TOWARDS COMPREHENSIVE INTERPRETATION OF THE STATE PARAMETER FROM CONE PENETRATION TESTING IN COHESIONLESS SOILS

by

MOHSEN GHAFGHAZI

B.Sc., Isfahan University of Technology, 2002
M.Sc., Sharif University of Technology, 2004

A THESIS SUBMITTED IN PARTIAL FULFILLMENT OF THE
REQUIREMENTS FOR THE DEGREE OF

DOCTOR OF PHILOSOPHY

in

THE FACULTY OF GRADUATE STUDIES

(Civil Engineering)

THE UNIVERSITY OF BRITISH COLUMBIA
(Vancouver)

April 2011

Abstract

The Cone Penetration Test (CPT) is widely used for determining in-situ properties of soil because of its continuous data measurement and repeatability at relatively low cost. The test is even more attractive in cohesionless soils such as sands, silts and most tailings due to difficulties associated with retrieving undisturbed samples in such soils. Behaviour of soils is highly dependent on both density and stress level. The state parameter is widely accepted to represent the soil behaviour encompassing both density and stress effects. Hence, determining the in-situ state parameter from CPT is of great practical interest.

The CPT was analysed using a large strain spherical cavity expansion finite element code using a critical state soil model (NorSand) capable of accounting for both elasticity and plastic compressibility. The constitutive model was calibrated through triaxial tests on reconstituted samples. The state parameter was then interpreted from CPT tip resistance, and the results were verified against an extensive database of calibration chamber tests. The efficiency of the method was further investigated by analysing two well documented case histories confirming that consistent results could be obtained from different in-situ testing methods using the proposed framework. Consequently, cumbersome and expensive testing methods can be substituted by a combination of triaxial testing and finite element analysis producing soil specific correlations.

One of the difficulties in analysing the cone penetration problem is the less researched effect of high stresses developing around the cone on the behaviour of the soil. A hypothesis was put forward on the particle breakage process at the particle level and its implications for the behaviour of sands at higher stress levels were discussed. A series of triaxial tests were performed, focusing on the effects of particle breakage on the location of the critical state line. The hypothesis was used to explain the observed behaviour. Particle breakage was shown to

cause additional compression and a parallel downward shift in the critical state line. The magnitude of the shift was linked to the amount of breakage and it was argued that significant breakage starts after the capacity for compression due to sliding and rolling is exhausted.

Preface

The research topics presented in the thesis were chosen jointly by Dr. D.A. Shuttle and me. I was responsible for performing all the numerical analyses, triaxial compression tests on Fraser river sand and data reduction work associated with the research. Initial versions of all thesis chapters were drafted by me, reviewed by Dr. D.A. Shuttle (and also Dr. Roberto Olivera for Chapter 7), and based on comments received I revised the thesis contents prior to submission. Dr. Roberto Olivera also provided guidance on the laboratory testing procedures described in Appendix A.

The following is the list of publications presented in this thesis:

Ghafghazi M., and Shuttle D.A. 2006. Accurate Determination of the Critical State Friction Angle from Triaxial Tests. Proceedings of the 59th Canadian Geotechnical Conference, Vancouver, 278-284, (*Chapter 2*) .

Ghafghazi M., and Shuttle D.A. 2008. Evaluation of Soil State from SBP and CPT: A Case History. Canadian Geotechnical Journal, (45)6: 824-844, (*Chapter 5*) .

Ghafghazi M., and Shuttle D.A. 2008. Interpretation of Sand State from Cone Penetration Resistance. Géotechnique, 58(8): 623–634, (*Chapter 4*) .

Ghafghazi M., and Shuttle D.A. 2009. Confidence and Accuracy in Determination of the Critical State Friction Angle. Soils and Foundations, 49(3): 391-395, (*Chapter 3*) .

Ghafghazi M., and Shuttle D.A. 2010. Interpretation of the In-situ Density from Seismic CPT in Fraser River Sand. Proceedings of the 2nd International Symposium on Cone Penetration Testing, Huntington Beach, California, (*Chapter 6*) .

Ghafghazi M., Shuttle D.A., and Olivera R.R. 2011. Particle Breakage and the Critical State of Sand. submitted, (*Chapter 7*) .

Table of Contents

List of Tables

List of Figures

List of Symbols and Abbreviations

a	[-]	Net area ratio
A_c	[L^2]	Projected cone area
A_s	[L^2]	Friction sleeve area
B	[-]	Skempton's pore pressure parameter, $B = \dfrac{\Delta u}{\Delta \sigma_3}$
B_q	[-]	CPTu excess pore pressure ratio, $B_q = \dfrac{u_2 - u_0}{\left(q_t - \sigma_{v0}\right)}$
CPT	[-]	Cone penetration test
CSL	[-]	Critical state locus
D	[-]	Total dilatancy, $\dot{\varepsilon}_v / \dot{\varepsilon}_q$
D^p	[-]	Plastic dilatancy, $\dot{\varepsilon}_v^p / \dot{\varepsilon}_q^p$
D_r	[-]	Relative density, $D_r = \dfrac{e_{max} - e}{e_{max} - e_{min}}$
e	[-]	Void ratio
e_c	[-]	Void ratio at the critical state for the current mean stress
e_{min}	[-]	Minimum void ratio, ASTM D4254
e_{max}	[-]	Maximum void ratio, ASTM D4253
F_r	[-]	Normalised friction ratio, $F_r = \dfrac{f_s}{q_t - \sigma_{v0}} \times 100$
f_s	[FL^{-2}]	Friction sleeve stress measurement
F_s	[F]	Sleeve friction resistance force
G	[FL^{-2}]	Elastic shear modulus
G_s	[-]	Specific gravity
H	[-]	Dimensionless plastic hardening modulus for loading
I_c	[-]	Soil classification index from Been and Jefferies (1992)
		$I_c = \sqrt{\left\{3 - \log\left(Q\left(1 - B_q\right) + 1\right)\right\}^2 + \left\{1.5 + 1.3\left(\log F_r\right)\right\}^2}$
I_r	[-]	Dimensionless elastic shear rigidity, G/p'
k	[-]	Soil-specific coefficient in equation [1-4]
K_0	[-]	In-situ lateral effective stress ratio, σ'_h / σ'_v
m	[-]	Soil-specific coefficient in equation [1-4]
M	[-]	Value of ratio η at the critical state (varies with lode angle)
M_i	[-]	Absolute value of $(M\text{-}\eta)$ used in the flow rule
M_{tc}	[-]	Value of ratio η at the critical state under triaxial compression conditions
n	[-]	Stress exponent
N, N^*	[-]	Volumetric coupling parameter
p	[FL^{-2}]	Mean total stress , $p = \left(\sigma_1 + \sigma_2 + \sigma_3\right)/3$

p'	[FL^{-2}]	Mean effective stress , $p' = (\sigma'_1 + \sigma'_2 + \sigma'_3)/3$
p_0	[FL^{-2}]	In-situ mean total stress
p'_0	[FL^{-2}]	In-situ mean effective stress , $p_0' = (\sigma'_{x0} + \sigma'_{y0} + \sigma'_{z0})/3$
p_a	[FL^{-2}]	Atmospheric pressure
p'_i	[FL^{-2}]	Mean effective stress at the image state
q	[FL^{-2}]	Deviatoric stress invariant, $q = (\tfrac{1}{2}(\sigma_1 - \sigma_2)^2 + \tfrac{1}{2}(\sigma_2 - \sigma_3)^2 + \tfrac{1}{2}(\sigma_3 - \sigma_1)^2)^{\tfrac{1}{2}}$
Q	[-]	Dimensionless CPT resistance based on mean stress required by mechanics, $Q = (q_t - p_0)/p'_0$
q_c	[FL^{-2}]	Tip resistance
Q_c	[F]	Cone tip resistance force
q_t	[FL^{-2}]	Corrected tip resistance, $q_t = q_c + (1-a)u_2$
Q_{tn}	[-]	Dimensionless CPT resistance based on vertical stress required by mechanics, $Q_{tn} = [(q_t - \sigma_{v0})/p_a](p_a/\sigma'_{v0})^n$
r	[-]	Chamber size correction factor
R	[-]	Overconsolidation ratio, $R = p'_{max}/p'_{current}$
SBP	[-]	Self-bored pressuremeter test
SD	[-]	Standard deviation
s_u	[FL^{-2}]	Undrained shear strength
u	[FL^{-2}]	Excess pore pressure
u_0	[FL^{-2}]	In-situ pore pressure
u_2	[FL^{-2}]	Pore pressure measured by CPT during sounding (at shoulder location)
χ_{tc}	[-]	Proportionality coefficient, relating minimum dilation to state
Δe_b	[-]	Reduction in void ratio caused by particle breakage
Δe_{sr}	[-]	Change in void ratio caused by sliding and rolling of particles
ε	[-]	Strain
ε^e_v	[-]	Volumetric strain, $\varepsilon^e_v = \varepsilon^e_1 + \varepsilon^e_2 + \varepsilon^e_3$, e superscript indicates elastic
ε^p_v	[-]	Volumetric strain, $\varepsilon^p_v = \varepsilon^p_1 + \varepsilon^p_2 + \varepsilon^p_3$, p superscript indicates plastic
$\dot{\varepsilon}_q$	[-]	Shear strain measure work conjugate with $\dot{\sigma}_q$, dot superscript denotes rate, $\dot{\varepsilon}_q = \tfrac{1}{3}\left((\sin\theta + \sqrt{3}\cos\theta)\dot{\varepsilon}_1 - 2\sin\theta\,\dot{\varepsilon}_2 + (\sin\theta - \sqrt{3}\cos\theta)\dot{\varepsilon}_3\right)$
ϕ'	[-]	Effective friction angle
ϕ_c	[-]	Constant volume (critical state) friction angle
η	[-]	Dimensionless shear measure as ratio of stress invariants, $\eta = q/p'$
η_L	[-]	Limiting stress ratio
Γ	[-]	'Altitude' of CSL, defined at 1 kPa
λ_{10}	[-]	Slope of CSL, defined on base 10
λ, λ_e	[-]	Slope of CSL on natural logarithmic scale

ν	[-]	Poisson's ratio
θ	[Rad]	Lode angle, $\sin(3\theta) = -13.5\,\sigma'_1\,\sigma'_2\,\sigma'_3\,/\,q^3$
σ	[FL^{-2}]	Total stress
σ'	[FL^{-2}]	Effective stress
σ'_{h0}	[FL^{-2}]	In-situ effective horizontal stress
σ_{v0}	[FL^{-2}]	In-situ total vertical stress
σ'_{v0}	[FL^{-2}]	In-situ effective vertical stress
ψ	[-]	State parameter, $e - e_c$
ψ_0	[-]	Initial state parameter

Acknowledgements

Dedication

To my parents and my wife whose love and support made this thesis a wonderful experience.

Chapter 1.

Introduction and Background

1.1.   Introduction

In-situ testing techniques are widely used to characterise the engineering properties of soils in engineering practice. The Cone Penetration Test (CPT) has been widely used for this purpose because of its continuous data measurement and repeatability at relatively low cost. The test is even more attractive in cohesionless soils such as sands, silts and most tailings due to difficulties associated with retrieving undisturbed samples in such soils.

The behaviour of cohesionless soils strongly depends on their density as well as the stress level. While relative density, D_r, is an almost universally used density index for sand, it is easy to show that it can be misleading (e.g. Tavenas, 1973). Alternatives to D_r that capture both the effect of void ratio and the effect of mean stress such as Bolton (1986) relative density index and the state parameter, ψ, (Been and Jefferies, 1985) can better represent soil behaviour.

The difficulty with any penetration test, however, is that the state measure of interest (e.g. D_r, ψ)

is not what is measured. Instead it is calculated from the penetration resistance; a process usually referred to as interpretation. This interpretation involves solution of an inverse boundary value problem to obtain mechanical properties of the soil from test measurements. But the large deformations associated with the CPT, along with the nonlinear behaviour of the soil and complicated boundary conditions, make this analysis an extremely difficult task, and the solution non-unique. The interpretation framework is also difficult to establish. No simple closed-form solution for ψ or D_r from CPT has been developed; and, nobody - to date - has provided a full numerical simulation of drained penetration that matches calibration data, although several have tried (de Borst and Vermeer, 1982; Willson et al., 1988; van den Berg, 1994; Huang et al., 2004; and Ahmadi et al. 2005). Two different directions have emerged to estimate soil state from CPT data: calibration chamber tests and analytical treatments.

Ideally, the adequacy and accuracy of interpretation methods should be verified against direct measurements of the in-situ density, such as undisturbed sampling. However sampling is particularly difficult in cohesionless soils with in-situ ground freezing being the only widely accepted technique; but such methods are prohibitively expensive and time consuming (Hoffman et al., 2000). Another problem with developing interpretation methods based on direct measurement of in-situ density is the unknown state of stress in the ground. The relation is affected by the horizontal stress (σ'_{h0}) in addition to the readily determined in-situ vertical effective stress σ'_{v0} (Baldi et al., 1986; Been et al. 1987; Schnaid, 1990), so that the horizontal geostatic stress ratio K_0 becomes important to accurate determination of ψ or D_r.

The need for controlled test conditions is not unique to this problem and is a common reason for resorting to laboratory testing. Calibration chamber testing has been the standard method adopted in the literature for developing interpretation methods for CPT.

Calibration chambers are circular steel tanks, typically about a metre in diameter and similar height. Sand is deposited at a known density and consolidated to the desired stress state within the tank. A cone penetration test is then performed along the vertical axis of the sample. Each test provides a tip resistance q_c for the given value of density and stress of the sample. A large number of tests, covering the range of densities and stresses of interest, provide the relation between q_c, in-situ effective stresses (σ'_1, σ'_2, σ'_3), and the density (usually expressed as ψ or D_r) for the tested material. The in-situ state ψ_0 (the subscript "0" denotes the initial value) is then obtained from the CPT by comparison of field CPT q_c measurements at the estimated in-situ stresses, to the $q_c-\sigma'-\psi_0$ relation determined in the calibration chamber.

Calibration chamber testing has been successfully used for calibrating CPT results to the state parameter (e.g. Been et al., 1987). However, the difference between the fabric and age of sample and the in-situ conditions still remains one of the major problems of extending calibration chamber results to in-situ CPT calibration. Moreover, this method is very time consuming and expensive; consequently, only a limited number of soils have been tested in calibration chambers and these are mostly at the research level. The $q_c-\sigma'-\psi_0$ relation differs from one soil to another so that, although the form remains common among soils, the coefficients involved are particular to the calibrated soil.

Different theoretical solutions have arisen as alternatives to calibration chamber testing for interpretation of the Cone Penetration Test. These methods have the advantage of being relatively easy and cheap to perform while providing insight into the parameters affecting the interpretation. This insight is a product of the theoretical methods incorporating some intrinsic material characteristic and thus relating them to the interpretation scheme.

Consequently, theoretical solutions have the potential to account for the basic differences

between calibration chamber tests and in-situ conditions such as fabric and age. Extending the argument to the effects of other material characteristics on the interpretation suggests that sufficiently advanced solutions should be able to provide material specific correlations for soils that have not been tested in calibration chambers.

A variety of methods have been used for modelling the deep penetration problem (mainly CPT and pile driving). The earliest methods approached the deep penetration phenomenon as a bearing capacity problem (e.g. Meyerhof, 1951; Vesic, 1963; and Sokolovskii, 1965). These bearing capacity idealisations assumed perfect plasticity and did not consider the deformations caused by the cone penetration.

The finite element method has been used for the analysis of the deep penetration problem for almost three decades (e.g. de Borst and Vermeer, 1982). Early efforts made significant simplifying assumptions to deal with the complexities of the problem; for example, prescribed deformation patterns were applied to replicate the penetration (e.g. Cividini and Gioda, 1988) or small strain formulation was used (e.g. Griffiths, 1982). With the advances in computational power, capabilities such as large strain formulation, adaptive mesh refinement and contact interface have been incorporated into the numerical analyses. More recent efforts (e.g. Susila and Hryciw, 2003; and Huang et al., 2004) have captured the geometric aspects of the problem with minimal simplifying assumptions.

Although significant progress has been made in capturing the geometrical aspects of cone penetration, less attention has been given to realistic modelling of soil behaviour. Elastic-perfectly plastic models with different flow rules are dominant for representing frictional soil (e.g. Huang et al., 2004; and Susila and Hryciw, 2003). Simple critical state models such as Modified Cam Clay have been used by some researchers (e.g. Sheng et al., 2005), but these

models have certain deficiencies in modelling density dependent behaviour of sand. Since the cone penetration is a deformation controlled process, it is necessary to simulate the dilation behaviour of the soil to an acceptable extent; a more sophisticated model is necessary to do so. Such a model should be able to simultaneously capture the behaviour of the part of the domain that is critical, dilating, or contracting; with the exact behaviour being a function of position.

Despite the obvious advances in modelling the problem in both sand and clay, it seems that the objective of determining soil properties from CPT has been lost in most efforts adopting finite element modelling; most attention has been directed towards modelling the problem itself assuming that the soil parameters are known. Ahmadi (2000) commented that no comprehensive comparison between experimental data and finite element results had been made. Most works are limited to comparing a few tests on a single soil and are primarily focused on predicting the resistance profile, while the steady value of resistance is what matters in uniform deposits.

Between the bearing capacity methods and full 3-D numerical modelling of the complete CPT penetration using a realistic soil model, lie a variety of simplified approaches such as spherical cavity expansion (e.g. Bishop et al., 1945; Yu and Houlsby, 1991; Salgado, 1993; and Shuttle and Jefferies, 1998) and steady state analyses (e.g. Baligh, 1985; and van den Berg, 1994). These methods make simplifying assumptions which induce certain limitations to their application for interpretation purposes. However, it is fair to say that they have contributed much to the understanding of the factors affecting the deep penetration problem as well as correlating in-situ parameters to the penetration resistance.

The cavity expansion is an especially attractive approach because of its relative ease of implementation and application even in comparison to steady state analyses. This makes it

useful to most geotechnical engineering projects requiring a practical CPT interpretation framework.

The reduction of the problem from its actual geometry to spherical symmetry necessarily results in applying only one stress invariant on the boundaries – as opposed to different vertical and horizontal stress components applied to the 3-D problem. However, this may not be a deficiency in itself if it is shown that the stress invariant applied at the boundaries can normalise any stress effects on q_c. Many researchers have pointed out the relation between q_c , the soil density (D_r or ψ) and the mean effective stress, p' (Clayton et al., 1985; Baldi et al., 1986, and Been et al., 1987). The data obtained with sands in calibration chamber testing show that there is negligible influence of K_0 , provided that the mean stress is used in normalising the data (Houlsby and Hitchman, 1989).

In this thesis the cavity expansion analogy is employed along with a constitutive model capable of capturing the density dependent behaviour of cohesionless soils to determine the state parameter from the CPT tip resistance q_c. Special attention is directed to

- Independent calibration of the numerical model to material behaviour through laboratory element tests on reconstituted samples
- Thorough verification and validation of the analysis against an extensive database of calibration chamber tests and in-situ measurements
- Associating confidence levels in estimating the state parameter to different levels of accuracy

The cone penetration was analysed as the expansion of a spherical cavity using a large strain

finite element code incorporating a critical state soil model (NorSand) capable of accounting for both elasticity and plastic compressibility. The constitutive model was calibrated through triaxial tests on remoulded samples. The state parameter was interpreted from CPT tip resistance, and the results were verified against a database of calibration chamber tests on natural sands and tailings, in addition to the laboratory standard sands. The efficiency of the method was further investigated by analysing two well documented case histories confirming that consistent results could be obtained from different in-situ testing methods using the proposed analysis technique. Consequently, cumbersome large scale testing methods, such as calibration chamber testing, can be replaced by a combination of triaxial testing and finite element analysis to produce soil specific interpretations.

There are two fundamental limitations in capturing the true behaviour of the material around the cone in the current analysis: The assumption that the elastic moduli remain unchanged during penetration and ignoring the particle breakage phenomenon.

For a certain material, the elastic moduli are known to be mainly affected by the stress level and void ratio, and to a lesser degree by other characteristics such as fabric. The penetration of the cone significantly increases the stresses in its vicinity while reducing the void ratio. Both of these will increase the elastic moduli around the cone resulting in a stiffer response. However, this effect has not been incorporated into the model due to numerical stability issues arising with elasticity approaching rigidity.

Another difficulty in understanding the cone penetration problem is the less researched effect of high stresses developing around the cone on the behaviour of the soil. Such stresses cause breakage in the particles increasing the compressibility of the soil. Russell and Khalili (2002) provided one of the earliest attempts at incorporating the effect of particle breakage into CPT

interpretation, by assuming a steepening of the Critical State Locus (CSL) with increasing mean stress, into a cavity expansion analysis using a critical state based model. The effect of this change was a reduction in the limiting cavity expansion pressure, inferring denser soil states for identical CPT tip resistances. However, the idea of a steepening CSL is theoretically questionable and fails to explain some of the behaviour observed in laboratory experiments.

While the changes in elasticity are relatively well understood and the problem is now reduced to a purely numerical one, the modelling of the particle breakage is still in its infancy especially within the critical state soil mechanics. Thus an attempt was made at further developing the state of knowledge on the subject.

A simple hypothesis on particulate behaviour of the material is proposed to understand the movement of the Critical State Locus due to shearing. The hypothesis was tested using a series of triaxial compression tests on a local sand.

1.2.   Verification and Validation

Any theoretical framework has to be verified and validated against an acceptable amount of data before being used as a reliable interpretation technique. This makes a method only as accurate as the experimental data that it has been verified against. But more importantly, there will be a limit to the extent that a method can be generalised for application to materials different from those included in the verification process. This limit is set by the number of material characteristics that can affect the interpretation and are properly accounted for in the theoretical framework.

For example, assume that elasticity is known to play a role in the interpretation of the state

parameter from CPT tip resistance, and a method has been verified for a number of materials with a certain range of elastic moduli. The validity of the application of this method to materials with elastic moduli outside of that range will depend on the capability of the method to adequately capture the effect of elasticity on the interpretation.

Validation immediately raises the issue of determining 'ground truth'. This situation has arisen in other aspects of in-situ testing of soil, and it is usual to evaluate the soil properties determined by one test method against those determined by another method in evaluating reliability of the two methods, for example, work at 'national test sites' by Nash et al. (1992) and Woods et al. (1994). In case of in-situ state of cohesionless materials, direct measurements of the void ratio were done in a few cases using ground freezing techniques (e.g. Wride et al., 2000; Plewes et al., 1994). Such cases would provide ideal validation cases for a theoretical method verified against a database of calibration chamber tests.

1.3. The NorSand Constitutive Law

The constitutive model adopted, NorSand (Jefferies, 1993), is an isotropically hardening - isotropically softening generalised critical state model that captures a wide range of particulate soil behaviour. The primary attribute of NorSand for this work is that it dilates in a realistic manner, thereby allowing the effect of volume change on the CPT resistance to be well represented. NorSand can be regarded as a super-set of the well-known Cam Clay model (Schofield and Wroth, 1968), with Cam Clay being obtained as a special case of NorSand by appropriate choice of the soil properties and initial conditions. NorSand has been well documented in the literature. The version used herein is that for monotonic loading of general

3-D stress states with constant principal stress direction as described in Jefferies and Shuttle (2002) but with one modification to improve accuracy (described below); a good overview of this version of the model is provided in Jefferies and Shuttle (2005).

The critical state, which is the condition at which soils deform continuously and indefinitely at constant volume, is used as the reference framework. The void ratio at the critical state e_c depends on the mean effective stress p', and various relations have been proposed for this. These different relations are details that do not affect the overall approach, and preference for one relation over another is given to fit the behaviour of a particular soil. For most purposes the familiar $e_c = \Gamma - \lambda \ln p'$ idealisation is both simple and sufficiently accurate. Γ is the intercept of CSL, defined at 1 kPa and λ is its slope on a logarithmic scale.

An infinity of Normal Consolidation Loci (NCL) for cohesionless soils (Ishihara et al., 1975) forces two parameters to characterise the state of a cohesionless soil: ψ and R. The state parameter ψ is a measure of the location of an individual NCL in $e - p'$ space. The overconsolidation ratio R represents the proximity of a state point to its yield surface when measured along the mean effective stress axis. Note in particular that R and ψ are not alternate identities as implied by Cam Clay or its variants; R and ψ represent measures of different things as illustrated in Figure 1-1.

The critical state is also a relation between mean and shear stress, and this has been extensively investigated. To a high precision and high stress levels, the critical state is fitted by $q_c = Mp'_c$ (where the subscript 'c' denotes critical conditions and M is a soil property; q_c is the deviator stress invariant at the critical state and should not be confused with its application as the CPT cone resistance in the rest of the thesis). More precisely, M varies with the proportion of

intermediate principal stress (usually given as the lode angle θ) and the soil property is conventionally defined under triaxial compression conditions as M_{tc} with the subscript '*tc*' being used to indicate this. M_{tc} is related to the critical state friction angle ϕ_c through Equation 1-1:

$$M_{tc} = \frac{6\sin\phi_c}{3 - \sin\phi_c} \qquad\qquad \text{[Eq. 1 - 1]}$$

NorSand is a plasticity model for soil. As such, and in common with other plasticity models, it comprises three items: (1) a yield surface; (2) a flow rule; and, (3) a hardening law. These three aspects of the NorSand model are described below, with the equations of the model summarised in Table 1-1.

The NorSand yield surface has the familiar bullet-like shape of the classical Cam Clay model but with one important difference – there is an internal cap so that the soil cannot unload to very low mean stresses without yielding. This internal cap is taken as a flat plane, and its location depends on the soil's current state parameter. Figure 1-2 illustrates the NorSand yield surface for two cases, a very loose soil and a very dense soil. As illustrated on Figure 1-2, the location of the internal cap controls the limiting stress ratio η_L that the soil can sustain; what is sometimes called the Hvorslev Surface is seen to be a hardening limit for the true yield surface. This internal cap generalises the ideas of Drucker et al. (1957), the key insight of which is that the familiar Mohr Coulomb strength envelope is not a yield surface, and gives realistic dilatancy with normality. Yield surfaces have a 'bullet' shape that intersects the Mohr Coulomb strength envelope at the critical state.

The plastic dilatancy D^p is determined from the idealised stress-dilatancy relation that underlies the model, but as there are three strain rates this is insufficient to determine each of them. The intermediate principal strain rate is therefore interpolated depending on the lode angle. This interpolation approach is somewhat unusual for plasticity models, but is taken to ensure consistency with the work dissipation postulate that is the basis of the model.

The third aspect of the model is the hardening law, which describes how the yield surface increases or decreases in size with plastic straining. The size of the yield surface is controlled by what is termed the image stress p'_i and which forms the object of the hardening law. It is called the image stress because it represents a situation in which one of the two conditions for the critical state (zero volume change) is met, and the meaning is readily apparent from Figure 1-2. NorSand has isotropic hardening which expands or contracts the yield surface, as required by the hardening law, while retaining its shape. The position of the internal cap evolves with the changing state parameter. Whether the yield surface hardens or softens depends on two things: the current state parameter and the direction of loading. Loading past the internal cap always softens the yield surface, as does principal stress rotation. However, the key determinant in the general hardening is the state parameter. As illustrated on Figure 1-2, the critical state does not usually intersect the yield surface (this is the largest single difference between NorSand and Cam Clay). This divergence of yield surface from critical state is used as the basis of the hardening law, and the hardening law acts to move the yield surface towards the critical state under the action of plastic shear strain – which directly captures the essence of critical state principles.

Elasticity in soils is arguably a more complicated aspect than plasticity. Various elastic models can be used depending on the trade off between complexity and accuracy. Pestana and Whittle

(1995) looked at elastic models that accounted for the effect of void ratio in some detail with Jefferies and Been (2000) suggesting a further refinement. However, for most situations involving soil modelling this sophistication is unwarranted. On one hand the soil fabric affects modulus and thus elastic modulus should be measured in-situ. On the other hand, plastic strains often dominate. For most purposes a simple constant shear rigidity I_r and constant Poisson's ratio is a sufficient representation of elasticity and this approach is used here. This is equivalent to the constant κ idealisation of the classic CSSM models.

NorSand is a sparse model. For the variant presented here, in which the CSL has been taken as the approximate semi-log form and with the simplest representation of elasticity, there are eight model parameters. These are summarised on Table 1-2 with typical ranges in values for sands indicated. How to determine the model parameters is presented later in the chapters and in detail in Jefferies and Shuttle (2005); examples of calibrated parameter sets are given there. All the parameters are dimensionless, although Γ has a reference stress level associated with it. Most of the parameters are familiar including $\Gamma, \lambda, M_{tc}, I_r$ and v. Only three parameters may be unfamiliar.

The parameter χ_{tc} is the slope of the trend line for minimum dilatancy versus the state parameter at minimum dilatancy. In the original version of NorSand this trend was thought to be a model constant. But, further data have shown that χ_{tc} varies somewhat from soil to soil and could also be a function of soil fabric. The reference condition is taken as triaxial compression because dilatancy is itself a function of the lode angle.

A feature of the original version of NorSand was a volumetric coupling parameter N for stress-dilatancy. Subsequently, Jefferies and Shuttle (2002) suggested that N could be eliminated from the model since $N\chi_{tc} \approx 1$ (based on average values of a large quantity of triaxial tests on different

sands). However, individual soils demonstrate a variety of $N\chi_{tc}$ values and some accuracy is sacrificed by following this suggestion. Adding N back to the model neither increases the complexity of the model, nor constitutes additional effort in calibration of the model, as N is obtained with M_{tc} from the stress-dilatancy plot and reintroduction of this parameter resulted in better replication of the soil behaviour. For the current work N was obtained as the slope of the post peak stress-dilatancy plots, rather than using the Bishop (1971) methodology and is termed N^* for clarity.

The plastic hardening modulus H can in principle be a function of soil fabric, and data to date suggests that it is often a function of ψ. There is some evidence that H is proportional to $1/(\lambda-\kappa)$ which is what might be anticipated from NorSand's similarity to to Cam Clay. On the other hand, such a linkage should also be anticipated to be affected by soil fabric.

1.4. Literature Review

1.4.1. Cone Penetration Test

Since being developed in early 1930s as a geological tool for stratigraphic purposes, the cone penetration test has attracted attention from the geomechanics perspective. The main advantage of the CPT is the interesting combination of a continuous data record with excellent repeatability and accuracy at relatively low cost.

The first cone penetrometers were made in 1932 by P. Barentsen, an engineer at the Department of Public Works in Netherlands (Lunne et al., 1997). The first electric cone penetrometer was most likely developed in Berlin during the Second World War (Lunne et al., 1997). Much of the

14

subsequent developments occurred in the Netherlands (Broms and Flodin, 1988). The work was continued in Canada by Campanella and his students (Campanella et al., 1983; Robertson and Campanella, 1983[a,b], 1986; Robertson et al., 1986; Robertson and Wride, 1998; and Robertson, 2009), and by many other workers worldwide.

The cone penetration test is conducted by pushing a penetrometer with a conical tip attached to the end of a series of rods into the ground at a constant rate; continuous measurements are made of the resistance of the tool to penetration. The standard electronic cone penetrometer (ASTM D5778) has a conical point with 60° apex angle and a projected cone base of 10 cm^2 (see Figure 1-3). The cone penetrometer is advanced through soil at a constant rate of 20 mm/sec. The cone tip resistance (Q_c) and sleeve friction resistance (F_s) are the basic readings of CPT results (both in force units). The excess pore water pressure (u) can be obtained through a piezometer on or behind the cone tip. It is common to have the piezo-element 5 mm above the cone and the pore pressure recorded at this location is denoted by u_2. Nowadays a cone penetrometer can contain many sensors and measurements of electrical conductivity, inclination, temperature and shear wave velocity can also be performed during cone penetration. Readings from the electronic measuring devices are usually recorded automatically in a computer during penetration.

Q_c divided by the projected area of the cone, A_c, produces the tip resistance q_c. q_c is corrected for the effect of the net area ratio (a) through Equation 1-2

$$q_t = q_c + (1-a)u_2$$ [Eq. 1 - 2]

q_t and q_c are essentially the same in drained penetration (as in cohesionless soils) due to low pore water pressures around the cone. F_s divided by the surface area of the friction sleeve, A_s,

produces sleeve resistance (f_s). The normalised friction ratio F_r is defined as a percentage with

$$F_r = \frac{f_s}{q_t - \sigma_{v0}} \times 100$$

[Eq. 1 - 3]

Since f_s is measured about 10 *cm* behind the cone tip (for a typical ASTM D5778 cone), the value of f_s and q_t in Equation 1-3 should not be the values recorded at the same time. Instead, the values recorded at the same depth should be used; i.e. f_s should be shifted to account for the distance between the cone tip and the centre of the friction sleeve.

1.4.2. Interpretation of the State Parameter from CPT Tip Resistance

The CPT provides three measurements; the tip resistance, the sleeve friction, and the pore pressure. A combination of the three is usually used in a qualitative way for soil classification (i.e. Been and Jefferies, 1992; Robertson and Wride, 1998). The CPT in sand provides just two outputs; the tip resistance and the sleeve friction as the penetration is drained so the pore pressure transducer simply measures the in-situ pore pressure.

Once a soil type has been identified it is common practice to correlate certain soil parameters with one of the measurements. The shear strength parameters (e.g. s_u, friction angle and density indices) are usually estimated through the tip resistance.

The state measure used in this work is the state parameter, ψ (Been and Jefferies, 1985). Because ψ is used as an internal state variable in the numerical model, the subscript '0' is used

to denote the in-situ (or initial) value of ψ_0 under geostatic conditions to be consistent with the original usage by Been and Jefferies.

Initial work with determining ψ_0 from CPT data comprised triaxial testing of sands for which chamber test data was available to define the CSL of each sand, and then processing the chamber test data to develop dimensionless relations (Been et al., 1986, 1987) of the form:

$$Q = k \exp(-m\psi_0)$$
[Eq. 1 - 4]

Where Q is the tip resistance normalised by the initial mean total and effective stresses, p_0 and p'_0:

$$Q = \frac{q_t - p_0}{p'_0}$$
[Eq. 1 - 5]

Been et al. (1987) suggested that the two coefficients k and m in Equation 1-4 depend on the compressibility of the soil through the slope of the critical state line λ. They used a database of five different clean sands to develop their correlations for obtaining the state parameter from CPT tip resistance.

Plewes et al. (1992) looked at a database of clean sands as well as silty clays and suggested that λ_{10} (on logarithm base 10) can be approximated by the normalised friction ratio F_r (written as a decimal) according to Equation 1-6:

$$\lambda_{10} = F_r/10 \qquad\qquad\qquad\qquad\qquad\qquad \text{[Eq. 1 - 6]}$$

Following the idea of Been et al. (1987) for correlating k and m to λ, Plewes et al. (1992) provided generalised equations that can be applied to both sands and clays:

$$k/M_{tc} = 3 + 0.85/\lambda_{10} \qquad\qquad\qquad\qquad \text{[Eq. 1 - 7]}$$

$$m = 11.9 - 13.3\lambda_{10} \qquad\qquad\qquad\qquad \text{[Eq. 1 - 8]}$$

Equation 1-7 implies that k and m in turn the interpreted state parameter are functions of the critical state friction ratio M_{tc}.

Konrad (1997) adopted Equation 1-4 and suggested that the in-situ state parameter can be determined by normalising the state parameter with respect to e_{min} and e_{max}. He also developed a correlation for correcting the stress level effect based on data from Ticino sand. He suggested that in the absence of material specific correlations, this stress level correlation can be used for other materials.

Robertson (2009) developed contours of state parameter on the material type behaviour charts of Robertson and Wride (1998) based on laboratory and field investigation data. The contours are shown on Figure 1-4 where normalised tip resistance, Q_{tn} is plotted against normalised friction ratio, F_r. Q_{tn} is defined by

$$Q_{tn} = \left[(q_t - \sigma_{v0})/p_a\right]\left(p_a/\sigma'_{v0}\right)^n \qquad\qquad \text{[Eq. 1 - 9]}$$

n is a stress exponent that varies from 0.3 to 0.9 for most coarse grained soils. p_a is a reference pressure assumed to be equal to 100 *kPa* and is used to preserve the non-dimensionality of the normalizations.

Combinations of measurements from independent in-situ tests have also been adopted for obtaining the state parameter in sands. Yu et al. (1996) used the ratio of measured cone tip resistance and pressuremeter limit pressure to calculate the peak friction angle and the state parameter. Schnaid and Yu (2007) used the ratio of elastic stiffness to the cone tip resistance to estimate the same parameters.

1.4.3. Calibration Chamber Testing

A calibration chamber test involves preparing a large sand specimen in the laboratory, consolidating it to a desired stress level, and then performing a CPT test under given boundary conditions. Since the entire experiment is conducted in the laboratory, the test quality can be readily controlled. The large sand specimen, with uniform deposition and known engineering properties, provides reference values for the interpretation and thus calibration of the in-situ test method. A cone penetration test is then performed along the axis of the sample. Each CPT test provides one value of q_c corresponding to the chamber's initial density and stress state. A number of tests, covering the range of densities and stresses of interest, provide a relation between q_c, density and stresses. To interpret the properties of a soil, the measurements of CPT in the field are compared with the measurements for the same soil in calibration chambers.

Chamber tests have been in use for over 40 years. The first advanced calibration chamber (including measurement of boundary stresses and strains) was built in 1969 at the Country

Roads Board (CRB) in Australia (Holden, 1991). Nowadays, the chamber tests differ in a number of ways such as dimensions, nature and form of control of boundaries, deposition procedure, and capability to handle saturated specimens. In 1991 Ghionna and Jamiolkowski provided a list of 19 calibration chamber tests reported in the literature. More calibration chambers have been built since then (e.g. Hsu and Huang, 1998; Ajalloeian and Yu, 1998; and Tan et al., 2003). Table 1-3 is an extension of a compilation of calibration chambers by Ghionna and Jamiolkowski (1991) to encompass some of the recent works.

Holden (1991) summarised the advantages of the calibration chamber as follows:

1. The lateral boundaries are flexible. It is possible to produce the normally consolidated (NC) or overconsolidated (OC) specimens under K_0 conditions.
2. The boundary stresses are known and controlled.
3. The chamber specimen can be large enough to perform a full scale CPT.
4. By means of pluvial methods, the chamber specimens are uniform and reproducible.

Been et al. (1988) and Ghionna and Jamiolkowski (1991) reviewed the problems associated with calibration chamber testing. Sample age, limited number of sands tested, and sample size and boundary effects are among the important limitations of calibration chamber testing. Calibration chamber tests are performed on specimens of freshly reconstituted sands. The fabric of these samples of sand will likely be different from that of the natural soil deposit in situ. The structure and ageing effects have been reported to have a significant effect on measured cone resistance (Schmertmann, 1991). Most calibration chamber tests have been performed on uniform, clean predominantly silica sands. Natural sand deposits are seldom as uniform, and generally contain

some amount of fines that may significantly influence their behaviour. In addition, many relevant engineering problems are linked to crushable and compressible materials such as carbonate sands which may also be slightly cemented. Strictly speaking, the correlations are only valid for sands of similar gradation, particle shape, and mineralogy to the sands the correlations are based upon. To extend calibration chamber research to more realistic soils such as silty, crushable, and cemented sands is a desirable aim for future work.

1.4.3.1.   Boundary effects

It is well known that the value of penetration resistance measured during the test is influenced by the conditions at the sample boundaries (Parkin and Lunne, 1982; Baldi et al. 1982; Bellotti et al., 1982; Been et al., 1987; Sisson, 1990; Mayne and Kulhawy, 1991; Salgado, 1993; Zohrabi et al., 1995; Huang and Hsu, 2005). As summarised in Table 1-4, five different boundary conditions have been used in calibration chambers. The differences between the five types of boundary conditions are in the type of stress or displacement boundary conditions imposed on the top, bottom, and circumferential surfaces of the sample. Been et al. (1988) based on a limited amount of data, indicated that boundary conditions on top and bottom of the chamber specimen had little effect on CPT results.

Boundary effects are more apparent in dense sand than in loose sand. The influence also decreases with the compressibility of sand. For loose sand, chamber results are relatively independent of boundary conditions, even when the ratio of chamber to cone diameter (D/d_c) is as low as 21; for dense sand, all calibration chamber results are affected by boundary conditions, even for D/d_c of 60 or greater (Parkin, 1988).

BC1 and BC4, both corresponding to a constant lateral stress during cone penetration, generate approximately the same penetration resistance values, all other factors being equal. Similarly, BC2 and BC3 generate comparable penetration resistance values under the same conditions. None of these four boundary conditions perfectly represent free-field conditions, so q_c in the calibration chamber is generally different from q_c in the field. The difference between chamber and field q_c values decreases as the ratio of chamber to cone diameter (D/d_c) increases. Whether the chamber q_c values are bigger or smaller than the in-situ values also depends on the type of boundary conditions. Under BC1 conditions, q_c is always lower than in the field, because a constant lateral stress during penetration underestimates the lateral stresses that will develop during penetration in the field. Ideal BC3 conditions, with a perfectly rigid lateral wall, would always impose boundary effects that lead to higher q_c values than those measured in the field. Additionally, a rigid wall does not offer the same degree of control during the sample preparation, consolidation, and penetration stages of the test.

In recent years, there have been attempts to simulate real soil response at boundaries of a calibration chamber specimen. The idea is that the lateral boundary deforms in response to the cone penetration test conducted within the soil specimen. The boundary deformation should then induce variation of stress on the lateral boundary due to the reaction of soil from beyond the lateral boundary, if the soil extended to infinity as in field conditions. Such chambers are called servo-controlled calibration chambers. The servo-controlled systems reported by Ghionna and Jamiolkowski (1991) and Foray (1991) allowed the stress to vary but remain uniform throughout the lateral boundary. Hsu and Huang (1998) developed a servo-controlled (BC5) calibration chamber that allowed the boundary response to be independently controlled at

different depths. However, there is little information about the efficiency of these methods and most available data still come from tests with the first four boundary conditions.

1.4.3.2.   Correction and Normalisation of Boundary Conditions Effect

Recognising the boundary effects on calibration chamber data, researchers have developed correlations and graphs to correct for them. Looking at calibration chamber data on Ticino sand at D/d_c=34.2, Baldi et al. (1982) reported a series of chamber size correction factors, r defined as

$$r = \frac{q_{c,field}}{q_{c,cc}}$$

[Eq. 1 - 10]

where $q_{c,cc}$ is the experimental value of tip resistance observed in the calibration chamber and $q_{c,field}$ is the tip resistance expected to be measured in the field for the same sand with the same relative density and the same in-situ stresses as in the chamber. They suggested that the value of r increases with density and the over consolidation ratio.

Lunne and Christophersen (1983), based on chamber test results using Hokksund sand, suggested that for a chamber to cone diameter ratio of 50, the difference between the tip resistance obtained in the chamber and the field is small.

Jamiolkowski et al. (1985) proposed a formula to relate the tip resistance obtained in the chamber to the tip resistance obtained in the field based on data from Ticino and Hokksund sands under BC1 and BC3 type boundary conditions.

$$\frac{q_{c,field}}{q_{c,cc}} = \left(1 + \frac{0.2\left(D_r(\%) - 30\right)}{60}\right)$$

[Eq. 1 - 11]

Equation 1-11 implies that for loose sand with a relative density of 30%, the experimental result of the chamber and the field are similar and no calibration size effect should be considered. However, as the relative density of sand in the chamber increases, the size effect will become larger (e.g. 1.13 for relative density of 70%).

Been et al. (1986) used previously published data to study the chamber size effects on normalised cone resistance. They used data from Hokksund and Ticino sands with different boundary conditions to normalise the cone resistance to that of a chamber size with D/d_c of 50. Figure 1-5 illustrates the variation of the Normalisation factors in different boundary conditions versus the state parameter. It should be noted that the factors are derived based on a particular design of chamber and for a limited number of sands. Hence they should be cautiously applied to other soils and chamber test designs. They acknowledged that a D/d_c of 50 may not be analogous to the field and is only used as a base for comparing different data.

Mayne and Kulhawy (1991) assumed that, regardless of the relative density and stress state, a chamber diameter to cone diameter ratio of 70 is sufficient to achieve the "free field" condition. This means that in order to prevent boundary effects for the standard cone diameter of 3.57 *cm*, a 2.5 *m* diameter chamber is required. They proposed a relation to correct the cone resistance for boundary effects that includes the chamber over cone diameter ratio and the relative density. This relation is based on some of the 24 sets of data of cone penetration test results performed in conventional calibration chambers.

$$\frac{q_{c,field}}{q_{c,cc}} = \left(\frac{(D/d_c) - 1}{70} \right)^{\frac{-D_r(\%)}{200}}$$

[Eq. 1 - 12]

In a 1.2 m wide chamber the equation returns correction factors of 1.12 for $D_r = 30\%$ and 1.30 for $D_r = 70\%$. Cudmani and Osinov (2001) adopted the form of the Mayne and Kulhawy (1991) correlation and generalised it as

$$\frac{q_{c,field}}{q_{c,cc}} = \left(\frac{(D/d_c) - A}{(D/d_c)_0} \right)^{-I_D^*/B}$$

[Eq. 1 - 13]

where $(D/d_c)_0$ is the ratio at which the influence of the chamber size vanishes, and A and B are constants to be determined. I_D^* is a normalised state parameter varying between 0 and 1 and being negative for very loose states. They suggest $A=0$ and $(D/d_c)_0=60$ and suggest the values in Table 1-5 for different sands based on previously published experimental data.

Salgado (1993) proposed an analytical scheme to correct the boundary effects based on cylindrical cavity expansion considering the dilatancy effects. Salgado et al. (1997) too used the spherical cavity expansion and concluded that the tip resistance is a function of relative density, stress state, and intrinsic parameters of the sand. This work was then used in Salgado et al. (1998) to obtain correction factors for chamber tests and was compared to experimental data. They proposed charts for obtaining correction factors that were dependent on relative density, stress state, and intrinsic parameters of the sand.

In summary, different researchers have tried to determine the ratio of chamber to cone diameter at which boundary conditions have little effect on the cone resistance; Values of D/d_c between

50 to 200 have been suggested. Since the correction factors are sensitive to the type of sand being tested as well as the boundary conditions, they should be used cautiously. The ideal approach is to apply factors developed for each sand under a certain set of boundary conditions, to the same sand and boundary conditions; but such information is not available in most cases. Since the differences between the various boundary effect corrections is usually about an order of magnitude smaller than the random variability in the calibration chamber data, for most practical purposes application of any reasonable correlation is expected to sufficiently reduce the error caused by the boundary effects.

The correction factor suggested by Been et al. (1987) has been used in this work, and indicates correction factors between 0.9 and 1.5 to the tip resistance q_c. This correction generally falls midrange between those of Jamiolkowski et al. (1985) and Mayne and Kulhawy (1991). Using Been et al. (1987) correlation provides a uniform treatment of the boundary effects amongst all the materials.

1.4.4. Analytical and Numerical CPT Interpretation Methods

A range of analytical and numerical methods have been used to analyse the deep penetration problem, some focusing on interpreting in-situ parameters from Cone Penetration Testing. These methods include the bearing capacity theory, the steady cone penetration and strain path methods, the cavity expansion theory, finite element method and other analysis techniques such as finite difference and discrete element methods. Yu and Mitchell (1998) provided a general overview of different methods used for analysis of the cone penetration. These methods are reviewed in this section to the extent that they relate to this work.

1.4.4.1.   Bearing Capacity Theory

One of the first methods used for the analysis of cone penetration was to treat it as a bearing capacity problem. The cone resistance is assumed to be equal to the collapse load of a deep circular foundation in soil. Two analytical approaches, namely limit equilibrium and slip-line analysis, have been used to determine the cone resistance. The limit equilibrium method adopts the concept of Terzaghi's (1943) bearing capacity theory. Under an assumed failure mechanism, q_c is computed based on global equilibrium of the soil mass which is treated as a rigid body (e.g., Meyerhof, 1951; Durgunoglu and Mitchell, 1975). In the slip-line analysis, the stress field in the plastic zone generated by cone penetration is simulated as a network of slip-lines. A yield criterion (such as the Mohr-Coulomb or Tresca) is combined with the equations of equilibrium to give a set of differential equations of plastic equilibrium in the soil mass. The value of q_c is determined by the distributed contact pressure acting on the cone face (e.g., Sokolovskii, 1965; de Simone and Golia, 1988; Koumoto, 1988). Although the stress field obtained from the slip-line method satisfies both the yield criterion and the equilibrium condition inside the slip-line network region, the stress distribution outside this region is not defined.

Yu and Mitchell (1998) summarised the bearing capacity solutions for cone resistance in both cohesive and cohesionless soils. A major advantage of this approach is its relative simplicity. It can be easily accepted by many engineers who are already familiar with bearing capacity calculations. However, the relative simplicity of the approach also typically extends to the use of very simple, and unrealistic, idealisations of soil behaviour. In addition, the bearing capacity approach for the analysis of cone penetration has serious limitations, some of which are described by Yu and Mitchell:

- In bearing capacity analysis, deformations of the soil are neglected, and this means the dependence of the cone resistance on soil stiffness and compressibility, as observed in laboratory and field testing, cannot be predicted.

- The bearing capacity approach ignores the influence of the cone penetration process on the stress states around the shaft. In particular, the horizontal stress tends to increase around the cone shaft above the cone, and the influence of this change on the cone resistance is not considered in bearing capacity analysis.

- Slip-line analysis is more rigorous than the limit equilibrium method, as it satisfies both the equilibrium equations and the yield criterion everywhere within the slip-line network. The limit equilibrium method only satisfies the global equilibrium.

- Shear surfaces assumed are usually not observed accompanying deep cone penetration.

1.4.4.2. Steady Cone Penetration and Strain Path Method

Although the initial insertion of the cone into the ground is a transient process, the penetration in a uniform material is a steady process. In steady state analysis of the penetration it is assumed that the cone penetration has proceeded for a long enough length that steady-state conditions have been reached. In other words, it is assumed that an observer situated on the cone penetrometer observes steady-state conditions in the soil passing the penetrometer during the penetration process. According to Yu et al. (2000) this approximation requires that the soil deposit is an infinite, isotropic, homogeneous mass with a known initial stress state. The assumption of homogeneity in the vertical direction removes the possibility of material property,

initial stress, or strength dependence with depth within the zone of influence of the cone penetrometer. This assumption limits the applicability of these methods in modelling the behaviour of layered soil. Another requirement is that the cone penetrometer is inserted into the ground with a constant velocity. This requirement is usually fulfilled as constant velocity is a requirement of ASTM D5778.

One of the first methods for conducting steady-state analysis of cone penetration in soil was the strain path method (Baligh, 1985). This method, which has long been used in modelling steady state cone penetration of incompressible soils such as clays (Baligh, 1985; Acar and Tumay, 1986; Huang, 1989; Gill and Lehane, 2000), is based on the assumption that the soil deformation is completely decoupled from the soil strength parameters. Sagaseta et al. (1998) extended the method to analyse shallow penetration problems. A combination of a strain path and the finite element method have been proposed by Teh and Houlsby (1991).

In the development of the method, soil deformations were estimated using velocity fields from potential theory (where the material properties correspond to an ideal, incompressible and inviscid fluid). Using this approximation, different penetrometer geometries can be modelled through combinations of sources and sinks or other surface mapping techniques such as the boundary element method. For simple penetrometer geometries, the velocity and strain rate components can be obtained from closed-form expressions, while the displacements and strains are solved by numerical integration along the streamlines. Once the strain paths of individual soil elements are known, the material constitutive equations can be used to derive the effective soil stresses. For undrained penetration in clays, the constitutive equations can be represented using either total stresses (relating shear stresses and shear induced pore pressures to shear strains) or effective stress models. In either case, due to incompressibility, there is one stress

component (either the excess pore pressure or the mean stress) that cannot be obtained from the stress–strain relations and must be solved from the equilibrium equations. In general, it is not possible to match all of the equilibrium equations with a single unknown function (i.e. field of u or p). A unique solution for this stress component is only possible if the strain field (derived for an inviscid fluid) is exact.

The main idea of Baligh's strain path method is that the soil deformations and strains caused by the CPT are independent of soil strength and stiffness parameters and can then be estimated, for example, from irrotational flow of an ideal fluid. This assumption was based on experimental observations on deep penetration in clay. As shown in Ladanyi (1963) and Collins and Yu (1996), for 1-D problems such as cavity expansion in undrained clay, the soil deformations and strains can be determined from the incompressibility condition without considering stresses and strength. In other words, for 1-D cavity expansion problems in undrained clays, the strains are completely independent of soil strength parameters. Considering that cavity expansion theory has long been used with reasonable accuracy to model much of the soil behaviour during deep penetration, Baligh (1985) logically assumed that the soil deformation caused by cone penetration may also be determined with reasonable accuracy purely from an incompressibility requirement. It has been found, however, that the resulting stresses derived from this approach may not satisfy all the equilibrium equations. This is because for 3-D problems, such as cone penetration in undrained clays, the soil deformation is not completely decoupled from the soil strength parameters, although the coupling is believed to be quite weak for undrained problems (Yu et al., 2000). In order to account for this problem, Baligh (1985) and Houlsby et al. (1985) proposed an iterative procedure between the assumed velocity field (equivalent to the strain path) and the stresses obtained from the method in order to reduce the imbalance in the

equilibrium equation. However, as reported by Whittle (1992) this procedure cannot remove all the errors that exist in the strain path stress solutions.

The application of the strain path method is mainly restricted to undrained clays. The application to cohesionless soils is almost impossible as the initial estimate of flow field for frictional-dilatant soils is very difficult to obtain. The reason is that the method is based on the assumption that the soil deformation is completely decoupled from the soil strength parameters. While the coupling is believed to be quite weak for undrained problems, it is much stronger in drained behaviour of dilatant soils. Other limitations of the strain path method are that the roughness of cone and shaft cannot be modelled, and that this method is not applicable to cone penetration in layered deposits.

Van den Berg (1994) used a Eulerean framework, which is a special case of the Arbitrary Lagrangian Eulerean (ALE) method, to model penetration in both sands and clays. In this method the movement of the element nodes and the material points is decoupled. In other words, the material can flow through the mesh. In van den Berg's work, the mesh is fixed, so the problem of extensive element distortion due to large displacements is solved. Simply speaking, the analysis is performed using a split algorithm; first, implicitly a Lagrangian step is calculated and, subsequently convection is taken into account explicitly in a remap loop over the nodes. The basic idea is the introduction of continuous stress and strain fields by interpolation of nodal point stresses and strains. So the next step starts with the mesh nodes at the initial location, but with an updated stress and strain field. This approach has long been applied to fluid mechanics problems, but is relatively new to geotechnical literature.

Since in the model the constitutive behaviour of the material is coupled to the fixed elements, the method is capable of giving reasonable results only for homogeneous materials throughout

the complete finite element discretisation. In order to model layered soil, a tracking algorithm was proposed enabling the material properties to stream through the mesh as well. In other words, the material particles' movement through the fixed finite element mesh is captured by tracking their constitutive behaviour. Van den Berg et al. (1996) mentioned that this algorithm may cause sudden imbalances in the numerical iteration procedure. This implies that in practice the difference between both sets of material parameters is limited, depending on the element size, the stress conditions and the total number of elements.

Van den Berg (1994) used the Tresca yield criterion to model the behaviour of clay and both Drucker-Prager and Mohr-Coulomb yield criteria with hardening-softening capability and a non-associated flow rule for modelling behaviour of sand. The standard cone was modelled with a completely smooth surface. As illustrated in Figure 1-6, cone penetration was modelled by moving the lower boundary upwards, while keeping the cone in its original place. There were no changing boundary conditions, or element distortions associated with the problem because of the approach taken.

Although chamber tests have been performed and reported in van den Berg (1994), no direct comparison of numerical results with measured values of cone penetration outputs was done. Instead, the focus of the testing was on the deformation field around the cone. However, the numerical approach of this work was notable for its time and the attention paid to modelling layered soil (both numerically and experimentally) is very important in the sense that even today very few works have been published in this regard.

The finite element approach used by Yu et al. (2000) focused on the penetration process at a particular instant in time and used the spatial variation of the stress state instead of time integration of finite element matrices to obtain the solution at a certain point in the domain (e.g.

point P in Figure 1-7). Thus, the state of stress at point P is obtained by an integration process considering all points below P until the initial stress state of undisturbed soil is reached. This process converges, as the finite-element grid is refined, in the same way that a time marching scheme converges as the time steps are made progressively smaller.

The dependency of the cone factor on soil stiffness, shaft roughness, in-situ state, and OCR were evaluated. The results were found to be similar to that of strain path method. The finite-element results on soil strain paths confirm the validity of the basic assumption in strain path method and that is, for undrained clay (i.e., incompressible materials), the coupling between soil deformation induced by steady cone penetration and soil strength or stiffness properties is very weak. It is therefore not surprising to note that the finite-element results (in particular, the dependence of cone factor on stiffness index G/S_u) are similar to those of the strain path method. Advantages of the finite element procedure over the strain path method for steady state analysis include:

- Equilibrium equations are fully accounted for in the finite-element method so that errors due to equilibrium imbalance can be minimised.
- Cone geometry can be properly modelled in the finite-element approach.
- Cone and shaft roughness can be accounted for through contact elements.
- The finite-element approach can be easily modified for application to frictional-dilatant soils.

1.4.4.3. Cavity Expansion Theory

Many simplified theoretical treatments have used spherical (and occasionally cylindrical) cavity expansion as analogues to the cone penetration test, essentially the same approach as used in conventional design of end bearing capacity of piles. The spherical cavity expansion analogy idealises the CPT as a cavity in a uniform medium under an isotropic stress state, with the internal pressure of the cavity initially equal to the in-situ mean effective stress p'_0. The cavity is expanded by monotonically increasing its radius until a limiting (constant) pressure is obtained, this being the pressure of interest. This idealisation greatly simplifies the analysis because the symmetry allows only radial displacements and in turn this permits a one-dimensional description of the problem.

The initial work by Bishop et al. (1945) and Hill (1950) addressed incompressible materials with associated flow rules, corresponding to the familiar and simple idealisation of the undrained behaviour of clay. Chadwick (1959) derived the pressure-expansion relation for a Mohr-Coulomb material with an associated flow rule. Vesic (1972) gave the general solution to the cavity expansion problem in an elastic-perfectly plastic material with a Mohr-Coulomb material with a non-associated flow rule. Vesic (1977) suggested that the bearing capacity of the soil around the tip of a pile can be estimated from the limit pressure required to expand a spherical cavity. The interesting further development of cavity expansion theory for non-associated flow has been considered by a number of workers including Carter et al. (1986) and Yu and Houlsby (1991). The central assumption of these studies has been that both the friction and dilation angles remain constant during shearing. Salgado (1993) and Salgado et al. (1997) advanced the work in a different direction by invoking a comprehensive database of well

documented calibration chamber tests into the analysis. Their work too used constant dilation and friction angles. Although constant dilation and friction angles led to analytical or semi-analytical solutions for cavity expansion, the idealisation has the fundamental deficiency that soil does not behave in such a manner – the nuances of soil behaviour being of first-order significance to realistic modelling of cavity expansion in soil.

Collins et al. (1992) provided the first realistic model for cavity expansion in soil using a state parameter based numerical analysis. Their results showed that the relation between normalised CPT tip resistance and ψ_0 was still affected by the stress level (as suggested by Sladen, 1989) and depended on material properties of the sand. Yu et al. (1996) used the same approach and combined it with cylindrical cavity expansion analysis of accompanying pressuremeter tests to interpret the state parameter as well as the friction angle from a combination of CPT tip resistance and pressuremeter limit pressures.

Shuttle and Jefferies (1998) used a general work hardening/softening critical state model (NorSand) to evaluate changes in CPT calibration in terms of material properties that can be measured in situ (including elasticity G) or determined in routine triaxial testing of reconstituted samples (including the critical state parameters M, Γ, λ). They showed that CPT behaviour in Hilton Mines sand, currently one of the most unusual of the published calibrations, could be predicted based on Ticino sand data by allowing for the changes in fundamental soil properties between Hilton Mines and Ticino.

The analogy of the cone penetration to expansion of a sphere in soil is based on the existence of a limit cavity expansion pressure; although it has long been recognised that there is an inherent mismatch between spherical cavity expansion analysis results and those of calibration chamber tests. The magnitude of the mismatch is enlarged with the application of realistic models that

capture the variable nature of strength and dilation angle. Their predecessors likely masked the mismatch by assuming constant friction and dilation angles. The difference between the spherical cavity analogy and the actual CPT geometry is usually accounted for by a *shape factor* (scaling the spherical results to the true in-situ resistance). Shuttle and Jefferies (1998) showed that there is a one to one correspondence between the normalised tip resistance obtained from spherical cavity expansion and that obtained in chamber testing on both Ticino and Hilton Mines sand. Cudmani and Osinov (2001) suggested a common shape factor for five different sands that was a function of the relative density corrected for stress level effects.

It is interesting that although particle breakage is known (e.g. De Beer, 1963; Yang et al., 2010) to occur at the high stresses usually induced by CPT in cohesionless soils, only a few of the preceding analyses explicitly model the effects of particle breakage on the limiting cavity pressure. Russell and Khalili (2002) considered this issue by incorporating one effect of particle breakage, a steepening of Critical State Locus with increasing mean stress, into a cavity expansion analysis using a critical state based model. The result was a reduction in the limiting cavity expansion pressure, inferring an increase in the shape factor required to match the chamber penetration resistance.

1.4.4.4.   Finite Element Method

CPT and pile driving analyses are interchangeably considered in reviewing the research done on finite element modelling of the deep penetration problem. The early finite element models (de Borst and Vermeer, 1982; and Griffiths, 1982) considered the problem in undrained clay using elasto-perfectly plastic models. The problem of deep penetration in sand was first dealt

with by Willson (1985) where sand was modelled as a Mohr-Coulomb material. The first large strain analysis of the penetration process was performed by Cividini and Gioda (1988).

Cividini and Gioda's work was also important in the sense that it was the first attempt to clarify the similarity of cavity expansion to penetration in soil through a finite element model. Another advantage of their work was that they pointed out the importance of a varying boundary condition at the tip of the cone and tried to address it by discretising the penetration process.

Advances were made in accounting for different aspects of the deep penetration problem focusing on undrained penetration in clay (Kiousis et al., 1988; Mabsout et al.,1995; Abu-Farsakh et al., 1998; Voyiadjisa and Kim, 2003; Lu et al., 2004; and Wei et al., 2005). More sophisticated models (e.g. modified Cam-Clay) were used and the interface friction between the cone (or concrete in case of piles) and the soil were accounted for.

The reason to use a 'good' constitutive model for modelling the cone penetration problem in sand is that, in general, part of the domain will be deforming at constant volume, other parts dilating, and other parts contractive; with the exact behaviour being a function of position relative to the cone tip. The works of Susila and Hryciw (2003), Sheng et al. (2004) and Huang et al. (2004) made significant advances in capturing the geometric aspects of the cone penetration problem in sand, but failed to satisfactorily capture the material behaviour.

Susila and Hryciw (2003) modelled the cone penetration in normally consolidated sand using an updated Lagrangian large strain formulation and auto-adaptive remeshing technique; this technique was utilised for handling the very large distortion of the mesh surrounding the cone tip. The Drucker-Prager soil model with a non-associated flow rule was used to simulate the soil behaviour. Their analysis showed that the distribution of sleeve resistance along the cone sleeve is not uniform. It is significantly lower close to the cone tip and becomes uniform higher up

along the sleeve. Cone tip resistance was plotted against friction angle and vertical effective stress and a chart was proposed to obtain the friction angle from cone resistance. It was also shown that finite element results are in good agreement with previously published cavity expansion solutions and average values from calibration chamber test data.

Sheng et al. (2004) modelled pile penetration in sand using a large strain finite element scheme. The pile was modelled with a conical tip instead of the flat end pile geometry. The pile had a tip angle of 60° which made it identical to CPT. A Modified Cam Clay soil model was used to simulate the behaviour of fine Silica sand and the pile was assumed to be rigid. Application of the Modified Cam Clay model to sands has serious limitations and does not capture their stress-dilatancy controlled behaviour.

The computed total and shaft resistances during pile installation were first compared with measured values from centrifuge tests, which indicated that the total resistance was well predicted by the finite element model, but the shaft resistance was not. The computed stress paths indicate that both the mean and deviator stresses first increase when the pile is above or at the level of the observation point in the soil, and then decrease once the pile has moved below the observation point.

They concluded that when the soil is represented by the modified Cam clay model, a thin soil layer of one pile radius immediately around the pile, extending from the ground surface to a distance of one pile radius above the pile tip, is under elasto-plastic expansion. Just outside this expansion (softening) zone, a compression zone of a U form was observed.

Huang et al. (2004) modelled the cone penetration test using a large strain (updated Lagrangian) finite element scheme. The penetrometer deformation was assumed to be negligible, so the cone was treated as a rigid body. Mohr-Coulomb soil model with a non-associated flow rule was used

to simulate the soil behaviour. The interface between the cone and the soil was modelled using a friction contact interface.

Parametric studies were performed to investigate the influence of the pressure level p_0, the shear modulus G, the soil internal friction angle ϕ, and the dilation angle. Effects of these parameters on the cone resistance and the plastic zone around the cone were studied in detail and the results were compared to those of cavity expansion and bearing capacity theories. Parametric studies showed that the cone resistance is influenced more by deformation parameters (such as shear modulus and dilation angle) than by shear strength parameters (such as the friction angle). This finding was in agreement with the general understanding of the cone penetration as a deformation controlled process.

Foster et al. (2005) performed a 3-D modelling of cone penetration into a cubic medium. The cone was modelled as an elastic shell while the soil was modelled using a model with 14 parameters. The model seems to take into account the critical state concept and assumes a constant elastic shear modulus. Another assumption of the model is that the plastic strain is proportional to the total strain. A master and slave surface concept was used with a frictional contact model to simulate the interface of cone and soil.

Data from Norfolk sandy loam and Decatur clay loam were used to verify the performance of the model. Results of simulation were compared to experimental data for a limited number of tests plotted as cone factor versus displacement up to about 200 *mm* of penetration.

Foster et al. (2005) used a realistic soil model for modelling behaviour of both sand and clay, but the approach of their work being mostly towards computational aspects of the problem and not the geotechnical aspects, makes it difficult to be used by the geotechnical community. Moreover, like many other works, it was not well verified with experimental data.

39

1.4.4.5. Other Methods

In addition to the methods previously discussed, there have been a few efforts to use other numerical techniques such as discrete element (Cundall and Strack, 1979) and finite difference methods to model the cone penetration problem.

Huang and Ma (1994) were the first to apply discrete elements method to the cone penetration problem. Tannant and Wang (2002) used the method to model penetration of a wedge into oil sands. Iqbal (2004) used a 2-D discrete element method code to model CPT in a coarse grained soil with rigid single sized particles. He reports acceptable agreement between the results of the method and experimental and other numerical methods.

The discrete element method, being a relatively new method in geomechanics, has not been verified against experimental data as widely as other numerical methods have. Computational effort required for the method is higher than that of continuum methods and this has restricted the application of the model to problems with a limited number of particles or problems dealing with coarse granular materials. All the works mentioned were done using 2-D codes; in other words they are all solving the problem of penetration of a wedge into a stock of cylinders. The method can be very helpful in understanding the penetration mechanism (especially with the more recent availability of 3-D codes) and issues such as fabric effect and changes of fabric during penetration about which other methods such as finite element method have failed to yield useful results.

Ahmadi et al. (2005) used a commercial finite difference package (FLAC) to model the cone penetration test in sands. They used the Mohr-Coulomb elasto-plastic model with stress-dependent elastic moduli and friction and dilation angles to account for the high stresses

developed around the cone. The standard cone was modelled and it was assumed to be infinitely rigid. Large strain effects were accounted for by updating the mesh after each step. In order to tackle the changing boundary conditions created by penetration along the axis of symmetry, the analysis was carried out for an axisymmetric body with a pre-existing small hole along its axis of symmetry.

The penetration was modelled using prescribed displacements. The main criterion considered in estimating the prescribed displacements was producing a deformation pattern in the analysis that was consistent with a penetrating cone and similar to that of the experiments. Generalising such a deformation field to all sands may cause major errors. As discussed in reviewing the steady state methods, different deformation fields will be generated in different cohesionless soils with different densities. This is the main reason methods such as the strain path method are not applicable to cohesionless soils.

An important aspect of their work was that the results of the analysis were compared with experimental data obtained in chamber tests; previously published data on Ticino sand were used for this purpose. The ratio between the vertical and horizontal prescribed displacements at the cone boundary that yielded the best match between the analysis and the experimental data was determined by performing a parametric study; a ratio of 0.85 yielded the best fit. This adjustment makes the comparison to the experimental data a means of calibration, rather than verification.

Ahmadi and Robertson (2005) extended the analysis to layered soils including two layers of different sands or sand and clay and thin layers of sand embedded in soft clay. They discussed the effects of thin layers on cone resistance and proposed a correction factor.

The application of the finite difference method to the Cone Penetration Test used by Ahmadi and coworkers is essentially identical to finite element method used by others. Hence their work can be viewed along with the finite element analyses performed by others.

1.4.5. Particle Breakage

The significance of particle breakage on the behaviour of granular materials has been recognised since the earliest days of soil mechanics (Bridgman, 1918). He looked at the problem from the point of view of geology and the existence of cavities in rocks at depth. De Beer (1963) looked at the scaling effect in using cone penetration data to design of pile foundations and studied the compression during cone penetration into a dense sand reaching pressures of up to 35 *MPa*. He suggested that the amount of breakage was affected by the characteristics of the material and was greatly intensified by introduction of large shear strains.

Construction of large earth dams brought the shearing behaviour of granular materials at high stresses to the spotlight again in the 60s and 70s; interest was directed to the changes in strength, compressibility and permeability under high pressures.

Bishop (1966) looked at the behaviour of a number of sands under a range of stresses of up to 10 *MPa* and concluded that the particle breakage is to a large extent caused by shearing rather than consolidation. He also suggested that during shearing the gradation shifts towards a well graded soil such as that observed in natural glacial tills and by doing so the soil can sustain a higher level of stress by increasing the number of inter-particle contacts carrying the stresses.

Lee and Farhoomand (1967) investigated the effect of high stress levels on compressibility and particle breakage of a number of soils ranging from gravels to fine sands. They showed that

breakage starts from the finer part of the gradation curve. Uniform and angular soils demonstrate more breakage than well graded and round grained soils. They pointed out that particle breakage induces additional compressibility and showed that higher deviator stresses result in more breakage.

Vesic and Clough (1968) looked at the behaviour of sands under a wide range of pressures and identified three ranges: very low pressures where dilatancy controls the behaviour and the breakage is negligible, higher pressures where breakage becomes more pronounced and suppresses dilatancy effects, and very high pressures where all effects of initial density vanish and sand behaves like a linear elastic material.

Billam (1971) related the particle breakage to the tensile strength of particles. He also suggested that particle breakage increases the axial strain to failure by "reducing the rate at which the material can accept additional stress".

Different variants of the gradation curve have been used to quantify particle breakage. Miura and O-Hara (1979) suggested the increase in the surface area of the soil sample as a measure for the amount of particle breakage. They also suggested that the amount of particle breakage is a function of the plastic work done and proposed a relation between this plastic work and increase in the surface area.

The idea of a breakage potential function and a total breakage function was introduced by Hardin (1985) based on the area between the gradation curves before and after breakage and investigated the effects of different factors such as initial particle distribution, particle shape, the amount of shearing and the stress path, initial void ratio, particle hardness and the presence of water. He concluded that the amount of breakage is increased by an increase in shear stress, initial density and particle angularity.

The effect of high pressures on the critical state of cohesionless soils has become of interest with the emergence of the constitutive models that are based on critical state soil mechanics. According to critical state theory, once a volume of soil reaches the critical state, it is expected to continue to shear at constant stress and constant volume. A two or three part linear CSL in $e - \log p'$ space has been generally accepted (Been et al., 1991; Konrad, 1998; Russell and Khalili, 2004) for the full range of mean effective stress.

That the changing gradation caused by the breakage imposes a downward shift on the CSL was first suggested by Daouadji et al. (2001). Muir Wood (2007) developed this idea, suggesting that during shearing at higher stresses the CSL moves down towards a final location associated with a fractal gradation (McDowell et al., 1996). A third dimension was proposed to the $e - \log p'$ space called the "grading state index"; a parameter between 0 and 1 which identifies soil's state on a scale between uniform and fractal gradations. Muir Wood and Maeda (2008) showed, using a discrete element analysis, that the effect of particle breakage on the CSL location in $e - \log p'$ space is essentially a parallel downward shift as a function of the grading state index.

A question pertinent to proper modelling of the particle breakage phenomenon is the existence of a final stable gradation. It is always possible to imagine a gradation where all voids are filled with progressively smaller and smaller particles (Fuller and Thompson, 1907) as emphasised by the works of McDowell and co-workers. Such a "fractal" gradation would be linear on a log-log plot of particle size and proportion finer than that size. Been et al. (1991), Konrad (1998), and Russell and Khalili (2004) by adopting the three part CSL framework implicitly assumed that a continual constant volume state will be achieved once the tests approach the second part of the CSL. The data presented by Russell and Khalili (2004) suggest that for higher stress levels (above 1 *MPa*) the loose tests do not reach a constant volume and continue to contract. Lade and

Yamamuro (1996) made the same observation on tests presented in Yamamuro and Lade (1996) and concluded that the critical state conditions can only be achieved at low pressures (the first part of CSL) or at extremely high pressures where particle breakage has ceased (the third part of CSL).

An experimental study on a granitic soil by Lee and Coop (1995) suggested that the amount of particle breakage at the critical state is path independent and solely a function of the value of p' on the CSL. In order to investigate whether the critical state can be achieved at higher stress levels, Luzzani and Coop (2002) used ring shear tests to take samples of a carbonate sand to more than 700% shear strain. They concluded that "the volumetric compression appeared to be directly related to the particle breakage, and the rate of increase of both reduced with increasing shear strain apparently tending towards constant values. It appears therefore that a constant volume will only be reached when the breakage ceases, but this will only be at strains about an order of magnitude greater than those achieved in our [their] work".

In a later attempt, Coop et al. (2004) used ring shear tests to take samples of a carbonate sand to up to 100,000% shear strain. They concluded that particle breakage continues to very large strains beyond those reached in triaxial tests, but a constant gradation is reached at very large strains. This constant gradation is dependent not only on the stress level but also on the uniformity and particle size of the original gradation.

There have been a number of attempts at modelling the consequences of particle breakage in the past ten years (e.g. Daouadji et al., 2001; Indraratna and Salim, 2002; Russell and Khalili, 2002; Einav, 2007; and Muir Wood, 2007). Russell and Khalili (2002) incorporated the effect of particle breakage into a bounding surface plasticity model, by assuming a steepening of the CSL with increasing mean stress. The more plausible idea of a shifting CSL with the change in

material during breakage (Daouadji et al., 2001; and Muir Wood, 2007) has yet to be validated against experimental data.

1.5. Overview of the Proposed Research

Looking at the body of the work reported to date on interpretation of the in-situ density of cohesionless soils through CPT reveals that significant progress has been made in realistic modelling of the cone penetration process, and in performing calibration chamber tests. However, none of the works to date offer a reliable framework for interpreting in-situ density of the soil. The numerical models have usually failed to adequately capture the material behaviour. In addition, not enough attention has been paid to clear and independent determination of material parameters. Finally, systematic verification and validation of the analyses is rather scarce in the literature.

Calibration chamber tests provide correlations between soil properties and CPT data but they are prohibitively expensive, limiting them to a small number of very large projects. The issue of different fabric and age between reconstituted chamber samples and in-situ conditions and variability of in-situ soils further limits the application of calibration chamber testing for engineering projects.

In this research, an analytical framework feasible for most engineering programs is laid out for analysing the Cone Penetration Test in cohesionless soils. The framework has three important aspects: Independent calculation of soil parameters, realistic constitutive modeling of soil behaviour, and comprehensive verification and validation of the results.

A central feature of the framework is the application of a critical state constitutive model that adequately captures the behaviour of cohesionless materials over a range of material properties and states. Another important aspect of the analysis is independent and thorough calibration of the constitutive model to material behaviour using element tests. The influence of number and quality of the element tests on estimated material properties is investigated.

Spherical cavity expansion analysis is chosen for modelling the cone penetration problem. This method has the advantage of being numerically stable and fast and is thus suitable for modelling a large number of tests. A unique shape function is identified for converting the spherical cavity expansion results to CPT tip resistance.

Special attention has been directed towards verification of the analytical method against experimental data. A comprehensive database of calibration chamber tests from the literature is processed and used to verify the framework. The method is also validated against in-situ measurements of soil density by comparison to other testing methods (the Self-Bored Pressuremeter testing in this case) as well as direct measurements through ground freezing techniques. The confidence and accuracy in the interpretation results and ways of improving them are discussed.

An important phenomenon pertinent to the cone penetration in cohesionless materials is particle breakage. However, it has been generally overlooked in the analyses of the CPT. One of the reasons has been a lack of understanding of the basics of the phenomenon. An extensive laboratory testing program is performed and the results are used to support a hypothesis for treating particle breakage within the critical state soil mechanics. The work provides a foundation for implementing the particle breakage in the analysis of the Cone Penetration Test.

The content is organised in the following order:

1. ***<u>Chapter one (Introduction and Background)</u>*** The problem of CPT interpretation in cohesionless soils is explained, different aspects of the problem and different solutions available in the literature are reviewed. A gap is identified in linking the experimental and analytical solutions, as well as theoretical understanding of the particle breakage phenomenon, which is pertinent to CPT interpretation. The need for a comprehensive theoretical framework verified against different experimental data is justified. The scope and structure of the dissertation is presented.

2. ***<u>Chapter two (Determination of the Critical State Friction Angle from Triaxial Tests)</u>*** The critical state friction angle is one of the parameters affecting the material behaviour and one of the most important ones influencing CPT resistance. Different methods of estimating this parameter from triaxial compression tests are compared and discussed.

3. ***<u>Chapter three (Confidence and Accuracy in Determination of Critical State Friction Angle)</u>*** A statistical investigation is performed to identify the effect of the number and quality of triaxial compression tests used to calculate critical state friction angle on the accuracy of the estimated parameter. Recommendations are made on the number and distribution of the tests necessary to achieve different levels of accuracy.

4. ***<u>Chapter four (Interpretation of Sand State from CPT Tip Resistance)</u>*** There is an inherent mismatch between measured CPT tip resistance and the limit cavity pressure obtained from

analysis. Calibration chamber data are presented for nine soils, comprising a range of soil types and material properties, for which triaxial testing is also available. Cavity expansion analysis is performed and a unique and unbiased relation between limit cavity expansion pressure and calibration chamber normalised tip resistance is identified, defined as the shape function. This approach recovered values of soil state ψ, with a precision close to that of the published calibration chamber data.

5. ***Chapter five (Evaluation of Soil State from SBP and CPT: A Case History)*** Validation of the interpretation framework requires knowledge of the ground truth. Comparing the data obtained from different in-situ testing methods performed in close proximity is one common way of assessing the reliability of either method. The chapter compares interpretations of the in-situ state parameter obtained from CPT and SBP testing performed off-shore in a uniform hydraulic fill. Extensive calibration chamber tests and high quality triaxial compression tests are available to calibrate the constitutive model. The SBP and CPT tests are independently analysed, considering the effects of fabric. The predictions of in-situ state for the fill from the CPT are close to those derived from the SBP. Although not proof of accuracy (validation) of either test, since ground truth is not known, the results lend support to the adequacy of the interpretation methodology used for both. Further improvements are discussed.

6. ***Chapter six (Interpretation of the In-situ Density from Seismic CPT in Fraser River Sand)*** The ideal validation for an interpretation framework would come from a comparison of the predicted state parameter with direct measurements of the in-situ state parameter. Such

direct measurements are usually obtained from void ratio measurements on undisturbed samples. This chapter describes an application of the CPT interpretation framework presented in Chapter 4 to obtain the state parameter from CPT tip resistances in the CANLEX (CANadian Liquefaction EXperiment) dataset. The CANLEX database provides a rare combination of reliable in-situ measurements and laboratory element testing on undisturbed and reconstituted samples, allowing for direct evaluation of the capability of the method in obtaining ground truth (validation). The effects of differing gradations and soil fabrics have been captured and reflected in the resultant state parameter interpretation. Accuracy is evaluated by comparison to in-situ density measurements and comparison to other published interpretation methods.

7. ***Chapter seven (Particle Breakage and the Critical State of Sand)*** Particle breakage has important implications for soil behaviour during shearing. In particular the change in a soil's gradation during particle breakage changes its critical state, which is a fundamental input to the majority of advanced constitutive models. It is a phenomenon pertinent to the analysis of CPT due to the high stresses that develop at the cone tip during cone penetration, and can directly affect the interpretation process. This chapter provides a hypothesis on the particle breakage process at the particle level and expands its implications for the critical state of sands at higher stress levels. Experimental data are presented and the hypothesis is used to explain the observed behaviour. The data support the proposition that breakage shifts the CSL down in the void ratio-mean effective stress space without changing its slope. It is suggested that the void ratio shift in the CSL is equal to the reduction in void ratio due to breakage. It is also proposed that significant particle breakage in a particulate material does

50

not occur unless two conditions are satisfied: Capability of the materials for contraction merely by sliding and rolling of the particles is exhausted; and, a stress level threshold is surpassed. Finally it is speculated that particle breakage does not directly affect the evolution of soil state towards the critical state and is merely a factor working alongside dilatancy imposing additional compressibility on the soil.

8. ***Chapter eight (Summary and Conclusion)*** A summary of key findings and conclusions is presented along with the limitations of the methods and results. Potential future studies to further advance the knowledge in this field are also identified.

9. ***Appendix A*** The testing procedures and equipment are explained in detail and the laboratory data obtained as part of this research are presented.

10. ***Appendix B*** A bibliography of the manuscripts included in this thesis is presented.

This document has been prepared in accordance with UBC's formatting principles for manuscript-based theses. A manuscript-based thesis is constructed around one or more related manuscripts. As a result, some information such as background information, numerical procedures and the constitutive model, and material descriptions is repeated in various chapters. The introduction provides background and context to the manuscripts. In this thesis, chapters two to seven are the individual manuscripts; it is a UBC requirement that at least one of them is appropriate for publication as a journal paper. The writer of the thesis can be either the sole author or a senior co-author of the manuscripts. The place of publication for the manuscripts is

provided as a footnote at the start of each chapter and a list of all the publications is provided in

Appendix B. The concluding chapter summarises the main findings from the individual chapters

in the context of interpretation of the in-situ state parameter in cohesionless soil using the CPT.

Table 1- 1 Summary of NorSand (Jefferies and Shuttle, 2005)

Internal Model Parameters	$\psi_i = \psi - \lambda \ln(p_i'/p')$ where $\psi = e - e_c$ $M_i = M\left(1 - N^* \chi_{tc} |\psi_i|/M_{tc}\right)$
Critical State	$e_c = \Gamma - \lambda \ln(p')$ AND $\eta_c = M = \frac{1}{2}(M_{MC} + M_{MN})$ where $M_{MC} = \left(3\sqrt{3}\right)/\left(\cos\theta(1 + 6/M_{tc}) - \sqrt{3}\sin\theta\right)$ and $\dfrac{27 - 3M_{MN}^2}{3 - M_{MN}^2 + \frac{8}{9}M_{MN}^3 \sin(\theta)\left(\frac{3}{4} - \sin^2(\theta)\right)} = \dfrac{27 - 3M_{tc}^2}{3 - M_{tc}^2 + \frac{2}{9}M_{tc}^3}$
Yield Surface and Internal Cap	$\dfrac{\eta}{M_i} = 1 - \ln\dfrac{p'}{p_i'}$ with $\left(\dfrac{p_i'}{p'}\right)_{max} = \exp\left(-\chi_{tc}\psi_i/M_{tc}\right)$
Hardening Rule	On yield surface: $\dfrac{\dot{p}_i'}{p_i'} = H\,\dfrac{M_i}{M_{tc}}\left(\dfrac{p'}{p_i'}\right)^2\left[\exp\left(\dfrac{-\chi_{tc}\psi_i}{M_{tc}}\right) - \dfrac{p_i'}{p'}\right]\dot{\varepsilon}_q^p$ On internal cap: $\dfrac{\dot{p}_i'}{p_i'} = -\dfrac{H}{2.7}\dfrac{M_i}{M_{i,tc}}\left|\dot{\varepsilon}_q^p\right|$
Stress Dilatancy and Plastic Strain Rate Ratios	$D^p = M_i - \eta \Rightarrow D_{tc}^p = D^p M_{i,tc}/M_i$ and $D_{te}^p = D^p M_{i,te}/M_i$ define $z_{3,tc} = \dfrac{2D_{tc}^p - 3}{6 + 2D_{tc}^p}$ and $z_{3,te} = \dfrac{2D_{te}^p - 6}{3 + 2D_{te}^p}$ $\Rightarrow \dfrac{\dot{\varepsilon}_3}{\dot{\varepsilon}_1} = z_{3,tc} - (z_{3,tc} - z_{3,te})\cos(\dfrac{3\theta + 90}{2})$ define $a = (\sin\theta + \sqrt{3}\cos\theta)/3$, $b = -2\sin\theta/3$, $c = (\sin\theta - \sqrt{3}\cos\theta)/3$ $\Rightarrow \dfrac{\dot{\varepsilon}_2}{\dot{\varepsilon}_1} = (aD^p - 1 + \dfrac{\dot{\varepsilon}_3}{\dot{\varepsilon}_1}(cD^p - 1))/(1 - bD^p)$
Elasticity	$I_r = \dfrac{G}{p'}$ with $K = G\dfrac{2(1+\nu)}{3(1-2\nu)}$

Table 1- 2 NorSand soil parameters and values for sands (Jefferies and Shuttle, 2005)

Parameter	Typical Range	Remark
CSL		
Γ	0.9 –1.4	Intercept of CSL, defined at 1 kPa
λ	0.01 – 0.07	Slope of CSL, defined on base e
Plasticity		
M_{tc}	1.2 – 1.5	Value of ratio q/p' at the critical state. Triaxial compression used as reference condition
N^*	0 – 0.5	Volumetric coupling parameter
H	50 – 500	Plastic hardening modulus for loading, often $f(\psi)$
χ_{tc}	2.5 – 4.5	Relates minimum dilatancy to ψ_i .
Elasticity		
I_r	100-800	Dimensionless shear rigidity
ν	0.1 – 0.3	Poisson's ratio, 0.2 commonly adopted

Table 1- 3 Current calibration chambers in the world, expanded after Ghionna and Jamiolkowski (1991)

Calibration chamber	sample diameter (m)	sample height (m)	Boundary Conditions			Reference	Soil Type
			Radial	Bottom	Top		
Cornell University, U.S.A.	2.10	2.90	Flexible	Rigid	Rigid	Ghionna & Jamiolkowski, 1991	
Country Roads Bureau, Australia	0.76	0.91	Flexible	Flexible	Rigid	Ghionna & Jamiolkowski, 1991	
ENEL-CRIS, Milan, Italy	1.20	1.50	Flexible	Flexible	Rigid	Ghionna & Jamiolkowski, 1991	Ticino sand
Golder Associates, Calgary	1.40	1.00	Flexible	Rigid	Flexible	Ghionna & Jamiolkowski, 1991	Erksak sand, Syncrude Tailings
ISMES, Bergamo, Italy	1.20	1.50	Flexible	Flexible	Rigid	Ghionna & Jamiolkowski, 1991	Ticino sand
Louisiana State University	0.55	0.82	Flexible	Rigid	Rigid	Kim, 1999	67% fine sand and 33% Kaolin
Monash University, Australia	1.20	1.80	Flexible	Flexible	Rigid	Ghionna & Jamiolkowski, 1991	
NCTU, Taiwan	0.79	1.60	Flexible[*]	Rigid	Flexible	Hsu & Huang, 1998	Da Nang sand
NCTU, Taiwan	0.51	0.76	Flexible	Rigid	Rigid	Hsu & Huang, 1999	Mai-Liao sand
North Carolina State University	0.94	1.00	Flexible	Rigid	Rigid	Ghionna & Jamiolkowski, 1991	
Norwegian Geotechnical Institute	1.20	1.50	Flexible	Flexible	Rigid	Ghionna & Jamiolkowski, 1991	
Oxford University, England	0.90	1.10	Flexible	Flexible	Rigid	Ghionna & Jamiolkowski, 1991	
Tokyo University, Japan	0.90	1.10	Flexible	Rigid	Rigid	Ghionna & Jamiolkowski, 1991	
UFRJ-COPPE,Rio	1.20	1.50	Flexible	Flexible	Rigid	Ghionna & Jamiolkowski, 1991	
University of California, Berkeley	0.76	0.80	Flexible	Rigid	Rigid	Ghionna & Jamiolkowski, 1991	Monterey sand
Clarkson University,USA	0.51	0.76	Flexible	Rigid	Rigid	Ghionna & Jamiolkowski, 1991	
University of Florida, Gainesville	1.20	1.20	Flexible	Flexible	Rigid	Ghionna & Jamiolkowski, 1991	Reid Bedford, Ottawa and Hilton Mines tailings
University of Grenoble, France	1.20	1.50	Flexible	Flexible	Flexible	Ghionna & Jamiolkowski, 1991	
University of Houston	0.76	2.54	Flexible	Flexible	Flexible	Ghionna & Jamiolkowski, 1991	
University of Newcastle, Australia	1.00	1.00	Flexible	Flexible	Rigid	Ajalloeian & Yu, 1998	
University of Oklahoma	0.61	0.45-1.42	Flexible	Flexible	Rigid	Tan et el., 2003	Minco silt
University of Sheffield, U.K.	0.79	1.00	Flexible	Rigid	Flexible	Ghionna & Jamiolkowski, 1991	
University of Texas at Austin	0.88	0.85	Flexible	Rigid	Flexible	Ghionna & Jamiolkowski, 1991	
Virginia Tech, Blacksburg	1.50	1.50	Flexible	Rigid	Rigid	Ghionna & Jamiolkowski, 1991	Yatesville silty sand
Waterways Experiment Station	0.80-3.00	variable	Flexible	Rigid	Rigid	Peterson & Arulmoli, 1991	

[*] Can be controlled by a computer to simulate field conditions.

Table 1- 4 Boundary conditions in conventional calibration chamber and simulator tests (Huang and Hsu, 2005)

Boundary Conditions	Top and bottom boundary		Lateral boundary	
	Stress	Strain	Stress	Strain
BC1	Constant	-	Constant	-
BC2	-	0	-	0
BC3	Constant	-	-	0
BC4	-	0	Constant	-
BC5	Constant	-	Servo-controlled	

Table 1- 5 Summary of B values (Equation 1-13) proposed for different sands by Cudmani and Osinov (2001)

SAND	Ticino	Monterey	L. Buzzard	Hokksund	Toyoura
B	1.3	2.3	3.5	4.0	4.0

Figure 1-1 Definition of state parameter ψ and overconsolidation ratio R (after Jefferies and Shuttle, 2005)
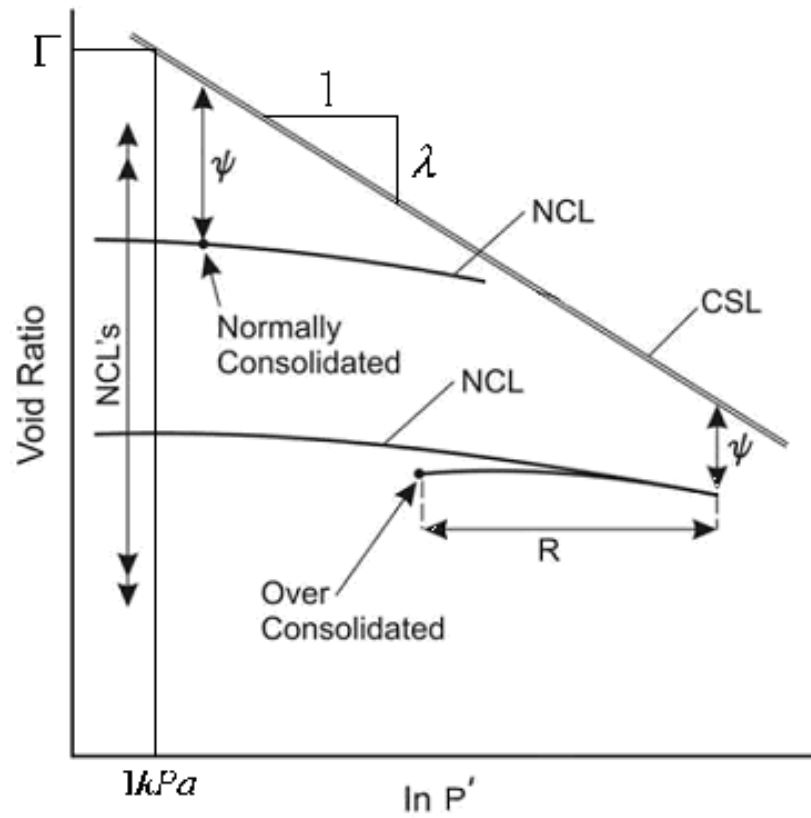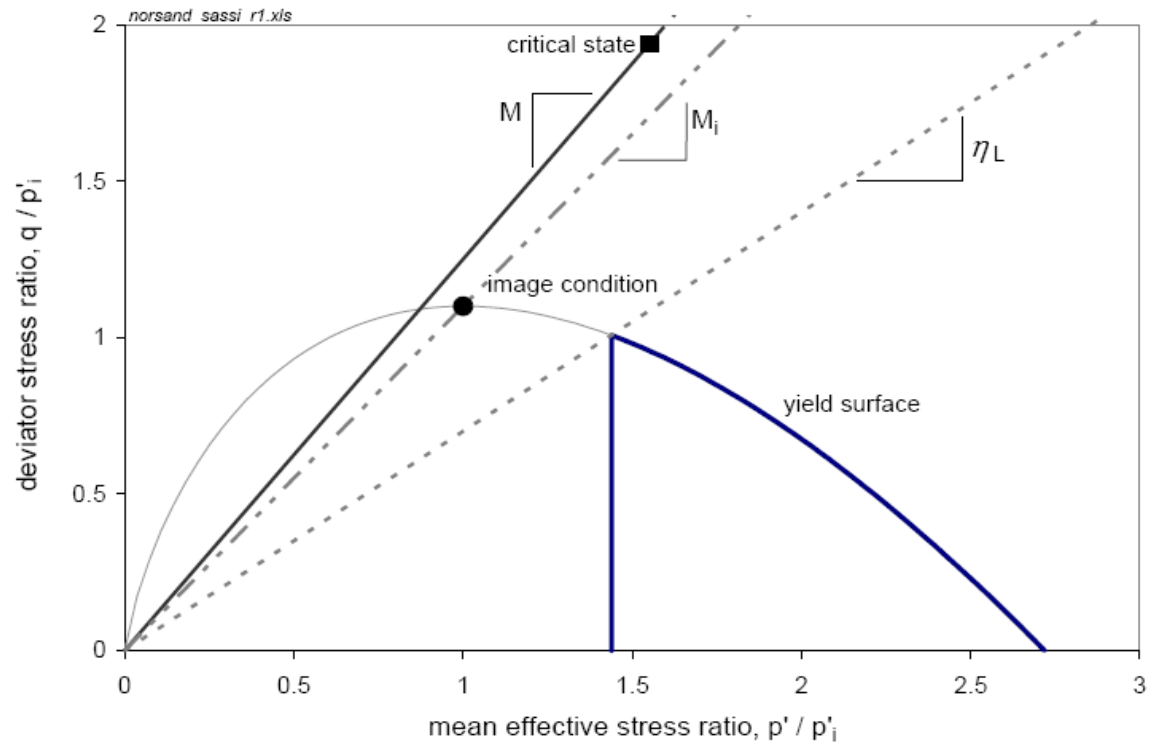
a) Very loose sand
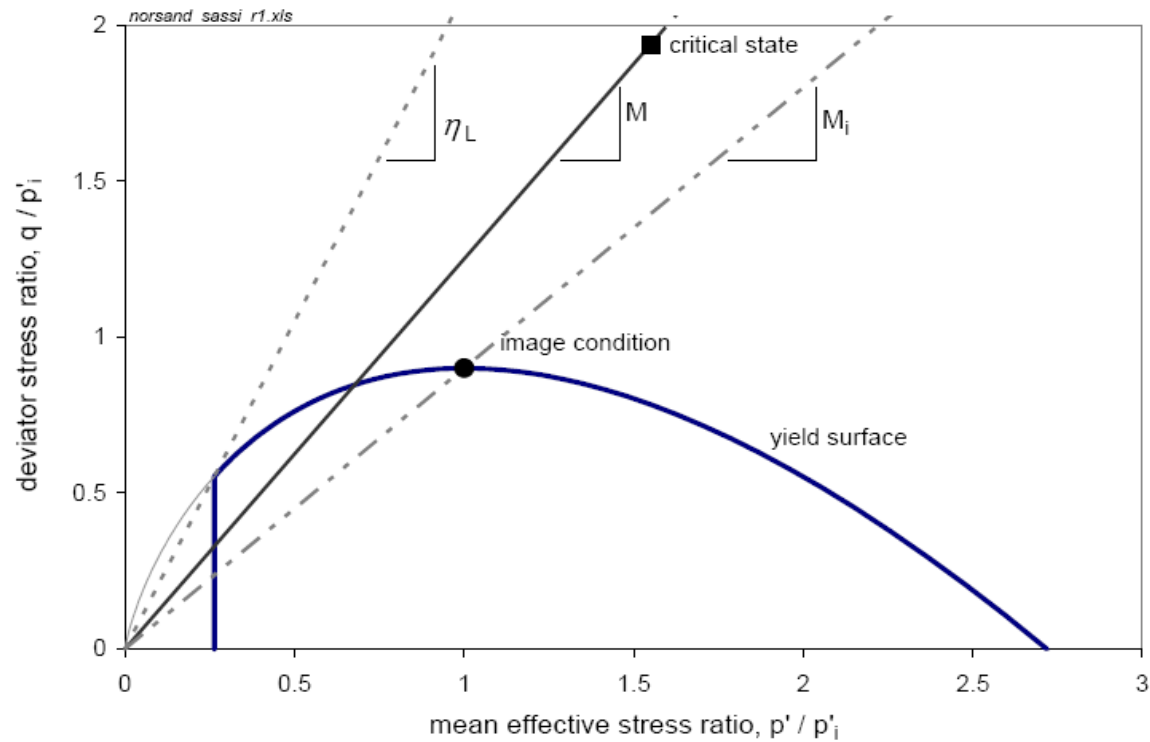
b) Very dense sand
Figure 1-2 Illustration of NorSand yield surfaces and limiting stress ratios (Jefferies and Shuttle, 2005)
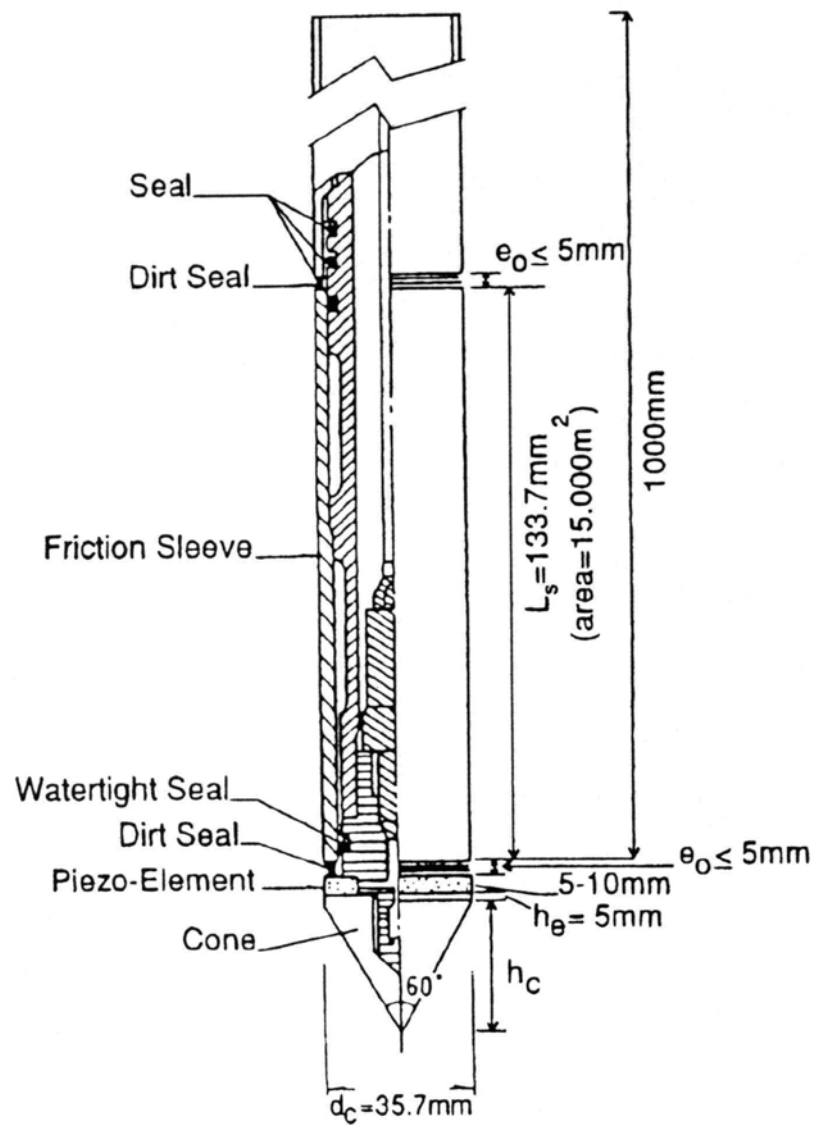
Figure 1-3 The standard electrical cone penetrometer (ASTM D5778)
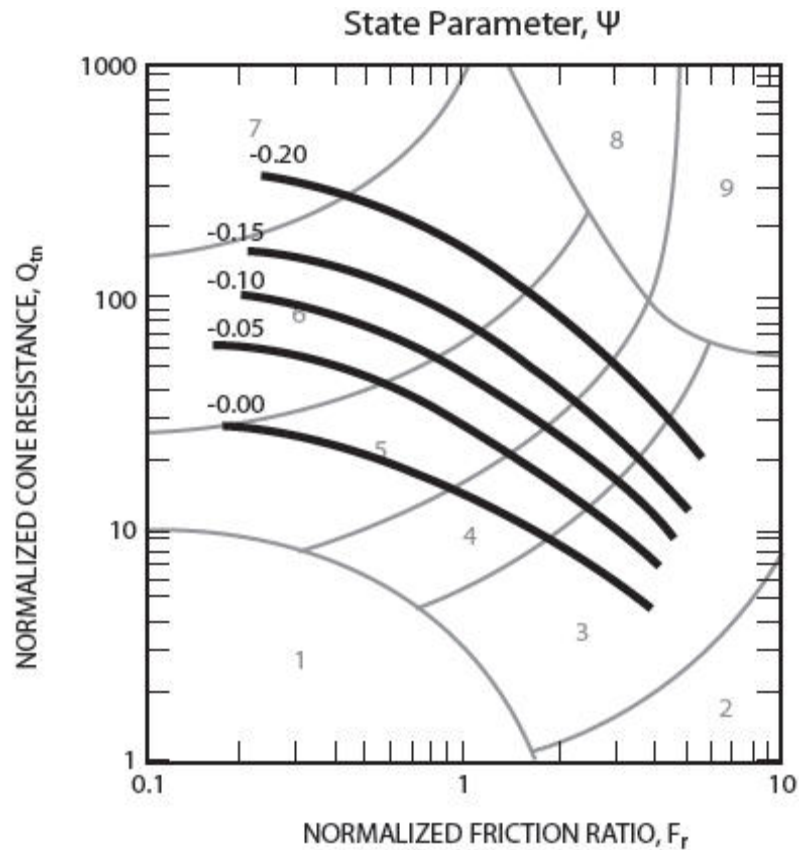
Figure 1-4 Contours of state parameter (Robertson, 2009)
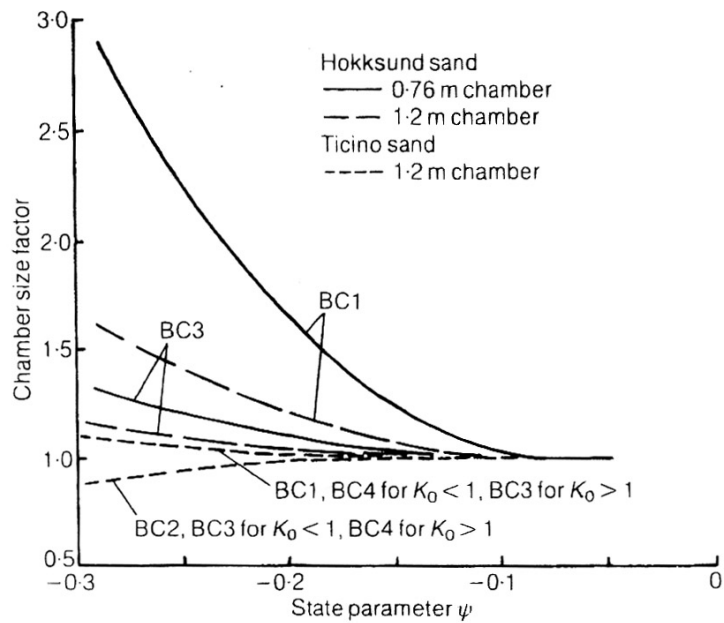
Figure 1-5 Normalisation factors for calibration chamber size and boundary conditions (Been et al., 1987)
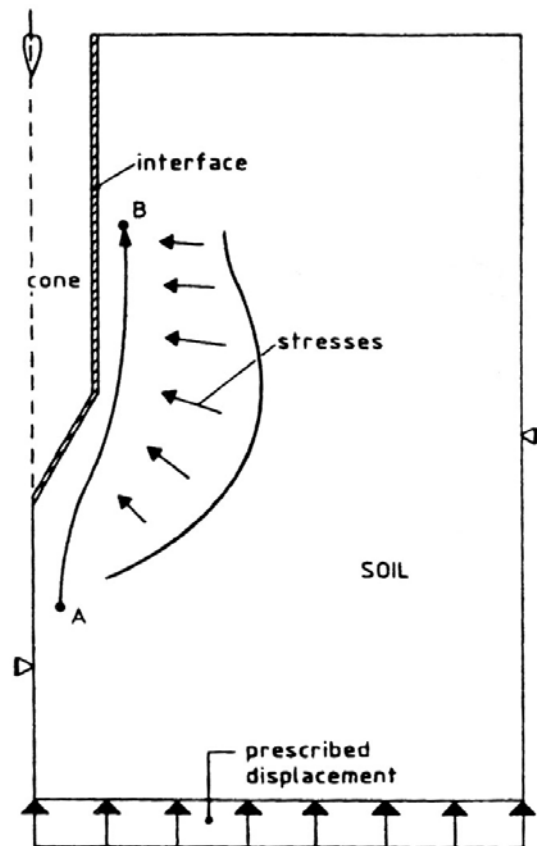
Figure 1-6 Schematic view of the Eulerean approach to the cone penetration problem (van den Berg et al., 1996)

Cone penetrometer

v_0 E

D

Soil Mass

Position of cone tip at a past time T–dt

r

Position of cone tip at current time T

undeformed location

$P(r,z)$ $P'(r',z')$

deformed location at time T

$Q(r, z + v_0 dt)$

z

$R(r, z + 2v_0 dt)$

A

$S(r, z + 3v_0 dt)$

C

B
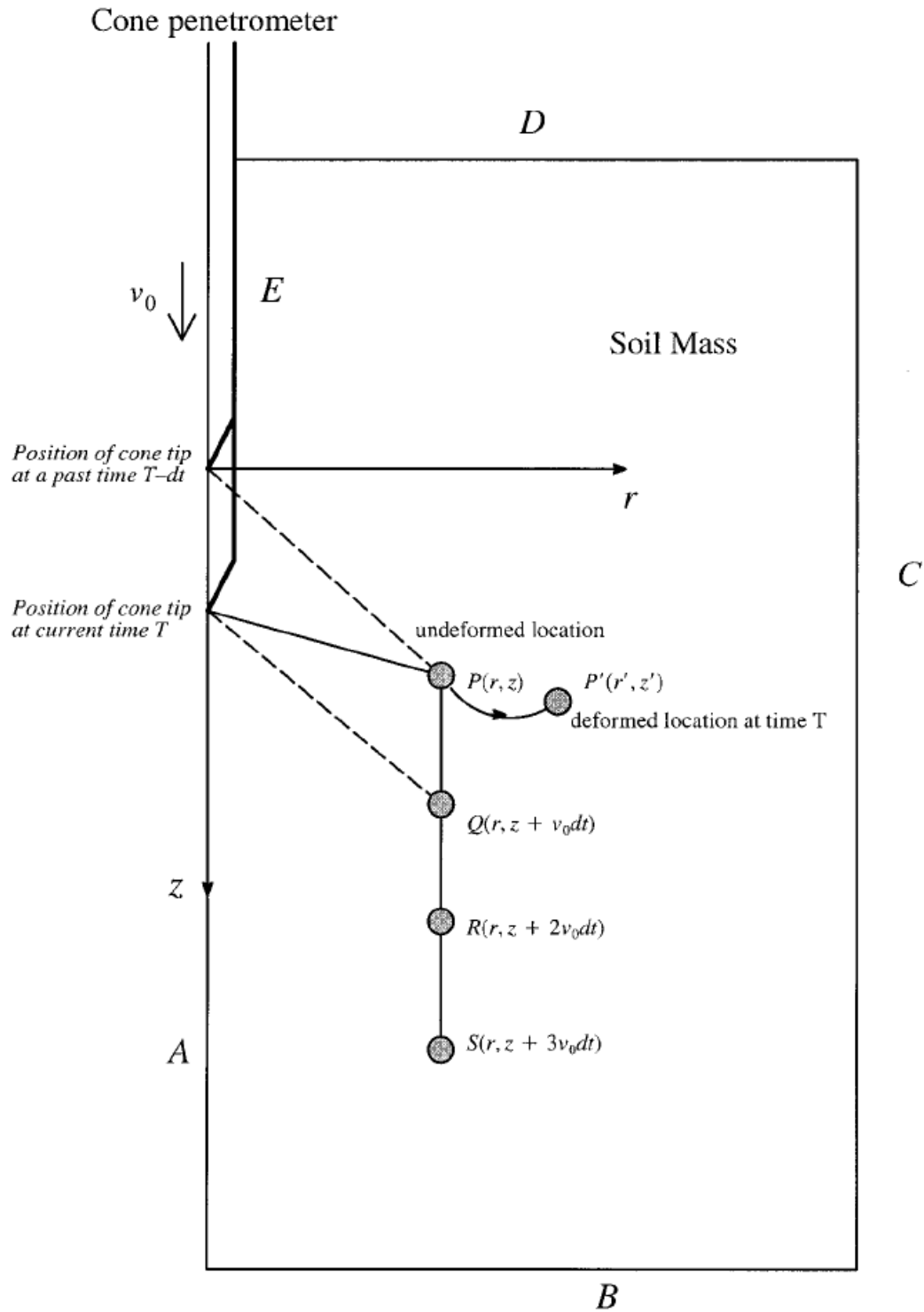
Figure 1-7 Steady-State behaviour and boundary conditions (Yu et al., 2000)

62

1.6. References

Abu-Farsakh M.Y., Voyiadjis G.Z., and Tumay M.T. 1998. Numerical Analysis of the Miniature Piezocone Penetration Tests (PCPT) in Cohesive Soils. International Journal for Numerical and Analytical Methods in Geomechanics, 22: 791-818.

Acar Y.B., and Tumay M.T. 1986. Strain Field around Cones in Steady Penetration. Journal of Geotechnical Engineering, 112(2): 207-213.

Ahmadi M.M, and Robertson P.K. 2005. Thin-Layer Effects on the CPT q_c Measurement. Canadian Geotechnical Journal, 42: 1302–1317.

Ahmadi M.M. 2000. Analysis of Cone Tip Resistance in Sand. PhD thesis, University of British Columbia, Vancouver, Canada.

Ahmadi M.M., Byrne P.M., and Campanella R.G. 2005. Cone Tip Resistance in Sand: Modeling, Verification, and Applications. Canadian Geotechnical Journal, 42: 977–993.

Ajalloeian R., and Yu H.S. 1998. Chamber Studies of the Effects of Pressuremeter Geometry on Test Results in Sand. Géotechnique, 48(5): 621-636.

ASTM D5778 - 07 . Standard Test Method for Electronic Friction Cone and Piezocone Penetration Testing of Soils. Published : November 2007.

Baldi G., Bellotti R., Ghionna V., Jamiolkowski M., and Pasqualini E. 1982. Design Parameters for Sands from CPT. Proceedings of the 2nd European Symposium on Penetration Testing, Amsterdam, 2: 425-432.

Baldi G., Bellotti R., Ghionna V., Jamiolkowski M., and Pasqualini E. 1986. Interpolation of CPTs and CPTUs part 2, Drained-Penetration of Sands. Proceedings of the 4th

International Geotechnical Seminar. Field instrumentations and in situ measurements, Singapore, 143-156.

Baligh M.M., 1985. Strain Path Method. Journal of Geotechnical Engineering, ASCE, 111: 1108–1136.

Been K., and Jefferies M.G. 1985. A State Parameter for Sands. Géotechnique, 35(2): 99-112.

Been K., and Jefferies M.G. 1992. Towards Systematic CPT Interpretation. Proceedings of Wroth Memorial Symposium, Thomas Telford, London, 121-134.

Been K., Crooks J.H.A., and Rothenburg L. 1988. A Critical Appraisal of CPT Calibration Chamber Tests. Proceedings of the 1st International Symposium on Penetration Testing (ISOPT), 2: 651-660.

Been K., Crooks J.H.A., Becker, D.E., and Jefferies M.G. 1986. The Cone Penetration Test in Sands. Part I: State Parameter Interpretation. Géotechnique, 36(2): 239-249.

Been K., Jefferies M.G., Crooks J.H.A., and Rothenburg L. 1987. The Cone Penetration Test in Sands. Part II: General Inference of State. Géotechnique, 37(3): 285-299.

Been K., Jefferies M.G., and Hachey J.E. 1991. The Critical State of Sands. Géotechnique, 41(3): 365-381.

de Beer E.E. 1963. The Scale Effect in the Transposition of the Results of Deep-Sounding Tests on the Ultimate Bearing Capacity of Piles and Caisson Foundations. Géotechnique, 13(1): 39-75.

Bellotti R., Bizzi G., and Ghionna V. 1982. Design, Construction, and Use of a Calibration Chamber. Proceedings ESOPT II, Balkema, Amsterdam, Netherlands, 2: 439-446.

van den Berg P. 1994. Analysis of Soil Penetration. PhD Thesis, Delft University of Technology, ISBN 90-407-1004-X.

van den Berg P., de Borst R., and Huetink H. 1996. An Eulerean Finite Element Model for Penetration in Layered Soil. International Journal of Numerical and Analytical Methods in Geomechanics, 20: 865-886.

Billam J. 1971. Some Aspects of the Behaviour of Granular Materials at High Pressures. Proceedings of the Roscoe Memorial Symposium, R.H. Parry (ed.), Henley-on-Thames: Foulis, 69-80.

Bishop A.W. 1966. Strength of Soils as Engineering Materials. 6th Rankine Lecture, Géotechnique, 16: 89-130.

Bishop R.F., Hill R., and Mott N.F. 1945. Theory of Indentation and Hardness Tests. Proceedings of the Physical Society, 57: 147–159.

Bolton M.D. 1986. The Strength and Dilatancy of Sands. Géotechnique 36(1): 65-78.

de Borst R., and Vermeer P.A. 1982. Finite Element Analysis of Static Penetration Tests. Proceedings of the 2nd European Symposium on Penetration Testing, Amsterdam, Netherlands, 457-562.

Bridgman P.W. 1918. The Failure of Cavities in Crystals and Rocks under Pressure. American Journal of Science, 45: 243-268.

Broms B.B. and Flodin N. 1988. History of Soil Penetration Testing. Proceedings of the International Symposium on Penetration testing, Penetration Testing 1988, ISOPT-1, Orlando, Vol. 1, J. de Ruiter (ed.), Balkema, Rotterdam, 157-220.

Campanella R.G., Robertson P.K., and Gillespie D. 1983. Cone Penetration Testing in Deltaic Soils. Canadian Geotechnical Journal, 20:23-35.

Carter J.P., Booker J.R., and Yeung S.K. 1986. Cavity Expansion in Cohesive Frictional Soils. Géotechnique, 36(3): 349–358.

Chadwick P. 1959. Quasi-Static Expansion of Spherical Cavity in Metals and Ideal Soils. The Quarterly Journal of Mechanics and Applied Mathematics, 12(1): 52-71.

Cividini A., and Gioda G. 1988. A Simplified Analysis of Pile Penetration. Proceedings of the 6th International Conference on Numerical Methods in Geomechanics, Balkema, Rotterdam, Netherlands, 1043-1049.

Clayton C.R.I., Hababa M.B., and Simons N.E. 1985. Dynamic Penetration Resistance and the Prediction of the Compressibility of a Fine-Grained Sand – A Laboratory Study. Géotechnique, 35: 19-31.

Collins I. F., and Yu H. S. 1996. Undrained Cavity Expansions in Critical State Soils. International Journal of Numerical and Analytical Methods in Geomechanics, 20(7): 489–516.

Coop M.R., Sorensen K.K., Bodas Freitas T., and Georgoutsos G. 2004. Particle Breakage during Shearing of a Carbonate Sand. Géotechnique, 54(3): 157-163.

Cudmani R., and Osinov V.A. 2001. The Cavity Expansion Problem for the Interpretation of Cone Penetration and Pressuremeter Tests. Canadian Geotechnical Journal, 38: 622-638.

Cundall P.A., Strack O.D.L. 1979. A Discrete Numerical Model for Granular Assemblies. Géotechnique, 29: 47-65.

Daouadji A., Hicher P. Y., and Rahma A. 2001. An Elastoplastic Model for Granular Materials Taking into Account Grain Breakage. European Journal of Mechanics - A/Solids, 20: 113–137.

Drucker D.C., Gibson R.E., and Henkel D.J. 1957. Soil Mechanics and Work Hardening Theories of Plasticity. Transactions of the American Society of Civil Engineers, 122, ASCE, Paper No. 2864, 338–346.

Durgunoglu H.T., and Mitchell J.K. 1975. Static Penetration Resistance of Soils, I-Analysis, II-Evaluation of Theory and Implications for Practice. Proceedings of the Specialty Conference in In-Situ Measurements of Soil Properties, ASCE, Raleigh, N.C., 1: 151-189.

Einav I. 2007. Breakage Mechanics – Part II: Modelling Granular Materials. Journal of the Mechanics and Physics of Solids, 55: 1298-1320.

Foray P. 1991. Scale and Boundary Effects on Calibration Chamber Pile Tests. Proceedings of the 1st International Symposium on Calibration Chamber Testing, Potsdam, New York, 147-160.

Foster W.A., Johnson C.E., Chiroux R.C., and Way T.R. 2005. Finite Element Simulation of Cone Penetration. Applied Mathematics and Computation, 162: 735-749.

Fuller W., and Thompson S.E. 1907. The laws of proportioning concrete. Transactions of the American Society of Civil Engineers. Paper no 1053: 67-143.

Ghionna V.N., and Jamiolkowski M. 1991. A Critical Appraisal of Calibration of Calibration Chamber Testing of Sands. Proceedings of the 1st International Symposium on Calibration Chamber Testing, ISOCCT 1, Potsdam, New York, 13-39.

Gill D.R., and Lehane B.M. 2000. Extending the Strain Path Method Analogy for Modelling Penetrometer Installation. International Journal of Numerical and Analytical Methods in Geomechanics, 24: 477-489.

Griffiths D.V. 1982. Elasto-Plastic Analysis of Deep Foundations in Cohesive Soil. International Journal of Numerical and Analytical Methods in Geomechanics, 6: 211-218.

Hardin B.O. 1985. Crushing of Soil Particles. ASCE, Journal of Geotechnical Engineering, 111(10): 1177-1192.

Hill R. 1950. The Mathematical Theory of Plasticity. Oxford University Press, Oxford.

Hofmann B.A., Sego D.C., and Robertson P.K. 2000. In Situ Ground Freezing to Obtain Undisturbed Samples of Loose Sand. Journal of Geotechnical and Geoenvironmental Engineering, ASCE, 126(11): 979-989.

Holden J.C. 1991. History of the First Six CRB Calibration Chambers. Proceedings of the 1st International Symposium on Calibration Chamber Testing, ISOCCT 1, Potsdam, New York, 1–12.

Houlsby G.T., Wheeler A.A., and Norbury J. 1985. Analysis of Undrained Cone Penetration as a Steady Flow Problem. Proceedings of the 5th International Conference on Numerical Methods in Geomechanics, 4: 1767–1773.

Houlsby G.T., and Hitchman R. 1988. Calibration Chamber Tests of a Cone Penetrometer in Sand. Géotechnique, 38(1): 39–44.

Houlsby G.T., and Hitchman R. 1989. Calibration Chamber Tests of a Cone Penetrometer in Sand. Discussion. Géotechnique, 39(4): 727–731.

Hsu H.H., and Huang A.B. 1998. Development of an Axisymmetric Field Simulator for Cone Penetration Tests in Sand. Geotechnical Testing Journal, 21(4): 348-355.

Hsu H.H., and Huang A.B. 1999. Development Calibration of Cone Penetration Test in Sand. Proceedings of the National Science Council. ROC(A), 23(5): 579-590.

Huang W., Sheng D., Sloan S.W., and Yu H.S. 2004. Finite Element Analysis of Cone Penetration in Cohesionless Soil. Computers and Geotechnics, (31): 517–528.

Huang A.B. 1989. Strain-Path Analyses for Arbitrary Three-Dimensional Penetrometers. International Journal of Numerical and Analytical Methods in Geomechanics, 13: 551-564.

Huang A.B., and Hsu H.H. 2004. Advanced Calibration Chambers for Cone Penetration Testing in Cohesionless Soils. Proceedings of ISC-2 on Geotechnical and Geophysical Site Characterization, Viana da Fonseca and Mayne (eds.), 147-166.

Huang A.B., and Hsu H.H. 2005. Cone Penetration Tests under Simulated Field Conditions. Géotechnique, 55(5): 345-354.

Huang A.B., and Ma M.Y. 1994. An Analytical Study of Cone Penetration Tests in Granular Material. Canadian Geotechnical Journal, 31(1): 91–103.

Indraratna B., and Salim W. 2002. Modelling of Particle Breakage of Coarse Aggregates Incorporating Strength and Dilatancy. Proceedings of the Institution of Civil Engineers, Geotechnical Engineering, 144(4): 243-252.

Iqbal M.S. 2004. Discrete Element Modeling of Cone Penetration Testing in Coarse Grain Soils. M.S. thesis, Civil and Environmental Engineering, University of Alberta, Edmonton.

Ishihara K., Tatsuoka F., and Yasuda S. 1975. Undrained Deformation and Liquefaction of Sand Under Cyclic Stresses. Soil and Foundations, 15(1): 29-44.

Jamiolkowski M., Ladd C.C., Germaine J.T., and Lancellotta R. 1985. New Developments in Field and Laboratory Testing of Soils. Proceedings of the 11th ICSMFE, San Francisco, CA, 1: 54-154.

Jefferies M.G. 1993. Nor-sand: a Simple Critical State Model for Sand. Géotechnique, 43(1): 91-103.

Jefferies M.G., and Been K. 2000. Implications for Critical State Theory from Isotropic Compression of Sand. Géotechnique, 50(4): 419-429.

Jefferies M.G., and Shuttle D.A. 2005. NorSand: Features, Calibration and Use. Proceedings of the Specialty Conference on Soil Constitutive Models: Evaluation, Selection, and Calibration, ASCE Geotechnical Special Publication 128: 204-236.

Jefferies M.G., and Shuttle D.A. 2002. Dilatancy in General Cambridge-Type Models. Géotechnique, 52(9): 625-638.

Kim D. 1999. Numerical Simulation and Experimental Verification of Cone Penetration Rate and Anisotropy in Cohesive Soil. PhD Thesis, Department of Civil Engineering, Louisiana State University.

Kiousis P.D., Voyiadjisa G.Z., and Tumay M.T. 1988. A Large Strain Theory and its Application in the Analysis of the Cone Penetration Mechanism. International Journal of Numerical and Analytical Methods in Geomechanics, 12: 45-60.

Konrad J.-M. 1997. In Situ Sand State from CPT: Evaluation of a Unified Approach at Two CANLEX Sites. Canadian Geotechnical Journal. 34(1): 120–130.

Konrad J.-M. 1998. Sand State from Cone Penetrometer Tests: A Framework Considering Grain Crushing Stress. Géotechnique, 48(2): 201–215.

Koumoto T. 1988. Ultimate Bearing Capacity of Cones in Sand. Proceedings of the 1st International Symposium on Penetration Testing, ISOPT-1, Orlando, Florida, De Ruiter (ed.), Balkema, Rotterdam, 809-813.

Ladanyi B. 1963. Expansion of a Cavity in a Saturated Clay Medium. Journal of the Soil Mechanics and Foundations Division, ASCE, 89(4): 127–161.

Lade P.V., and Yamamuro J.A. 1996. Undrained Sand Behaviour in Axisymmetric Tests at High Pressures. Journal of Geotechnical Engineering, 122(2): 120-129.

Lee I.K., and Coop M.R. 1995. Intrinsic Behaviour of a Decomposed Granite Soil. Géotechnique, 45(1): 117-130.

Lee K.L., and Farhoomand I. 1967. Compressibility and Crushing of Granular Soil in Anisotropic Triaxial Compression. Canadian Geotechnical Journal, 4(1): 68-86.

Lu Q., Randolph M.F., Hu Y., and Bugarski I.C. 2004. A Numerical Study of Cone Penetration in Clay. Géotechnique, 54(4): 257–267.

Lunne T., and Christophersen H.P. 1983. Interpretation of Cone Penetration Data for Offshore Sands. Proceedings of the 15th Annual Offshore Technology Conference, Houston, Texas, 181-192.

Lunne T., Robertson P.K., and Powell J.J.M. 1997. Cone Penetration Testing in Geotechnical Practice. Routledge, Blackie Academic & Professional. London.

Luzzani L., and Coop M.R. 2002. On the Relationship between Particle Breakage and the Critical State of Sands. Soils and Foundations, 42(2): 71-82.

Mabsout M.E., Reese L.C., and Tassoulas J.L. 1995. Study of Pile Driving by Finite-Element Method. Journal of Geotechnical Engineering, ASCE, 121(7): 535-543.

Matsuoka H., and Nakai T. 1974. Stress-Deformation and Strength Characteristics of Soil under Three Different Principal Stresses. Trans. JSCE, 6: 108-109.

Mayne P.W., and Kulhawy F.H. 1991. Calibration Chamber Database and Boundary Effects Correction for CPT Data. Proceedings of the 1st International Symposium on Calibration Chamber Testing, ISOCCT 1, Potsdam, New York, 257-264.

McDowell G.R., Bolton M.D., and Robertson D. 1996. The Fractal Crushing of Granular Materials. Journal of the Mechanics and Physics of Solids, 44(12): 2079-2101.

Meyerhof G.G. 1951. The Ultimate Bearing Capacity of Foundations. Géotechnique, 2(4): 301-332.

Miura N., and O-Hara S. 1979. Particle-Crushing of a Decomposed Granite Soil under Shear Stresses. Soils and Foundations, 19(3): 1-14.

Muir Wood D. 2007. The Magic of Sands. The 20th Bjerrum lecture presented in Oslo, 25 November 2005, Canadian Geotechnical Journal, 44: 1329-1350.

Muir Wood D., and Maeda K. 2008. Changing Grading of Soil: Effect on Critical States. Acta Geotechnica, 3: 3-14.

Nash D.F.T., Powell J.J.M., and Lloyd I.M. 1992. Initial Investigations of the Soft Clay Test Site at Bothkennar. Géotechnique, 42: 163-181.

Parkin A., and Lunne T. 1982. Boundary Effects in the Laboratory Calibration of a Cone Penetrometer in Sand. Proceedings of ESOPT II, Balkema, Amsterdam, The Netherlands, 2: 761-768.

Parkin A.K. 1988. The Calibration of Cone Penetrometers. Proceedings of the 1st International Symposium on Penetration Testing, ISOPT-1, Orlando, Florida, Vol.1, pp.221-243.

Pestana J.M., and Whittle A.J. 1995. Compression Model for Cohesionless Soils. Géotechnique, 45: 611-631.

Peterson R.W., and Arulmoli K. 1991. Overview of a Large Stress Chamber System. Proceedings of the 1st International Symposium on Calibration Chamber Testing, Potsdam, New York, 329-338.

Plewes H.D., Davies M.P., and Jefferies M.G. 1992. CPT Based Screening Procedure for Evaluating Liquefaction Susceptibility. Proceedings of the 45th Canadian Geotechnical

Conference, Toronto, Ont., 26-28 Oct. 1992, Canadian Geotechnical Society, Alliston, Ont., 4: 1-9.

Plewes H.D., Pillai V.S., Morgan M.R., and Kilpatrick B.L. 1994. In Situ Sampling, Density Measurements, and Testing of Foundation Soils at Duncan Dam. Canadian Geotechnical Journal, 31: 927–938.

Robertson P.K. 2009. Interpretation of Cone Penetration Tests – a Unified Approach. Canadian Geotechnical Journal, 46(11): 1337-1355.

Robertson P.K., and Campanella R.G. 1983[a]. Interpretation of Cone Penetration Tests. Part I: Sand. Canadian Geotechnical Journal, 20(4): 718-733.

Robertson P.K., and Campanella R.G. 1983[b]. Interpretation of Cone Penetration Tests. Part II: Clay. Canadian Geotechnical Journal, 20(4): 734-745.

Robertson P.K., and Campanella R.G. 1986. Guidelines for the Use and Application of the CPT and CPTU. Soil Mechanics series No. 105, Department of Civil Engineering, The University of British Columbia, 187 p.

Robertson P.K., and Campanella R.G., Gillespie D., and Greig J. 1986. Use of Piezometer Cone Data. In Use of In Situ Tests in Geotechnical Engineering, Proceedings of In Situ '86, a Specialty Conference sponsored by the Geotechnical Engineering Division of the American Society of Civil Engineers, S.P. Clemence (ed.), American Society of Civil Engineers, Geotechnical special publication No. 6, 1263-1280.

Robertson P.K., and Wride C.E. 1998. Evaluating Cyclic Liquefaction Potential Using the Cone Penetration Test. Canadian Geotechnical Journal, 35(3): 442-459.

Russell A.R., and Khalili N. 2002. Drained Cavity Expansion in Sands Exhibiting Particle Crushing. International Journal of Numerical and Analytical Methods in Geomechanics, 26(4): 323–340.

Russell A.R., and Khalili N. 2004. A Bounding Surface Plasticity Model for Sands Exhibiting Particle Crushing. Canadian Geotechnical Journal, 41(6): 1179-1192.

Sagaseta C., Whittle A.J., Santagata M., 1998. Deformation Analysis of Shallow Penetration in Clay. International Journal of Numerical and Analytical Methods in Geomechanics, 21(10): 687 – 719.

Salgado R. 1993. Analysis of Penetration Resistance in Sands. PhD thesis, Department of Civil Engineering, University of California at Berkeley.

Salgado R., Mitchell J.K., and Jamiolkowski M. 1997. Cavity Expansion and Penetration Resistance in Sand. Journal of Geotechnical and Geoenvironmental Engineering, 123(4): 344-354.

Salgado R., Mitchell J.K., and Jamiolkowski M. 1998. Calibration Chamber Size Effects on Penetration Resistance in Sand. Journal of Geotechnical and Geoenvironmental Engineering., ASCE, 124(9): 878-888.

Schmertmann J.H. 1991. The Mechanical Ageing of Soils. Journal of Geotechnical Engineering, ASCE, 117(12): 1288-1330.

Schnaid F. 1990. A Study of the Cone-Pressuremeter Test in Sand. PhD thesis, Magdalen College, University of Oxford, Oxford.

Schnaid F., and Yu H.S. 2007. Interpretation of the seismic cone test in granular soils. Géotechnique, 57(3): 265-272.

Schofield A.N., and Wroth C.P. 1968. Critical State Soil Mechanics. McGraw-Hill.

Sheng D., Eigenbrod K.D., and Wriggers P. 2005. Finite Element Analysis of Pile Installation Using Large-Slip Frictional Contact. Computers and Geotechnics, 32: 17–26.

Shuttle D.A., and Jefferies M.G. 1998. Dimensionless and Unbiased CPT Interpretation in Sand. International Journal of Numerical and Analytical Methods in Geomechanics, 22: 351-391.

de Simone P., and Golia G. 1988. Theoretical Analysis of the Cone Penetration Test in Sands. Proceedings, 1st International Symposium on Penetration Testing, ISOPT-1, Orlando, Florida, de Ruiter (ed.), Balkema, Rotterdam, 729-753.

Sisson R.C. 1990. Lateral Stresses on Displacement Penetrometers. PhD thesis, University of California at Berkeley.

Sladen J.A. 1989. Problems with Interpretation of Sand State from Cone Penetration Test. Géotechnique, 39(2): 323-332.

Sokolovskii V.Y. 1965. Statics of Granular Media. Pergamon Press, Tarrytown, N.Y.

Susila E., and Hryciw R.D. 2003. Large Displacement FEM Modelling of the Cone Penetration Test (CPT) in Normally Consolidated Sand. International Journal for Numerical and Analytical Methods in Geomechanics, 27: 585-602.

Tan N.K., Miller G.A., and Muraleetharan K.K. 2003. Preliminary Laboratory Calibration of Cone Penetration in Unsaturated Silt. Proceedings of the 12th Pan American Conference on Soil Mechanics and Geotechnical Engineering, Cambridge, Massachusetts, 1: 391-396.

Tannant D.D., and Wang C. 2002. PFC Model of Wedge Penetration into Oil Sands. Discrete Element Methods: Numerical Modeling of Discontinua. Proceedings of the Third International Conference, Santa Fe, September 2002, Reston, Virginia, ASCE, 311-316.

Tavenas F.A. 1973. Difficulties in the Use of Relative Density as a Soil Parameter. Evaluation of Relative Density and its Role in Geotechnical Projects Involving Cohesionless Soils,

American Society for Testing and Materials, Selig E.T., and Ladd R.S. (eds.), Philadelphia, ASTM Special Technical Publication 523: 478-483.

Teh C.I., and Houlsby G.T. 1991. An Analytical Study of the Cone Penetration Test in Clay. Géotechnique, 41: 17-34.

Terzaghi K. 1943. Theoretical Soil Mechanics. John Wiley & Sons, New York, N.Y.

Vesic A.S. 1963. Bearing Capacity of Deep Foundations in Sand. Highway Research Board, Record No. 39, Stresses in Soils and Layered System, 112-153.

Vesic A.S. 1972. Expansion of cavities in infinite soil mass, Journal of Soil Mechanics and Foundations Division, ASCE, 98(SM3): 265-290.

Vesic A.S. 1977. Design of pile foundations. National Research Council, Washington, D.C.

Vesic A.S., and Clough G.W. 1968. Behavior of Granular Materials under High Stresses. Journal of the Soil Mechanics and Foundations Division, American Society of Civil Engineers, 94 (SM3): 661-688.

Voyiadjisa G.Z., and Kim D. 2003. Finite Element Analysis of the Piezocone Test in Cohesive Soils Using an Elastoplastic–Viscoplastic Model and Updated Lagrangian Formulation. International Journal of Plasticity, 19: 253–280.

Wei L., Abu-Farsakh M.Y., and Tumay M.T. 2005. Finite-Element Analysis of Inclined Piezocone Penetration Test in Clays. International Journal of Geomechanics, ASCE, 5(3): 167-178.

Whittle A.J. 1992. Constitutive Modelling for Deep Penetration Problems in Clay. Proceedings of the 3rd International Conference on Computational Plasticity: Fundamentals and Applications, 2: 883–894.

Willson S.M. 1985. Finite Element Analysis of Piles and Penetrometers. PhD thesis, University of Manchester, UK.

Willson S.M., Ims B.W., and Smith I.M. 1988. Finite Element Analysis Of Cone Penetration. Penetration testing in the UK, Thomas Telford, London, 157-159.

Woods R.D., Benoît J., and deAlba P. 1994. National Geotechnical Experimentation Sites. Geotechnical News, 12(1): 39-44.

Wride (Fear) C.E., Hofmann B.A., Sego D.C., Plewes H.D., Konrad J.-M, Biggar K.W., Robertson P.K., and Monahan P.A. 2000. Ground Sampling Program at the CANLEX Test Sites. Canadian Geotechnical Journal, 37(3): 530–542.

Yamamuro J.A., and Lade P.V. 1996. Undrained Sand Behaviour in Axisymmetric Tests at High Pressures. Journal of Geotechnical Engineering, 122(2): 109-119.

Yang Z.X., Jardine R.J., Zhu B.T., Foray P., and Tsuha C.H.C. 2010. Sand Grain Crushing and Interface Shearing During Displacement Pile Installation in Sand. Géotechnique, 60(6): 469-482.

Yu H.S., and Houlsby G.T. 1991. Finite Cavity Expansion in Dilatant Soils: Loading Analysis. Géotechnique, 41(2): 173–183.

Yu H.S., and Mitchell J.K. 1998. Analysis of Cone Resistance: Review of Methods. Journal of Geotechnical and Geoenvironmental Engineering, ASCE, 124(2): 140-149.

Yu H.S., Schnaid F., and Collins I.F. 1996. Analysis of Cone Pressuremeter Tests in Sands. ASCE, Journal of Geotechnical Engineering, 122(8): 623-632.

Yu H.S., Herrmann L.R., and Boulanger R.W. 2000. Analysis of Steady Cone Penetration in Clay. ASCE, Journal of Geotechnical and Geoenvironmental Engineering, 126(7): 594-605.

Zohrabi M., Sibbald A. and Fairfield C.A. 1995. Boundary Conditions and Chamber Size Effects on CPT. Proceedings of the International Symposium on Cone Penetration Testing, Linkoping, Sweden, 2: 363–368.

Chapter 2.

Determination of the Critical State Friction Angle from Triaxial Tests[2]

2.1. Introduction

The idea that soils sheared to very high values of strain will eventually reach a constant void ratio, e_c, and friction angle, ϕ_c, is well established in soil mechanics. This constant volume state, usually termed the critical state, is also inherent in many, if not most, advanced constitutive soil models, including the well known critical state soil models Cam Clay and Modified Cam Clay. Geotechnical predictions are sensitive to the assumed shear strength parameters. Hence it is important that geotechnical engineers have access to good parameter estimates. However, despite the importance of the critical state to understanding soil behaviour, measurement of ϕ_c

---

[2] A version of this chapter has been published. Ghafghazi M., and Shuttle D.A. 2006. Accurate Determination of the Critical State Friction Angle from Triaxial Tests. Proceedings of the 59th Canadian Geotechnical Conference, Vancouver, 278-284.

remains problematic. This is particularly the case in engineering practice, where typically only a limited number of soil tests are available.

This chapter describes four methods from the literature to obtain the critical state friction ratio in triaxial conditions. The accuracy of each of these methods is discussed based on previously published data for Ticino sand taking into consideration the limited number of tests typically available in practice. Then the two most promising methods are used to determine shear strength parameters for Erksak sand, to investigate the repeatability of the methods. Finally recommendations are made on how to acquire the most accurate parameters from a limited amount of data.

2.2. Definition of the Critical State

The critical state (also called steady state) was defined by Roscoe et al. (1958) as the state at which a soil "continues to deform at constant shear stress and constant void ratio". Poulos (1981) gives a more precise definition as "the steady state of deformation for any mass of particles is that state in which the mass is continuously deforming at constant volume, constant normal effective stress, constant shear stress and constant velocity". Writing these definitions in a logical form we have:

$$\exists C(e,q,p')\big|_{p'=0} \ni \dot{\varepsilon}_v \equiv 0 \wedge \ddot{\varepsilon}_v \equiv 0 \forall \varepsilon_q \qquad \text{[Eq. 2 - 1]}$$

Where $C(\ )$ is the function defining the *CSL*, e is the void ratio, q is the deviatoric stress invariant, p' is the mean effective stress and ε_v and ε_q are volumetric and deviatoric strain

invariants respectively. The above equation includes two important conditions: first, the volumetric strain rate must be zero; second, the rate of change of this strain rate must also be zero. Hence, both dilatancy and rate of change of dilatancy must be zero during shearing at the critical state. There are no strain rate terms in *C( )*, making the *CSL* identical to the steady state of Poulos (1981). Constant mean stress is invoked in the equation to avoid a less easily understood definition for the situation in which mean stress is increased while the soil is continuously sheared at the critical state (Jefferies, 1993).

These definitions can be used to infer the existence of a unique Critical State Locus (not necessarily linear) in $e - \log p'$ space. This line is the locus of end points of state paths ($e - \log p'$) for different tests sheared to large strain values. Many authors have presented data on the existence of a unique Critical State Locus (e.g. Castro, 1969; Been and Jefferies, 1985; Been et al., 1991; Vaid and Sasitharan, 1992; Garga and Sedano, 2002).

Equation 2-1 also requires the existence of a unique critical state locus in $p' - q$ space. Since the models are cast in terms of stress invariants, and the relation between these invariants needs to be expressed for the critical state, it is convenient to replace the critical state friction angle with a parameter which is directly related to the stress invariants. The convention is to introduce a critical stress ratio, *M*, such that at the critical state:

$$q = Mp'$$
[Eq. 2 - 2]

Constant *M* does not imply a constant friction angle and experimental data suggest that constant *M* yields unrealistic friction angles in general 3-D stress space (e.g. Bishop, 1966; Wanatowski and Chu, 2006). A constant friction angle may be obtained by treating *M* as a function of the

intermediate principal stress, represented by the lode angle, θ. Friction angle is also likely not constant with θ (Jefferies and Shuttle, 2002). In this work triaxial compression conditions are taken as the reference case for which soil properties are determined. Thus, M_{tc} becomes the soil property (where subscript '*tc*' denotes triaxial compression), and $M(\theta)$ is evaluated in terms of this property. For known stress conditions the friction angle is directly related to stress ratio and the two parameters can be applied interchangeably; for example, in triaxial compression we have

$$M_{tc} = \frac{6\sin\phi_c}{3 - \sin\phi_c} \qquad\qquad\qquad \text{[Eq. 2 - 3]}$$

This chapter only considers triaxial compression conditions.

2.3. Stress-Dilatancy Definitions

The stress-dilatancy plot, which consists of the stress ratio $\eta = q/p'$ versus plastic dilatancy, $D^p = \dot{\varepsilon}_v^p / \dot{\varepsilon}_q^p$ is very useful in understanding the behaviour of soils. When plotting data from triaxial tests, to reduce the noise in the raw data a central-difference approach is employed to compute D^p. That is,

$$D_j^p = \frac{\varepsilon_{v,j+1}^p - \varepsilon_{v,j-1}^p}{\varepsilon_{q,j+1}^p - \varepsilon_{q,j-1}^p} \qquad\qquad\qquad \text{[Eq. 2 - 4]}$$

where j subscript means that the value of parameter at j^{th} data point is considered.

Stress-dilatancy is a concept regarding plastic strain rates, and thus, Equation 2-4 is not itself sufficient to reduce test data, as there is an elastic component of strain rate. The plastic dilatancy is estimated as

$$D_j^p = \frac{\dot{\varepsilon}_v^p}{\dot{\varepsilon}_q^p} = \frac{\left(\varepsilon_{v,j+1} - \varepsilon_{v,j-1}\right) - \left(p'_{j+1} - p'_{j-1}\right)/K}{\left(\varepsilon_{q,j+1} - \varepsilon_{q,j-1}\right) - \left(q_{j+1} - q_{j-1}\right)/3G}$$

[Eq. 2 - 5]

where K is the elastic bulk modulus and G the elastic shear modulus.

2.4.   Determination of the Critical State Friction Ratio

The critical state of soils is usually achieved at very large strains. The widely used triaxial testing apparatus typically cannot achieve the strains required to get to the critical state, and after the peak stress is reached, shear banding may occur making the measured stress ratio unreliable. This has resulted in many researchers attempting to obtain critical state shear strength properties using peak and pre-peak triaxial data.

2.4.1.   End of Test (ET) Method

A direct way of obtaining M_{tc} from soil samples is to plot the stress ratio, $\eta = q/p'$, versus deviatoric strain, ε_q, for a drained test sheared up to about 20% of strain. The final stress ratio of such a test is taken as M_{tc} for that test. Figure 2-1 shows the stress ratio versus deviatoric strain

from a drained triaxial test on a dilatant specimen of Ticino sand. M_{tc} obtained using this method

is denoted by $(M_{tc})_{ET}$ in this work; where the ET subscript stands for "end of test".

The major problem with this method is that the sample has likely not reached the critical state.

We are also dealing with triaxial data obtained at relatively large strains, where localisation may

occur.

As shown in Figure 2-1, at the end of the test neither the stress ratio nor the volumetric strain

has reached a constant value. Hence this dense sample has not yet reached the critical state.

2.4.2. Maximum Contraction (MC) Method

Maximum contraction during shearing of a soil sample is identified as the point where the

sample reaches its minimum volume as illustrated in Figure 2-1. At this point only one of the

conditions of critical state, $\dot{\varepsilon}_v = 0$ in Equation 2-1 is satisfied.

Negussey et al. (1988) suggested obtaining the critical state friction angle ϕ_c from mobilised

friction angle at maximum contraction based on data including ring shear tests on Ottawa sand,

two tailings sand, granular copper, lead shot and glass beads. M_{tc} parameter obtained from this

method will be denoted by $(M_{tc})_{MC}$ in the following; where MC subscript stands for "maximum

contraction".

2.4.3. Bishop Method (BM)

Bishop (1972) suggested a method of obtaining the critical state friction angle using the results

of drained tests on dense samples at varying densities. For each test the value of peak dilatancy

D_{min} at peak strength ϕ'_{peak} is computed, making use of the fact that at peak strength the elastic strain increment is zero. In elasticity strain increments are linearly related to stresses. At peak the stresses change from increasing (elastic compression) to decreasing (elastic expansion), and correspondingly the elastic strain rate changes from positive to negative giving an instantaneous zero elastic strain increment. With zero elastic component, the total and plastic strain increments are identical. This method relies on the experimental observation that dilatancy, and hence peak friction angle, increase with density. And for a sand that reaches the critical state directly, i.e. without any dilation, the peak stress ratio corresponds with the critical state where $\eta = M_{tc}$ and $D_{min} = 0$. M_{tc} can then be determined by extrapolation to zero dilatancy. For convenience, we plot η_{max} instead of ϕ'_{peak} and the corresponding dilation rate (peak dilatancy is $D_{min} \leq 0$ because of the compression-positive convention). Figure 2-2 shows the application of this method in $\eta_{max} - D_{min}$ space applied to Ticino sand.

The slope of this line, $(1 - N)$, has been used by some researchers as a material parameter (Nova 1982; Jefferies, 1993); N is called the volumetric coupling parameter.

2.4.4. Stress-Dilatancy (SD) Method

By definition the stable stress ratio at which no volume change occurs, $D = 0$, and remains there with continuing shearing, $\dot{D} = 0$, is the stress ratio at the critical state. Most triaxial tests do not reach the critical state within the strain limitations of the apparatus. As discussed earlier, localisation may occur post peak making the measured stress ratio unreliable. But it is possible to infer M_{tc} by extrapolating the post-peak portion of a stress ratio versus dilatancy plot to zero dilatancy (the vertical axis where $D = 0$).

The post-peak (hook) portion of the graph is usually linear, and this extrapolation to the critical state has been done by assuming that a linear trend continues to the critical state. The line drawn through the stress-dilatancy plot in Figure 2-3 illustrates how this method is applied to a triaxial test on a dense sample.

Post peak data should be used with significant caution. From an experimental viewpoint, shear banding and localisation may happen as soon as the sample strains beyond peak strength towards critical state. At larger strains (above 15%) other problems such as a higher effect of membrane penetration, tilting or bulging of the sample can occur; hence the data should be looked at very cautiously.

In this method the closer the test gets to the critical state, without developing shear bands, or other sources of error, the more accurate the extrapolation will be. In the case where the dilatancy path deviates from the linear trend approaching the end of the test, it is recommended that the initial part of the hook gets a higher weight in determining the location of the extrapolation line, and the second part be discarded. In this work the slope of this line is identified as $(1 - N^*)$.

2.5.   Obtaining the Critical State Stress Ratio of Ticino Sand

Ticino sand is a medium to coarse predominantly quartz sub-angular sand. A summary of its properties and the test program used here is available in Been et al. (1987) and Bellotti et al. (1996). Data presented here are from tests performed in 1987 at Golder Associates' Calgary laboratory. All samples were dry pluviated and taken from bulk samples known as Ticino 04, 08 and 09.

2.5.1. Ticino Data Processing

For the elastic properties of Ticino sand, Shuttle and Jefferies (1998) suggest using

$$G = \frac{6.5}{e^{1.3}}\left(\frac{p'}{p_a}\right)^{0.48}$$

[Eq. 2 - 6]

where p_a is a reference pressure equal to 100 kPa. The equation is obtained from bender element testing data presented by Bellotti et al. (1996). For test 09-CID-D169 with p'=300 kPa and e=0.686 at the beginning of the test, we can calculate $D - D^p$ for the whole test, which is plotted against stress ratio as shown in Figure 2-4.

Theoretically, the difference between total and plastic dilatancy ($D - D^p$) is equal to zero at the peak. One important observation from Figure 2-3 is that the difference between the total and plastic dilatancy ($D - D^p$) is negligible post-peak. Hence, as the emphasis is on the latter part of the stress-dilatancy plot, it is possible to use total dilatancy, D, instead of plastic dilatancy, D^P, as a reasonable approximation. This is convenient because elastic modulus is not measured using bender elements in all triaxial tests. Total dilatancy (D) has been used instead of plastic dilatancy (D^P) in the rest of this work.

Figure 2-5 shows a comparison between M_{tc} obtained using the four methods described earlier; the values of M_{tc} range from 1.25 for MC to 1.445 for ET with BM and SD yielding similar values of 1.33 and 1.345 respectively.

2.5.2. Discussion of Results for Ticino Sand

The strength from the end of test method, $(M_{tc})_{ET}$ =1.445 appears to overestimate M_{tc} for the dense specimen used here; the sample is not at the critical state at the end of the test, as expected for a relatively dense sample. Even for loose sand reaching the critical state within the strain limits of the triaxial test is problematic. That test 09-CID-D169 is not at the critical state as confirmed in Figure 2-5, where the dilation rate is not zero at the end of the test.

The MC method is based on the assumption that the post-peak *hook* in the stress-dilatancy plot corresponds to the maximum contraction point when the sample reaches the critical state. Although this is assumed by many stress-dilatancy rules, including that of Cam-Clay and Nova, it is not a requirement of critical state theory. None of the triaxial data considered for this work demonstrates such behaviour and, as illustrated in Figure 2-5, this method predicts a much lower shear strength, $(M_{tc})_{PT}$ =1.25, than the Stress Dilatancy (SD) and Bishop (BM) methods. The large difference between $(M_{tc})_{MC}$ and the critical state strength predicted by the SD and BM methods, combined with lack of a conceptual rationale as to why the maximum contraction and the critical state should generally be coincident, casts doubt on the accuracy of M_{tc} estimated from the maximum contraction point.

$(M_{tc})_{SD}$ = 1.345 is very close to $(M_{tc})_{BM}$ = 1.33 and the difference is smaller than the ± 0.03 resolution of M_{tc} determination suggested by Jefferies and Been (2006). In order to show how BM results compare to the results of obtaining M_{tc} from the stress-dilatancy plot, the results are plotted in the same space in Figure 2-6.

It can be seen that the two tests for which the entire stress-dilatancy path is plotted are coincident with the line passing through the peak points. That is, the second part of stress-

dilatancy path (the hook) lies on this line. Consequently, the Bishop Method yields the same results as the stress-dilatancy method; we have $(M_{tc})_{SD} = (M_{tc})_{BM}$ and $N = N^*$. Note that $N = N^*$ is necessary for these two methods to yield equal M_{tc} values; if $N \neq N^*$ then the hook part of stress-dilatancy plot will leave Bishop's line after the peak and intersect the $D = 0$ axis at a different M_{tc}. As the stress-dilatancy plots for all of the ten tests show a relatively good agreement with Bishop's method, we can use Bishop's M_{tc}=1.33 and N=0.4 for Ticino sand with confidence.

2.6.   Obtaining the Critical State Stress Ratio of Erksak Sand

Erksak sand is a uniformly graded, medium to fine grained predominantly quartz, sub-rounded sand. A complete description of this sand and the test program undertaken is available in Been et al. (1991). The gradation referred to here has 0.7% fines content and D_{50}=330 μm. Nine tests on wet pluviated samples are used here. These tests are presented in Table 2-1.

2.6.1. Erksak Data Processing

The ET and MC methods were shown not to yield accurate M_{tc} values. Hence, only the BM and SD methods are applied to Erksak data and discussed here.

$D_{min} - \eta_{max}$ pairs are plotted in Figure 2-7 in order to locate Bishop's line. Another line can be drawn passing through six points with a very good resolution and ignoring the three points which are off the line. This results in M_{tc}=1.10 and N=0.065; this N value is lower than the expected range of 0.2-0.4 casting doubt about the reliability of this chosen line. The best fit

trend-line through all nine tests is also plotted in Figure 2-7. This results in M_{tc}=1.25 and N=0.41, which are more common values for these two parameters.

Still there is quite a scatter around this line (R^2=0.79) and it does not seem reasonable to merely rely on this line to obtain the critical state parameters. This example shows that Bishop's method is very sensitive to selection of data and the approach taken in drawing the line.

To obtain an accurate critical state stress ratio from a limited number of tests, we now consider the stress dilatancy plot for the entire stress paths. Figure 2-8 shows how the extrapolation for test CID-G667, where the earlier portion of the hook is preferentially weighted, has been done. The same process was applied to all nine tests, and the M and N^* parameters obtained are reported in Table 2-1. The average values of M_{tc}=1.28 and N^*=0.40 are very close to those obtained from the Bishop approach using the best fit line and including all data points.

2.6.2. Discussion of Results for Erksak Sand

It is of interest to note that this set of nine triaxial tests on dense samples would be considered a luxurious set of data in most engineering, and even academic, projects. Hence it is very important to be able to estimate the critical state friction angle (or stress ratio) with acceptable accuracy relying on this number of tests. In this case, we have the advantage of having results of a research project (Vaid and Sasitharan, 1992) on the same sand, allowing comparison of the two proposed Bishop's lines as well as the average SD values. M_{tc}=1.276 and N=0.41 are obtained from Vaid and Sasitharan (see Figure 2-9); these numbers are in good agreement with those obtained from fitting the best line passing through nine data points in BM and the average values obtained from SD method.

It is interesting to note that for test CID-G667 (and many other tests) although the $D_{min} - \eta_{max}$ coincides with Bishop's line, the dilatancy path leaves this line and estimates a higher M_{tc} than that of Bishop method; this also implies $N \neq N^*$. However, as shown in Table 2-1, the average values of M_{tc} and N^* are only slightly higher than those estimated from Bishop's method. Based on the above discussion $M_{tc}=1.27$ and $N=0.40$ are reasonable estimates for Erksak sand based on both the Stress-Dilatancy and Bishop's methods.

2.7.   Summary

Four methods of obtaining critical state friction angle were summarised and the advantages and disadvantages of each method were investigated using previously published data from drained triaxial tests on two sands.

Two of the methods "end of test" and "maximum contraction" (ET and MC) are inconsistent with the definition of the critical state and were found to give unrealistic estimates of M_{tc}.

While Bishop method is the reference method for assessing the critical state friction angle in most cases and especially where a large number of tests are available, most triaxial testing programs include only a limited number of tests. With only a small number of tests available, the Bishop method alone is sensitive to any outlying data points.

An advantage of the Stress-Dilatancy method is that it yields an estimate of M_{tc} for every single test, which can then be compared with that of Bishop's method. This makes Stress-Dilatancy method especially helpful when dealing with a small number of tests.

It is therefore recommended that the whole stress-dilatancy path of tests be plotted and used in conjunction with the Bishop approach.

Table 2 - 1 M_{tc} and N^* parameters (from the Stress-Dilatancy method) for nine wet pluviated triaxial tests on dense Erksak 330/0.7

Test name	$P'_0(kPa)$	OCR	e	M_{tc}	N^*
CID-G661	140	1.0	0.676	1.28	0.36
CID-G662	60	1.0	0.595	1.26	0.36
CID-G663	300	1.0	0.601	1.30	0.70
CID-G664	300	1.0	0.570	1.23	0.33
CID-G665	130	1.0	0.610	1.18	0.30
CID-G666	60	1.0	0.637	1.24	0.20
CID-G667	130	1.0	0.527	1.38	0.41
CID-G761	250	4.0	0.589	1.32	0.45
CID-G762	250	4.0	0.491	1.32	0.50
Average				1.28	0.40
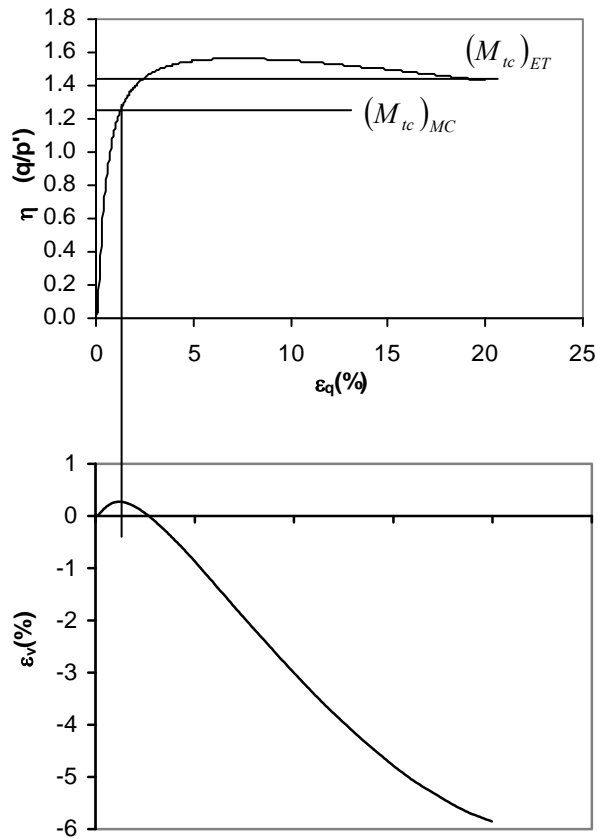
Figure 2 - 1 Stress ratio and volumetric strain versus deviatoric strain for Ticino sand
(test 09-CID-D169)
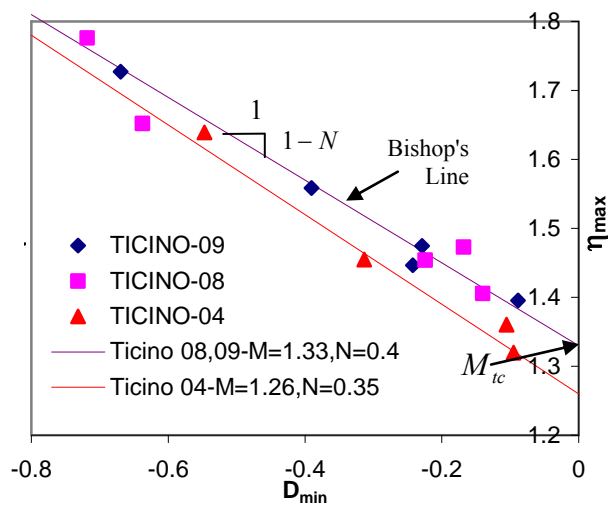
Figure 2 - 2 Application of Bishop's method to Ticino sand
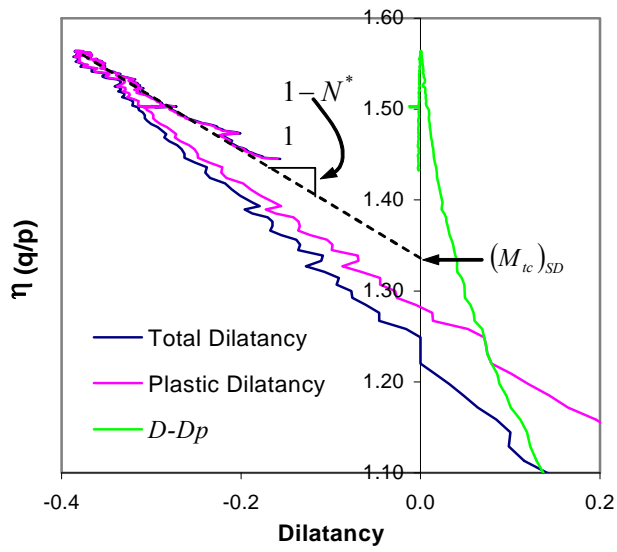
Figure 2 - 3 Stress-dilatancy plot ($D - \eta$), around peak
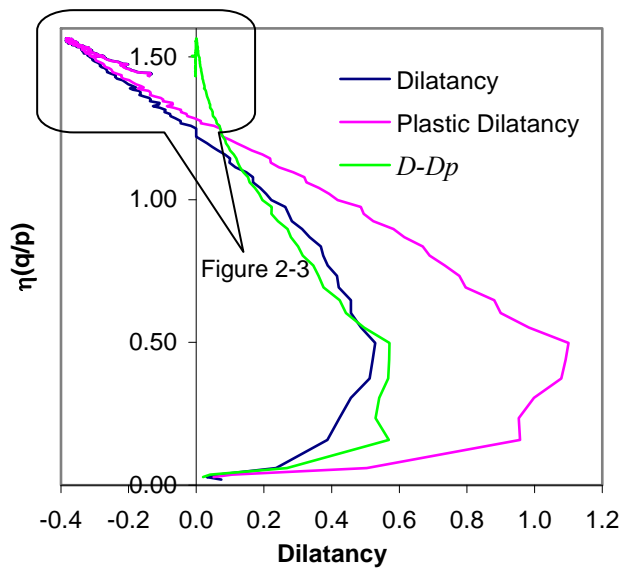
Figure 2 - 4 Stress-dilatancy plot ($D - \eta$) for Ticino sand (test 09-CID-D169)
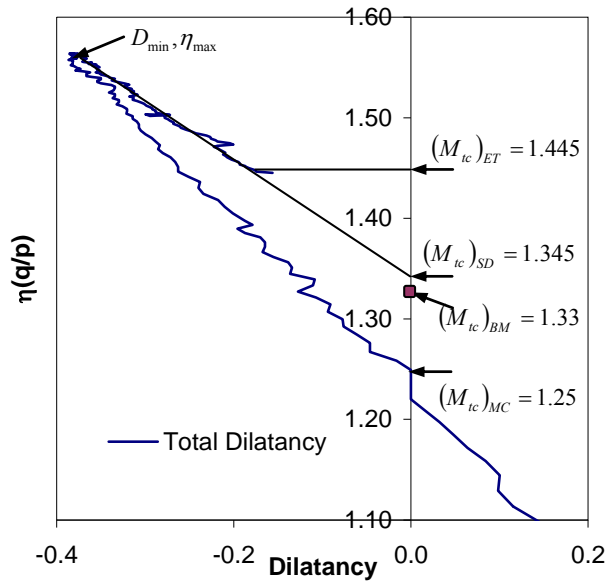
Figure 2 - 5 Stress-dilatancy plot ($D - \eta$) for Ticino sand (test 09-CID-D169), comparison of methods
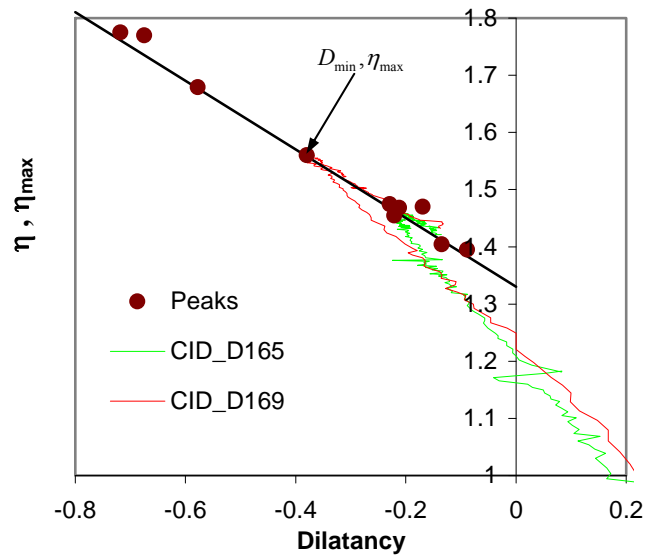
Figure 2 - 6 Stress-dilatancy plot ($D - \eta$) for Ticino sand
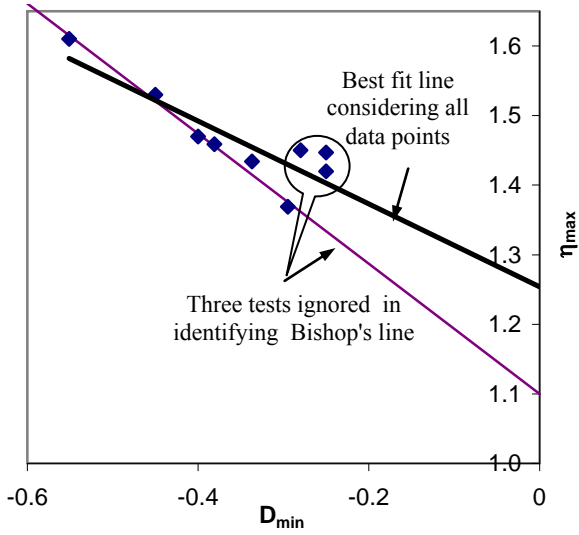
Figure 2 - 7 Stress-dilatancy ($D_{min} - \eta_{max}$) plot from triaxial data on Erksak 330/0.7 sand
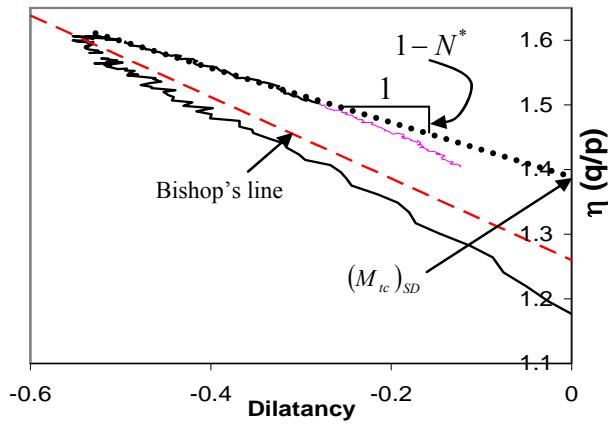
Figure 2 - 8 Stress-dilatancy plot ($D - \eta$) for Erksak 330/0.7 sand (test CID-G667)
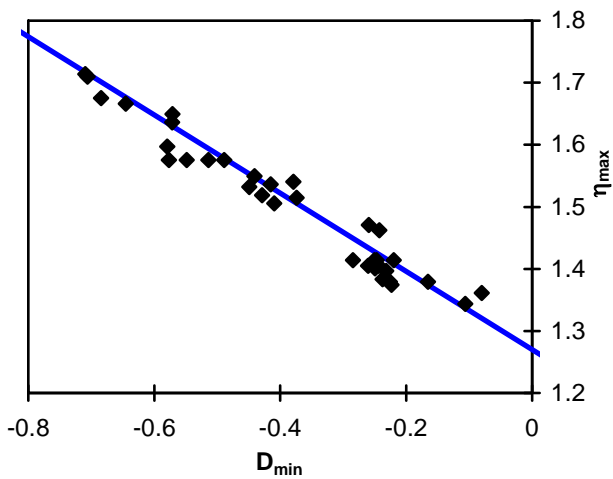
Figure 2 - 9 Stress-dilatancy ($D_{min} - \eta_{max}$) plot from triaxial data on Erksak 330/0.7 sand (data after Vaid and Sasitharan, 1992)

95

2.8. References

Been K., and Jefferies M.G. 1985. A State Parameter for Sands. Géotechnique, 35(2): 99-112.

Been K., Jefferies M.G., Crooks J.H.A., and Rothenberg L. 1987. The Cone Penetration Test in Sands: Part II, General Inference of State. Géotechnique, 37(3): 285-299.

Been K., Jefferies M.G., and Hachey J.E. 1991. The Critical State of Sands. Géotechnique, 41(3): 365-381.

Bellotti R., Jamiolkowski M., Lo Presti D.C.F., and O'Neil D.A. 1996. Anisotropy of Small Strain Stiffness in Ticino Sand. Géotechnique, 46 (1): 115-131.

Bishop A.W. 1966. Strength of Soils as Engineering Materials. 6th Rankine Lecture. Géotechnique, 16: 89-130.

Bishop A.W. 1972. Shear strength parameters for undisturbed and remolded soil specimens. In Proceedings, Roscoe Memorial Symposium, Cambridge University. Edited by R.H.G. Parry. G.T. Foulis & Co. Ltd., Yeovil, U.K., 3–139.

Bolton M.D. 1986. Strength and Dilatancy of Sands. Géotechnique, 36(1): 65-78.

Castro G. 1969. Liquefaction of Sands. PhD. Thesis, Harvard University, Cambridge, Mass. (Harvard Soil Mechanics Series 81).

Garga V.K., and Sedano J.A.I. 2002. Steady State Strength of Sands in a Constant Volume Ring Shear Apparatus. Geotechnical Testing Journal, 25(4).

Jefferies M.G. 1993. Nor-sand: a Simple Critical State Model for Sand. Geotechnicque, 43(1): 91-103.

Jefferies M.G., and Shuttle D.A. 2002. Dilatancy in General Cambridge-Type Models. Géotechnique, 52: 625-638.

Jefferies M.G., and Been K. 2006. Soil Liquefaction: A Critical State Approach. Taylor & Francis (Abingdon & New York). ISBN 0-419-16170-8.

Klotz E.U., Coop M.R. 2002. On the Identification of Critical State Lines for Sands. Geotechnical Testing Journal, 25(3).

Negussey D., Wijewickreme W.K.D., and Vaid, Y.P. 1988. Constant Volume Friction Angle of Granular Materials. Canadian Geotechnical Journal, 25: 50-55.

Poulos S.J. 1981. The Steady State of Deformation. Journal of Geotechnical Engineering, American Society of Civil Engineers, 17(G75): 553-562.

Roscoe K.H., Schofield A.N., and Wroth C.P. 1958. On the Yielding of Soils. Géotechnique, 8(1): 22-53.

Rowe P.W. 1962. The Stress Dilatancy Relation for Static Equilibrium of an Assembly of Particles in Contact. Proceedings of the Royal Society of London, A 269: 500-527.

Shuttle D.A., and Jefferies M.G. 1998. Dimensionless and Unbiased CPT Interpretation in Sand. International Journal for Numerical and Analytical Methods in Geomechanics, 22: 351-391.

Vaid Y.P., and Sasitharan S. 1992. The Strength and Dilatancy of Sand. Canadian Geotechnical Journal, 29: 522-526.

Wanatowski D., and Chu J. 2006. Stress-Strain Behavior of a Granular Fill Measured by a New Plane-Strain Apparatus. Geotechnical Testing Journal, 29(2): 1-9.

Chapter 3.

Confidence and Accuracy in Determination of

Critical State Friction Angle[3]

3.1. Introduction

Geotechnical predictions are sensitive to the shear strength parameters and so it is important for geotechnical engineers to have access to good parameter estimates. One widely used shear strength parameter is the critical state (or constant volume) friction angle, ϕ_c, a soil property that varies over a surprisingly wide range depending on soil mineralogy amongst other factors. Critical state soil mechanics is based on the idea that soils sheared to very high values of strain will eventually reach a constant void ratio, e_c, termed the critical void ratio, and constant friction angle, ϕ_c, termed the critical friction angle. Well established in soil mechanics since the late 1950s, critical state soil mechanics provides a basis for understanding the soil behaviour, with

---

many soil constitutive models based on this concept. Equally, the simplest engineering problems dealing with shear strength of soils require an estimate of the critical state friction angle, even if a critical state framework is not explicitly adopted, as ϕ_c is central to stress dilatancy (which is the micromechanical process governing cohesionless soil behaviour). For example Bolton (1986) relative density index provides a simplified but useful engineering relation which allows for estimating the peak friction angle ϕ_{peak} as a function of the relative density D_r if ϕ_c is known. Despite the importance of ϕ_c, the literature contains little guidance on how many laboratory tests are required to determine ϕ_c within the desired accuracy. This is particularly problematic in engineering practice, where typically only a limited number of soil tests are possible due to budget limitations. This situation is exacerbated by the lack of a consensus on the most accurate method of obtaining ϕ_c from standard laboratory tests.

This chapter uses an extensive triaxial testing program from the literature to determine ϕ_c using Bishop's method (1972), this being a standard method for determining ϕ_c. The database chosen is unusual in the sense that it comprises a large number of tests on a single material. By performing a statistical analysis of the database, guidance is obtained on the number, density range and pressure range of triaxial tests required to reach a specified level of accuracy and confidence in ϕ_c. Finally, the performance of the proposed methodology for estimating the accuracy of ϕ_c determination is tested against a smaller independent set of triaxial tests on the same sand, performed in a commercial testing laboratory.

3.2.   Triaxial Database

The material used for this study was Erksak sand, a sand used in several offshore construction projects in the Beaufort Sea (Jefferies et al., 1985). Erksak sand is a medium (D_{50} = 0.34 mm), uniform (U_c = 1.8), mainly quartz sand with sub-rounded particles. Testing of this sand was independently reported by Vaid and Sasitharan (1992) and Been et al. (1991).

The majority of the work in this chapter focuses on 34 drained triaxial compression tests performed in the University of British Columbia's (UBC) soils laboratory, as reported by Vaid and Sasitharan (1992). Samples were prepared using the water pluviation technique at three different relative densities; 26% (13 tests), 56% (13 tests) and 70% (8 tests) representing loose, medium dense and dense conditions. A smaller set of drained triaxial data was reported by Been et al. (1991), and comprised 9 triaxial compression tests performed in Golder Associates' Calgary commercial testing laboratory. The Been et al. tests were also prepared using water pluviation and had relative densities ranging between 20% and 74% with five loose, two medium and two dense samples. The terms loose, medium dense and dense refer to initial relative density values of 15-35%, 35-65%, and 65-85% respectively. It should be mentioned that even the loosest samples tested showed "dense" sand behaviour; i.e. having a clear peak strength and dilating towards the critical state. This lack of pressure dependence on soil behaviour is a pitfall of using D_r as the primary density index. However, despite this limitation D_r is used as the density index in this chapter due to its simplicity, and more importantly its widespread adoption in engineering practice.

3.3. Methodology Used for ϕ_c Determination

The critical state friction angle ϕ_c appears to be constant for a particular soil under triaxial compression conditions (e.g. Rowe, 1962; Negussey et al., 1988). However, there is no consensus on the most accurate method of determining its value. Ghafghazi and Shuttle (2006) (chapter 2) discussed four different methods of determining ϕ_c from triaxial compression tests. The first method, termed End of Test, assumes the measured friction angle at the end of the triaxial test is equal to ϕ_c. End of Test is simple, but most samples do not reach the critical state within the strain limits of the triaxial test and post-peak localisation could also render the measurements unreliable. The second method, Maximum Contraction, incorrectly assumes that the friction angle at maximum contraction is equivalent to ϕ_c and so provides poor ϕ_c values. The third method, Stress-Dilatancy, involves extrapolating a plot of the post-peak stress ratio versus dilatancy data to zero. This provides good predictions in the absence of localisation immediately post peak. However it is difficult to automate and involves user interpretation. The final method considered was Bishop's Method (1972), which has the advantage of yielding theoretically correct answers while being easily automated for any dataset of triaxial compression tests. This study uses Bishop's method.

Bishop's method of obtaining the critical state friction angle is based on the idea that, for constant mean stress, the peak friction angle of a soil increases with increasing density, and that a purely contractive soil will reach peak strength at critical state. Bishop used the parameters ϕ and $d\varepsilon_v/d\varepsilon_l$. However, the alternative identities η and D are preferred because these variables are, theoretically, linearly related (Schofield and Wroth, 1968; Nova, 1982). The dilatancy, D, is

defined as the ratio of rate of volume change to the rate of change in shear strain invariant. In mathematical form:

$$D = \frac{d\varepsilon_v}{d\varepsilon_q} \qquad\qquad \text{[Eq. 3 - 1]}$$

where ε_v [$=\varepsilon_1 + 2\varepsilon_3$] and ε_q [$= {}^2/_3 (\varepsilon_1 - \varepsilon_3)$] are the triaxial volumetric and deviatoric strain invariants respectively. The dilatancy at peak strength is negative because of the compression positive convention of soil mechanics. Mobilised stresses are represented by the stress ratio, η:

$$\eta = \frac{q}{p'} \qquad\qquad \text{[Eq. 3 - 2]}$$

where q [$= \sigma'_1 - \sigma'_3$] and p' [$= (\sigma'_1 + 2\sigma'_3)/3$] are the triaxial deviatoric stress and mean effective stress invariants respectively and σ'_1 and ($\sigma'_2 = \sigma'_3$) are the three principal effective stresses. For known stress conditions the friction angle is directly related to the stress ratio at the critical state and the two parameters can be applied interchangeably; for example, in triaxial compression we have

$$\phi_c = \arcsin\left(\frac{3M_{tc}}{6 + M_{tc}}\right) \qquad\qquad \text{[Eq. 3 - 3]}$$

where M_{tc} is the stress ratio η at the critical state under triaxial compression conditions.

With Bishop's method, a series of triaxial tests at differing densities are carried out. As illustrated in Figure 3-1, for each test the mobilised stress ratio, η, is plotted against dilatancy, D, and the peak point of the plot is chosen to represent the test on a plot of η_{max} vs. D_{min}. M_{tc} is determined by extrapolation of a linear regression through the D_{min} - η_{max} for all the 34 triaxial tests, with M_{tc} being the intercept at zero dilatancy, as shown in Figure 3-2. For a soil sample that reaches the critical state directly, i.e. without dilation, η_{max} (or equivalently ϕ_{peak}) corresponds with the critical state.

In this work it is assumed that the best fit regression line through all 34 Vaid and Sasitharan tests provides the "correct" answer. The trendline shown in Figure 3-2 yields $M_{tc} = 1.276$ (or $\phi_c = 31.75°$) with a coefficient of determination, $R^2 = 0.955$.

3.4. Determination of ϕ_c from Limited Number of Triaxial Tests

To determine accuracy in ϕ_c determination from fewer triaxial tests the simplest method would be to randomly sample the required number of tests from the database of 34 tests. However, this approach was felt to be unrealistic as most testing programs include a range of soil densities. Also, Bishop's approach is most accurate when the tests are spread over a range of D_{min}; using random tests would result in some unrepresentatively poor estimates of ϕ_c. Hence it was assumed that every combination of tests used to determine ϕ_c include at least one loose, one medium dense and one dense sample (i.e. one test at $D_r = 26\%$, 56% and 70% respectively for the Vaid and Sasitharan dataset). Additionally, no repetition was allowed in this procedure so that no test could be sampled twice in any realisation.

Adopting this statistical methodology led to ϕ_c being calculated with 3, 4, 5,…, 34 tests. Typically 3 to 20 tests are presented here: 20 tests being considered an upper bound for most practical testing programs. Each combination of loose, medium dense and dense tests comprising the total number of required tests was sampled 300 times. For example, 4 tests can comprise either 1 loose, 1 medium, 2 dense or 1 loose, 2 medium, 1 dense or 2 loose, 1 medium, 1 dense tests. After each of these three possible combinations was randomly realised 300 times, M_{tc} was again calculated from linear regression through the realised data points. Values of M_{tc} were then converted to ϕ_c using Equation 3-3.

The precision of the ϕ_c calculation, plotted as the percentage of tests falling within 0.1 degree bins, is shown in Figure 3-3 for 5, 10, 15 and 24 tests. As expected, with an increasing number of tests the accuracy of the ϕ_c prediction improves. However, Figure 3-3 also indicates that there is a slight bias towards over-prediction of ϕ_c for all numbers of tests. This bias is also evident in the determined M_{tc} data and may be related to the use of a real dataset. The magnitude of this bias is small: for 10 tests the bias in the results from quoting the average absolute error of 0.36 degrees, rather than the average over and under-prediction errors of 0.39 and 0.33 degrees respectively, is only 0.03. Hence the bias is ignored in the remainder of the work.

Figure 3-4 plots $|\varDelta\phi_c|$ versus number of tests for a range of confidence levels. At each confidence level the error rapidly decreases from 3 tests to around 8 tests. Thereafter a slower, almost linear, enhancement in accuracy is indicated. At the 85% confidence level this corresponds to a ±1.31 degree accuracy for 3 tests to better than ±0.75 degrees accuracy with 8 tests. The same information is provided in numerical form in Table 3-1 at 75%, 80%, 85%, 90%, and 95% confidence levels for 3 to 20 tests.

As discussed earlier, Figure 3-4 is obtained using one loose, medium dense and dense test in each realisation with the remaining tests randomly distributed. From a practical perspective it is of interest to determine whether improved accuracy could be obtained by further specifying the initial densities of the samples.

Figure 3-5 plots the magnitude of the average and standard deviation absolute error for all possible combinations of 9 tests including at least one loose, one medium and one dense test. The combinations are organised with the largest absolute error on the left hand side of the figure. The results show that of the 28 possible combinations of tests, the 10 combinations with the largest error have only one from each grouping. Moreover, the three combinations with 7 tests from one density grouping are among the worst 5 groups. Conversely, the average error is approximately half where the tests are better distributed between the three groups. Hence it is advisable that the program be designed to distribute tests equally between loose, medium and dense samples.

3.5.   Validation against Independent Triaxial Database

A high quality university testing program was used to compute the confidence levels shown in Table 3-1. Hence these confidence levels could be considered an upper bound on likely commercial accuracy. The general applicability of the confidence levels is tested using nine good quality commercial tests reported by Been et al. (1991). The full suite of nine tests shown in Figure 3-6 indicates M_{tc} = 1.254, corresponding to ϕ_c = 31.24° and suggesting an error compared to the original database of $\Delta\phi_c$ = 0.51° (associated with 67 % level of confidence).

To directly compare with the predicted confidence levels it is necessary to consider possible subsets of these data. If six tests are considered, there are 70 possible combinations of tests which include at least one loose, medium dense and dense test. Therefore from Table 3-1 we would expect 52 of the combinations to predict ϕ_c within an accuracy of ±0.70º at 75% confidence. The Been et al. data suggest a lower accuracy of only ±1.22º at 75% confidence (see Table 3-2).

Some reasons for the lower accuracy may be observed from Figure 3-6. The accuracy predicted from the Vaid and Sasitharan data is predicated on having one test from each density range. Although this criterion has been enforced for the Been et al. dataset as well, the effect of stress level (see Table 3-3) has resulted in one of the two medium dense tests being less dilative than all of the loose tests. Therefore the range of D_{min} between density ranges is reduced. Although this problem also exists for the large dataset, the few medium dense tests in the small dataset increase the inaccuracy. Additionally, comparison of Figure 3-2 with Figure 3-6 indicates that all of the "dense" tests for the Golder dataset are significantly less dilatant (D_{min} > -0.55) than the dense samples from the larger dataset (D_{min} < -0.55 for all but two samples). This problem could be reduced by maximising the range of D_{min} in Figure 3-6 by ensuring that for each confining pressure at least one loose and one dense test are undertaken. This is equivalent to defining a range of state parameters (Been and Jefferies, 1985), $\psi\ [= e - e_c]$, which accounts for the stress level effect on dilatancy, in addition to the void ratio accounted for in D_r.

3.6.   Summary and Conclusions

A statistical evaluation of a drained triaxial compression test database was performed to determine accuracy and confidence level in determining the critical state friction angle.

Critical state friction angle was obtained from a dataset comprising 34 triaxial tests using the methodology proposed by Bishop (1972); ϕ_c being obtained using linear regression. It was assumed that the correct ϕ_c was obtained if all 34 tests were included in the analysis. In determining the accuracy of smaller realisations of the dataset it was assumed that any test program will include at least one loose (D_r = 26 %), one medium dense (D_r = 56 %) and one dense (D_r = 70 %) sample tested under drained triaxial compression conditions.

Results were presented as error in ϕ_c versus number of tests for confidence levels of 75%, 85%, 90% and 95%. As the number of tests increased from 3 to 8, a sharp increase in accuracy was observed at all confidence levels. Hence it is recommended that any commercial testing program for evaluation of the critical state friction angle includes at least 6 tests (6 tests yielding an accuracy of ±1.0º from university quality data with 90% confidence). For academic purposes, where accuracy of ±0.5º with 90% confidence may be needed, more than 20 tests may be required.

Although the presented results were developed using one comprehensive academic testing program, their application to commercial data was encouraging. Although (unsurprisingly) the errors from the commercial dataset were slightly larger, the academic database provided a reasonable upper bound on likely achievable accuracy.

In conclusion, although soil type and gradation might be expected to affect sample uniformity during reconstitution and hence influence the repeatability (and hence accuracy) of the triaxial

testing program, distributing the triaxial tests over a wide range of initial D_r, or ideally initial ψ, should provide greater accuracy in ϕ_c for fewer tests.

Table 3 - 1 Confidence level, $|\Delta \phi_c|$, versus number of triaxial tests

Number of tests	3	4	5	6	7	8	9	10	11	12	13	14	15	16	17	18	19	20
Confidence Level (%) 95	1.67	1.42	1.28	1.16	1.06	0.98	0.93	0.89	0.86	0.85	0.82	0.81	0.80	0.76	0.73	0.69	0.66	0.62
90	1.46	1.22	1.09	1.00	0.88	0.84	0.80	0.77	0.75	0.73	0.71	0.70	0.69	0.67	0.64	0.61	0.57	0.54
85	1.31	1.08	0.97	0.87	0.79	0.75	0.71	0.70	0.67	0.65	0.64	0.63	0.62	0.60	0.58	0.55	0.52	0.49
80	1.18	0.98	0.88	0.77	0.71	0.69	0.65	0.63	0.61	0.59	0.58	0.57	0.57	0.55	0.53	0.50	0.48	0.45
75	1.06	0.87	0.79	0.70	0.64	0.62	0.59	0.58	0.55	0.54	0.52	0.52	0.52	0.50	0.48	0.46	0.44	0.41

Table 3 - 2 Confidence levels for 6 tests from the independent Been et al. (1991) dataset

Confidence Level (%)	75	80	85	90	95
Error $|\Delta \phi_c|$ (degrees)	1.22	1.29	1.39	1.96	2.00

Table 3 - 3 Summary of initial conditions for Been et al. (1991) triaxial tests

Test Name	Void ratio e	p' (kPa)	D_r (%)	ψ_0	D_{min}
CID G666	0.707	60	20.4	-0.055	-0.28
CID G665	0.687	130	29.2	-0.063	-0.295
CID G661	0.676	140	34.1	-0.073	-0.250
CID G662	0.675	60	34.5	-0.087	-0.381
CID G663	0.671	300	36.3	-0.066	-0.337
CID G761[1]	0.649	250	46.0	-0.091	-0.250
CID G664	0.630	300	54.4	-0.107	-0.400
CID G762[1]	0.601	250	67.3	-0.139	-0.450
CID G667	0.587	130	73.5	-0.163	-0.551

[1] The two tests G761 and G762 are performed on samples with over-consolidation ratio = 4
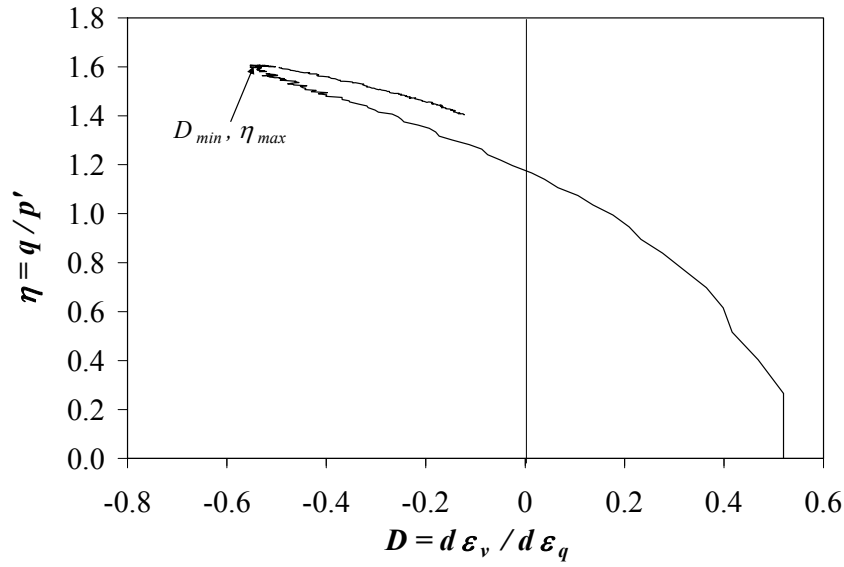
Figure 3 - 1 Stress-Dilatancy plot for test D-667 (Been et al., 1991) on Erksak sand
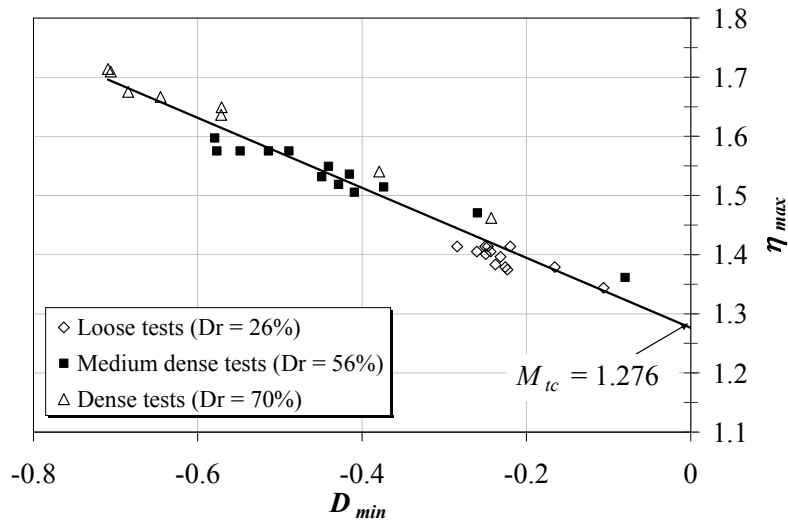
Figure 3 - 2 η_{max} vs. D_{min} of 34 triaxial compression tests on Erksak sand (after Vaid and Sasitharan, 1992)
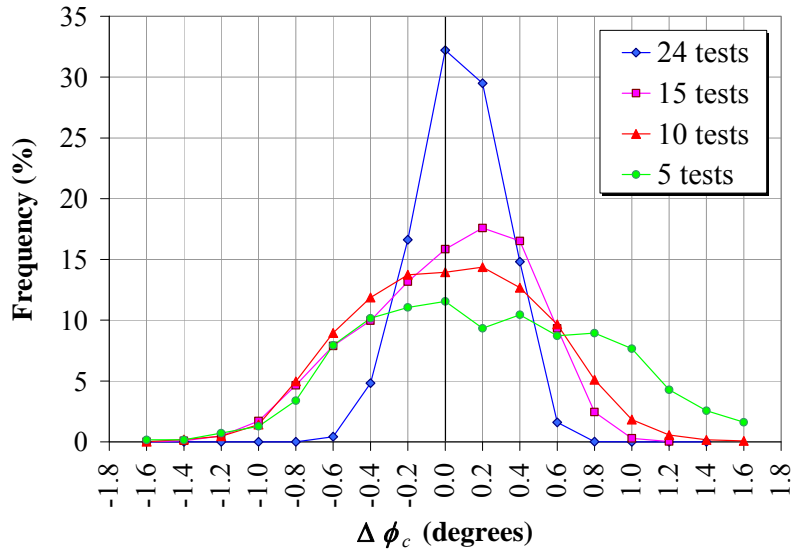
Figure 3 - 3 Frequency of error in ϕ_c for 5, 10, 15 and 24 tests
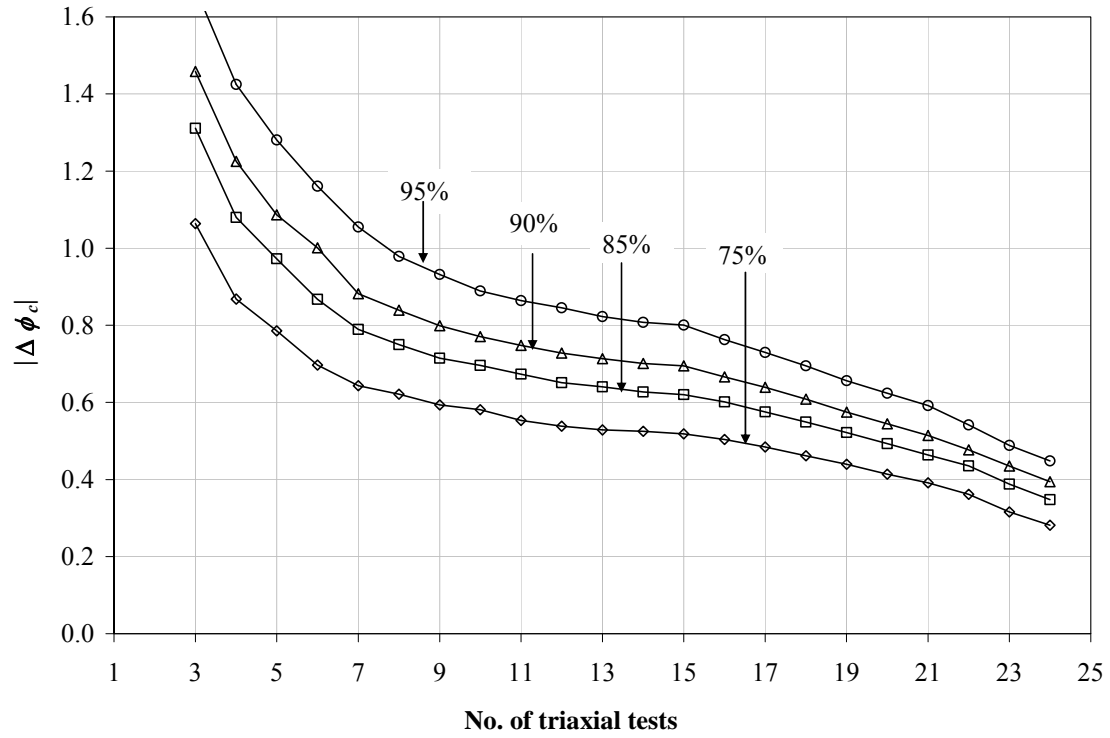
Figure 3 - 4 Error in ϕ_c vs. number of triaxial tests at different confidence levels
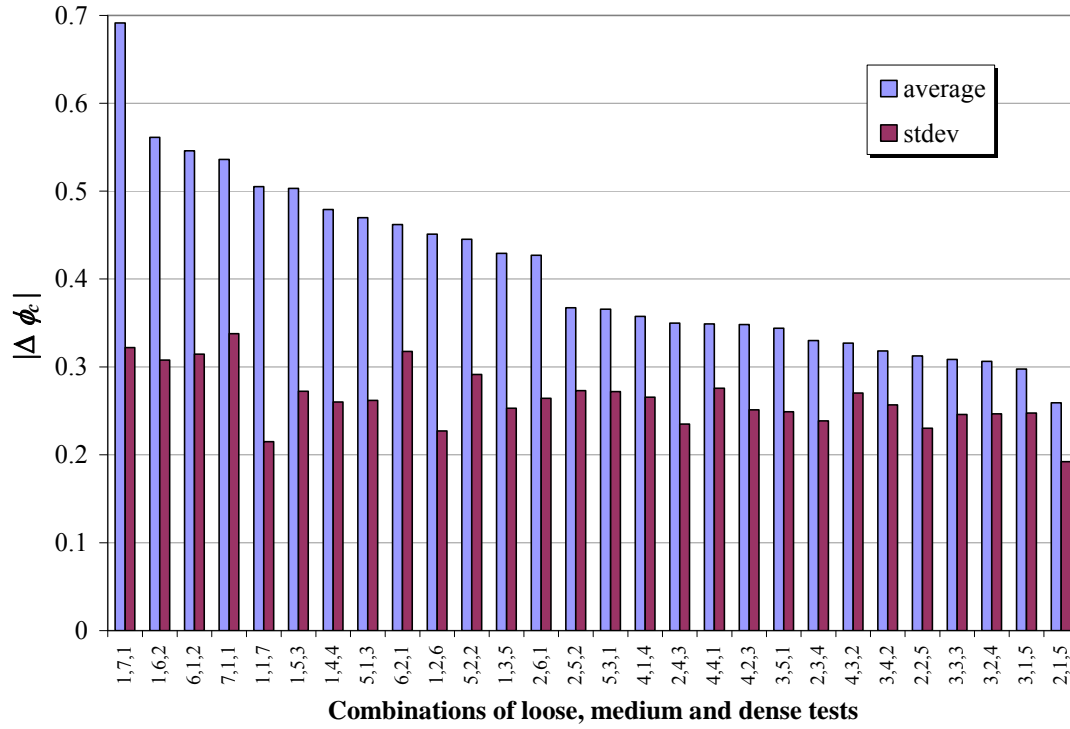
Figure 3 - 5 Error in calculation of ϕ_c obtained from 9 tests with different combinations of loose, medium and dense tests
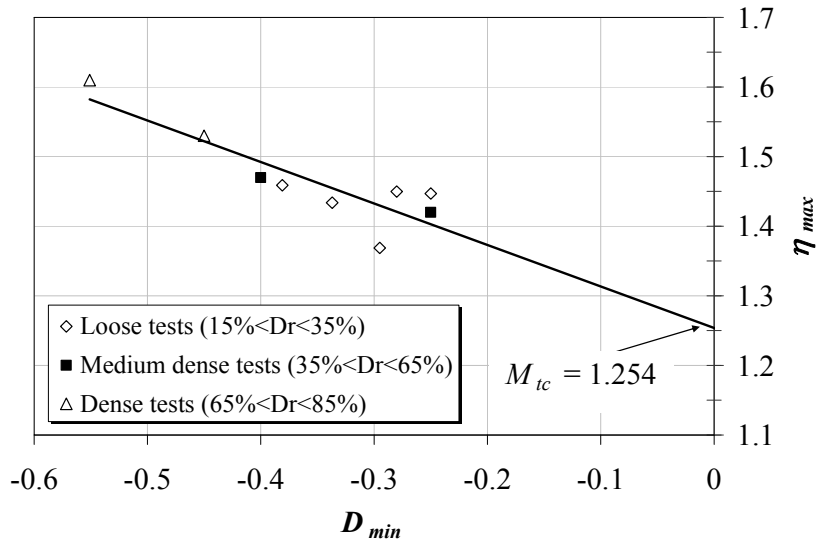
Figure 3 - 6 η_{max} vs. D_{min} of 9 triaxial compression tests on Erksak sand (after Been et al., 1991)

3.7.   References

Been K., and Jefferies M.G. 1985. A state Parameter for Sands. Géotechnique, 35(2): 99-112.

Been K., Jefferies M.G., and Hachey J.E. 1991. The Critical State of Sands. Géotechnique, 41(3): 365-381.

Bishop A.W. 1972. Shear strength parameters for undisturbed and remolded soil specimens. In Proceedings, Roscoe Memorial Symposium, Cambridge University. Edited by R.H.G. Parry. G.T. Foulis & Co. Ltd., Yeovil, U.K., 3–139.

Jefferies M.G., Stewart H.R., Thomson R.A.A., and Rogers B.T. 1985. Molikpaq Deployment at Tarsiut P-45. Proceeding of ASCE Specialty Conference on Civil Engineering in the Arctic Offshore, San Francisco, CA, 1-27.

Ghafghazi M., and Shuttle D.A. 2006. Accurate Determination of the Critical State Friction Angle from Triaxial Tests. Proceedings of the 59th Canadian Geotechnical Conference, Vancouver, 278-284.

Negussey D., Wijewickreme W.K.D., and Vaid Y.P. 1988. Constant Volume Friction Angle of Granular Materials. Canadian Geotechnical Journal, 25(1): 50-55.

Nova R. 1982. A Constitutive Model under Monotonic and Cyclic Loading. Proceedings of Soil Mechanics – Transient and Cyclic Loads, Pande and Zienkiewicz (eds.), Wiley, 343-373.

Rowe P.W. 1962. The Stress Dilatancy Relation for Static Equilibrium of an Assembly of Particles in Contact. Proceedings of the Royal Society of London, Series A, 269: 500-527.

Schofield A.N., and Wroth C.P. 1968. Critical State Soil Mechanics. McGraw-Hill, London. Download: http://www.geotechnique.info/ .

Vaid Y.P., and Sasitharan S., 1992. The Strength and Dilatancy of Sand. Canadian Geotechnical Journal, 29: 522-526.

Chapter 4.

Interpretation of Sand State from

CPT Tip Resistance[4]

4.1.   Introduction

The behaviour of cohesionless soils (sands, silts, tailings) strongly depends on their density. While relative density D_r is an almost universally used density index for sand, it is easy to show that it can be misleading (e.g. Tavenas, 1973). An alternative to D_r that captures both the effect of void ratio and the effect of mean stress on soil behaviour is the state parameter, ψ (Been and Jefferies, 1985). Different soils, or the same soil at different stress levels, display similar behaviour at the same value of ψ. However, determining the in-situ ψ (or D_r) in the laboratory is very difficult because of density changes during sampling – an "undisturbed" cohesionless sample is essentially impossible to obtain in normal engineering practice. Penetration tests have

---

[4] A version of this chapter has been published. Ghafghazi M., and Shuttle D.A. 2008. Interpretation of sand state from cone penetration resistance. Géotechnique, 58(8): 623–634.

thus become routine practice for testing cohesionless soils, with the modern electronic CPT offering continuous data measurement, and excellent repeatability and accuracy at relatively low cost.

The difficulty with any penetration test, however, is that the state measure of interest (e.g. D_r, ψ) is not measured. Instead it is deduced from the penetration resistance; a process usually referred to as interpretation. This interpretation involves solution of an inverse boundary value problem to obtain mechanical properties of the soil from test measurements. But the large deformations associated with the CPT, along with the nonlinear behaviour of the soil and complicated boundary conditions, make this analysis an extremely difficult task, and renders the solution non-unique. The interpretation framework is also difficult to establish. No simple closed-form solution for ψ or D_r has been developed from CPT; and, nobody - to date - has provided a full numerical simulation of drained penetration that matches calibration data, although several have tried (de Borst and Vermeer, 1982; Willson et al., 1988; van den Berg, 1994; Huang et al., 2004; and Ahmadi et al. 2005). Two different directions have emerged to deduce soil state from CPT data: calibration chamber tests and simplified theoretical treatments.

Calibration chambers are circular steel tanks typically about a metre in diameter and similar height. Sand is deposited at a known density and consolidated to the desired stress state within the tank. A cone penetration test is then performed along the vertical axis of the reconstituted specimen exactly as in natural ground. Each test provides a tip resistance q_c for the given value of density and applied stress. A large number of tests, covering the range of densities and stresses of interest, provide the relation between q_c, effective stresses (σ'_1, σ'_2, σ'_3), and the density (more usually expressed as ψ or D_r) for the tested material. The in-situ state ψ_0 is then

obtained from the CPT by comparison of field CPT q_c measurements at the estimated in-situ stresses, to the $q_c-p_0'-\psi_0$ relation determined in the calibration chamber.

The first CPT calibration chamber was built in 1969 at the Country Roads Board (CRB) in Australia (Holden, 1991). Chamber tests are now reported in the literature with differing dimensions, nature and form of control of boundaries, method of specimen reconstitution, and capability to handle saturated specimens. While improvements have been made to reconstitute more consistent specimens, most effort has been devoted to minimising and quantifying the influence of sample boundaries on the penetration resistance (e.g. Bellotti et al., 1982; Jamiolkowski et al., 1985; Been et al. 1987[a]; Mayne and Kulhawy, 1991; and Salgado, 1998). Chamber ratios, defined as the ratio of the chamber to cone diameter (D/d) of up to 200 have been proposed as the minimum ratios required to eliminate boundary effects on measured CPT tip resistance (Salgado et al., 1998).

A large body of calibration chamber data is available for clean sands, through decades of testing. These data show that the calibration is soil specific. This soil specific calibration is also affected by the stress history and, possibly, fabric. But, for most projects, it is not practical to conduct calibration chamber tests for the soil of interest at the different conditions expected to be encountered in the field. Thus, the case for an analytical method of CPT interpretation that can be calibrated for a specific soil based on easier laboratory tests seems compelling.

Robertson and Campanella (1983) first suggested that the difference between the CPT calibrations in various sands might be understood in terms of the intrinsic 'compressibility'. However, the compressibility measure was not defined. Subsequently, Been et al. (1987[a]) invoked the slope of the critical state line λ as the compressibility index. The basic problem with both of these approaches was that no mechanistic framework was offered.

Many simplified theoretical treatments have used spherical cavity expansion as an analogue of the penetration test on which to develop a mechanistic framework, essentially the same approach as used in conventional design of end bearing capacity of piles. The initial work by Bishop et al. (1945) and Hill (1950) addressed incompressible materials with associated flow rules, corresponding to the familiar and simple idealisation of the undrained behaviour of clay. Chadwick (1959) derived the pressure-expansion relation for a Mohr-Coulomb material with an associated flow rule, and further development of cavity expansion theory for non-associated flow has been considered by a number of workers including Carter et al. (1986) and Yu and Houlsby (1991). The central assumption of these studies has been that both the friction and dilation angles remain constant during shearing.

Although constant dilation and friction angles lead to analytical or semi-analytical solutions for cavity expansion, the idealisation has the fundamental deficiency that soil does not behave in such a manner – the nuances of soil behaviour being of first-order significance to realistic modelling of cavity expansion in soil. Realistic simulation of cavity expansion requires a stress-strain model that captures the evolution of dilatancy with accumulated strain and stress, as it is this behaviour that distinguishes one sand from another. The consequences of realistic modelling of dilatancy are magnified by the confinement of the cavity expansion. In more comprehensive evaluations 'good' soil models have been used allowing for plastic hardening, strain softening, etc.

Collins et al. (1992) provided the first realistic model for cavity expansion in soil using a state parameter based numerical analysis. Their results showed that the relation between normalised CPT tip resistance and ψ_0 was still affected by the stress level (as suggested by Sladen, 1989) and depended on material properties of the sand. Shuttle and Jefferies (1998) used a general

117

work hardening/softening critical state model to evaluate changes in CPT calibration in terms of critical state parameters M and λ that can be determined in routine triaxial testing of reconstituted specimens. These authors showed that CPT behaviour in Hilton Mines sand, currently the most unusual of the published calibrations, could be predicted based on Ticino sand data by allowing for the changes in fundamental soil properties between Hilton Mines and Ticino.

The analogy of the cone penetration to expansion of a sphere in soil is based on the existence of a limit cavity expansion pressure, although it has long been recognised that there is an inherent mismatch between spherical cavity expansion analysis results and those of calibration chamber tests. The magnitude of the mismatch is enlarged with the application of realistic models that capture the variable nature of strength and dilation angle. Their predecessors likely masked the mismatch by assuming constant friction and dilation angles. The difference between the spherical cavity analogy and the actual CPT geometry is usually accounted for by a *shape factor*. Shuttle and Jefferies (1998) showed that there is a one to one correspondence between the normalised tip resistance obtained from spherical cavity expansion and that obtained in chamber testing on Ticino sand. Cudmani and Osinov (2001) suggested a common shape factor for five different sands that is a function of the relative density corrected for stress level effects.

It is interesting that although particle breakage is known to occur at the high stresses usually induced during cone penetration, none of the preceding analyses explicitly model the effects of particle breakage on the limiting cavity pressure. Russell and Khalili (2002) incorporated one effect of particle breakage, a steepening of Critical State Locus (CSL) with increasing mean stress, into a cavity expansion analysis using a critical state based model. The effect of this change was a reduction in the limiting cavity expansion pressure, inferring an increase in the

shape factor required to match the chamber penetration resistance. Investigation into particle breakage is still in its infancy, with issues of changing stress-dilatancy due to energy dissipation during breakage yet to be resolved, and hence this effect is not explicitly modelled in this work. In this chapter spherical cavity expansion is applied to a database of nine soils including laboratory standard and natural sands, as well as relatively clean sand-size tailings for which both chamber testing and triaxial compression data are available in the literature. The soil behaviour is captured by the isotropically hardening - isotropically softening generalised critical state model, NorSand (Jefferies, 1993; Jefferies and Shuttle, 2002; and Jefferies and Shuttle, 2005), independently calibrated to triaxial tests. A unique relation between cavity expansion and calibration chamber normalised tip resistances, termed the *shape function* is identified for all database sands. This shape function is used to predict the calibration chamber results from spherical cavity expansion simulations with the same level of accuracy as observed in published experimental data. A framework for interpreting the state parameter from CPT tip resistance is then presented that eliminates the need to perform calibration chamber tests to obtain soil specific q_c–p_0'–ψ_0 correlations. Calibrations to triaxial testing determine material parameters that are then used in numerical analysis to predict the in-situ state, without sacrificing accuracy, and without resorting to expensive and difficult calibration chamber tests.

4.2. Background to CPT Interpretation in Sand

The CPT in sand provides just two outputs; the tip resistance and the sleeve friction (the penetration is drained so the pore pressure transducer simply measures the in-situ pore pressure). This is why most CPT data are interpreted in terms of one parameter alone, commonly relative

density, but sometimes peak friction angle. The state measure used in this work is the state parameter, ψ (Been and Jefferies, 1985). Because ψ is used as an internal state variable in the numerical model, the subscript '0' is used to denote the in-situ (or initial) value of ψ_0 under geostatic conditions to be consistent with the original usage by Been and Jefferies.

Initial work on determining ψ_0 from CPT data comprised triaxial testing of sands for which chamber test data were available to define the CSL of each sand, and then processing the chamber test data to develop dimensionless relations (Been et al., 1986, 1987[a]) of the form:

$$Q = k \, exp(- m\psi_0)$$
[Eq. 4 - 1]

Where Q is the tip resistance normalised by the initial mean effective stress, p'_0:

$$Q = \frac{q_c - p_0}{p'_0}$$
[Eq. 4 - 2]

The two coefficients k and m in Equation 4-1 differ from one sand to another.

Since all analytical methods of interpreting ψ_0 from CPT results must be verified against available calibration chamber data, the scatter in experimental results limits the accuracy of any interpretation method. Experimentalists have tried to measure reproducibility of calibration chamber results by repeating tests on specimens with exactly the same density and stress conditions. These efforts have resulted in $\pm$ 25% variability in measured Q in the most recent works (e.g. Hsu, 1999). However, the majority of available data suggest that $\pm$ 50% accuracy in measured repeatability of Q is 'good' quality data. Of course translating the accuracy in Q to the

accuracy in ψ_0 involves interpretation, but a rough estimate based on average k and m values for Ticino 4 sand (Shuttle and Jefferies, 1998) would suggest that $\pm\,0.05$ accuracy in ψ_0 is about the best accuracy that can be expected in predicting any particular test in the available calibration chamber data.

4.3.   Materials and Testing

The nine soils used in this research were chosen based on availability of reliable triaxial and calibration chamber test data. They include two natural sands, Da Nang and Erksak sands; four laboratory standard sands, Hokksund, Ottawa, Ticino and Toyoura sands; and two mine tailings, Syncrude oil tailings and Hilton Mines sand. Table 4-1 contains the index properties of these soils as reported by different researchers. The database includes median grain sizes of 160 to 1130 μm and rounded to angular grain shapes. Most calibration chamber tests are performed on dry specimens. There was little or no fine grained material in the soils, resulting in completely drained penetration even in cases where water was present in the chamber.

Triaxial compression tests were used to determine soil properties based on reconstituted specimens. Table 4-2 summarises the drained triaxial testing used to calibrate NorSand. In cases where undrained tests were available they were only used to determine the CSL in $e - \log p'$ space.

Previously published calibration chamber tests performed between 1974 and 1998, and summarised in Table 4-3, have been used to illustrate the utility of this approach. Although some over-consolidated chamber tests were available, this work focuses on the normally consolidated tests.

rs between 0.9 and 1.5 to the tip resistance q_c. This correction generally falls midrange between those of Jamiolkowski et al. (1985) and Mayne and Kulhawy (1991).

4.4. Constitutive Model

The reason to use a 'good' sand model for cavity expansion analysis is that, in general, part of the soil domain will be critical, other parts strongly dilating, and other parts contractive; with the exact behaviour being a function of the soil's position relative to the cone tip. Accordingly, it is helpful to look at the computed behaviour of the sand before examining the computed limiting pressures as a function of initial state.

The constitutive model adopted is NorSand, an isotropically hardening - isotropically softening generalised critical state model that captures a wide range of particulate soil behaviour. The version used is that for general 3-D stress states with constant principal stress direction as described in Jefferies and Shuttle (2002) but with a further extension to improve accuracy. A feature of the original version of NorSand was a volumetric coupling parameter N for stress-dilatancy. Subsequently, Jefferies and Shuttle (2002) suggested that N could be eliminated from the model since $N\chi \approx 1$ (based on average values of a large quantity of triaxial tests on different sands). However, individual soils demonstrate a variety of $N\chi$ values and some accuracy is given up by following this suggestion. The N model parameter neither increases the complexity of the model, nor constitutes additional effort in calibration of the model, as N is obtained with

M_{tc} from the stress-dilatancy plot and reintroduction of this parameter resulted in better replication of the soil behaviour. For the current work 'N' was obtained from the post-peak stress-dilatancy plot (see Figure 4-1), rather than the slope of the line passing through peak points of the stress-dilatancy plot, and hence is referred to as N^* in the remaining text.

Like most elasto-plastic models, NorSand has four basic aspects: a yield surface; a work hardening law; a plastic flow rule (stress-dilatancy); and, elasticity. Many material parameters in NorSand will be familiar from Cam Clay. Three parameters describe the critical state, these being the critical friction ratio M_{tc} (the tc denoting the reference triaxial compression condition and allowing M to vary with lode angle, θ) and Γ, λ which describe the CSL for the semi-log idealisation used. There are two parameters relating to the plastic behaviour: χ_{tc} and H. The property χ_{tc} scales the maximum dilatancy to ψ. In some ways this is similar to specifying a relation between peak strength and ψ. The dimensionless hardening modulus H is required because the state parameter approach de-couples the yield surface from the CSL and hence the slope of the CSL no longer acts as a plastic compliance. A finite elastic shear modulus G is also adopted. The rigid-plastic idealisation in shear used by Cam Clay is both unrealistic, and inconvenient for use with numerical methods. Various forms of elasticity can be used within the same framework. For the current work both elastic parameters G and ν are assumed to be constant during the test. Although G is treated as a soil property, the sensitivity of the modulus to soil fabric argues in favour of elastic modulus perhaps being viewed as a further state measure rather than as a property. To preserve the dimensionless nature of NorSand, it is convenient to specify G in terms of the dimensionless rigidity I_r ($= G/p'_0$).

Despite compressibility having an important influence on CPT resistance (Robertson and Campanella, 1983), similar to most constitutive models, compressibility is not represented

within NorSand by a single material property. Both plastic and elastic compressibility play an important part in the limiting spherical cavity pressure. Plastic compressibility is incorporated in NorSand primarily through the parameters λ (also used as a compressibility metric by Been et al., 1987[a]) and H. Elastic compressibility is equally important to the cavity resistance, although often neglected in the CPT literature, and is specified in NorSand as the rigidity I_r.

4.5.   Calibration of NorSand

The aim in calibrating NorSand to a particular soil is to obtain a consistent set of material parameters that adequately represents that soil's behaviour over the range of pressures and states. Hence the goodness of fit for any individual test is, by necessity, compromised to obtain a better representation of the overall soil response. This calibration process is summarised below; the reader is directed to Jefferies and Shuttle (2005) for a more detailed discussion of the calibration procedures.

Determining the soil's critical state is independent of the NorSand model, as any critical state model will have the same parameter set. For the semi-log idealisation of the CSL, a best-fit line is put through the critical states judged from high strain results on loose samples as shown in Figure 4-2 for Ticino 4 sand. Figure 4-3 compares all the CSLs for the nine investigated soils. As illustrated in Figure 4-1, N^* and M_{tc} are obtained from the slope and intercept of the post peak portion of the stress-dilatancy plot for each triaxial test (Ghafghazi and Shuttle, 2006). Average values are then chosen to represent the overall soil behaviour.

The plasticity parameter χ, was also derived from η -D plots, this time plotting dilation at peak stress ratio from Figure 4-1 against the state parameter at the image condition at the same point

d NorSand

parameters for all nine soils.

As the sand properties were taken from the literature, elastic shear modulus was obtained in a variety of ways (see Table 4-4). Bender element measurements in the triaxial samples were used to measure G for Hokksund, Ottawa, Syncrude, Ticino and Toyoura sands. Consolidation measurements of unload-reload were used to infer elasticity for Erksak sand. No measurement of elasticity was made for Hilton mines tailings and Da Nang sand. Da Nang sand elasticity was estimated by curve-fitting to the triaxial tests. For Hilton mines, G was assumed to be similar to Toyoura sand.

4.6.   Spherical Cavity Expansion Analysis

The spherical cavity expansion analogy idealises the CPT as a cavity in an infinite uniform medium under an isotropic stress state, with the internal pressure of the cavity initially equal to the in-situ mean effective stress p'_0. The cavity is expanded by monotonically increasing its radius until a limiting (constant) pressure is obtained, this being the pressure of interest. This idealisation greatly simplifies the analysis because the spherical symmetry allows only radial displacements and in turn this permits a one-dimensional description of the problem. The corresponding stresses are a radial and two equal hoop stresses.

The spherical cavity finite element code used by Shuttle and Jefferies (1998), modified to incorporate changes to the NorSand model, is used in this study. The underlying code and finite element mesh remained the same, hence retaining the verified large displacement performance of the code. The one-dimensional problem was analysed using 70 elements, with a single stress sampling location at the centre of each element. The problem has no intrinsic measure of scale and so, for convenience, the original cavity radius was set to unity. The outer boundary was set as a zero displacement node at a distance of 500, chosen to avoid artefacts of boundary conditions. To capture the rapid variation of stress close to the cone, the element spacing was set to logarithmically increase with distance from the cavity. Similarly, a second-order numerical difference was used to extrapolate the element stresses to the cavity wall to accurately capture the high stress gradients present in the vicinity of the cavity.

4.7. Numerical Formulation

The soil response during spherical expansion obviously depends on the initial state of the sand. To observe the key aspects of this behaviour, cavity expansion from a dense initial state may be considered. And, because computation starts from "at rest" conditions, the behaviour of an element close to the cavity wall is typical because there is no intrinsic scale in the analysis. Figure 4-5a illustrates the stress path of an element of Ticino 4 sand initially at 74 *kPa* effective stress and with an initial void ratio of 0.596, corresponding to ψ_0 = -0.285 based on the CSL from Table 4-4. Even though spherical cavity expansion is often referred to as being analogous to triaxial conditions, the stress path really amounts to a rapid excursion from isotropic conditions to the Mohr-Coulomb envelope followed by dilation up the envelope (which is

curved because it is a function of the state parameter which decreases as the sand dilates to critical conditions at a shear strain of more than 50%).

The state path of the sand is shown in Figure 4-5b. Note that the sand moves up the CSL as the critical state is approached because the cavity has not reached its limiting expansion pressure at the time this particular element achieves criticality, and so the element tracks down the CSL as the confining stress increases.

4.8.   Comparison to Calibration Chamber Data

In the current work the soil parameters for every calibration chamber test may be calculated knowing p'_0 and e, and by inference ψ_0. Each chamber test is modelled and the limit cavity pressure is calculated at 500% strain. The cavity pressure, being analogous to CPT q_c, is then normalised by the initial mean stresses using Equation 4-2 to obtain Q_{sph}. The results are then plotted versus ψ_0 as illustrated in Figure 4-6 for Ticino 4 sand. In order to compare the results with those obtained in calibration chamber testing, normalised tip resistance Q_{cc} for the Ticino 4 calibration chamber tests are also plotted on the same figure. It can be seen that Q_{cc} results are significantly higher than Q_{sph}. This mismatch is observed for every soil in the dataset and is quantified using a shape function.

While the ratio between normalised tip resistances (Q_{cc} / Q_{sph}) is a function of ψ_0, plotting Q_{cc} versus Q_{sph} in Figure 4-7 suggests that for Ticino sand there is a one on one correlation between them (termed the *shape function*) irrespective of ψ_0 or the stress level. Figure 4-7 shows that 91% of the data fall within the two dashed boundary lines at ±70% of the average trendline defined by Equation 4-3:

$$Q_{cc} = 0.7 \left(Q_{sph} \right)^{1.7}$$ [Eq. 4 - 3]

This accuracy is close to the repeatability of Q typically achieved in calibration chamber testing itself. Hence a large part of the scatter in Figure 4-7 stems from the scatter in calibration chamber data itself, which is the maximum accuracy achievable by any analytical approach. Plotting Q_{cc} versus Q_{sph} for all of the database soils in Figure 4-8 shows that the shape function defined by Equation 4-3 appears independent of the soil type for all of the nine normally consolidated clean sand-size soils considered. Interestingly, all these soils fall within the boundary lines drawn for Ticino 4 sand, with essentially the same overall confidence level of 89%, suggesting that no extra error has been introduced by comparing different soils.

4.9.   Inverse form for Interpretation of CPT

Shuttle and Jefferies (1998) showed that Equation 4-1 may be used to recover ψ_0 from calibration chamber data provided k and m are functions of soil characteristics and the stress level. Using a spherical cavity expansion analysis, we can summarise the effect of different soil characteristics as NorSand parameters in the following equation:

$k_{sph} = f_1(G/p'_0,\ M_{tc},\ N,\ H,\ \chi, \lambda, \nu)$ [Eq. 4 - 4a]

$m_{sph} = f_2(G/p'_0,\ M_{tc},\ N,\ H,\ \chi, \lambda, \nu)$ [Eq. 4 - 4b]

where k_{sph} and m_{sph} are introduced as the spherical cavity expansion equivalents to k and m in Equation 4-1.

All the NorSand parameters in Equation 4-4 are constants, or known functions of e and p'. At a particular ψ_0 all the variables in Equation 4-4 take a single value derived from Table 4-4 except for G/p'_0 (the stress level effect) as illustrated for Ticino 4 sand in Figure 4-9. Hence the trend of k_{sph} and m_{sph} with ψ may be determined for a single value of G/p'_0 from Q_{sph} using Equation 4-4. This analysis is then repeated with different values of G/p'_0. By plotting the computed k_{sph} and m_{sph} as functions of G/p'_0, as illustrated for Ticino 4 sand in Figure 4-9, the complete functions are recovered. Values of k_{sph} and m_{sph} as functions of G/p'_0 are given for all nine investigated sands in Table 4-5.

For each calibration chamber test, having Q_{sph} determined from Equation 4-3, and k_{sph} and m_{sph} from the equations in Table 4-5, one can infer the initial state parameter of the chamber sample from Equation 4-5 which is directly deduced from writing Equation 4-1 for spherical cavity expansion:

$$\psi_0 = \frac{-\ln\left(Q_{sph}\middle/ k_{sph}\right)}{m_{sph}}$$

[Eq. 4 - 5]

The inferred ψ_0 is plotted versus the one obtained by experimentally measuring the void ratio in Figure 4-10.

Two boundary lines are drawn beside the line of equivalency in Figure 4-10, presenting ±0.04 and ±0.07 error margins. Table 4-6 summarises the number of tests with ψ_0 calculated within these error margins, as well as the level of confidence that the method can predict ψ_0 within both error margins.

From 301 calibration chamber tests investigated in this work, 66 predictions produced a $\Delta\psi_0$

129

error of more than 0.04 and only 24 tests predicted $\Delta\psi_0$ of more than ±0.07, equivalent to confidence levels of 78% and 92% respectively. However, the method did not produce equal accuracy for all sands. Ottawa, Toyoura 160 and Syncrude Oil Tailings showed excellent prediction. Da Nang and Ticino yielded an accuracy close to the average. Lower accuracy was obtained with Hokksund, Hilton Mines and Erksak sands.

Hokksund calibration chamber data was collected from different sources and had the greatest scatter in Q - ψ_0 among the database soils. As a result of this scatter in the raw data this sand yields a poor ψ_0 prediction. The second "problem" sand, Hilton Mines, has long been known for being the most compressible among those tested in calibration chambers. The poor ψ_0 prediction for Erksak sand is less well understood, but may have resulted from the consolidation unload-reload loops under-predicting the elastic stiffness. In addition, Erksak sand had the highest fines content of any of the sands considered here. The presence of fines can make sample uniformity much more difficult to achieve. This can in turn reduce the repeatability of the tests and affect the accuracy of the predictions. Eliminating these three soils from the database would improve predictions to 84.3% confidence of $\Delta\psi_0$ less than ±0.04 and 97.2% less than ±0.07.

4.10. Discussion

The CPT is an important and widely used test, with particular relevance for cohesionless soils. However, theoretical understanding of the test has not matched its widespread use. In part this is because detailed simulation of the CPT presents a substantial challenge in mechanics. The present work adopted an intermediate step, using the analogy of limit pressure in spherical cavity expansion to CPT tip resistance. Cavity expansion allows fast numerical computation of

limit pressure, with a large strain approach and using sophisticated soil models. Of course, a central question then follows: how close is the cavity expansion analogy to the real CPT. This issue was dealt with by introducing a shape function; defined by Equation 4-3. This shape function incorporates the spherical to true geometry scaling, as well as model simplifications including neglecting particle breakage and use of constant elasticity. A central finding of the present work is that this shape function is the same for all nine soils evaluated, from which we can infer that the shape function is unique since the sands involved cover a reasonable range of properties.

The finding of a unique shape function should not be influenced by the constitutive model adopted (e.g. Cudmani and Osinov, 2001), although the state parameter is central. Advanced plasticity models for soil with density independent parameters are, to date, almost invariably based on the state parameter (e.g. Manzari and Dafalias, 1997; Wan and Guo, 1998; Li et al., 1999; Gajo and Wood, 1999). Their properties are also similar – for example, the semi-log idealisation for the CSL is verging on ubiquitous and leads to Γ, λ being common. Similarly, the concept of a critical friction ratio (angle) has been uncontroversial for at least half a century. Plastic hardening, which will have a model-dependent parameter scaling it, is central to any work hardening idealisation – so, although a different parameter to H occurs with the various models, these hardening parameters have a similar role and can be expected to affect the computed results as much as H does. As for elasticity, an isotropic shear modulus will be the default starting point for any elasto-plastic model.

A unique function means that spherical cavity solutions using a 'good' soil model (i.e. one whose parameters are density independent) can provide the framework for estimating ψ_0 from the CPT q_c data for any cohesionless soil. But this misses an important opportunity. Although

more practical than calibration chamber testing, the dependence of the inversion from q_c to ψ_0

on soil properties is inconvenient since properties change from one stratum to the next and it is

clearly desirable to avoid a suite of triaxial tests for each soil type in a CPT profile. There is an

opportunity to minimise supporting laboratory testing by using additional information measured

by the CPT – for example, friction sleeve data are widely used as a basis to infer soil type.

Plewes et al. (1992) suggested that at least λ might be estimated this way. Looking to the future,

the success of the spherical cavity analogy presented here should be viewed as the starting point

for proper understanding of the CPT. Although difficult, detailed modelling of actual CPT

penetration in NorSand (or similar theoretical soil) will allow understanding of how H, λ etc.

can be related to sleeve friction – markedly improving the available precision in inferring ψ_0 in

practical situations.

Turning to accuracy in estimating ψ_0, the spherical approach is shown to provide excellent

resolution for six of the nine sands investigated. The question then becomes, how can resolution

be improved for all soils? Hokksund sand appears to provide poor predictions due to the

variability in its calibration chamber database, rather than any systematic failing in the

approach. This calibration chamber variability is illustrated on Figure 4-6 for Ticino 4 where the

recorded CPT resistance for Tests E139 and I169 differ by more than a factor of 2, but the tests

have virtually identical initial conditions in terms of stress state, geostatic stress ratio (K_0), and

void ratio. Hilton Mines tailings sand also shows no systematic bias in error over the range of

ψ_0. Looking at Table 4-6 one can see that the soils yielding the best accuracy in ψ_0 are those

with bender elements measurements of the elastic shear modulus G (i.e. Ottawa, Syncrude, and

Toyoura). High quality G measurement has shown that G can easily vary by ± 50% because of

sample preparation all else equal (Bellotti et al., 1982). Hence the lack of repeatability seen in

the chamber test data could credibly be caused by changes in G from one calibration chamber experiment to the next, even under ostensibly similar situations. Shuttle and Jefferies (1998) suggest a factor of $\pm\ 50\%$ on G will produce about $\pm\ 0.03$ on ψ_0, which is about half the residual uncertainty. Therefore it is strongly recommended that G be measured to eliminate an unnecessary error in evaluation of the in-situ state parameter.

It is well known that both fabric and ageing affect the soil response. Hence while critical state parameters are independent of fabric, and can be determined from triaxial testing, and G may be measured in-situ using the seismic CPT; hardening modulus H will likely vary between the lab and the field. Despite this, inspection of Table 4-2 and Table 4-3 suggests that differing reconstitution methods in calibration chamber and triaxial tests did not significantly reduce the accuracy of the inversion for ψ_0. Hence one might expect reasonable state predictions in-situ.

4.11.   Summary and Conclusion

A framework for evaluation of in-situ soil state parameter ψ_0 from CPT q_c data has been developed based on a spherical cavity expansion analogue. Central to the approach is a shape function that relates the normalised spherical and calibration chamber limiting pressure.

A database of nine normally consolidated soils, including laboratory standard and natural sands as well as tailings materials, was compiled for which both calibration chamber tests and triaxial tests were available. The NorSand critical state soil model was calibrated for each of the nine soils using the triaxial data. Spherical cavity expansion analysis was then performed for 301 normally consolidated calibration chamber tests and the results compared with those obtained experimentally. All nine soils followed the same trend with a scatter equivalent to that observed

for the most intensely tested calibration chamber sand, Ticino. A unique and consistent shape function between the normalised experimental CPT and spherical cavity limit pressures was identified. The shape function was shown to be insensitive to soil type and density.

Estimation of accuracy of the proposed framework is constrained by the repeatability seen in the calibration chamber data. For known soil properties (from triaxial compression tests) the soil specific k and m relation recovers q_c to near perfect accuracy, and without bias. Individual calibration chamber results cannot be recovered to this accuracy, but that appears a consequence of the intrinsic variability in the calibration chamber data. Consequently, it was shown that the normalised cone resistance can be analytically reproduced with an accuracy of ±70% to 89% confidence.

The spherical analysis results were then used to back calculate ψ_0 using Equation 4-5 for all 301 chamber tests and the resulting states compared to those measured in the lab. The method predicted ψ_0 to within ±0.04 with 78% confidence and to within ±0.07 with 92% confidence.

Two sources of error were explicitly identified; inherent variability in the calibration chamber testing and elastic modulus. Clearly no analytical method can predict ψ_0 with accuracy higher than the repeatability of the calibration chamber data set itself, and this inherent variability between calibration chamber tests likely accounts for about half the observed error. For Ticino sand the estimated error in interpreted ψ_0 due to variations in G was estimated as up to ±0.03. Hence, it is recommended that G be measured in-situ to eliminate an unnecessary source of error.

Table 4 - 1 Index properties of studied sands and tailings

Property \ Sand/Source	Da Nang: Hsu, 1999	Erksak 355/3.0: Been et al., 1987 [b]	Hilton Mines tailings: Been et al., 1987 [a]	Hokksund: Been et al., 1987 [a]	Ottawa: Been et al., 1987 [a]	Syncrude Oil Tailings: Golder Associates, 1987 [a]	Ticino 4: Been et al., 1987 [a]	Ticino 9: Golder Associates Report, 1987 [b]	Toyoura 160: Fioravante et al., 1991
Mineralogy	Quartz, minor amounts of chert	Quartz, minor amounts of chert	Quartz, some feldspar, muscovite, mica, heavy minerals	Feldspar, Quartz, some mica	Quartz	Quartz Small amount of bitumen as discrete gravel sized lumps	Quartz Trace of Mica	Assumed to be similar to that of Ticino 4 sand	Mainly Quartz, 3% chert
Median grain size D_{50}: μm	1130	355	200	390	530	207	530	530	160
Effective grain size D_{10}: μm	680	180	110	210	350	-	360	-	-
Uniformity coefficient	1.84	2.2	2.0	2.0	1.7	1.9	1.6	-	1.5
Percentage passing no. 200 sieve	0	3-6	2.5	0	0	3.5	0	0	0
Specific gravity of particle	2.61	2.65	3.02	2.70	2.66	2.64	2.70	2.67	2.65
Average sphericity	-	0.75	0.72	0.77	0.83	-	0.79	-	-
Average roundness	-	-	0.23	0.32	0.55	-	0.38	-	-
Grain description	sub-angular to angular	Sub-rounded	Angular	Sub-angular	Rounded	Angular to sub-angular, mostly cubical	Sub-rounded	-	Sub-angular
Maximum voids ratio e_{max}	0.808	0.963	1.05	0.91	0.79	0.898	0.89	0.90	0.977
Minimum voids ratio e_{min}	0.515	0.525	0.62	0.55	0.49	0.544	0.60	0.60	0.605

Table 4 - 2 Summary of drained triaxial compression tests used in calibration of NorSand

Sand	Reference	Number of tests	Sample preparation	Range of void ratio	Range of mean stress p_0' (kPa)
Da Nang	Hsu, 1999	15	Wet pluviated	0.56-0.66	50-400
Erksak 355/3.0	Been et al., 1987[b]	4	Moist tamped	0.54-0.63	50-400
Hilton Mines	Golder Associates, 1985	6	Moist tamped	0.71-0.87	80-1000
Hokksund	Norwegian Geotech. Inst.,1982	15	Unknown	0.51-0.72	34-233
Ottawa	Golder Associates, 1985	6	Moist tamped	0.53-0.74	50-220
Syncrude Oil Tailings	Golder Associates, 1987[a]	5	Wet pluviated	0.53-0.71	100-500
Ticino 4	Golder Associates, 1986	5	Moist tamped	0.65-0.85	100-200
Ticino 9	Golder Associates, 1987[b]	5	Dry pluviated	0.64-0.81	50-300
Toyoura 160	Golder Associates, 1989	14	Wet pluviated	0.61-0.84	33-1000

Table 4 - 3 Summary of calibration chamber tests on normally consolidated soils

Sand	Reference	No. of tests	BC[1]	Sat.	Chamber ratio D/d	Sample prep.	void ratio e	p_0' kPa	Chamber descrip.
Da Nang	Hsu, 1999	38	BC5	Dry	22.1, 44.2	Dry pluv.	0.56-0.73	33-150	Hsu & Huang, 1998
Erksak 355/3.0	Been et al., 1987[b]	14	BC4	Sat.	38	Moist tamped	0.53-0.66	25-300	Been et al., 1987[b]
Hilton Mines	Harman, 1976	20	BC1, BC3	Dry, Sat.	34.2	Dry pluv.	0.65-0.95	30-180	Laier et al., 1975
Hokksund	Parkin et al., 1980; Baldi et al., 1986; Been et al., 1987[a]	51	BC1, BC3	Dry	33.6-48	Dry pluv.	0.58-0.87	25-370	Bellotti et al. ,1982; Chapman, 1974
Ottawa	Harman, 1976	30	BC1, BC2	Dry, Sat.	34.2	Dry pluv.	0.54-0.73	30-200	Laier et al., 1975
Syncrude Oil Tailings	Golder Associates, 1987[a]	8	BC4	Sat., moist	38	Wet pluv. Moist tamped	0.55-0.70	30-400	Been et al., 1987[b]
Ticino 4	Baldi et al., 1986	90	BC1, BC2, BC3, BC4	Dry	33.6	Dry pluv.	0.50-0.90	50-500	Bellotti et al., 1982
Ticino 9	Golder Associates, 1987[b]	9	BC4	-	38	-	0.63-0.88	30-315	Been et al., 1987[b]
Toyoura 160	Iwasaki et al., 1988; Fioravante et al., 1991	39	BC1, BC2, BC3	Dry, Sat.	22.1-120	Dry pluv.	0.64-0.85	30-177	Iwasaki et al., 1988; Bellotti et al., 1982

[1] Boundary conditions: BC1, constant stress side and base restraints; BC2, constant volume side and base restraints; BC3, constant volume side restraint, constant stress base restraint; BC4, constant stress side restraint, constant volume base restraint (Salgado et al., 1998); BC5, servo-controlled side restraint, constant volume base restraint.

Table 4 - 4 NorSand parameters for nine CPT calibration chamber sands

Parameter	CSL			Plasticity			Elasticity[1]	
	Γ	λ_e	M_{tc}	N^*	H	χ	I_r	ν
Da Nang	0.99	0.0317	1.25	0.35	$40\text{-}220\,\psi_0$	4.3	$300\text{-}2000\,\psi_0$ From fitting to triaxial data	0.2
Erksak 355/3.0	0.834	0.019	1.25	0.32	$100\text{-}400\,\psi_0$	3.8	$\dfrac{195}{\left(e-e_{min}^*\right)} \times \left(\dfrac{p'}{p_{ref}}\right)^{-0.50}$ After Jefferies and Been (2006) $=0.355$ is the void e_{min}^* ratio at which volumetric compressibility becomes zero.	0.2
Hilton Mines	1.315	0.0738	1.40	0.20	50	3.5	Equal to Toyoura 160	0.2
Hokksund	0.934	0.0235	1.00	0.40	$138+513\,\psi_0+2250\,\psi_0^2$	4.0	$\dfrac{720}{e^{1.30}} \times \left(\dfrac{p'_0}{p_{ref}}\right)^{-0.54}$ After Lo Presti et al. (1992)	0.2
Ottawa	0.754	0.0122	1.24	0.45	$180\text{-}400\,\psi_0$	4.0	$\left(\dfrac{2.66+e}{1+e}\right) \times \left(38.1-25.9e\right)^2$ $\times \left(\dfrac{p'_0}{p_{ref}}\right)^{-0.48}$ After Robertson et al. (1995)	0.2
Syncrude, Oil Tailings	0.890	0.0283	1.27	0.28	$43\text{-}296\,\psi_0 + 1927\,\psi_0^2$	5.8	$\left(\dfrac{2.64+e}{1+e}\right) \times \left(31.1-18.8e\right)^2$ $\times K_0^{0.26} \times \left(\dfrac{p'_0}{p_{ref}}\right)^{-0.48}$ After Cunning et al. (1995)	0.2
Ticino 4	0.986	0.0243	1.27	0.40	$70\text{-}200\,\psi_0$	3.0	$\dfrac{650}{e^{1.3}}\left(\dfrac{p'_0}{p_{ref}}\right)^{-0.52}$ After Shuttle & Jefferies (1998)	0.2
Ticino 9	0.970	0.0217	1.33	0.40	$60\text{-}350\,\psi_0$	3.8	Equal to Ticino 4	0.2
Toyoura 160	0.983	0.019	1.28	0.41	100	4.4	$878 \times \dfrac{(2.17-e)^2}{1+e}\left(\dfrac{p'_0}{p_{ref}}\right)^{-0.47}$ After Chaudhary et al. (2004)	0.2

[1] p_{ref} is equal to 100 kPa or equivalent

Table 4 - 5 Equations for k_{sph} and m_{sph} as functions of G/p'_0 for database soils

Sand	k_{sph}	m_{sph}
Da Nang	$5.52 + 0.0007 \, G/p'_0$	$4.50 + 0.465 \ln(G/p'_0)$
Erksak 355/3.0	$6.42 + 0.58 \ln(G/p'_0)$	$0.86 + 0.79 \ln(G/p'_0)$
Hilton Mines	$3.19 + 0.90 \ln(G/p'_0)$	$2.68 + 0.081 \ln(G/p'_0)$
Hokksund	$15.0 - 1.31 \ln(G/p'_0)$	$-5.37 + 1.78 \ln(G/p'_0)$
Ottawa	$8.05 + 0.66 \ln(G/p'_0)$	$1.26 + 0.733 \ln(G/p'_0)$
Syncrude Oil Tailings	$11.21 - 0.51 \ln(G/p'_0)$	$-2.62 + 1.75 \ln(G/p'_0)$
Ticino 4	$5.27 + 0.56 \ln(G/p'_0)$	$2.62 + 0.316 \ln(G/p'_0)$
Ticino 9	$8.74 + 0.0006 \, G/p'_0$	$2.07 + 0.59 \ln(G/p'_0)$
Toyoura 160	$10.47 - 0.10 \ln(G/p'_0)$	$2.15 + 0.50 \ln(G/p'_0)$

Table 4 - 6 Summary of $\Delta\psi_0$ obtained for nine database soils

Sand	Total Number of tests	Number of tests with $\Delta\psi_0 > 0.04$	Number of tests with $\Delta\psi_0 > 0.07$	Confidence Level that $\Delta\psi_0 < 0.04$	Confidence Level that $\Delta\psi_0 < 0.07$
Da Nang	38	11	2	71.1 %	94.7 %
Erksak 355/3.0	14	6	2	57.1 %	85.7 %
Hilton Mines	20	11	5	45.0 %	75.0 %
Hokksund	51	15	11	70.6 %	78.4 %
Ottawa	30	1	0	96.7 %	100.0 %
Syncrude Oil Tailings	8	1	0	87.5 %	100.0 %
Ticino 4	90	16	3	82.2 %	96.7 %
Ticino 9	9	3	1	66.7 %	88.9 %
Toyoura 160	41	2	0	95.1 %	100.0 %
Sum	**301**	**66**	**24**	**78.1 %**	**92.0 %**
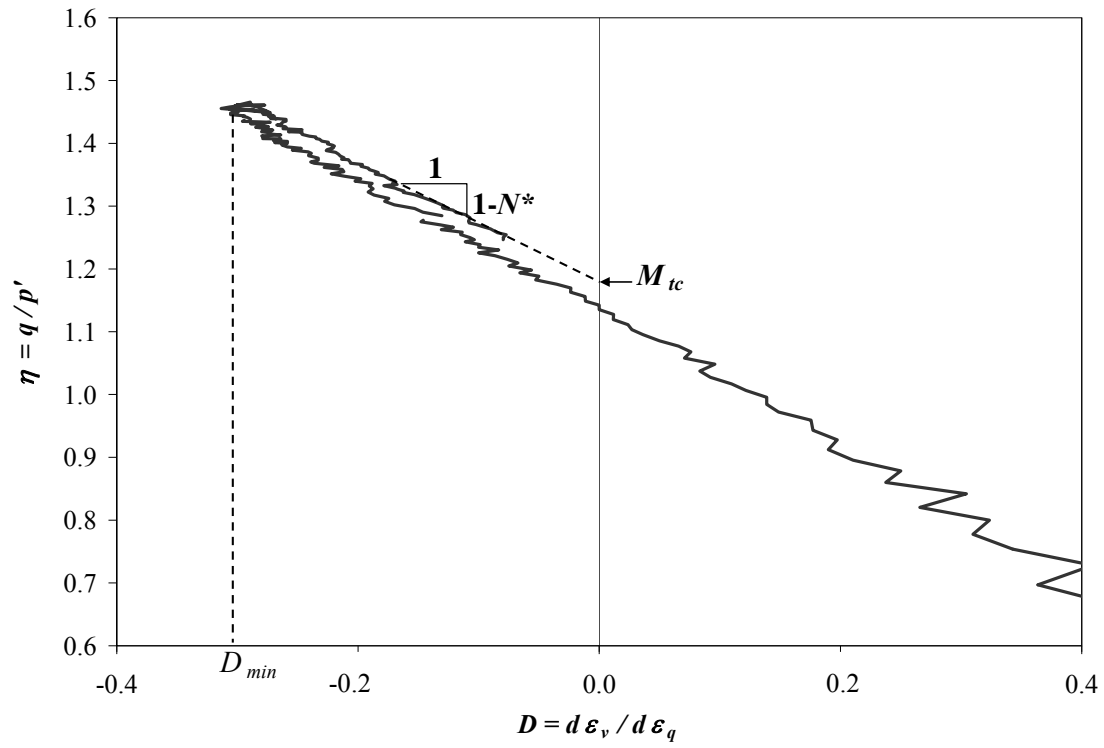
Figure 4 - 1 Stress-dilatancy plot (η - D) to obtain M_{tc} and N^* (Ticino 4, C264)
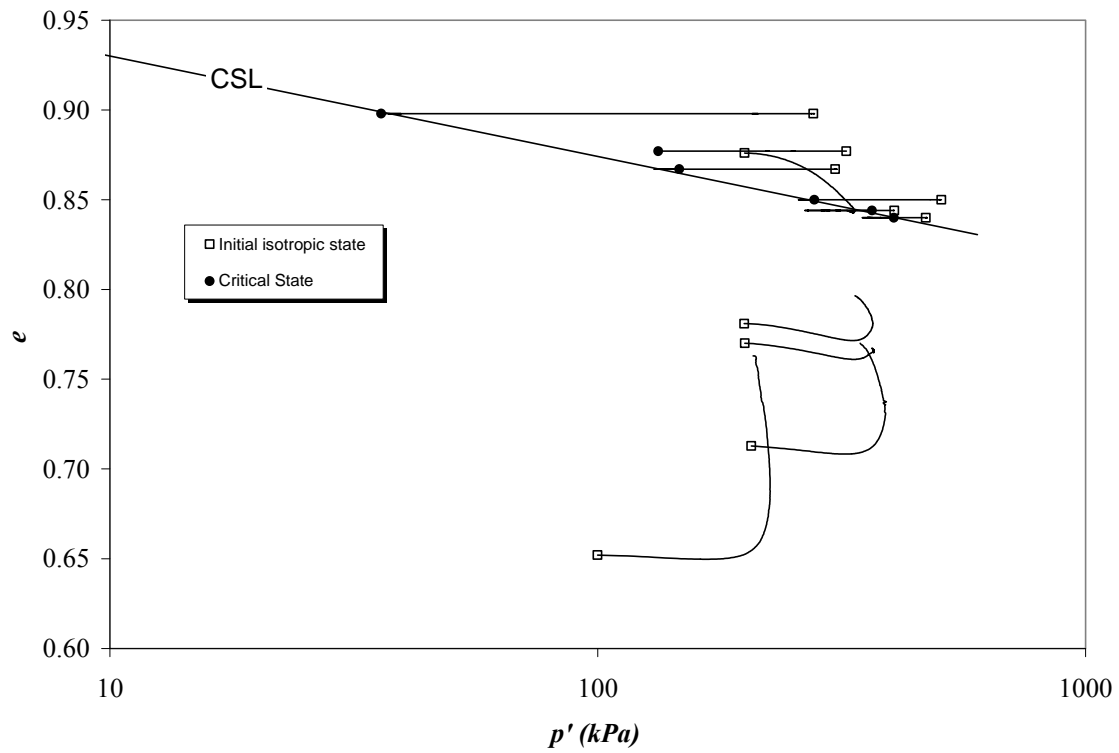
Figure 4 - 2 CSL determination for Ticino 4
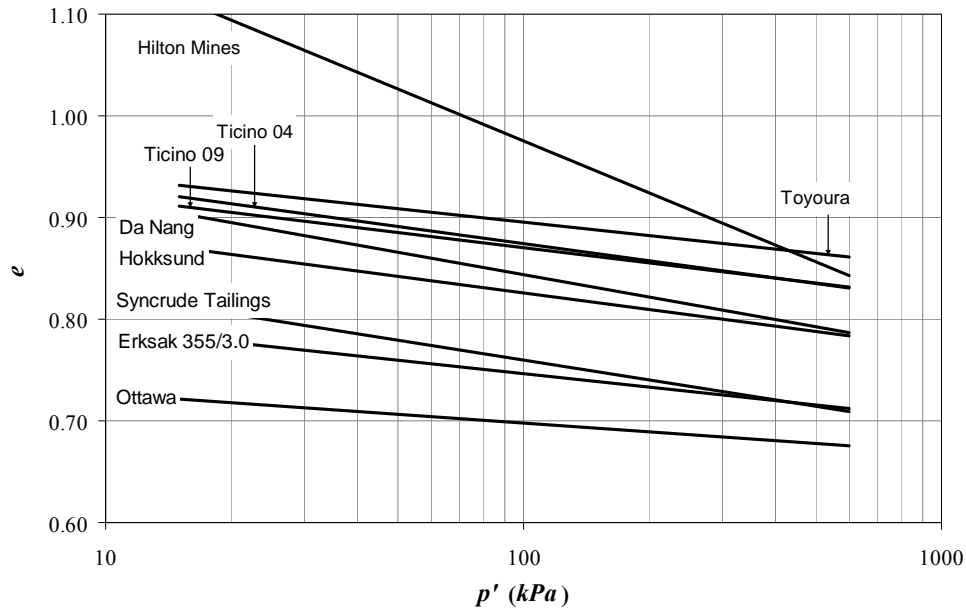
Figure 4 - 3 Comparison of CSL for all nine sands
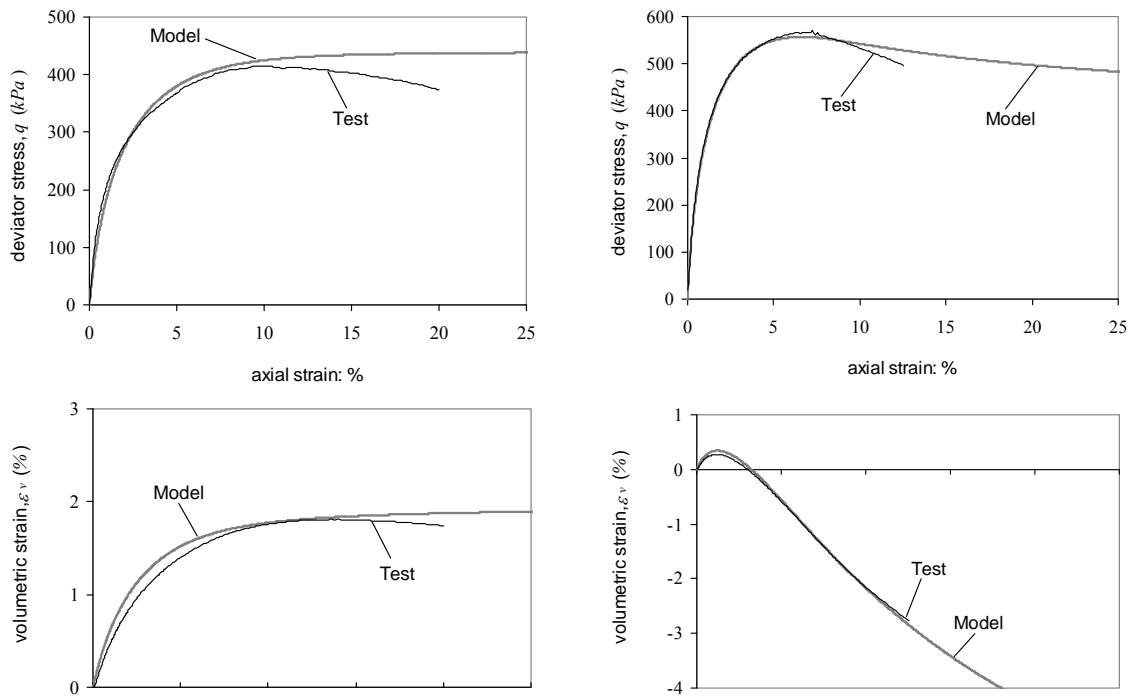
Figure 4 - 4 NorSand fits to loose and dense Ticino 4 triaxial data (C262, C264)

140
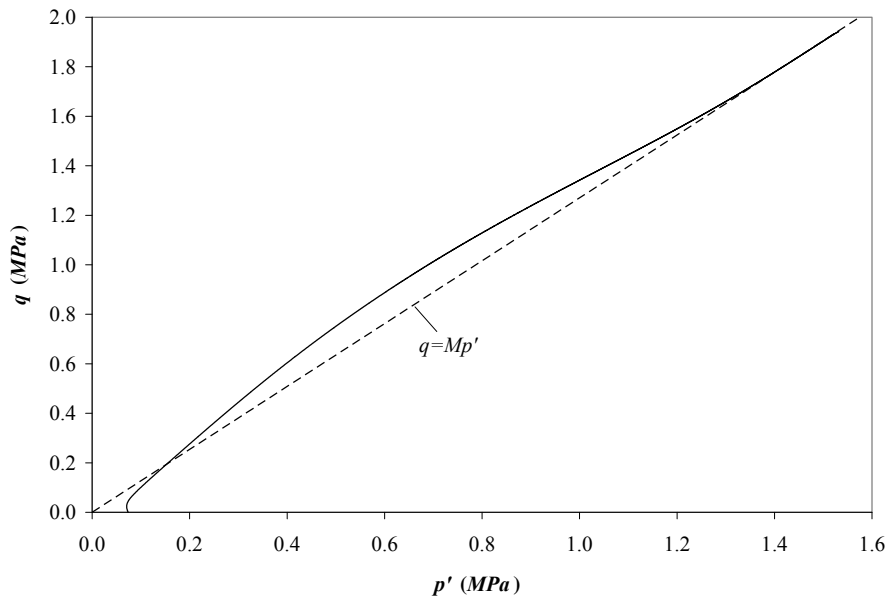
a) Stress path
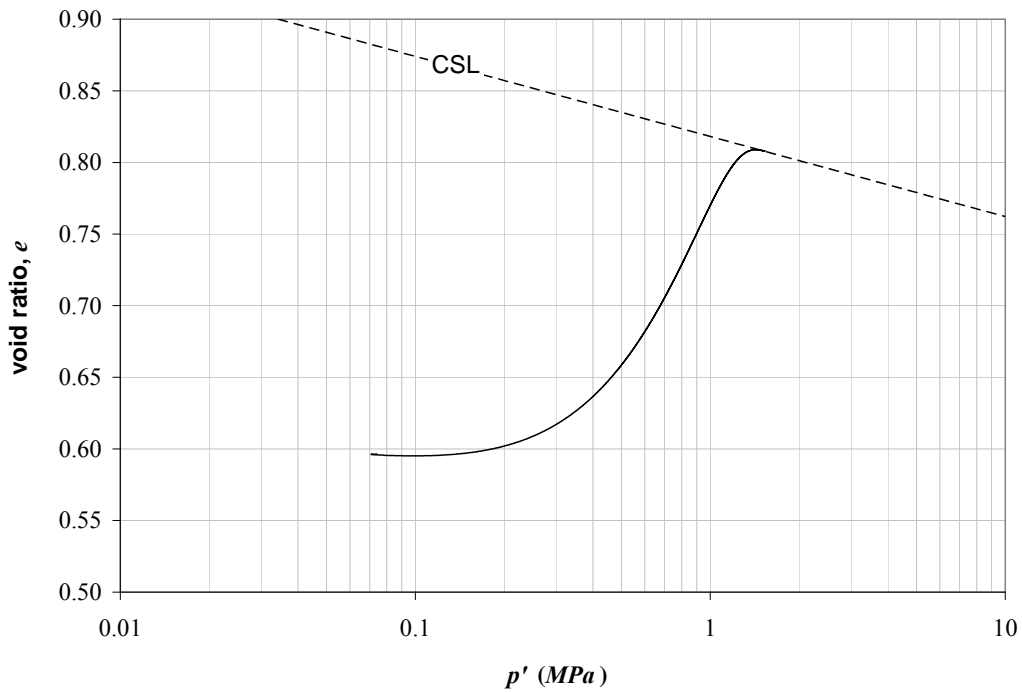
b) Void ratio versus log of mean effective stress

Figure 4 - 5 Behaviour of an element close to the cavity during spherical expansion
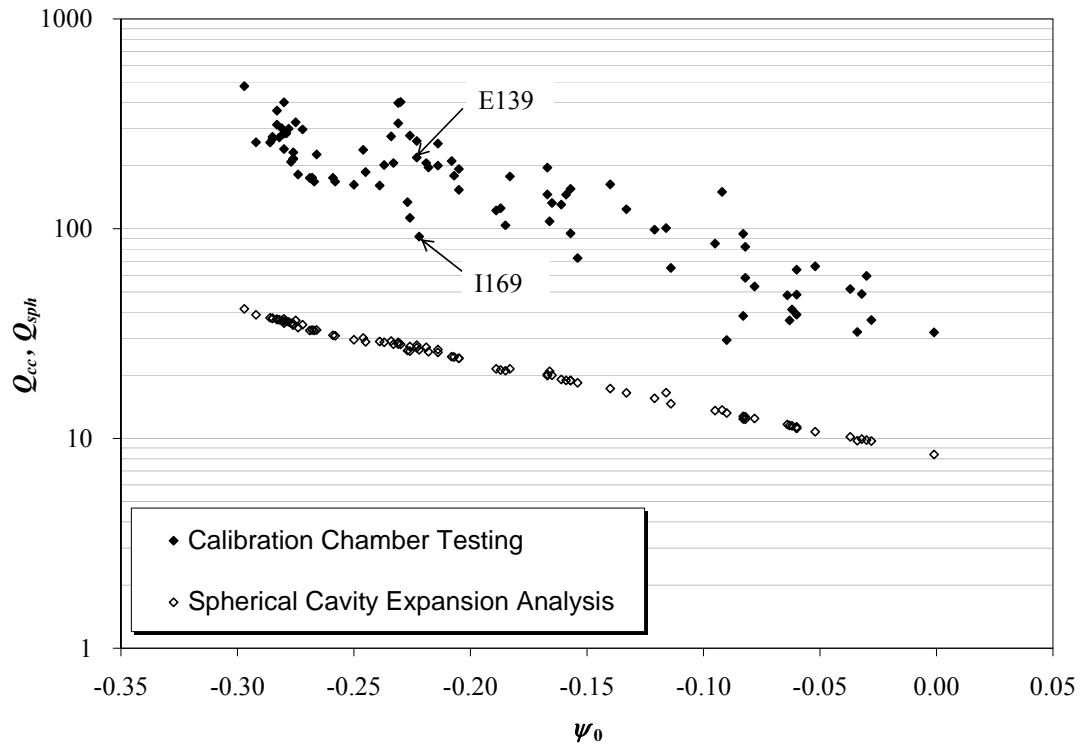
Figure 4 - 6 Q_{cc} and Q_{sph} vs. ψ_0 for Ticino 4 sand
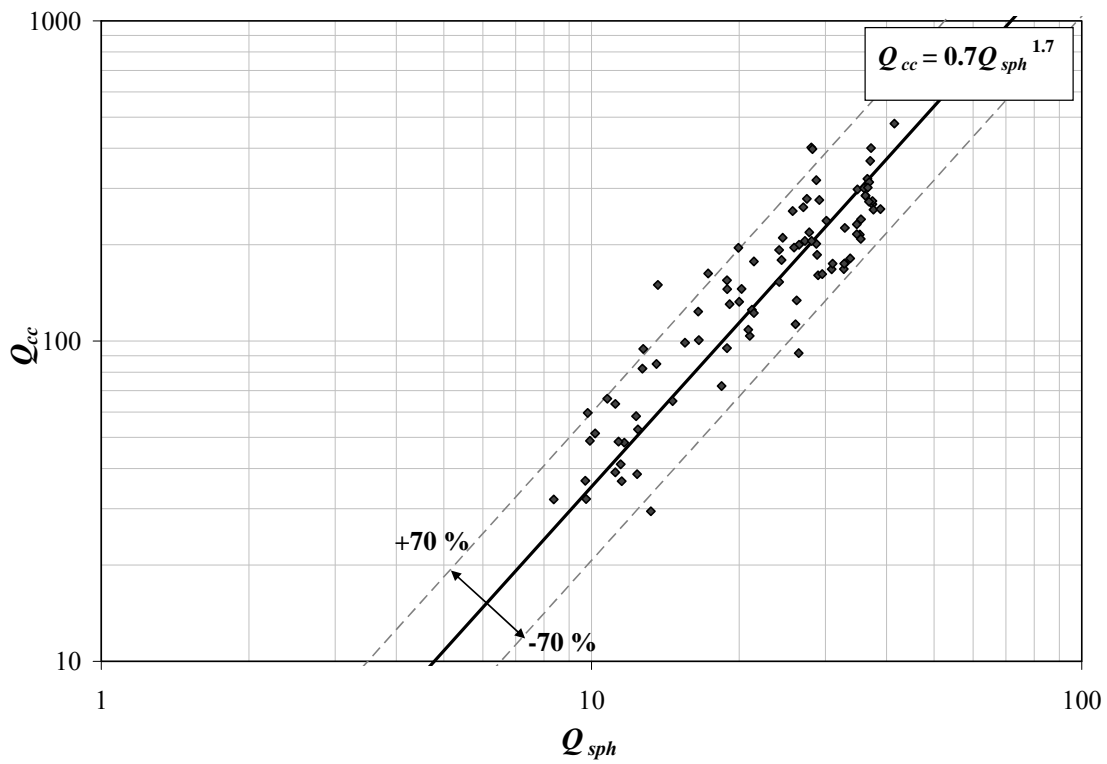
Figure 4 - 7 Q_{cc} vs. Q_{sph} for Ticino 4 sand
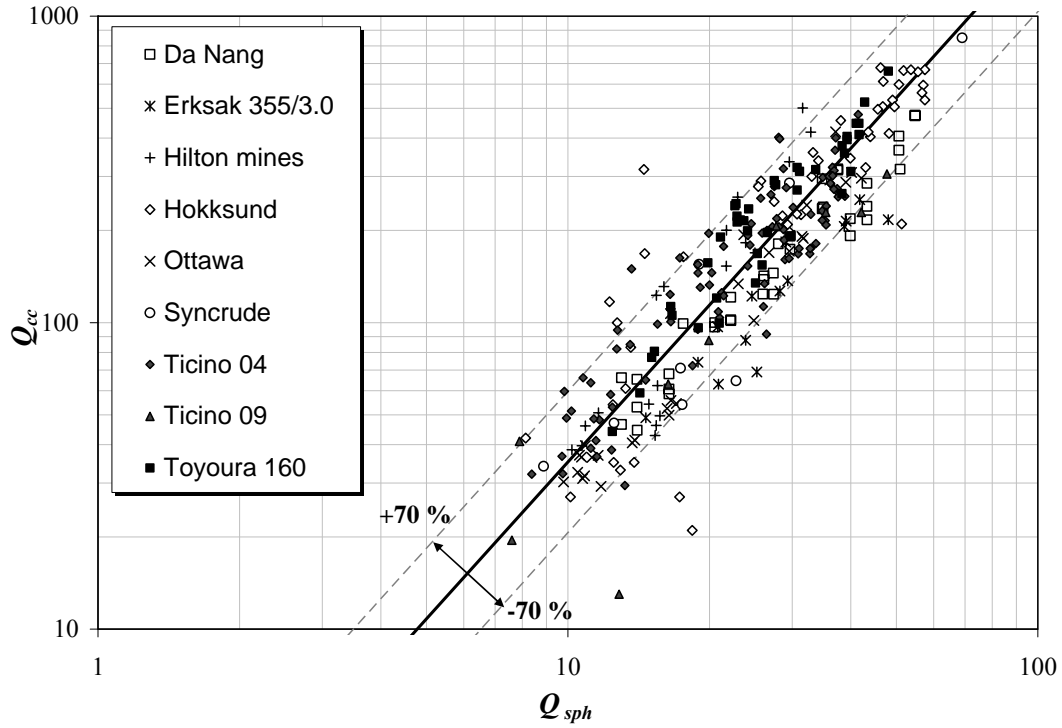
Figure 4 - 8 Q_{cc} vs. Q_{sph} for all nine database sands
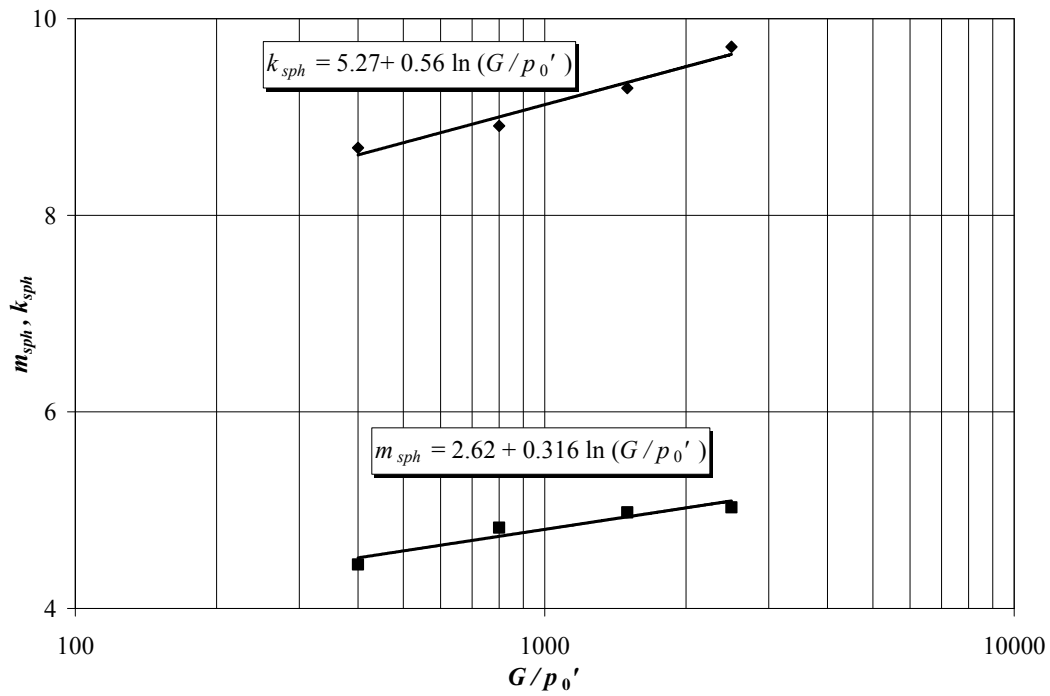
Figure 4 - 9 Effect of G/p'_0 on k_{sph} and m_{sph} for Ticino 4 sand
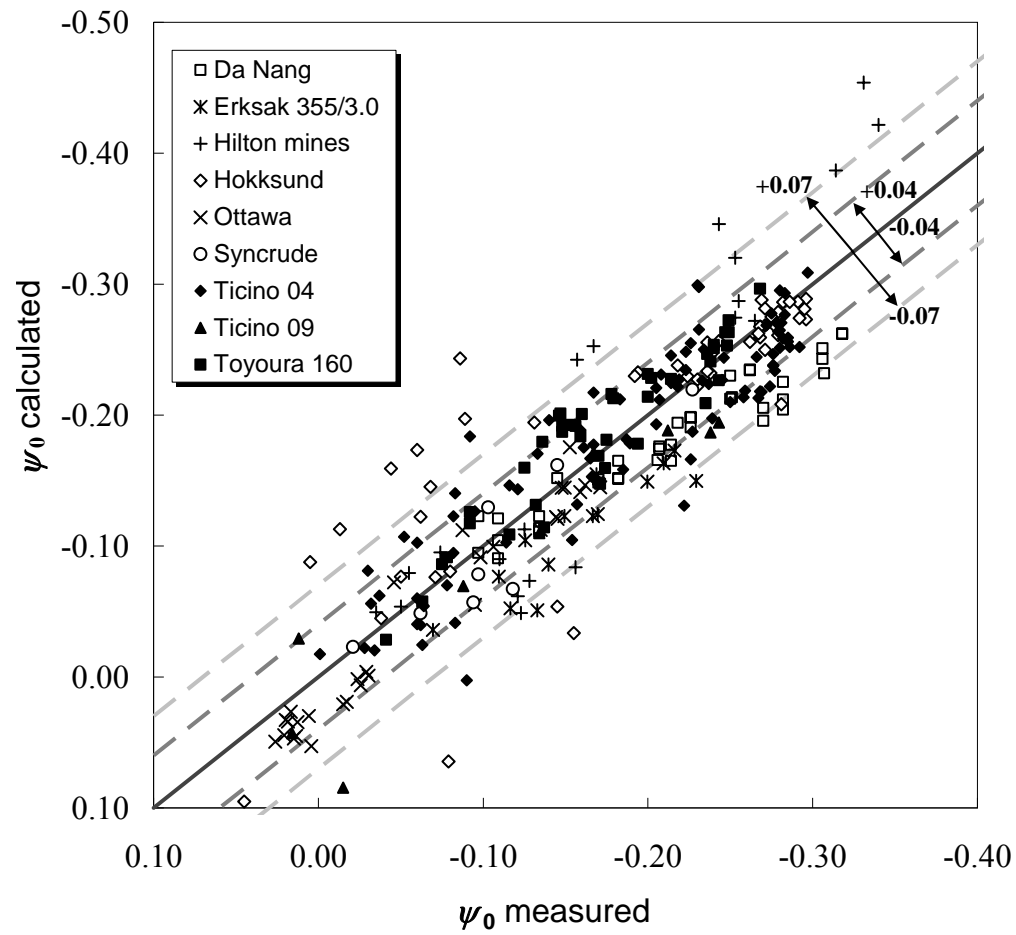
Figure 4 - 10 ψ_0 from Equation 4-5 vs. ψ_0 measured in the chamber

4.12. References

Baldi G., Bellotti R., Ghionna V.N., Jamiolkowski M., and Pasqualini E. 1986. Interpretation of CPTs and CPTUs, 2nd Part: Drained Penetration of Sands. Field Instrumentation and In-situ Measurements. Proceedings of the 4th International Geotechnical Seminar, Singapore, Nanyang Technological Institute, 143-156.

Been K., Jefferies M.G., Crooks J.H.A., and Rothenburg L. 1987[a]. The Cone Penetration Test in Sands. Part II: General Inference of State. Géotechnique, 37(3): 285-299.

Been K., Lingnau B.E., Crooks J.H.A., and Leach B. 1987[b]. Cone Penetration Test Calibration for Erksak (Beaufort Sea) Sand. Canadian Geotechnical Journal, 24: 601-610.

Been K., and Jefferies M.G. 1985. A State Parameter for Sands. Géotechnique, 35(2): 99-112.

Been K., Crooks J.H.A., Becker D.E., and Jefferies M.G. 1986. The Cone Penetration Test in Sands: Part I, State Parameter Interpretation. Géotechnique, 36(2): 239-249.

Bellotti R., Bizzi G., and Ghionna V. 1982. Design, Construction and Use of a Calibration Chamber. Proceedings of the 2nd European Symposium on Penetration Testing, Amsterdam, 2: 439-446.

van den Berg P. 1994. Analysis of Soil Penetration. Delft University of Technology, PhD Thesis, ISBN 90-407-1004-X.

Bishop R.F., Hill R., and Mott N.F. 1945. Theory of Indentation and Hardness Tests. Proceedings of Physics Society, 57: 147–159.

de Borst R., and Vermeer P.A. 1982. Finite Element Analysis of Static Penetration Tests. Proceedings of the 2nd European Symposium on Penetration Testing, Amsterdam, 2: 457-562.

Carter J.P., Booker J.R., and Yeung S.K. 1986. Cavity Expansion in Cohesive Frictional Soils. Géotechnique, 36(3): 349–358.

Chadwick P. 1959. Quasi-Static Expansion of Spherical Cavity in Metals and Ideal Soils. The Quarterly Journal of Mechanics and Applied Mathematics, 12(1): 52-71.

Chapman G.A. 1974. A Calibration Chamber for Field Test Equipment. Proceedings of the 1st European Symposium on Penetration Testing, Stockholm, 2: 59-65.

Chaudhary S.K., Kuwano J., and Hayano Y. 2004. Measurement of Quasi-Elastic Stiffness Parameters of Dense Toyoura Sand in Hollow Cylinder Apparatus and Triaxial Apparatus with Bender Elements. Geotechnical Testing Journal, 27(1): 1-13.

Collins I.F., Pender M.J., and Yan W. 1992. Cavity Expansion in Sands under Drained Loading Conditions. International Journal for Numerical and Analytical Methods in Geomechanics, 16: 3-23.

Cudmani R., and Osinov V.A. 2001. The Cavity Expansion Problem for the Interpretation of Cone Penetration and Pressuremeter Tests. Canadian Geotechnical Journal, 38: 622-638.

Cunning J.C., Robertson P.K., and Sego D.C. 1995. Shear Wave Velocity to Evaluate In Situ State of Cohesionless Soils. Canadian Geotechnical Journal, 32: 848-858.

Fioravante V., Jamiolkowski M., Tanizawa F. and Tatsuka F. 1991. Results of CPT's in Toyoura Quartz Sand. Calibration chamber testing. Huang A.B. (ed.), Elsevier, 135-146.

Gajo A., and Muir Wood D.A. 1999. Kinematic Hardening Constitutive Model for Sands: The Multiaxial Formulation. International Journal for Numerical and Analytical Methods in Geomechanics, 23(9): 925-965.

146

Ghafghazi M., and Shuttle D.A. 2006. Accurate Determination of the Critical State Friction Angle from Triaxial Tests. Proceedings of the 59th Canadian Geotechnical Conference, Vancouver, 278-284.

Golder Associates. 1985. Report No. 852-2041.

Golder Associates. 1986. Report No. 852-2042.

Golder Associates. 1987[a]. Cone Penetrometer Calibration Chamber Tests on Syncrude Tailings. Report No. 872-2402.

Golder Associates. 1987[b]. Report No. 862-2801.

Golder Associates. 1989. Report No. 892-2021.

Harman D.E. 1976. A Statistical Study of Static Cone Bearing Capacity, Vertical Effective Stress and Relative Density of Dry and Saturated Fine Sands in a Large Triaxial Testing Chamber. University of Florida, MSc. thesis.

Hill R. 1950. The Mathematical Theory of Plasticity. Oxford University Press, Oxford.

Holden J.C. 1991. History of the First Six CRB Calibration Chambers. Proceedings of the 1st International Symposium on Calibration Chamber Testing, Potsdam, New York, 1-12.

Hsu H.H. 1999. Cone Penetration Tests in Sand under Simulated Field Conditions. PhD thesis, Department of Civil Engineering, National Chiao Tung University, Hsin Chu, Taiwan.

Hsu H.H., and Huang A.B. 1998. Development of an Axisymmetric Field Simulator for Cone Penetration Tests in Sand. Geotechnical Testing Journal, 21(4): 348-355.

Huang W., Sheng D., Sloan S.W., and Yu H.S. 2004. Finite Element Analysis of Cone Penetration in Cohesionless Soil. Computers and Geotechnics, 31: 517–528.

Iwasaki k., Tanizawa F., Zhou S., and Tatsuka F. 1988. Cone Resistance and Liquefaction Strength of Sand. Proceedings of the 1st International Symposium on Penetration

Testing, Orlando, 20-24 March 1988, de Ruiter. J., and Balekma A.A. (eds.), Rotterdam, 2: 785-791.

Jamiolkowski M., Ladd C.C., Germaine J.T., and Lancellotta R. 1985. New Developments in Field and Laboratory Testing of Soils. Proceedings of the 11th ICSMFE, San Francisco, CA.

Jefferies M.G., and Shuttle D.A. 2005. NorSand: Features, Calibration and Use. Proceedings of the Specialty Conference on Soil Constitutive Models: Evaluation, Selection, and Calibration. ASCE Geotechnical Special Publication, 128: 204-236.

Jefferies M.G., and Shuttle D.A. 2002. Dilatancy in General Cambridge-Type Models. Géotechnique, 52(9): 625-638.

Jefferies M.G. 1993. Nor-Sand: a Simple Critical State Model for Sand. Géotechnique, 43(1): 91-103.

Jefferies M.G., and Been K. 2006. Soil Liquefaction: A Critical State Approach. Taylor & Francis, Abingdon & New York, ISBN 0-419-16170-8.

Laier J.E., Schmertmann J.H., and Schaub J.H. 1975. Effect of Finite Pressuremeter Length in Dry Sand. Proceedings of the Conference on Insitu Measurement of Soil Properties. Raleigh, ASCE, New York, 241-259.

Li X.S., Dafalias Y.F., and Wang Z.L. 1999. State-Dependent Dilatancy in Critical-State Constitutive Modelling of Sand. Canadian Geotechnical Journal, 36(4): 599-611.

Lo Presti D.C.F., Pedroni D.C.F., and Crippa V. 1992. Maximum Dry Density in Cohesionless Soil By Pluviation and by ASTM D 4253-83: A Comparative Study. Geotechnical Testing Journal, 15(2): 180-189.

Manzari M.T., and Dafalias Y.F. 1997. A Critical State Two-Surface Plasticity Model for Sands. Géotechnique, 47(2): 255-272.

Mayne P.W., and Kulhawy F.H. 1991. Calibration Chamber Database and Boundary Effects Correction for CPT Data. Proceedings of the 1st International Symposium on Calibration Chamber Testing, ISOCCT 1, Potsdam, New York, 257-264.

Norwegian Geotechnical Institute 1982. Report No. 842-2007.

Parkin A., Holden J., Aamot K., Last N., and Lunne T. 1980. Laboratory Investigation of CPTs in Sand. Norwegian Geotechnical Institute, Report 52-18-9.

Plewes H.D., Davies M.P., and Jefferies M.G. 1992. CPT Based Screening Procedure for Evaluating Liquefaction Susceptibility. Proceedings of the 45th Canadian Geotechnical Conference, Toronto.

Robertson P.K., and Campanella R.G. 1983. Interpretation of Cone Penetration Tests. Part I: Sand. Canadian Geotechnical Journal, 20(4): 718-733.

Robertson P.K., Sasitharan S., Cunning J.C., and Sego D.C. 1995. Shear-Wave Velocity to Evaluate In-Situ State of Ottawa Sand. ASCE Journal of Geotechnical Engineering, 121(3): 262-273.

Russell A.R., and Khalili N. 2002. Drained Cavity Expansion in Sands Exhibiting Particle Crushing. International Journal for Numerical and Analytical Methods in Geomechanics, 26(4): 323–340.

Salgado R., Mitchell J.K., and Jamiolkowski M. 1997. Cavity Expansion and Penetration Resistance in Sand. Journal of Geotechnical and Geoenvironmental Engineering, 123(4): 344-354.

Salgado R., Mitchell J.K., and Jamiolkowski M. 1998. Calibration Chamber Size Effects on Penetration Resistance in Sand. Journal of Geotechnical and Geo-environmental Engineering, ASCE, 124(9): 878-888.

Shuttle D.A., and Jefferies M.G. 1998. Dimensionless and Unbiased CPT Interpretation in Sand. International Journal for Numerical and Analytical Methods in Geomechanics, 22: 351-391.

Sladen J.A. 1989. Problems with Interpretation of Sand State from Cone Penetration Test. Géotechnique, 39(2): 323-332.

Tavenas F.A. 1973. Difficulties in the Use of Relative Density as a Soil Parameter. Evaluation of Relative Density and its Role in Geotechnical Projects Involving Cohesionless Soils, American Society for Testing and Materials, Selig E.T., and Ladd R.S. (eds.), Philadelphia, ASTM Special Technical Publication 523: 478-483.

Wan R.G., and Guo P.J. 1998. A Simple Constitutive Model for Granular Soils: Modified Stress-Dilatancy Approach. Computers and Geotechnics, 22(2): 109-33.

Willson S.M., Ims B.W., and Smith I.M. 1988. Finite Element Analysis of Cone Penetration. Penetration Testing in the UK, Thomas Telford, London, 157-159.

Yu H.S., and Houlsby G.T. 1991. Finite Cavity Expansion in Dilatant Soils: Loading Analysis. Géotechnique, 41(2): 173–183.

Chapter 5.

Evaluation of Sand State from SBP and CPT:

A Case History[5]

5.1.   Introduction

The behaviour of cohesionless soils depends strongly on their density. While relative density D_r

is an almost universally used density index for sand, it is easy to show that D_r can be misleading

(e.g. Tavenas, 1973). Apart from the lack of accuracy in identifying minimum and maximum

void ratios upon which D_r depends, it is well understood that behaviour of soils is also a

function of mean stress. An alternative to D_r that captures both the effect of void ratio and the

effect of mean stress on soil behaviour is the state parameter, ψ (Been and Jefferies, 1985).

Different soils, or the same soil at different stress levels, display similar behaviour at the same

value of ψ.

---

[5] A version of this chapter has been published. Ghafghazi M., and Shuttle D.A. 2008. Evaluation of Soil State from
SBP and CPT: A Case History. Canadian Geotechnical Journal, (45)6: 824-844.

Regardless of whether ψ or D_r is used as the characterisation parameter, outside of a few research situations it is impractical to obtain undisturbed samples of cohesionless soils. Engineering of cohesionless soils must be based on a combination of true properties determined from disturbed or reconstituted samples, with in-situ measurements to determine the value of the state measure adopted.

For most situations penetration tests are the basic in-situ reference tests. Both SPT and CPT have similarities, measuring a resistance (N or q_c respectively) to an imposed displacement of the tool. The modern electronic CPT emerged as the appropriate penetration test for the offshore oil industry in the 1970's, has been further enhanced over the subsequent decades with additional transducer channels (induced pore pressure in particular), in-tool correction for thermal drift, in-tool A-to-D conversion, and even wireless data transmission. Electronic CPT equipment is now displacing earlier mechanical CPT and SPT everywhere, this modern version offering a continuous data record, excellent repeatability, excellent accuracy, and relatively low cost. This chapter is based on modern electronic CPT data as described in ASTM D5778.

The difficulty with any penetration test, however, is that the state measure of interest (e.g. D_r, ψ) is not measured directly; instead the chosen state measure is calculated from the tip resistance q_c, a process usually referred to as interpretation. Interpretation based on mechanics involves the solution of an inverse boundary value problem to obtain mechanical properties of the soil from test results. But the large deformations associated with these penetration problems, along with the nonlinear behaviour of the soil and complicated boundary conditions make the analysis an extremely difficult task, and the solution non-unique. The interpretation framework is also difficult to establish. No simple closed-form solution for ψ or D_r from CPT (nor the more complex boundary conditions of SPT) has been developed; and, nobody - to date - has provided

a full numerical simulation of drained penetration that matches calibration data, although several have tried (e.g. De Borst and Vermeer, 1982; Willson et al., 1988; Van den Berg, 1994; Huang et al., 2004; and Ahmadi et al., 2005). Two different directions have emerged to estimate soil state from CPT data: correlations established through calibration chamber tests and simplified theoretical treatments.

Calibration chambers are circular steel tanks typically about a metre in diameter and similar height. Sand is deposited at a known density and consolidated to the desired stress state within the tank, and a cone penetration test is then performed along the vertical axis of the sample exactly as in natural ground. Each test provides a q_c for the given value of density and stress of the sample. A large number of tests, covering the range of densities and stresses of interest, provide the relation between q_c, in-situ effective stresses (σ'_1, σ'_2, σ'_3), and the density (more usually expressed as ψ or D_r) for the tested material. The in-situ state ψ is then obtained from the CPT by comparison of field CPT q_c measurements, at the estimated in-situ stresses, to the $q_c-\sigma'-\psi$ relation determined in the calibration chamber (and similarly for D_r).

There is a considerable history to calibrating the CPT in large chambers, with chambers increasing in size over time and becoming less subject to corrections for finite chamber size (boundary effects). The first advanced calibration chamber was built in 1969 at the Country Roads Board (CRB) in Australia (Holden, 1991). Chamber tests are now reported in the literature with differing dimensions, nature and form of control of boundaries, deposition procedure, and capability to handle saturated specimens. Ghionna and Jamiolkowski (1991) provided a list of 16 calibration chamber tests in the literature. More calibration chambers have been built since (e.g. Peterson and Arumoli, 1991; Hsu and Huang, 1998; Ajalloeian and Yu, 1998; and Tan et al., 2003).

Although chamber tests data appear to provide unarguable calibration for the CPT, this substantial body of experimental data is not sufficient in general. In addition to soil fabric and ageing which are known to complicate correlation of laboratory response to in-situ behaviour, there are two difficulties specific to CPT interpretation. First, the $q_c - \sigma' - \psi$ relation differs from one soil to another so that, although the form remains common among soils, the coefficients involved are particular to the calibrated soil. Second, the relation is controlled by the mean effective stress p', not the readily determined in-situ vertical effective stress σ'_v, so that the horizontal geostatic stress ratio K_0 becomes important to accurate determination of ψ or D_r. These two issues have been addressed below.

In the case of calibration coefficients changing from one soil to another, simplified theoretical modelling has been used to develop interpolations between different calibrations since it is impractical to calibrate the CPT for soils encountered in routine practice. A single chamber test involves preparing a uniform sample of between one and two tonnes at uniform density, and a calibration of the CPT in a chamber for one soil involves many chamber tests – an effort beyond that affordable by all but a few large projects. In addition, even large projects must account for the soil being non-uniform in gradation, with place to place variations even within a defined geological stratum.

Many simplified theoretical treatments have used spherical cavity expansion as an analogue of the penetration test, essentially the same approach as used in conventional design of end bearing capacity of piles. Robertson and Campanella (1983) first suggested that the difference between the CPT calibrations in various sands might be understood in terms of an undefined 'compressibility' of the sand involved. In more comprehensive evaluations of factors causing differing calibration, 'good' soil models have been used allowing for plastic hardening, strain

softening, etc. Shuttle and Jefferies (1998) used a general work hardening/softening critical state model to evaluate changes in CPT calibration in terms of critical state parameters M, λ (the critical state friction ratio and slope of the critical state line in $e - \log p'$ space, respectively) that can be determined in routine triaxial testing of reconstituted samples. They showed that CPT behaviour in Hilton Mines sand, currently the most unusual of the published calibrations, could be predicted based on Ticino sand data by allowing for the changes in fundamental soil properties between Hilton Mine and Ticino sand. However, this work is more in the nature of verification than validation since it does not involve independent evaluation of 'ground truth' in-situ at prototype scale – and stress conditions are perfectly known.

Turning to the issue of stress conditions, current practice appears to involve widespread neglect of K_0, despite the chamber test calibrations showing that K_0 is important. Jefferies et al. (1987) drew attention to the situation, pointing out the error caused by neglecting K_0 was credibly as large as the error caused by uncertainty in the effect of different sands on the CPT response. Although limited research has been done on using the hoop stress in the friction sleeve to infer K_0 (Huntsman et al., 1986; Jefferies et al., 1987) this approach is rarely used and has its own significant uncertainties. Clearly there is an issue with neglecting K_0, for example by using σ'_v rather than p', and thus there is a validation question of just how well ψ can practically be estimated from the CPT under normal circumstances.

Validation immediately raises the issue of determining 'ground truth'. This situation has arisen in other aspects of in-situ testing of soil, and it is usual to evaluate the soil properties determined by one test method against those determined by another method in evaluating reliability of the two methods (for example, work at 'national test sites' Nash et al., 1992 and Woods et al., 1994). This is the approach followed in this chapter.

Four alternative methods are found in the literature for density or state determination: the Self-Bored Pressuremeter test (SBP), flat plate Dilatometer Test (DMT) (Konrad, 1988), geophysically based density measurements (Plewes et al., 1988; Plewes et al., 1994; Hofmann et al., 2000), and shear wave velocity using geophysical methods (Cunning et al., 1995). Of these, the last two estimate void ratio, not ψ or D_r, and independent measurements of CSL (or e_{min} and e_{max}) and in-situ stress are also needed, making the predictions less accurate for characterising an in-situ deposit. The DMT is a difficult test to evaluate theoretically or numerically, and there is less calibration experience with it in comparison to the CPT – as such, it offers little in the way of a complementary test. In contrast the SBP is readily amenable to theoretical and numerical analysis. The attractiveness of the SBP in the present context is that it can easily be simulated using very advanced soil models. As such, SBP data provides a reasonably independent evaluation of ψ estimated from the CPT.

Many researchers have used Self-Bored Pressuremeter tests to determine soil density. The conventional approach to evaluation of SBP data follows the methodology developed by Hughes et al. (1977) in which the cylindrical cavity expansion analysis was adopted assuming a non-associated Mohr-Coulomb model with no elasticity. This type of analysis uses dilation angle as the index of material behaviour, a behaviour that is intimately linked to ψ. Carter et al. (1986) provided an improved solution that accounts for elasticity and included the effects of large strains. A different derivation using the same idealisation as Carter et al. was given five years later by Yu and Houlsby (1991). Numerical determination of the state parameter from the Self-Bored Pressuremeter during loading was first undertaken by Yu (1994). His numerical analysis concluded that there is a unique linear correlation between the slope of the pressuremeter expansion curve on logarithmic scale and the initial state parameter.

Yu et al. (1996) proposed an approach for obtaining the initial state parameter from the ratio of CPT tip resistance and the limit cavity pressure of SBP test. The major limitation of this approach is that SBP tests are rarely taken far enough to reach the limit pressure, rendering the method difficult to apply to most data. An alternative approach to interpreting SBP data is to fit the entire SBP load displacement curve. The mechanical parameters of the soil, including density, can then be determined for the chosen soil model (e.g. Shuttle and Jefferies, 2000; Shuttle, 2006).

In this chapter, finite element cavity expansion analysis with a critical state constitutive model has been used to obtain the state parameter from previously published CPT and SBP data obtained as part of a site investigation program on a hydraulically placed, clean quartz sand in Beaufort sea. The work is based on independent calibration of the constitutive model with triaxial tests. The state of the soil is then calculated from CPT data using calibration chamber testing results interpreted through numerical analysis. Soil state is also independently obtained from SBP data by fitting an analytical pressure-strain curve to the measured data. Effects of elasticity, ageing and fabric on the results are considered and reliability of the two test methods in estimating soil state is evaluated.

5.2. Tarsiut P-45 Case History

Exploration for hydrocarbons in the Canadian Arctic in the 70s and 80s was largely based on construction of artificial islands using sandfill. Islands were used rather than drill-ships because of the short open water season, and the presence of moving ice during the winter. Islands had sufficient mass to resist the forces of moving ice and thus allow extended drilling. These islands

became quite large over time, were constructed of rather uniform hydraulically placed sand, and had extensive engineering and quality assurance. Although two decades or more old, the testing was often at the state of the art and much of the data is of good quality even by current standards. Most importantly, not only are there literature contributions on the work (e.g. Stewart et al., 1983; Jefferies et al., 1985; Hicks and Smith, 1986; Hicks and Smith, 1988; Been et al., 1991; Jefferies et al., 1988; and Hicks and Onisiphorou, 2005) but the original data (as raw digital test data) supporting these contributions are in the public domain (www.golder.com/liq). These data provide: several CPT/SBP tests in close proximity, together with supporting laboratory tests; in-situ geophysical tests were used to determine elastic properties of the sandfill; and, most importantly, calibration of the CPT in a state-of-the-art calibration chamber using the construction sand. Together, this data set provides a unique opportunity to evaluate ψ inferred from CPT with ψ from SBP in a full scale case history – and is the subject of this chapter.

The island from which the data used in this chapter was obtained, was not a true island, but was a caisson with an inner core of hydraulically placed sand. This particular caisson was known as the Molikpaq (it was classified as a drilling barge, and hence named as if it were a ship). Figure 5-1a shows a view of this structure while it was operating in moving winter ice, with Figure 5-1b showing a cross section through the structure. Because the Molikpaq was designed for use at multiple sites of varying water depth, it had to be founded on a sandfill platform. This platform, referred to as a berm, enabled the caisson to be configured for a constant set-down depth across a range of water depths. Foundation failure beneath the berm was avoided by excavating any weak clay at the seabed, using a dredge, to create what was referred to as a subcut. With the subcut excavated, infilled with sand and the berm raised, the Molikpaq was

ballasted down onto the berm. Then, the hollow core of the Molikpaq was filled with sand.

The subcut infill, the berm, and the core were constructed of the same sand. For the case history used in this chapter, the initial deployment of the Molikpaq was at the Tarsuit P-45 location (see Figure 5-2) in 1984, and the construction sand came from the Erksak borrow pit (location also shown on Figure 5-2). All aspects of construction with sand involved hydraulic filling, using a trailer-hopper dredge, without any mechanical densification/compaction. However, the deposition methods differed between the subcut infill/berm and the core, resulting in very different in-situ densities being obtained by the different construction methods. Details of the construction methods and their achieved densities were given in Jefferies et al (1988) and can be summarised as follows. The infill and the berm were constructed by predominantly *bottom dump* placement from the dredge. In this method, the dredge is manoeuvred over the target and valves opened in the base of the hull, dropping 6,000 tonnes of sand into place in a few minutes. The core was filled by slurrying the sand in the hopper of the dredge and then pumping it through a floating pipeline across to the Molikpaq and discharging the slurry from a spigot in the centre of the core at sea level, a process referred to as *spigot placement*. The bottom dump placement produced sand with penetration resistance about double those achieved by spigotting. The focus of this chapter is on the core as it is looser, and hence of more interest from a stability viewpoint.

5.3. Erksak Sand

Erksak sand is a predominantly quartz, sub-rounded sand; Figure 5-3 illustrates the grain shape (fines content removed). The fines content of the sand in the borrow pit is about 10%, but most

hopper. Figure 5-4 shows histograms of mean grain size and fines content of the sand after it was loaded into the hopper of the dredge, the hopper being sampled using grab samples as well as a vibrocore drill. This variability is to be expected, as the borrow area from which the sand was extracted was some 1 *km* wide by 2 *km* long and with the dredge taking a pass along the pit with the draghead pulling sand from the seabed as the dredge slowly traversed the area.

Figure 5-5 shows a cross section through the core showing the 1985 investigation boreholes and the median grain size and fines content measured on samples in the core zone. The D_{50} of the as-placed sand lies between 224 and 480 microns, with an average of 330 microns. Silt contents in-situ are in the range 1 to 4%. Although soil behaviour is sensitive to fines content, the range observed at this site is considered narrow enough to treat the soil as a uniform material.

5.4. Laboratory Tests

Laboratory testing of Erksak sand concentrated on two gradations. Much of the testing to determine mechanical properties, and in particular the reliability of the critical state determination, was on 330/0.7[6] sand, this material being a composite of the various borehole samples from a subsequent Molikpaq deployment that used the same sand (see Been et al. (1991) for details). However, this volume of material was nothing like sufficient for the calibration chamber testing and a truckload of Erksak sand was shipped from the field to the testing laboratory. Once thoroughly mixed, this large sample had a 355/3.0 gradation; a slightly different gradation from the composite laboratory sample. Grain size distribution curves for

---

[6] The notation means D_{50}=330 μm and 0.7% of the soil passes #200 sieve.

these samples of Erksak sand are shown in Figure 5-6. Index properties are summarised in Table 5-1.

Both gradations of Erksak sand were tested in triaxial compression; Table 5-2 summarises this testing. Testing of the 330/0.7 gradation was extensive, and is documented in Been et al. (1991). Table 5-3 presents the comparable information for the 355/3.0 tests. Figure 5-7 shows the CSL determined for each gradation of Erksak sand while Figure 5-8 plots peak friction angle versus initial state parameter for the dense drained tests.

5.5. In-situ Tests

5.5.1.   CPT

A total of 33 CPTs were carried out in 1984 in the two weeks following placement and levelling of the sand core. Subsequently, this data was supplemented by another 5 CPTs some six months later in 1985 to investigate the effect of "ageing". The combined data set has been made available to researchers and has been the basis of extensive research into characterizing soil state variability and the consequence of that variability (e.g. Popescu et al, 1998).

Although the site was a manmade one with rigorous quality control and a uniform material and deposition method, considerable variability was observed amongst different CPT tests. For example the tip resistance of MACRES 01, 02 and 03 (locations shown in Figure 5-5) were different by a factor of 2 at any given depth. However, based on the assessment of the site data by the original investigators (Golder Associates, 1986) the variability was reduced when the CPT's were within about 1 to 2 *m* of each other. As illustrated in Figure 5-5 CPT test MACRES

d in determining the characteristic q_c associated with the SBP data.

Figure 5-9 shows MACRES 02 CPT data including tip resistance q_c, friction ratio F, pore pressure u_2 (measured at the 'shoulder' location) indicating a water table elevation at $3.5\ m$ depth, and material index I_c. The depths of the SBP tests are also shown on the tip resistance plot. Horizontal effective stresses inferred from SBP results (discussed later) are also presented on this figure.

5.5.2.   SBP

The 1984 investigation program included three SBP profiles in the core zones; these data were not available to the authors and have not been used in this paper. In 1985, 16 SBP tests were conducted in boring BM1 (see Figure 5-5) seven of which were used to evaluate soil state in the core zone; the rest being obviously disturbed, for example due to a large mismatch between the individual arm displacements (Jefferies and Been, 2006). The tests were carried out in undensified hydraulically placed Erksak sand, which was approximately six months old at the time of testing.

A correction was applied to account for the effect of membrane on the horizontal stress measurement. This membrane correction was developed during the fieldwork as a function of the hoop strain, ε_R; the engineers who carried out the testing reported that a pressure correction of $dP = 18 + \varepsilon_R\,(\%)$ should be used, giving values in the range $18\text{-}30\ kPa$. The effective horizontal stress measured by the pressuremeter was calculated by subtracting the in-situ pore water pressure from the total pressure measured with the water table at $3.5\ m$ depth.

e finite length of the pressuremeter (discussed below), is illustrated in Figure 5-10 and shows a consistently increasing trend with depth. G_{UR} indicates values between 10 and 90 *MPa* with an average of 50 *MPa*. The range of G_{UR} and its dependence on mean effective stress is generally consistent with the correlation suggested by Jefferies and Been (2006) from laboratory measurements. However, despite the apparent reliability of the measurements, the strain amplitude over which G_{UR} was measured varied between SBP tests. For consistency with the CPT interpretation, in the subsequent SBP analyses the elastic shear modulus from geophysical tests, *G*, has been used.

5.5.3. Elastic Stiffness from Geophysical Tests

Cross-hole and down-hole seismic velocity profiles were developed as part of the geophysical testing program. The shear wave velocities based on incremental shear wave velocity measured by Vertical Seismic Profile in Hole I 02 (not shown on Figure 5-5) are plotted against depth and mean effective stress (using the average K_0 of 0.66 obtained from the SBP tests' lower range) in Figure 5-10. The trend of the shear modulus *G* may be approximated by the relation $G = 1.9\, p'^{0.8}$ where *G* is given in *MPa* and *p'* in *kPa*.

5.6. Calibration Chamber

A feature of this case history is that CPT calibration chamber data are available for the sand used in large scale construction. This calibration testing involved 14 tests (Been et al., 1987[b]) at

163

relatively dense initial state parameters of -0.069 to -0.229 (see Table 5-4 and Figure 5-11). The calibration chamber at Golder Associates' Calgary laboratory can accommodate a soil sample up to 1.0 *m* in height with a diameter of 1.4 *m* (chamber to standard cone diameter ratio of 38). The top and bottom boundaries are rigid and the lateral boundaries impose constant stress on the soil sample. CPT chamber samples were prepared by moist tamping, which is similar to that used for triaxial sample preparation for all Erksak 355/3.0 and some of Erksak 330.0.7 samples but with some modifications because of the very large sample size. Successive layers were added and tamped until the desired sample height was obtained. The sample was weighed, sample dimensions recorded, and overall average void ratio calculated. A complete description of the chamber testing program and the material is presented in Been et al. (1987[b]).

5.7. Modelling Erksak Sand Behaviour

The approach to evaluating the state parameter from SBP data involves formal modelling of the pressure-hoop strain relation. Similarly, for the CPT, the relation between q_c and ψ in the calibration chamber has been established by modelling. As the same constitutive model is used in both situations, this model is overviewed and then calibrated for Erksak sand before discussing its application to each of the in-situ tests.

5.7.1. NorSand

The constitutive model adopted is NorSand (Jefferies, 1993), an isotropically hardening - isotropically softening generalised critical state model that captures a wide range of particulate soil behaviour. The version used is that for general 3-D stress states with constant principal

stress direction as described in Jefferies and Shuttle (2002) but with a further extension to improve accuracy as described below. NorSand can be regarded as a super-set of the well-known Cam Clay model (Schofield and Wroth, 1968), with Cam Clay being obtained as a special case of NorSand by appropriate choice of the material parameters and initial conditions.

A feature of the original version of NorSand was a volumetric coupling parameter N for stress-dilatancy. Subsequently, Jefferies and Shuttle (2002) suggested that N could be eliminated from the model since $N\chi \approx 1$ (based on average values of a large quantity of triaxial tests on different sands). However, individual soils demonstrate a variety of $N\chi$ values and some accuracy is given up by following this suggestion. The N model parameter neither increases the complexity of the model, nor constitutes additional effort in calibration of the model, as N is obtained with M_{tc} from the stress-dilatancy plot (see Figure 5-12) and reintroduction of this parameter resulted in better replication of the soil behaviour. For the current work a minor modification of the original N, termed N^* for clarity, was obtained as the slope of the post peak stress-dilatancy plots.

A central feature of NorSand is the use of the state parameter ψ as an internal rate variable, which allows the model to simulate soil behaviour ranging from liquefaction of loose soil when loaded undrained through to extreme dilation of very dense samples. This particular version of NorSand has been validated for stress paths ranging from plane strain (Jefferies and Shuttle, 2002) to systematically varied triaxial paths from compression through to extension (Jefferies and Shuttle, 2005[a,b]). All NorSand parameters apart from elasticity are invariant with soil density or stress level. The differing soil behaviours simulated are entirely controlled by the state measures.

As a critical state model, NorSand is based on the premise that soil's state tends to critical conditions as shear strain accumulates. Two modelling choices are involved to determine the level of accuracy desired in the representation of the CSL; and, to capture the influence of intermediate principal stress on M. For many soils, and much engineering, a semi-logarithmic approximation of the critical state locus is sufficient and that is used here. Regarding M, it has been known since Bishop (1966) that constant M was inconsistent with the no-tension behaviour of particulate materials. The analysis here adopts the empirical rule for $M(\theta)$ proposed by Jefferies and Shuttle (2002), which takes M_{tc} as the basic soil property (θ is called the Lode angle, and describes the proportion of the 3-D shear stress invariant attributable to the intermediate principal stress).

NorSand has four basic aspects: a yield surface; a work hardening law; a plastic flow rule (stress-dilatancy); and, elasticity. NorSand is a sparse model, with the fixed principal stress direction variant having eight material parameters, seven of which are dimensionless. Many soil properties in NorSand will be familiar from Cam Clay. Three properties describe the critical state, these being the critical friction ratio M_{tc} and Γ, λ which describe the CSL for the semi-log idealisation used. There are two additional properties relating to the plastic behaviour: χ_{tc} and H. The property χ_{tc} scales the maximum dilatancy to ψ. In some ways this is similar to specifying a relation between peak strength and ψ. The dimensionless hardening modulus H is required because the state parameter approach de-couples the yield surface from the CSL and hence the slope of the CSL no longer acts as a plastic compliance.

The rigid-plastic idealisation in shear used by Cam Clay theoretically requires that G is infinite. This is both unrealistic, and inconvenient for use with numerical methods. Within NorSand the physically real "finite" elastic shear modulus G is adopted. Various forms of elasticity can be

used within the same framework. For the purpose of the current research although the initial elastic shear modulus is assumed to depend on the void ratio and stress level, both G and ν are taken as constant during the test.

5.7.2. Calibration to Erksak 355/3.0 and Erksak 330/0.7 Sand

The aim in calibrating NorSand to a particular soil is not to fit one test as elegantly as possible. Rather, the objective is to obtain a consistent set of material parameters that are able to represent the behaviour of the sand over all available tests and covering the range of pressures and states. Hence the goodness of fit for any individual test is, by necessity, compromised to obtain a better representation of the overall soil response. This calibration process is summarised below; the reader is directed to Jefferies and Shuttle (2005[a]) for a more detailed discussion of the calibration procedures.

The critical state of the soil is not really a NorSand calibration, as any critical state model will have the same parameter set. For the semi-log idealisation of the CSL, a best-fit line is put through the critical states judged from high strain results on loose samples. A variety of methods are available to estimate M_{tc} (Ghafghazi and Shuttle, 2006). As illustrated in Figure 5-12, N^* and M_{tc} are respectively obtained as the slope and intercept of the post peak portion of the stress-dilatancy plot for each triaxial test. Average values were then chosen to represent the overall soil behaviour.

The plasticity parameter, χ_{tc}, was derived by plotting dilation at peak against the state parameter at the image condition (see Figure 1-2) ψ_i at peak, with χ_{tc} being the slope of the trend in Figure 5-13.

The last plasticity parameter, the hardening parameter H, is fabric dependent and can only be determined by iteratively fitting the NorSand model to triaxial data. In this iterative fitting, the parameters established as just described were kept constant, and H was determined by modelling the drained triaxial tests and selecting the parameter set that gave the best overall visual fit across all the tests. Figures 5-14 and 5-15 show the fits for two tests chosen from each sand and sample reconstitution method.

Elastic shear modulus G is also expected to be affected by fabric (and age of deposit). Jefferies and Been (2006) suggest a correlation between G, void ratio and stress level of the sample based on the unloading portion of a series of isotropic compression tests on Erksak 330/0.7 samples. No distinguishable difference was observed between moist tamped and wet pluviated samples, so the same relation of G against depth is applied to both Erksak sample types (Table 5-5). For the range of void ratio and mean effective stress at this site the correlation yields G values between 40 and 100 MPa. This range matches the values measured in the field (10-90 MPa from SBP and 40-120 MPa from geophysical measurements), and suggests that ageing had not significantly affected the stiffness of Erksak sand at the time of testing. Table 5-5 summarises the calibration of NorSand for Erksak 355/3.0 moist tamped samples.

The calibration of NorSand to Erksak 330/0.7 sand was documented in Jefferies and Shuttle (2005[a]). A difference between the two calibrations is that two sample reconstitution methods, moist tamping and water pluviation, were used in the case of 330/0.7 sand. Although the reconstitution method has no effect on the critical state parameters, it does affect the plastic hardening modulus, with the moist tamped sand being stiffer than water pluviated sand, thus yielding a higher H value for identical initial state conditions as reflected in Table 5-5.

5.8.   Evaluation of In-situ CPT Data

5.8.1.   Methodology

The original framework for the relation between penetration resistance and state was developed empirically (Been et al., 1986, 1987[a]). Triaxial testing was used to determine CSLs of the various sands for which chamber test data existed, allowing the calibration data base to be transformed from void ratio measurements to state parameter. The effect of stress level on the CPT was removed by transforming the CPT data to dimensionless form using:

$$Q = \frac{q_c - p}{p'}$$
[Eq. 5 - 1]

where q_c is the tip resistance for drained penetration (corrected for chamber size) and p and p' are the mean total and effective stresses respectively. Plotting chamber test data in this normalised form supported a simple dimensionless relation for any sand:

$$Q = k \exp(-m \psi_0)$$
[Eq. 5 - 2]

where the two coefficients k and m in Equation 5-2 differ from one sand to another. In the original work, it was suggested that both k and m were functions of the slope of the CSL, λ, but that no other soil properties were identified as being involved in the relation between Q and ψ_0.

Equation 5-2 is readily inverted to give ψ_0 provided that k and m are known from calibration studies (or otherwise):

$$\psi_0 = -\frac{\ln(Q/k)}{m}$$ [Eq. 5 - 3]

Sladen (1989) tested Equation 5-3 for bias using the extensive Ticino sand calibration data and found a systematic bias in Equation 5-3 with stress level despite the dimensionless formulation. Potential errors as much as $\Delta\psi_0 = \pm 0.2$ were suggested, in the order of 50% of the credible range in the parameter sought.

Sladen's identification of stress bias in a dimensionless formulation resulted in other workers turning to numerical analysis to resolve the conundrum. Collins et al. (1992) reported a drained cavity expansion analysis using a state parameter based model. Their results showed that there was an effect of stress level on the state parameter approach, consistent with the suggestion of Sladen, and further that the relation between Q and ψ_0 depended on material properties of the sand. Jefferies and Been (1995) compared Collins et al. results for Ticino sand and found that the computed effect of stress level was half the experimental scatter in the calibration chamber data, but clearly there was an unknown bias. Subsequently, Shuttle and Jefferies (1998) implemented NorSand in a finite element spherical cavity expansion analysis and demonstrated that Equation 5-2 was an accurate approximation of the numerical results for fixed soil properties. However, both k and m were found to be strong functions of G/p_0' (termed I_r), and it is this aspect that led to an apparent stress level bias within a dimensionless formulation. For constant I_r, Equation 5-2 fits all simulations regardless of the confining stress. The issue arises though, that I_r is not constant in real sands. Doubling the stress level produces less than a

doubling in the shear modulus, making I_r reduce as the stress level increases. It is this reduction in I_r that leads to apparent stress level bias because m and k also reduce with reducing I_r.

The result of exploring the stress level 'bias' identified by Sladen is that it is not a real bias at all. Rather, an important parameter group, I_r, had been omitted from the framework. Accurate evaluation of ψ from CPT data requires detailed knowledge of the shear modulus profile through the deposit, and, the trend of k and m with I_r has to be determined for the soil being tested.

Understanding the relation between k and m and I_r illustrates the limitations of physical testing – there is no independent control over shear modulus in the calibration chamber, so the relation cannot be determined experimentally and numerical simulations are essential. Parametric simulations provide data to develop influence functions for each of the material parameters, leading to the approximation (Shuttle and Jefferies, 1998):

$$k = (f_1(I_r) f_2(M) f_3(N) f_4(H) f_5(\lambda) f_6(\nu))^Z \qquad \text{[Eq. 5 - 4a]}$$

$$m = 1.45 f_7(I_r) f_8(M) f_9(N) f_{10}(H) f_{11}(\lambda) f_{12}(\nu) \qquad \text{[Eq. 5 - 4b]}$$

where the functions f_1 - f_{12} are simple algebraic expressions and Z is a scaling factor accounting for the inherent mismatch between cone penetration and spherical cavity expansion processes.

5.8.2. State Parameter from CPT Tests

The spherical cavity finite element code used by Shuttle and Jefferies (1998) was used in this study. The analysis code and finite element mesh remained the same, thus retaining the verified

large displacement performance of the code. In the current work for the calibration chamber tests, all moist tamped Erksak 355/3.0 soil parameters are either constant or known functions of ψ_0 , p' or e (see the fourth column in Table 5-5). The shear modulus is obtained from the correlation suggested by Jefferies and Been (2006), which corresponds to that of a newly prepared sample. Each chamber test is modelled as having the initial state, horizontal and vertical stresses and the Q obtained is plotted against that measured in the test in Figure 5-16.

It has been well understood that there is an inherent mismatch between spherical cavity expansion analysis results and those of calibration chamber tests. This difference stems from the assumptions made in the analogy of cone penetration and spherical cavity expansion, and is usually accounted for by a scaling factor. The scaling function[7] obtained for this NorSand representation of Erksak sand, and as shown in Figure 5-16, is:

$$Q_{cc} = 0.47\left(Q_{sph}\right)^{1.7}$$ [Eq. 5 - 5]

5.8.3. Inversion Parameters

The analysis developed is for Erksak 355/3.0 sand placed by moist tamping. However, this was not the in-situ placement method for the core, and laboratory observations clearly indicate sample preparation method does affect stress-strain behaviour. This creates a dilemma for engineering analysis. If forced to rely on reconstituting samples, how can real construction processes be simulated in the laboratory, and how can the soil fabric developed in one situation

---

[7] The analysis presented in this chapter was performed and published before those presented in chapter 4. Hence a different scaling function is applied. The two functions are numerically close as the scaling from Ticino sand is shown to be applicable to all the database sands as discussed later in chapter 4.

be checked against another? Perhaps a closer analogy to the full scale hydraulic fill placement is water pluviation, and therefore a new parameter set is generated by adopting the plastic hardening parameter H from tests on wet pluviated samples of Erksak 330/0.7 while keeping all the other parameters from the Erksak 355/3.0 calibration. A summary of this parameter set is presented in the fifth column of Table 5-5.

The elastic shear modulus for the in-situ CPT is obtained from down-hole seismic shear wave velocity measurements. This type of data is now frequently obtained with cone penetration and represents the in-situ soil elasticity.

With every parameter known as a constant or a function of ψ_0, the CPT inversion parameters k and m versus I_r trends are developed for the in-situ soil conditions using the spherical cavity expansion analysis ($k_{spherical}$, $m_{spherical}$). The $k_{spherical}$ and $m_{spherical}$ values are then scaled using the scaling factor obtained from calibration chamber data. Combining Equations 5-2 and 5-5 we can write

$$k = 0.47\left(k_{spherical}\right)^{1.7} \hspace{3cm} \text{[Eq. 5 - 6a]}$$

$$m = 1.7 \times m_{spherical} \hspace{3cm} \text{[Eq. 5 - 6b]}$$

and obtain k and m vs I_r, the results being shown in Figure 5-17.

The in-situ normalised cone tip resistance is calculated for the centre point of each SBP test from the procedure shown in Figure 5-18. Knowing the mean effective stress and G, we can calculate k and m for each depth. ψ_0 is then conveniently calculated from Equation 5-3. All the parameters and results are summarised in Table 5-6.

The state parameter at the location of each SBP was estimated from the CPT data allowing for variable penetration resistance along the length of the pressuremeter, and variable K_0 as described below.

The CPT penetration resistance is plotted in Figure 5-9, and the depths of the SBP tests are indicated. The best estimate of the q_c value at the CPT is taken as that at the mid-point of the SBP, with the upper and lower bounds for q_c being taken as the least and greatest value, respectively, over the length of the SBP. These values are tabulated as error margins in Table 5-6.

A main source of uncertainty in both CPT and SBP interpretation is the ambiguity in horizontal stress. In this project we have the luxury of good quality pressuremeter data to interpret a range of σ'_h and hence p' for each test depth (as explained in the next section). The variation in p' then results in a variation in G, I_r and Q leading to a range of ψ_0 predicted when superimposed with the variation in q_c.

The best estimate values of I_r shown in Table 5-6 are calculated using the best estimates of seismic shear modulus, G, with the best estimates of p'. The variation caused by the uncertainty in K_0 is presented as error margins for G. Variations in penetration resistance q_c along the length of the pressuremeter cause an additional variation in the normalised tip resistance Q (presented in Table 5-6) again resulting in uncertainty in the state parameter ψ_0.

5.9.   Evaluation of SBP Data

5.9.1.   Methodology

The SBP tests were analysed using Iterative Forward Modelling (IFM). IFM of a SBP involves estimating the parameter set for the test, computing the pressure-hoop strain curve, and comparing that curve with the measured one. The parameter set is varied and the procedure repeated until an acceptable fit is obtained in a procedure similar to that of Jefferies (1988) and subsequently adopted by Cunha (1994) and Shuttle and Jefferies (1995). IFM has the advantage of using all the available information while preventing inconsistent parameter combinations which may occur if the parameter selection is uncoupled.

The IFM work was based on the expanding cylindrical cavity idealisation of the pressuremeter, corrected for finite pressuremeter length. The original cavity radius was set equal to unity; the outer boundary was set as a zero displacement node at a distance of 800, and the logarithmic element spacing was used. The formulation assumes that the pressuremeter is infinitely long and so the soil around it is in a state of both plane strain and axial symmetry. A complete description of the formulation is presented in Shuttle (2006).

The idealisation of cylindrical symmetry is not as restrictive as might be thought because there appears to be a very simple relation between the cavity expansion pressure under the cylindrical assumption and that under a finite pressuremeter geometry. This aspect was explored experimentally by Ajalloeian and Yu (1998), who carried out experiments in a calibration chamber using several pressuremeter geometries and several sand densities. If the cavity expansion pressure under cylindrical symmetry is denoted as P_∞ and the cavity expansion

pressure for a finite SBP with a length (L) to diameter (D) ratio of $L/D = 6$ (typical of many commercial devices) as P_6, Shuttle (2006) used the experimental data to show that these two variables are related by

$$P_6 = P_\infty \left(1 + 0.1\varepsilon_R^{0.5}\right)$$
[Eq. 5 - 7]

where ε_R is the cavity hoop strain in percent at the pressuremeter-soil interface. Other SBP geometries have similar relations using different coefficients. Hence, it is convenient to rely on this result and use the simplification of cylindrical cavity expansion (Shuttle, 2006).

5.9.2. State Parameter from SBP Tests

In analysing the SBP data, sand parameters are known from the calibration summarised in Table 5-5, column 4 and 5, and with elastic shear modulus obtained from geophysical tests. Only two parameters remain to be determined by IFM: the initial horizontal stress σ_h' and the state parameter ψ_0. Despite the data being of good quality, disturbance is observed at the start of many of the tests, making determination of σ_h' from the lift-off pressure unreliable. Therefore both σ_h' and ψ_0 have been determined using IFM, with the fits constrained to pass through the higher strain SBP loading data where the effect of disturbance is lower. In addition, an upper limit of unity on K_0 was assumed as, although the sand was pumped at approximately 5000 t/hour via a 36 inch diameter central spigot using 8 MW and 15 MW pumps and higher values of K_0 could be anticipated, the sand was not overconsolidated. This methodology is summarised in Figure 5-19 and resulted in a non-unique, although constrained, predicted range

176

for σ'_h and ψ_0. The vertical effective stresses and K_0 values estimated for each SBP test are summarised in Table 5-6 and the credible range of "best fits" are plotted in Figure 5-20.

The quality of the fits to SBP curves is not equal for all tests. For some tests, including SBP 14, it was only possible to fit the last part of the curve by the model and K_0 and ψ_0 were not very well constrained. Conversely, visually an excellent fit is achieved for SBP 10, but this pressuremeter was expanded to less than 3% strain and the inferred ψ_0 is likely unrealistically dense.

5.10. Discussion

The goal of this study was to evaluate the in-situ state parameter of a sand deposit using two different in-situ methods so as to obtain an indication of the reliability with which state parameter can be determined. Two in-situ methods were used, the CPT and the SBP, each having differing constraints, attributes, and uncertainties. Data from the CPT and SBP were evaluated independently, and plotted in Figure 5-21 for comparison. Six of the seven evaluations (the exception being test 10 which is discussed below) indicate good correspondence between estimates for ψ_0 estimating the state parameter with a difference of 0 to 0.05. This is considered a very good level of consistency when compared to the common scatter observed in calibration chamber tests performed under controlled conditions in the laboratory.

In comparison to CPT, SBP tends to estimate more negative values of ψ_0 by approximately 0.02 indicating a denser deposit. Although small, this estimate is non-conservative relative to the CPT interpretation; so the results should be cautiously applied to engineering problems.

done on the densest material in the borehole, the SBP estimate seems unrealistic especially as no densification effort has been undertaken at the site. Looking at Table 5-6, one would realise that this test was continued to the lowest strain (2.8%) amongst all the SBP tests done at the site. Other tests are taken to at least 5.5% and up to 10.5%. Thus, it could be speculated that any SBP test taken to strains less than about 5% should be treated with extreme caution when it comes to determining the state parameter. The irony is that test 10 predicts too dense a state while in other tests the low strain data is generally softer than the numerical model results. Hence if we assume that test 10 would have followed the same trend as others, it should have become stiffer towards the end resulting in even denser ψ_0 predictions.

A striking feature of analysing these two different types of tests is the relative ease. The CPT is very easy to do in the field, but requires considerable care in estimating the state parameter. Conversely, with SBP it is challenging to get good data in sand but rather straightforward to analyse with the IFM approach.

The CPT interpretation would be aided by routine use of the seismic cone to provide the relevant shear modulus data. However, the biggest step for a range of soil types may be to use the data from the friction sleeve to indicate the appropriate soil compressibility behaviour. Plewes et al. (1992) initiated this approach based on field data, but enormous insights should be realisable from full numerical simulation of a real CPT geometry, and in which results are also computed for the friction sleeve.

Evaluation of SBP data in sand is at an early stage compared to the wealth of experience with the CPT. For example, the correction applied for limited pressuremeter length is purely

experimental and constant for different soil densities. Since the mismatch between CPT and SBP states increases with density (more negative ψ_0), and geometric corrections such as the one for limited boundaries of the CPT calibration chamber increase with density, it may be that the present finite geometry correction is too approximate. But this will diminish in importance in time when the IFM method runs fast enough to use real pressuremeter geometry in the finite element mesh of the numerical model.

The difference between ψ_0 interpreted by the two methods can also be magnified by an error in evaluating K_0 from SBP data, which is sensitive to disturbance. Obtaining a unique fit becomes more difficult because increased initial stress has a similar effect to decreased initial state. Further work is warranted on exploring the effect of disturbance, and in particular whether the contraction stage of the pressuremeter test might usefully constrain the estimate of σ_{h0} as is readily done in the case of clays (Shuttle and Jefferies, 1996).

5.11. Conclusion

State of the art methods were used to interpret the state parameter from in-situ SBP and CPT in a hydraulically placed clean quartz sand in Beaufort Sea. Calibration chamber test results have been modified for fabric effects to replicate in-situ soil conditions and used as reference.

SBP and CPT interpretation methods were used to estimate the in-situ state parameter with an acceptable consistency as compared to common scatter observed in laboratory testing performed under controlled conditions. CPT results appeared more consistent, and the state parameter values were more reasonable with respect to site conditions. However, since CPT calibration chamber testing has been used as a reference, and no independent measurement of the in-situ

One should keep in mind that although the CPT appears to produce a more reasonable and consistent state parameter interpretation for the site investigated, performing an adjacent pressuremeter test is necessary to obtain the horizontal stress required for the CPT interpretation formulation. In other words, the accuracy of CPT inferred state parameter relies on SBP measurement of horizontal stress levels.

SBP results can then be used to verify state parameters obtained from CPT testing through the analysis method employed in this research. However, any SBP test taken to strains of less than about 5 % should be treated with extreme caution in determining the state parameter.

For the site investigated in this program, which was six months old at the time of testing, ageing did not appear to have a significant effect and could be ignored in the interpretation. Conversely, fabric effects were deemed important and were accounted for in making use of laboratory measurements for site interpretation.

Table 5 - 1 Index properties of Erksak 330/0.7 and Erksak 355/3.0 sands

Sand/Source Property	Erksak 330/0.7 Been et al. (1991)	Erksak 355/3.0 Been et al. (1987[b])
Mineralogy	Quartz 73%, Feldspar 22%, Other 5%	Quartz, minor amounts of chert
Median grain size D_{50}: μm	330	355
Effective grain size D_{10}: μm	190	180
Uniformity coefficient	1.8	2.2
Percentage passing no. 200 sieve	0.7	3-6
Specific gravity of particle	2.66	2.65
Average sphericity	-	0.75
Grain description	Subrounded	Subrounded
Maximum void ratio e_{max}	0.753	0.963
Minimum void ratio e_{min}	0.527	0.525

Table 5 - 2 Summary of triaxial tests on Erksak 330/0.7 and Erksak 355/3.0 sands

Sand/Source	Erksak 330/0.7 Been et al. (1991)	Erksak 355/3.0 Been et al. (1987[b])
Number of undrained tests	40	5
Number of drained tests	16	5
Range of void ratio tested in drained triaxial apparatus	0.53-0.82	0.54-0.63
Range of mean effective stress applied in drained triaxial apparatus	60-1000 (kPa)	50-400 (kPa)

Table 5 - 3 Drained triaxial tests on moist tamped Erksak 355/3.0 sand

Test	Initial conditions			Test Conditions[1]		End of test					
	Void ratio	p' kPa	ψ_0	Drainage	Stress Path	Steady state [2]	σ'_3 kPa	p' kPa	q kPa	Void Ratio [3]	ϕ_c deg.
CID L1	0.628	100	-0.119	D	C	Mdil	100	185	255	0.689	33.4
CID L2	0.615	400	-0.105	D	C	Mdil	400	680	840	0.659	29.1
CID L3	0.709	195	-0.025	D	C	Con	195	300	313	0.705	25.4
CID D1	0.551	100	-0.196	D	C	Yes	100	190	268	0.658	32.8
CID C166	0.536	50	-0.224	D	C	Dil	50	86	109	0.590	32.3

[1] U, Undrained conditions; D, drained conditions; L, load-controlled compression; C, triaxial compression.
[2] Yes = critical state apparently reached; Dil/Con = sample still dilating or contracting at end of test; Mdil means small amount of dilation with sample close to critical state at end of test
[3] Void ratios corrected for membrane penetration

Table 5 - 4 Summary of CPT calibration chamber tests (after Been et al., 1987[b])

TEST	e	σ'_v kPa	σ'_h kPa	k_o	p' kPa	ψ_0	q_c MPa	Boundary Correction	Q
CC-3A	0.63	100	100	1.00	100.0	-0.117	6.7	1.00	63
CC-3B	0.58	100	100	1.00	100.0	-0.167	14.1	1.05	144
CC-05	0.53	127	89	0.70	102.0	-0.216	26.2	1.15	290
CC-6A	0.66	306	214	0.70	245.0	-0.069	12.4	1.00	49
CC-6B	0.62	307	214	0.70	245.0	-0.109	18.6	1.00	74
CC-6C	0.58	309	214	0.69	246.0	-0.149	30.4	1.00	122
CC-07	0.56	307	214	0.70	245.0	-0.169	31.5	1.05	133
CC-08	0.60	374	266	0.71	302.0	-0.126	29.7	1.00	97
CC-09	0.56	63	44	0.70	50.0	-0.200	10.5	1.11	229
CC-10	0.57	188	131	0.70	150.0	-0.169	27.8	1.05	193
CC-11	0.53	180	126	0.70	144.0	-0.210	31.2	1.12	240
CC-12	0.60	180	126	0.70	144.0	-0.140	12.9	1.00	88
CC-18	0.64	30	22	0.73	25.0	-0.133	1.9	1.00	65
CC-19	0.53	63	45	0.71	51.0	-0.229	11.5	1.20	260

Table 5 - 5 NorSand calibration to Erksak sand

Parameter	Erksak 330/0.7 (wet pluviated)	Erksak 330/0.7 (moist tamped)	Erksak 355/3.0 (moist tamped)	In-situ Soil: Erksak 355/3.0 (Hydraulic-ally placed)	Remark
Critical State					
Γ	0.828	0.828	0.834	0.834	Void ratio of CSL at 1 kPa
λ_e	0.0160	0.0160	0.019	0.019	Slope of CSL, defined on base e
M_{tc}	1.27	1.27	1.25	1.25	Critical state friction ratio
Plasticity					
H	$70-430\psi_0$	$100-400\psi_0$	$100-400\psi_0$	$70-430\psi_0$	Plastic hardening modulus for loading
χ_{tc}	5.40	5.40	3.80	3.80	Relates minimum dilatancy to ψ, again determined under triaxial compression conditions
N	0.40	0.40	0.32	0.32	Volumetric coupling parameter for stress-dilatancy rule
Elasticity					
G (kPa)	$\dfrac{195}{(e-e^*_{min})}\times(p'\,p'_{ref})^{0.50}$ After eq. 3.37 of Jefferies and Been, 2006	$\dfrac{195}{(e-e^*_{min})}\times(p'\,p'_{ref})^{0.50}$ After eq. 3.37 of Jefferies and Been, 2006	$\dfrac{195}{(e-e^*_{min})}\times(p'\,p'_{ref})^{0.50}$ After eq. 3.37 of Jefferies and Been, 2006	$1900\,p'^{\,0.8}$ from in-situ seismic shear wave velocity (Figure 5-10)	p' is the initial mean effective stress in kPa p'_{ref} is a reference stress equal to 100 kPa $e^*_{min}=0.355$ is the void ratio at which the volumetric compressibility becomes zero.
ν	0.20	0.20	0.20	0.20	Poisson's ratio, assumed value (measured values typically found to be in range 0.10- 0.25)

182

Table 5 - 6 Summary of data used in estimation of in-situ state from CPT and SBP tests

Test	Depth (m) note 1	$\bar{\sigma}'_v$ (kPa) note 2	K_0 (---)	p' (kPa)	q_c (MPa)	Q (---)	G (MPa)	k (---)	m (---)	ψ_0 from CPT	Maximum strain (%) in SBP test	ψ_0 from SBP
1	2.7	50	0.85 ± 0.15	45.0 ± 5.0	2.6 ± 0.3	64.3 ± 7.3	39.9 ± 3.5	19.59	11.18	-0.11 ± 0.01	8.4	-0.06 ± 0.02
9	10.7	135	0.77 ± 0.23	114.5 ± 20.7	9.2 ± 0.7	82.6 ± 21.2	84.1 ± 12.2	19.47	10.92	-0.13 ± 0.02	5.5	-0.17 ± 0.04
10	11.5	143	0.85 ± 0.15	128.8 ± 14.3	14.7 ± 5.0	114.0 ± 12.8	92.5 ± 8.2	19.45	10.88	-0.16 ± 0.01	2.8	-0.26 ± 0.04
11	16.2	189	0.80 ± 0.20	163.9 ± 25.2	12.3 ± 5.0	799 ± 43.0	112.1 ± 13.8	19.42	10.82	-0.11 ± 0.06	10.5	-0.12 ± 0.03
13	18.2	209	0.80 ± 0.20	180.8 ± 27.8	8.0 ± 2.0	45.2 ± 18.2	121.3 ± 15.0	19.41	10.79	-0.07 ± 0.04	8.0	-0.11 ± 0.03
14	20.0	226	0.77 ± 0.24	190.8 ± 35.5	12.7 ± 2.0	69.1 ± 23.5	126.5 ± 18.9	19.40	10.78	-0.11 ± 0.04	9.1	-0.13 ± 0.04
15	21.0	236	0.96 ± 0.04	229.8 ± 6.3	12.4 ± 3.0	52.6 ± 14.5	147.2 ± 3.2	19.38	10.72	-0.09 ± 0.03	8.0	-0.11 ± 0.00

Notes: (1) Depths are quoted to the strain arm measurement axis of the SBP.
 (2) Water Table estimated at 3.5 m from surface from adjacent CPTu.

a)
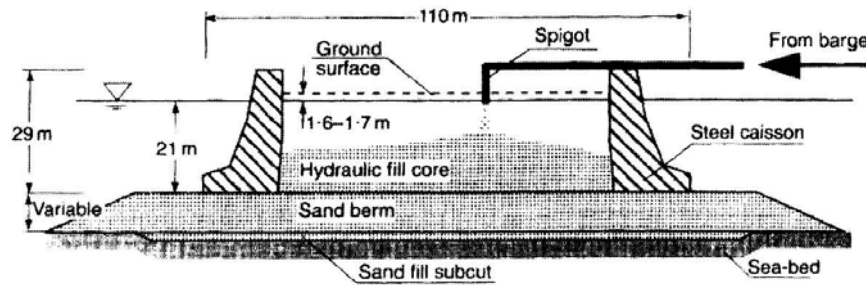
b)

Figure 5 - 1 a) Aerial photo of Molikpaq; b) Schematic cross section of Molikpaq at Tarsiut P-45 (Jefferies and Been, 2006)
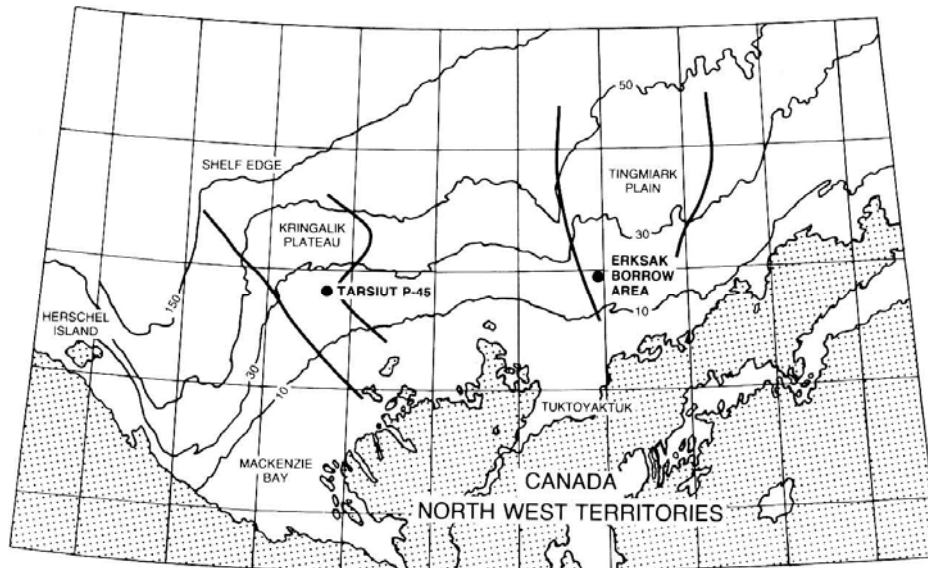

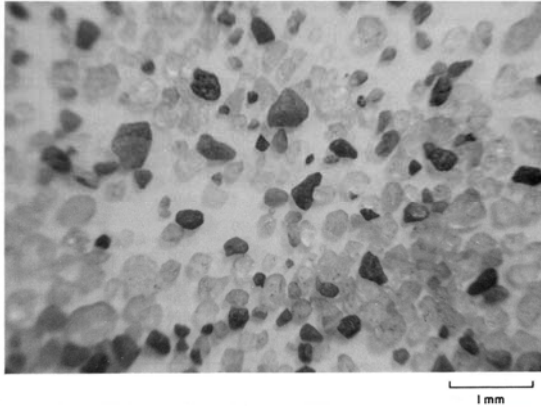Figure 5 - 2 Tarsiut location showing proximity of Erksak borrow (after Jefferies et al., 1985)

184

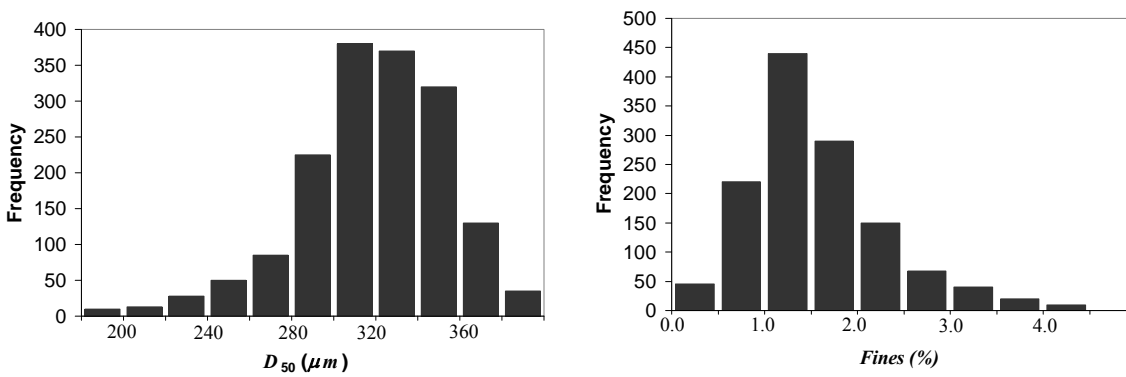Figure 5 - 3 Photograph of washed Erksak 355 sand particles (Been et al., 1987[b])

Figure 5 - 4 Particle size distribution of Erksak sand in hopper of dredge prior to placement (after Goldby et al., 1986)
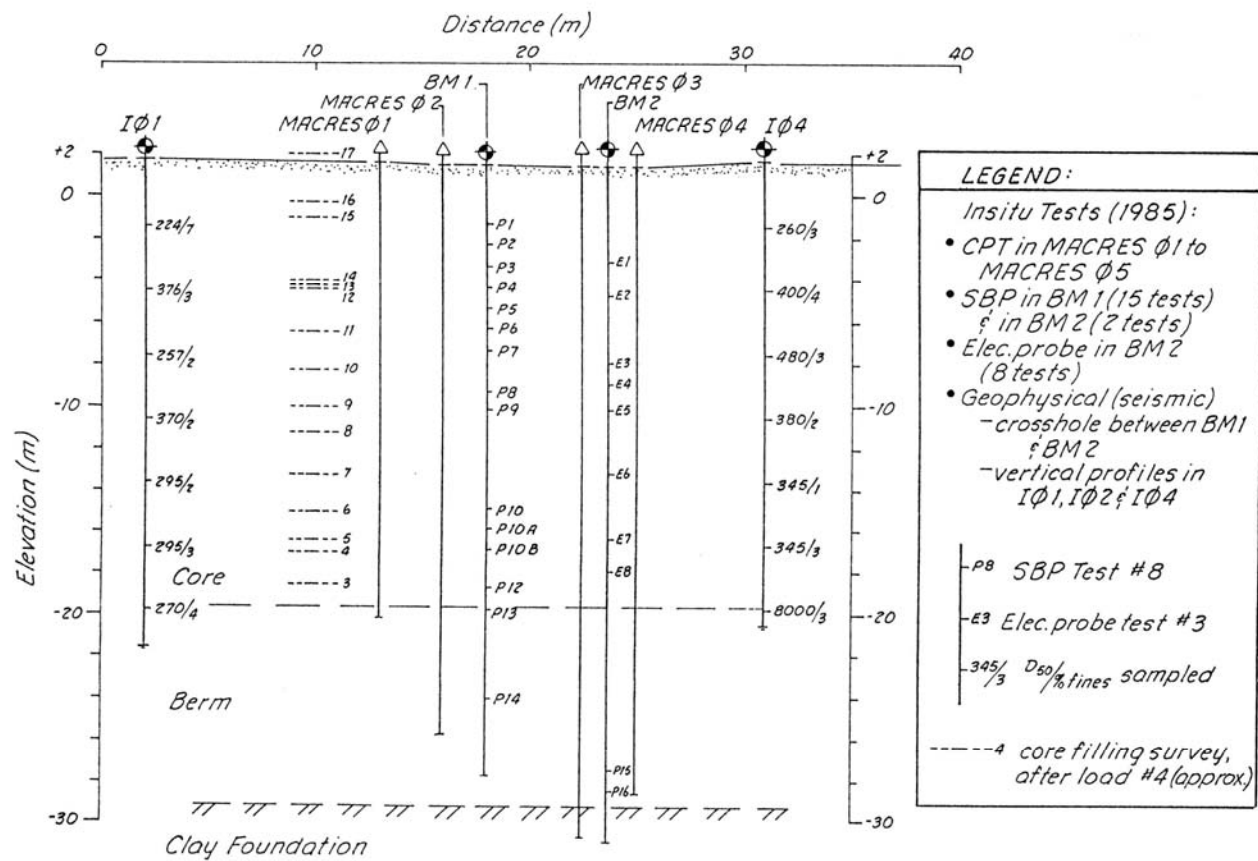
Figure 5 - 5 Section through the core showing the 1985 in-situ testing program and the results of gradation tests (Golder Associates Ltd., 1986)
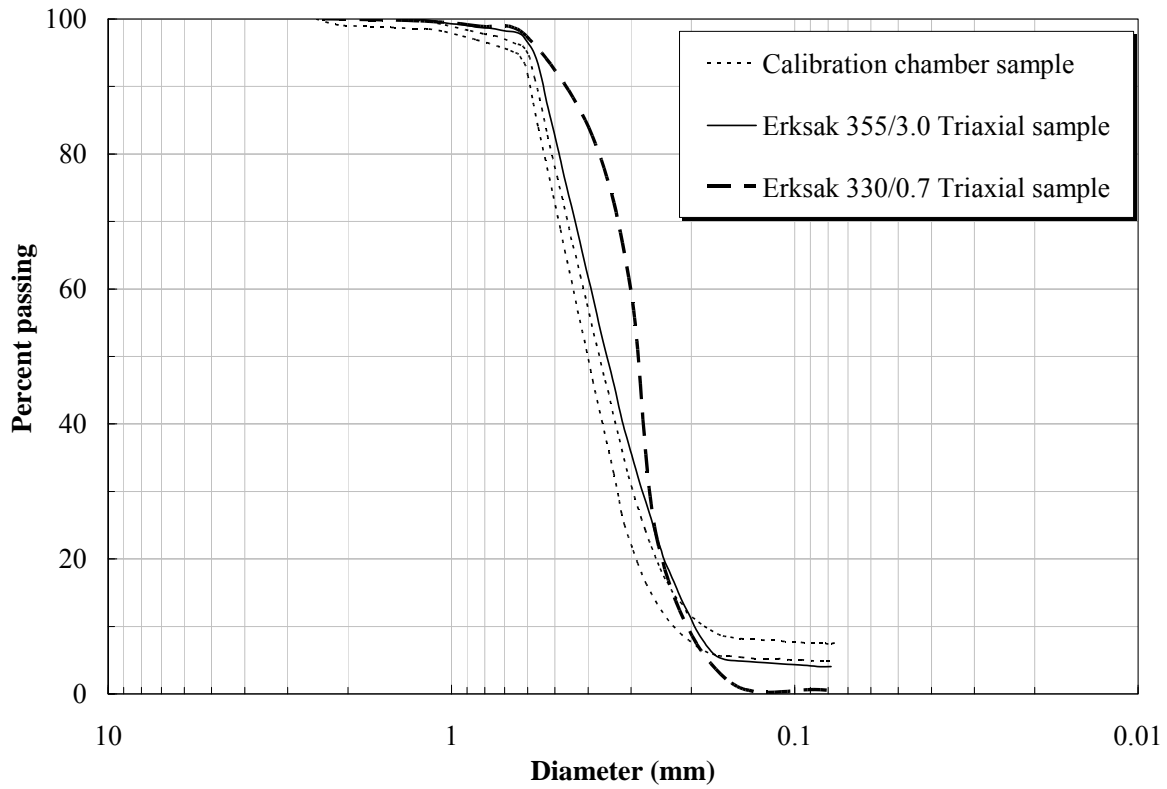
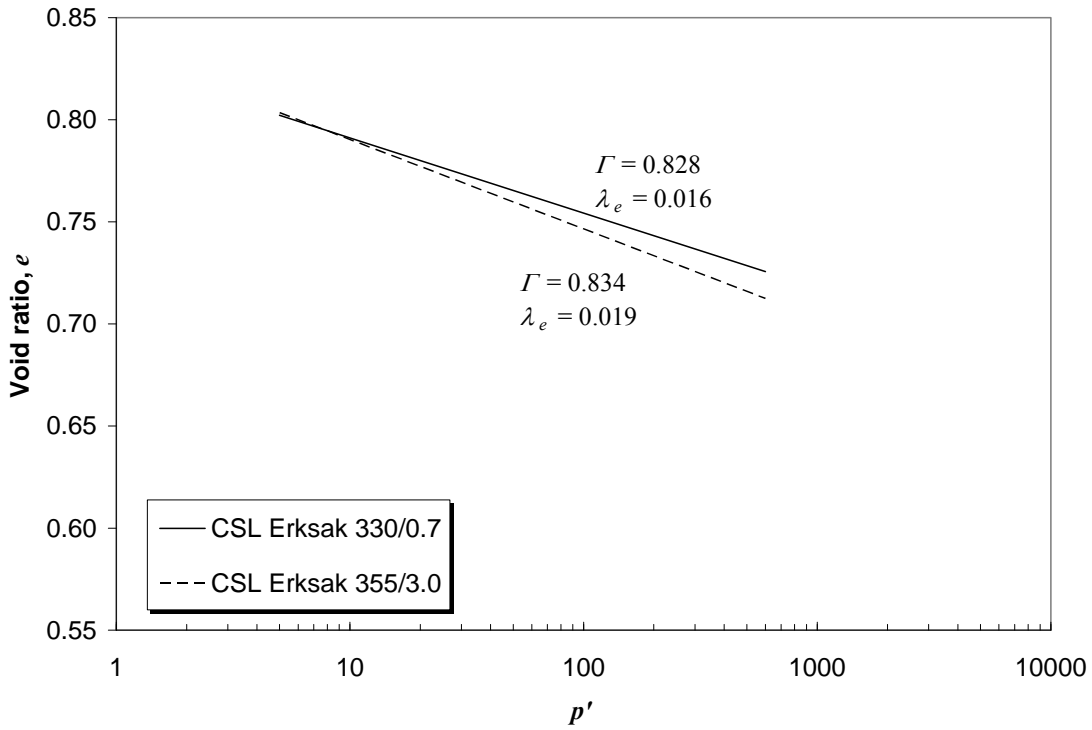Figure 5 - 6 Grain size distribution of different Erksak sand gradations: Erksak 355/3.0 and 330/0.7 (after Been et al., 1987[b], 1991)

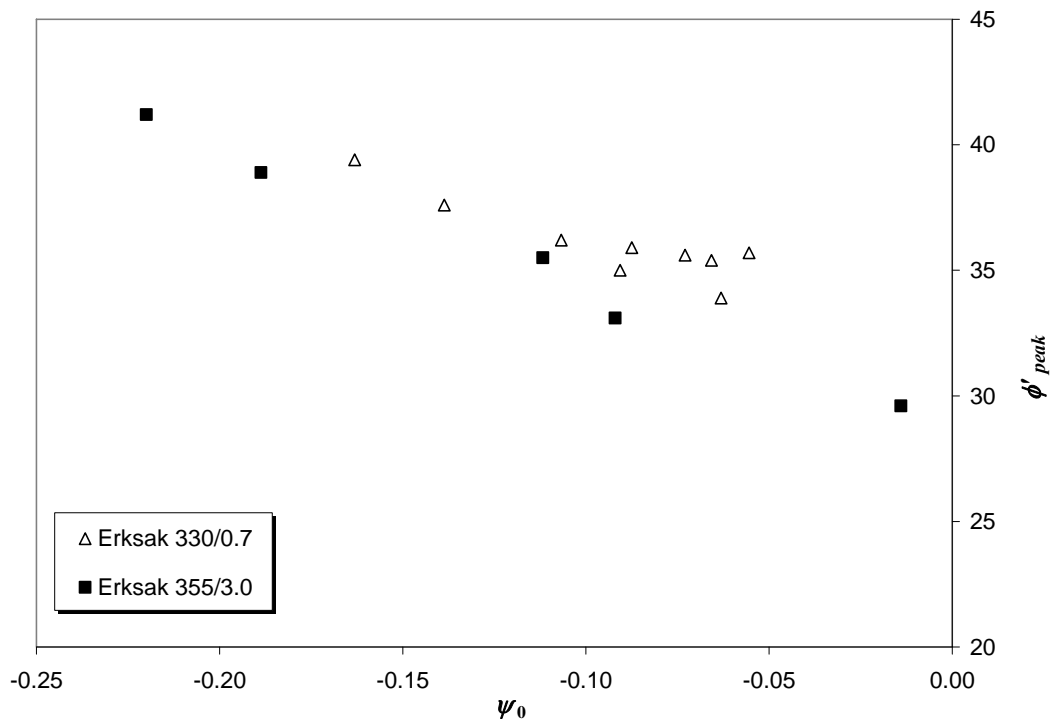Figure 5 - 7 CSL locations for Erksak 330/0.7 and Erksak 355/3.0

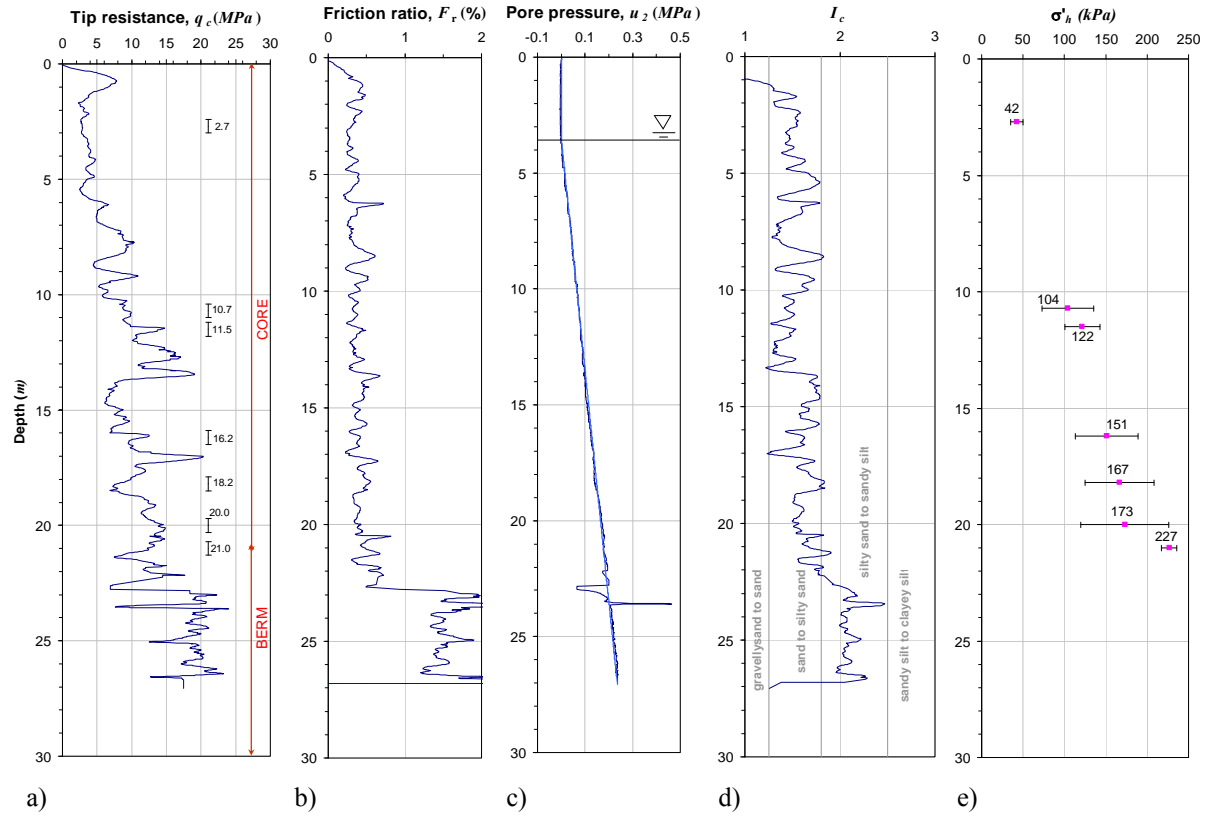Figure 5 - 8 Peak drained triaxial compression strength of dense Erksak sand samples

Figure 5 - 9 a) Cone tip resistance and SBP depths; b) Friction ratio; c) Pore water pressure u_2; d) material index I_c after Been and Jefferies (1992); e) Horizontal effective stress from SBP
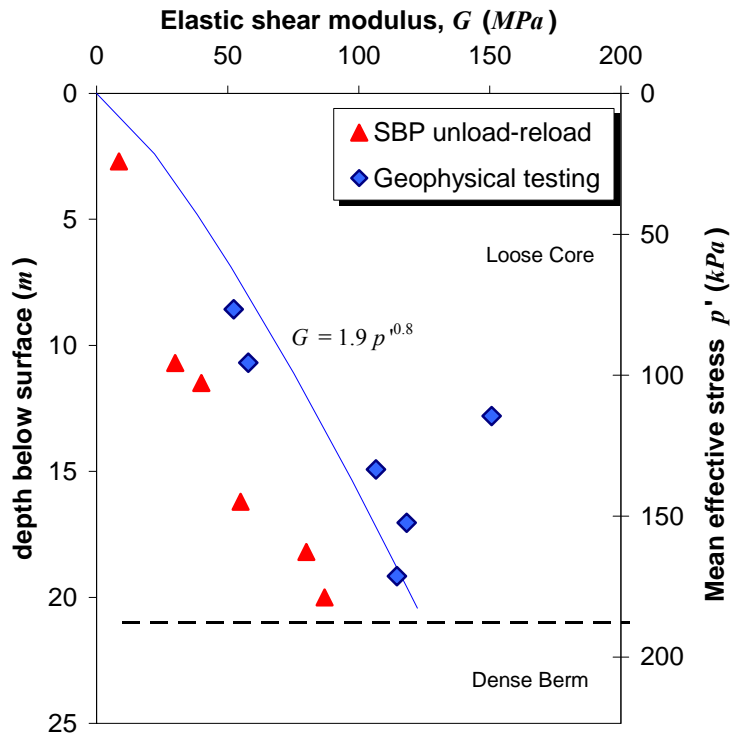
Figure 5 - 10 Shear modulus measurements from SBP unload-reload loops and geophysical testing (data from Golder Associates Ltd., 1986)
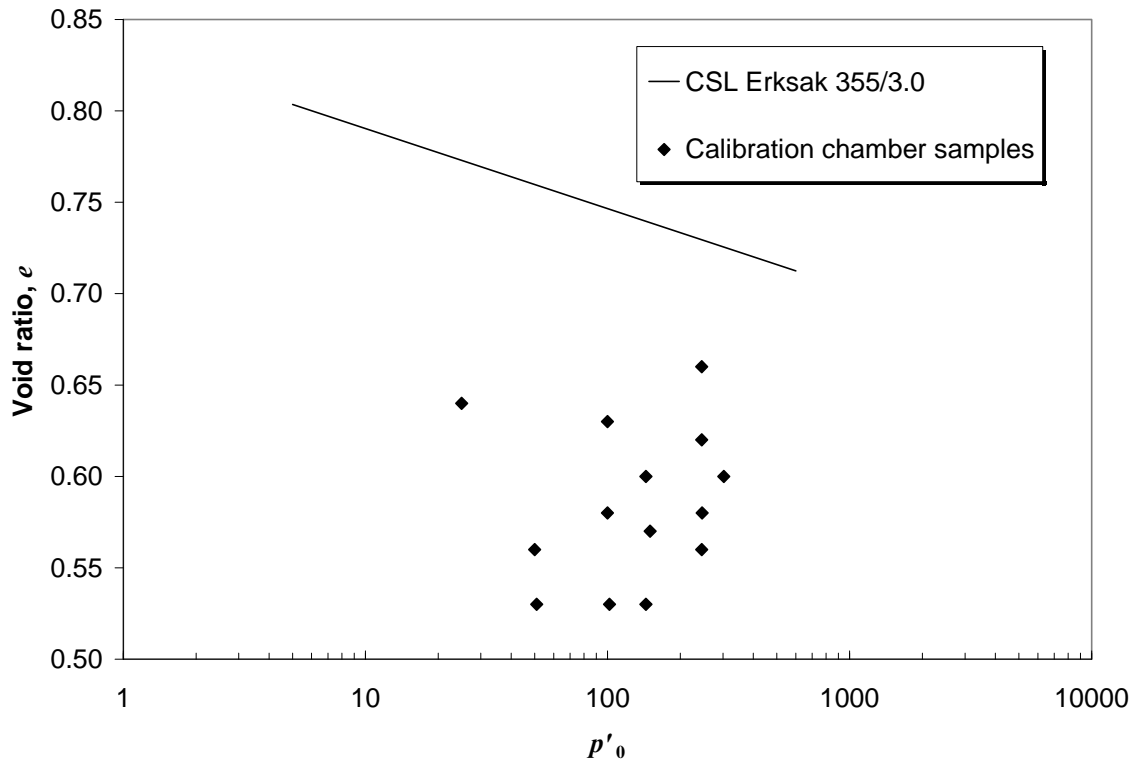

Figure 5 - 11 Initial state plot for CPT calibration tests in Erksak 355/3.0 sand
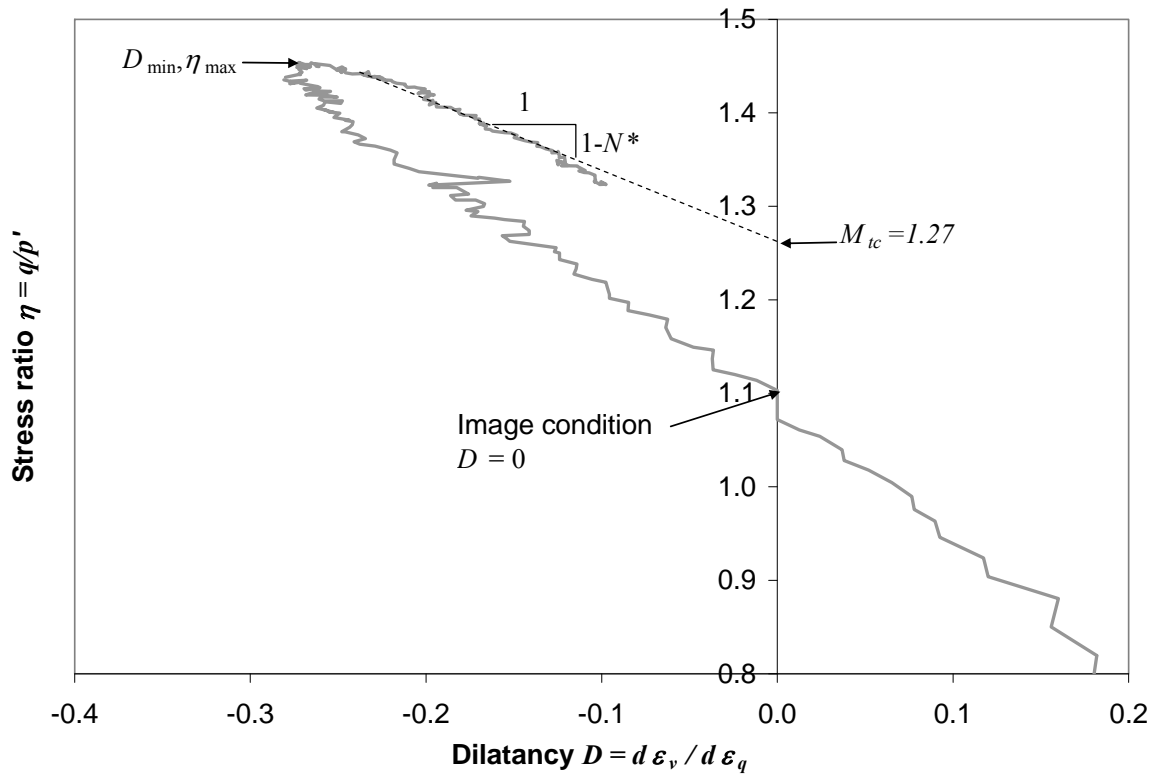
Figure 5 - 12 Stress-dilatancy plot (η - D) for Erksak 330/0.7 sand (test CID_G666)

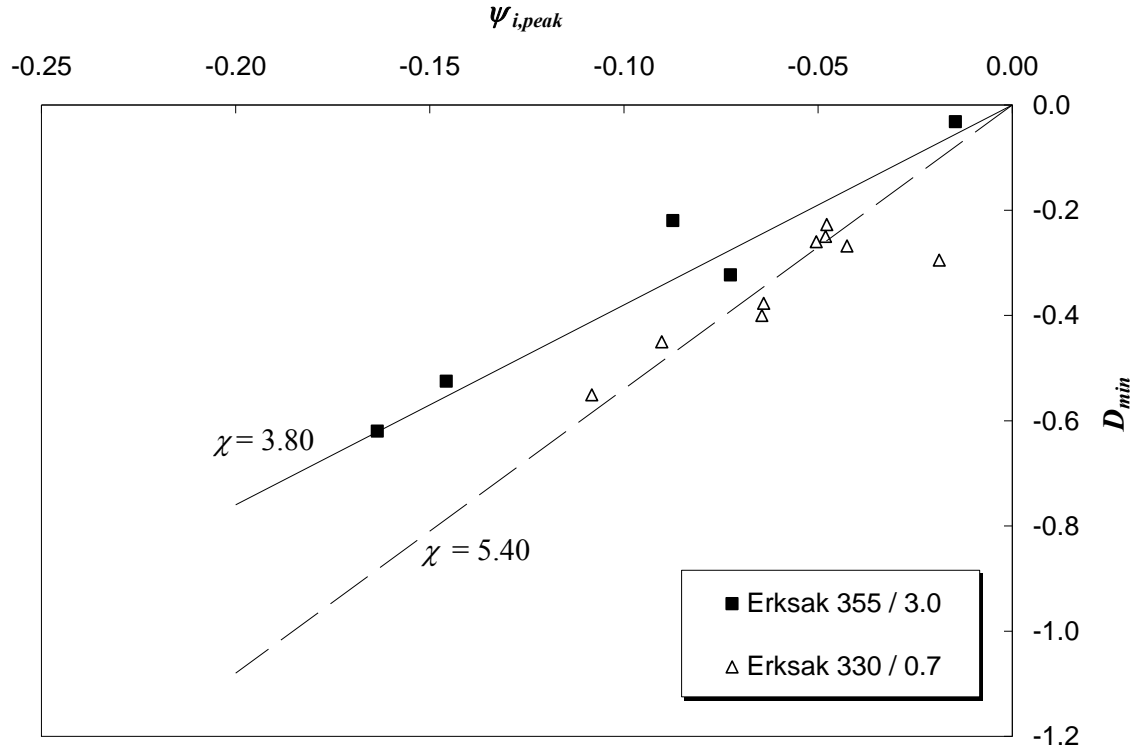Figure 5 - 13 Plot of dilatancy at peak, D_{min}, versus the state parameter at the image condition ψ_i at peak to determine the value of χ_{tc}
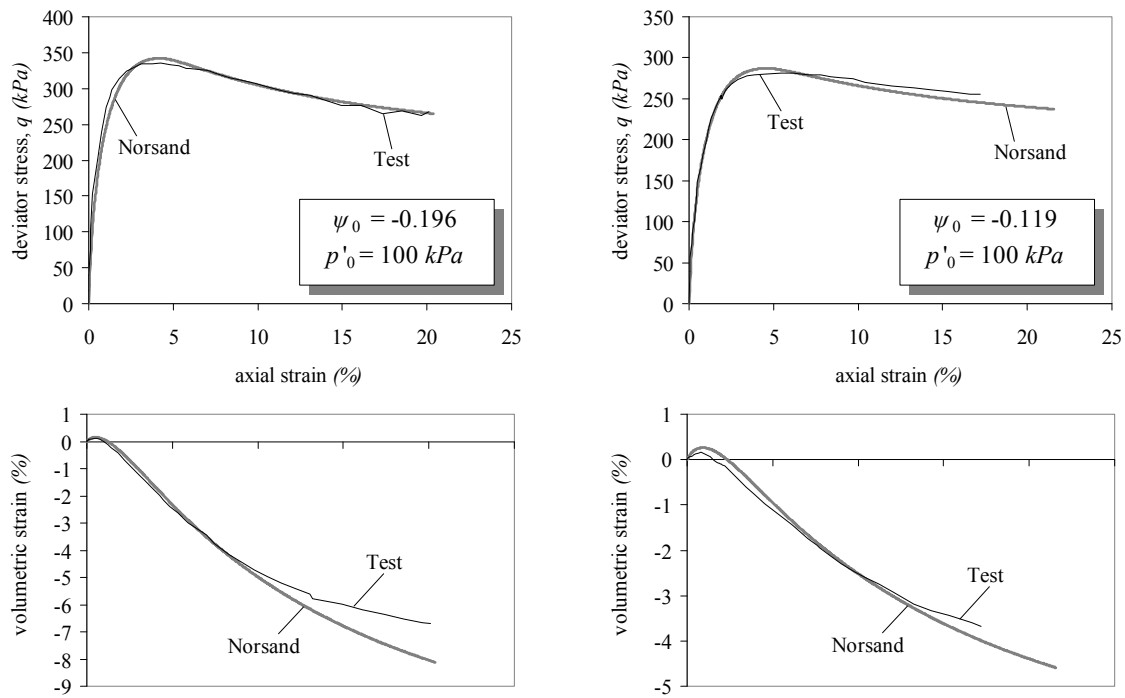
a) Test CID D1

b) Test CID L1

Figure 5 - 14 Fitting NorSand to triaxial tests on Erksak 355/3.0, Moist tamped
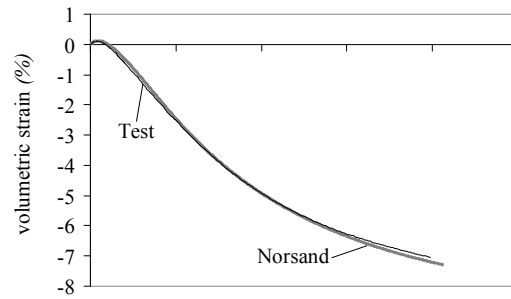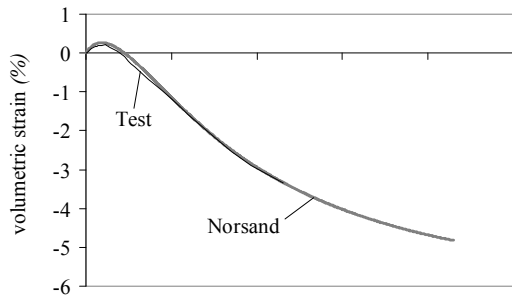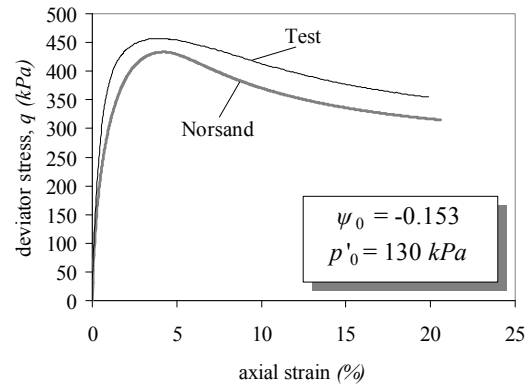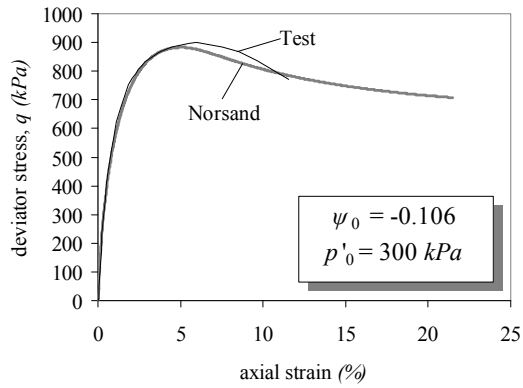
a) Test CID G664, Wet pluviated

b) Test CID G667, Wet pluviated
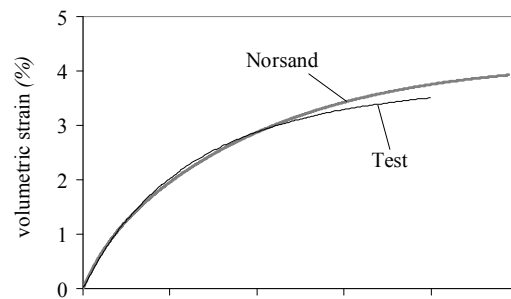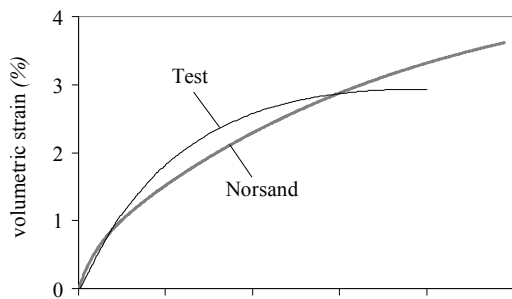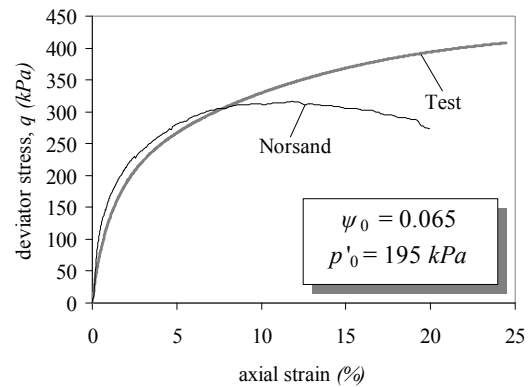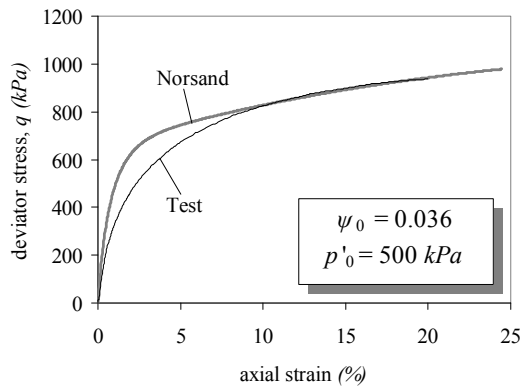
c) Test CID G682, Moist tamped

d) Test CID G685, Moist tamped

Figure 5 - 15 Fitting NorSand to triaxial tests on Erksak 330/0.7
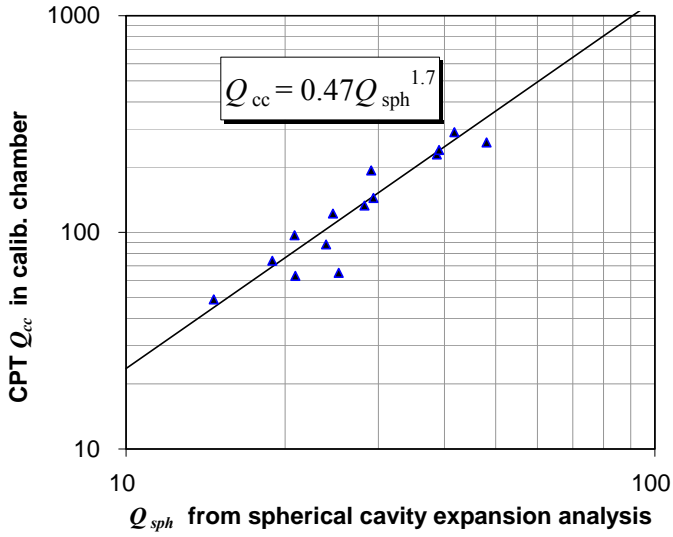
Figure 5 - 16 CPT in calibration chamber versus spherical cavity expansion: Erksak sand
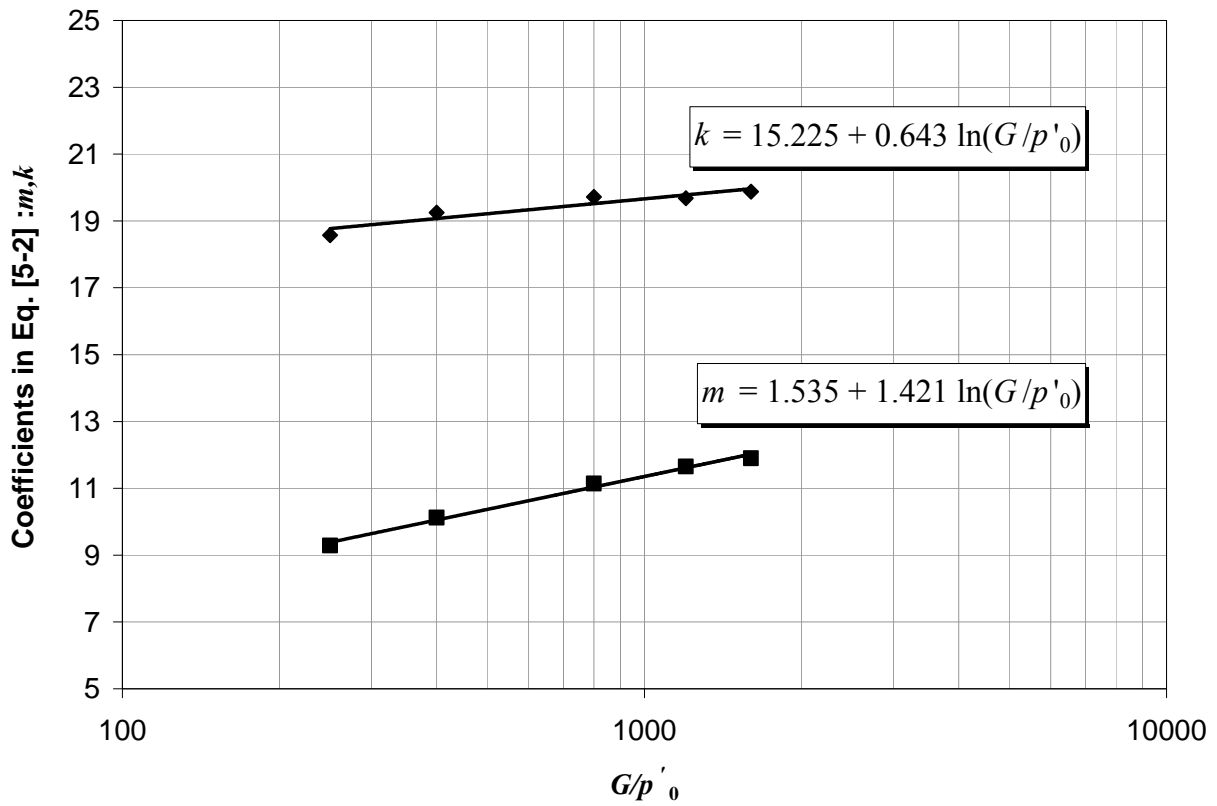
Figure 5 - 17 Computed effect of soil rigidity I_r on CPT calibration coefficients in hydraulically placed Erksak 355/3.0 sand
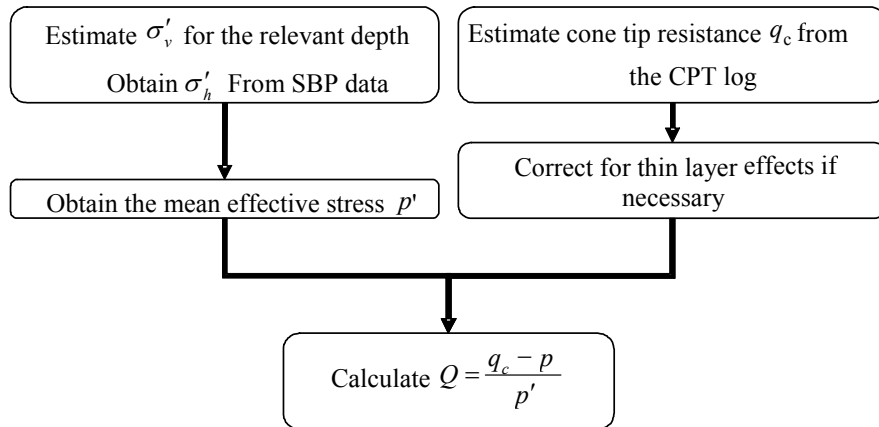
Figure 5 - 18 Procedure followed to obtain the normalised cone tip resistance Q from CPT data at depth of the adjacent SBP
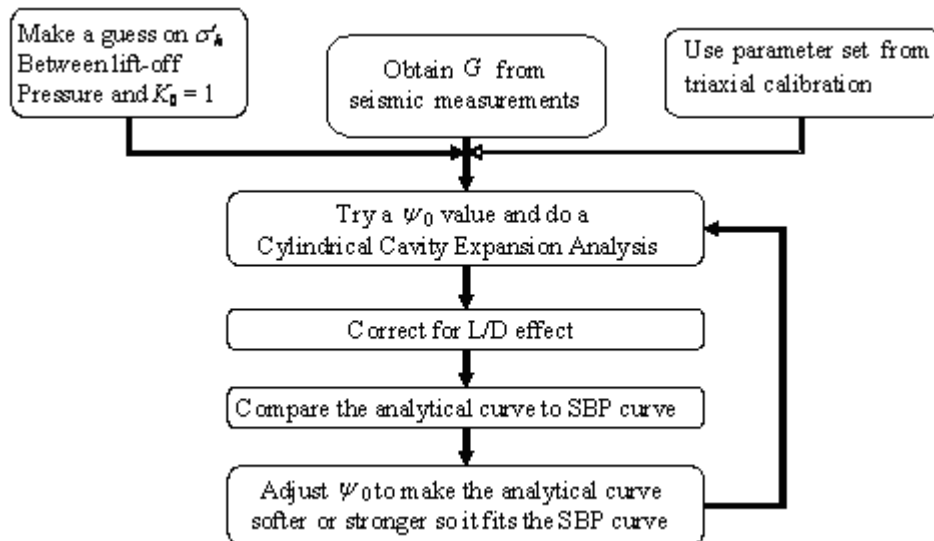
Figure 5 - 19 Procedure followed to obtain the initial state parameter ψ_0 from SBP data

a)

b)

c)

d)

e)

f)

g)
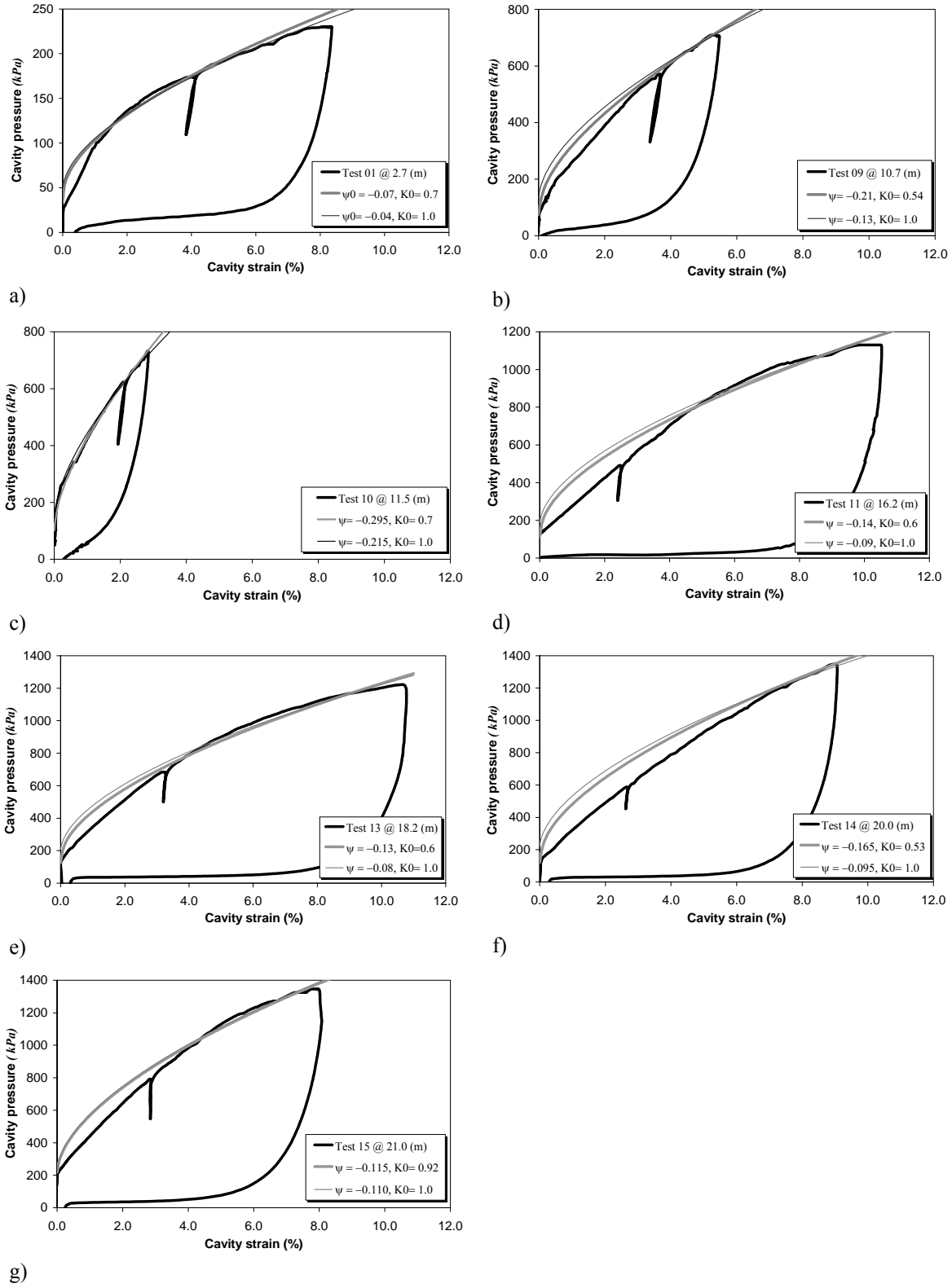
Figure 5 - 20 IFM calibration of SBP to determine range of ψ_0 and K_0 (SBP corrected for finite geometry effects)
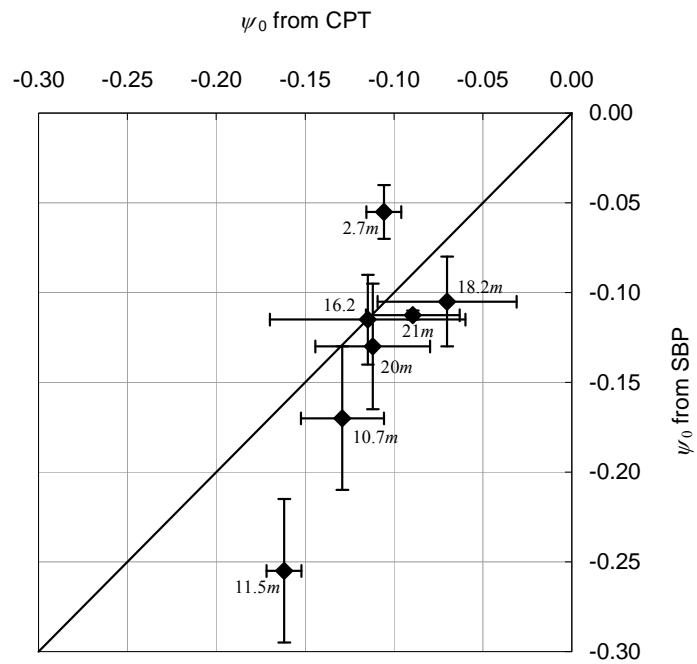
Figure 5 - 21 Comparison of ψ_0 back calculated from CPT and SBP (numbers on the figure indicate test depth)

5.12. References

Ahmadi M.M., and Robertson P.K. 2005. Thin-Layer Effects on the CPT q_c Measurement. Canadian Geotechnical Journal, 42: 1302–1317.

Ajalloeian R., and Yu H. S. 1998. Chamber Studies of the Effects of Pressuremeter Geometry on Test Results in Sand. Géotechnique, 48(5): 621–636.

ASTM D5778 - 07 . Standard Test Method for Electronic Friction Cone and Piezocone Penetration Testing of Soils. Published : November 2007.

Been K., and Jefferies M.G. 1985. A State Parameter for Sands. Géotechnique, 35(2): 99-112.

Been K., and Jefferies M.G. 1992. Towards Systematic CPT Interpretation. Proceedings Wroth Memorial Symposium, Thomas Telford, London, 121-134.

Been K., Crooks J.H.A., Becker, D. E., and Jefferies M.G. 1986. The Cone Penetration Test in Sands: Part I, State Parameter Interpretation. Géotechnique, 36(2): 239-249.

Been K., Jefferies M.G., Crooks J.H.A., and Rothenberg L. 1987[a]. The Cone Penetration Test in Sands: Part II, General Inference of State. Géotechnique, 37(3): 285-299.

Been K., Lingnau B.E., Crooks J.H.A., and Leach B. 1987[b]. Cone Penetration Test Calibration for Erksak (Beaufort Sea) Sand. Canadian Geotechnical Journal, 24: 601-610.

Been K., Jefferies M.G., and Hachey J. 1991. The Critical State of Sands. Géotechnique, 41(3): 365-381.

Bishop A.W. 1966. Strength of Soils as Engineering Materials. 6th Rankine Lecture, Géotechnique, 16: 89-130.

Carter J.P., Booker J.R., and Yeung S.K. 1986. Cavity Expansion in Cohesive Frictional Soils. Géotechnique, 36(3): 349-358.

Collins I. F., Pender M.J., and Yan W. 1992. Cavity Expansion in Sands under Drained Loading Conditions. International Journal for Numerical and Analytical Methods in Geomechanics, 16: 3–23.

Cunha R.P. 1994. Interpretation of Selfboring Pressuremeter Tests in Sand. PhD thesis, Department of Civil Engineering, the University of British Columbia.

Cunning J.C., Robertson P.K., and Sego D.C. 1995. Shear Wave Velocity to Evaluate in Situ State of Cohesionless Soils. Canadian Geotechnical Journal, 32(5): 848-858.

de Borst R., and Vermeer P.A. 1982. Finite Element Analysis of Static Penetration Tests. Proceedings of the 2nd European Symposium on Penetration Testing, Amsterdam, Netherlands, 457-562.

Ghafghazi M., and Shuttle D.A. 2006. Accurate Determination of the Critical State Friction Angle from Triaxial Tests. Proceedings of the 59th Canadian Geotechnical Conference, Vancouver, 278-284.

Ghionna V.N., and Jamiolkowski M. 1991. A Critical Appraisal of Calibration of Calibration Chamber Testing of Sands. Proceedings of the 1st International Symposium on Calibration Chamber Testing, ISOCCT 1, Potsdam, New York, 13-39.

Goldby H.M., Crooks J.H.A., Harper J.R., and Stuckert B. 1986. Novel Approach to Fill Material Quality Assessment near Real Time Grading of Dredged Sand. Proceedings of 3rd Canadian Conference on Marine Geotechnical Engineering, St. John's, Newfoundland, Canada, 1: 409-427.

Golder Associates (Western Canada) Ltd. 1986. Report on Review of In Situ Testing Tarsuit P-45 Research Project, April 1986.

Hicks M. A., and Smith I. M., 1986. Influence of Rate of Pore Pressure Generation on the Stress-Strain Behaviour of Soils. International Journal for Numerical Methods in Engineering, 22(3): 597-621.

Hicks M.A., and Smith I.M. 1988. Class A Prediction of Arctic Caisson Performance. Géotechnique, 38(4): 589-612.

Hicks M.A., and Onisiphorou C. 2005. Stochastic Evaluation of Static Liquefaction in a Predominantly Dilative Sand Fill. Géotechnique, 55(2): 123-133.

Hofmann B.A., Sego D.C., and Robertson P.K. 2000. In Situ Ground Freezing to Obtain Undisturbed Samples of Loose Sand. ASCE, Journal of Geotechnical and Geoenvironmental Engineering, 126(11): 979-989.

Holden J.C. 1991. History of the First Six CRB Calibration Chambers. Proceedings of 1st International Symposium on Calibration Chamber Testing, Potsdam, New York, 1-12.

Hsu H.H., and Huang A.B. 1998. Development of an Axisymmetric Field Simulator for Cone Penetration Tests in Sand. Geotechnical Testing Journal, 21(4): 348-355.

Huang W., Sheng D., Sloan S.W., and Yu H.S. 2004. Finite Element Analysis of Cone Penetration in Cohesionless Soil. Computers and Geotechnics, 31: 517–528.

Hughes J.M.O., Wroth C.P., and Windle D. 1977. Pressuremeter Tests in Sands. Géotechnique, 27(4): 455-477.

Huntsman S.R., Mitchell J.K., Klejbuk L.W. Jr., and Shinde S.B. 1986. Lateral Stress Measurement during Cone Penetration. Proceedings of In Situ '86, Use of In Situ Tests in Geotechnical Engineering, Blacksburg, VA, USA. ASCE Geotechnical Special Publication 6: 617-634.

Jefferies M.G. 1988. Determination of horizontal geostatic stress in clay with self-bored pressuremeter. Canadian Geotechnical Journal, 25(3): 559-573.

.Jefferies M.G. 1993. Nor-Sand: a Simple Critical State Model for Sand. Géotechnique, 43(1): 91-103.

Jefferies M.G., and Been K., 1995. Cone Factors in Sand. Proceedings of CPT '95, International Symposium on Cone Penetration Testing, Swedish Geotechnical Society, Linkoping, Sweden, Oct. 4-5 1995: 187-193.

Jefferies M.G., and Shuttle D.A. 2002. Dilatancy in General Cambridge-Type Models. Géotechnique, 52(9): 625-638.

Jefferies M.G., and Shuttle D.A. 2005[a]. NorSand: Features, Calibration and Use. Proceedings of Specialty Conference on Soil Constitutive Models: Evaluation, Selection, and Calibration. ASCE Geotechnical Special Publication, 128: 204-236.

Jefferies M.G., and Shuttle D.A. 2005[b]. NorSand: Calibration and Use. Proceedings of the 11th Conference of the International Association for Computer Methods and Advances in Geomechanics, Turin, 345-352.

Jefferies M.G., and Been K. 2006. Soil Liquefaction: a Critical State Approach. Taylor & Francis (Abingdon & New York). ISBN 0-419-16170-8.

Jefferies M.G., Stewart H.R., Thomson R.A.A., and Rogers B.T. 1985. Molikpaq Deployment at Tarsiut P-45. Proceedings of ASCE Specialty Conference on Civil Engineering in the Arctic Offshore, San Francisco, Ca., 1-27.

Jefferies M.G., Crooks J.H.A., Becker D.E., and Hill P.R. 1987. Independence of Geostatic Stress from Overconsolidation in Some Beaufort Sea Clays. Canadian Geotechnical Journal, 24(3): 342-356.

Jefferies M.G., Rogers B.T., Stewart H.R., Shinde S., James D., and Williams-Fitzpatrick S. 1988. Island Construction in the Canadian Beaufort Sea. Proceedings of specialty conference on Hydraulic Fill Structures, ASCE Geotechnical Special Publication, 21: 816-883.

Konrad J.M. 1988. Interpretation of Flat Plate Dilatometer Tests in Sands in Terms of the State Parameter. Géotechnique, 38(2): 263-277.

Nash D.F.T., Powell J.J.M., and Lloyd I.M. 1992. Initial Investigations of the Soft Clay Test Site at Bothkennar. Géotechnique, 42(2): 163-181.

Peterson R.W., and Arulmoli K. 1991. Overview of a Large Stress Chamber System. Proceedings of First International Symposium on Calibration Chamber Testing, Potsdam, New York, 329-338.

Plewes H.D., McRoberts E.C., and Chan W.K. 1988. Downhole Nuclear Density Logging in Sand Tailings. ASCE Geotechnical Special Publication, 21: 290-309.

Plewes H.D., Davies M.P., and Jefferies M.G. 1992. CPT Based Screening Procedure for Evaluating Liquefaction Susceptibility. Proceedings of the 45th Canadian Geotechnical Conference, Toronto.

Plewes H.D., Pillai V.S., Morgan M.R., and Kilpatrick B.L. 1994. In Situ Sampling, Density Measurements, and Testing of Foundation Soils at Duncan Dam. Canadian Geotechnical Journal, 31: 927–938.

Popescu R., Prevost J.H., and Deodatis G. 1997. Effects of spatial variability on soil liquefaction; some design recommendations. Géotechnique, 47(5): 1019-1036.

Robertson P.K., and Campanella R.G. 1983. Interpretation of Cone Penetration Tests. Part I: Sand. Canadian Geotechnical Journal, 20: 718-733.

Schofield A.N., and Wroth C.P. 1968. Critical State Soil Mechanics. McGraw Hill, London.

Shuttle D.A. 2006. Can the effect of sand fabric on plastic hardening be determined using self-bored pressuremeter? Canadian Geotechnical Journal, 43: 659-673.

Shuttle D.A. and Jefferies M.G. 1995. Reliable parameters from imperfect SBP tests in clays, ICE Conference on Advances in Site Investigation Practice, London, March 1995.

Shuttle D.A., and Jefferies M.G. 1996. Reliable Parameters from Imperfect SBP Tests in Clays. Advances in Site Investigation Practice: Proceedings of the International Conference Held in London on 30-31 March 1995, C. Craig (ed.), published January 1996 by Thomas Telford, ISBN: 0727725130, 571-585,

Shuttle D.A., and Jefferies M.G. 1998. Dimensionless and Unbiased CPT Interpretation in Sand. International Journal of Numerical and Analytical Methods in Geomechanics, 22: 351-391.

Shuttle D.A. and Jefferies M.G. 2000. Prediction and Validation of Compaction Grout Effectiveness. Proceedings of Geo-Denver 2000, Advances in Grouting and Ground Modification, August 5-8 2000, ASCE Geotechnical Special Publication, Krizek R.J., and Sharp K. (eds.), 104: 48-64

Sladen J.A. 1989. Problems with Interpretation of Sand State from Cone Penetration Test. Géotechnique, 39(2): 323-332.

Stewart H.R., Jefferies M.G., and Goldby H. M. 1983. Berm Construction for the Gulf Canada Mobile Arctic Caisson. Proceedings of Annual Offshore Technology Conference, 2: 339-346.

Tan N.K., Miller G.A., and Muraleetharan K.K. 2003. Preliminary Laboratory Calibration of Cone Penetration in Unsaturated Silt. Proceedings, 12th Pan American Conference on Soil Mechanics and Geotechnical Engineering, Cambridge, Massachusetts, 1: 391-396.

Tavenas F.A. 1973. Difficulties in the Use of Relative Density as a Soil Parameter. Evaluation of Relative Density and its Role in Geotechnical Projects Involving Cohesionless Soils, American Society for Testing and Materials, Selig E.T., and Ladd R.S. (eds.), Philadelphia, ASTM Special Technical Publication 523: 478-483.

van den Berg P. 1994. Analysis of Soil Penetration. PhD Thesis, Delft University of Technology, ISBN 90-407-1004-X.

Willson S.M., Ims B.W., and Smith I.M. 1988. Finite Element Analysis of Cone Penetration. Penetration Testing in the UK, Thomas Telford, London, 157-159.

Woods R.D., Benoît J., and deAlba P. 1994. National Geotechnical Experimentation Sites. Geotechnical News, 12 (1): 39-44.

Yu H.S. 1994. State Parameter from Self-Boring Pressuremeter Tests in Sand. ASCE, Journal of Geotechnical Engineering, 120(12): 2118-2135.

Yu H.S., and Houlsby G.T. 1991. Finite Cavity Expansion in Dilatant Soils: Loading Analysis. Géotechnique, 41(2): 173-183.

Yu H.S., Schnaid F., and Collins I.F. 1996. Analysis of Cone Pressuremeter Tests in Sands. ASCE Journal of Geotechnical Engineering, 122(8): 623-632.

Chapter 6.

Interpretation of the Sand State from CPT in Fraser River Sand: A Case History[8]

6.1.   Introduction

With the recent advances in the analysis and design techniques used in geomechanics, accurate interpretation of 'ground truth' has become of even greater significance to the geotechnical community. In the case of cohesionless soils, 'ground truth' includes knowledge of in-situ gradation, density, fabric and stress state, and the spatial variability of these parameters.

The behaviour of cohesionless soils strongly depends on their density. While relative density, D_r, is an almost universally used density index for sand, it is easily shown that D_r can be misleading (e.g. Tavenas, 1973). An alternative to D_r that captures both the effect of void ratio and mean stress on soil behaviour is the state parameter, ψ (Been and Jefferies, 1985). The state

---

[8] A version of this chapter has been published. Ghafghazi M., and Shuttle D.A. 2010. Interpretation of the In-situ Density from Seismic CPT in Fraser River Sand. Proceedings of the 2nd International Symposium on Cone Penetration Testing, Huntington Beach, California.

205

parameter is defined as the difference between the current void ratio of the soil and its critical void ratio at the same mean effective stress. However, determining the in-situ ψ (or D_r) is very difficult because of density changes during sampling – an "undisturbed" sample is essentially impossible in normal engineering practice. Penetration tests have thus become the norm for testing cohesionless soils, with the modern electronic CPT offering continuous data measurement with excellent repeatability and accuracy at relatively low cost.

The difficulty with any penetration test, however, is that the state measure of interest is not measured. Instead it is calculated from the penetration resistance; a process usually referred to as interpretation. This interpretation involves solving an inverse boundary value problem to obtain mechanical properties from the measurements.

Ghafghazi and Shuttle (2008) (presented in chapter 4) analysed a database of nine soils, including laboratory standard and natural sands, as well as relatively clean sand-size tailings, for which both chamber testing and triaxial compression data were available in the literature. This methodology offers a framework for interpreting the state parameter from CPT tip resistance.

The interpretation framework is applied to the Massey Tunnel site, an extensively investigated site in Fraser river delta in British Columbia, Canada. The effect of soil fabric on the interpretation results has been considered by adjusting the calibration parameters with respect to tests on undisturbed samples. The accuracy of the method is evaluated by comparison to in-situ density measurements and compared to other methods of interpreting the state parameter from CPT.

6.2. Site Investigation Program

The Canadian geotechnical community completed a major collaborative research project between 1993 and 1997 entitled the CANadian Liquefaction EXperiment (CANLEX). The project was divided into different phases. One of the sites investigated in Phase II was located south of Massey Tunnel, connecting Richmond and Delta (Figure 6-1a) in British Columbia.

The full program was reported in five companion papers (Robertson et al., 2000[a, b]; Wride et al., 2000[a, b]; and Byrne et al., 2000). Complete summary reports with all data were published in a five volume series; the data for the Massey site reported in this chapter are extracted from volume 4 (Wride and Robertson, 1997).

The site characterisation program was targeted at depths of 8 to 13 m and included two standard penetration tests (SPT), six seismic cone penetration tests (CPT), three boreholes with Self-Bored Pressuremeter tests (SBP), and two geophysical logs. Ground freezing and sampling was carried out, providing undisturbed cores which were trimmed into samples used in both triaxial and simple shear testing. Samples were also obtained using the Laval Large Diameter Sampler. Figure 6-1b shows the locations of the tests relevant to the current work.

The water table was measured at 2.3 m depth. Based on SBP tests Wride and Robertson (1997) suggested the coefficient of lateral earth pressure at rest of $K_0 = 0.5$ for the target depth range; this evaluation was adopted here. The frozen and Laval large diameter samples yield an average void ratio of 0.96 with standard deviation (SD) of 0.05. γ_{sat} and γ_{dry} were accordingly calculated as 18.2 kN/m^3 and 13.4 kN/m^3 respectively for computing the vertical stresses.

6.3.   Material and Testing

Fraser River Sand (FRS) is a uniform, angular to sub-angular with low to medium sphericity medium grained clean alluvial sand widely spread in the Fraser river delta. For Massey samples $e_{\min}$ (ASTM D4254) and $e_{\max}$ (ASTM D4253) are reported as 0.677 and 1.056 and $G_s = 2.68$. Laboratory testing of the Massey site samples included testing reconstituted and undisturbed ones to evaluate the soil response to both undrained monotonic and cyclic loading. Since this method requires drained triaxial compression tests over a range of stresses and densities, which were not available in the CANLEX database, a second set of data on a batch of FRS entitled the "UBC sample" has been used. The FRS sample fines content has been reduced to 0.8% to produce a clean sand for testing. $e_{\min}$ and $e_{\max}$ are reported as 0.627 and 0.989 and $G_s = 2.719$ by Shozen (1991). e_{min} was measured according to ASTM D2049 while e_{max} was reported as the initial deposition void ratio in the loosest state. Figure 6-2 illustrates the gradation curves of the two FRS samples used in this work.

6.4.   Methodology

The CPT in sand provides just two outputs; tip resistance (q_t) and sleeve friction (f_s); the penetration is drained so the pore pressure transducer simply measures the in-situ pore pressure. The state measure used in this work is the state parameter, ψ. Because ψ is used as an internal state variable in the numerical model, the subscript '0' is used to denote the in-situ (or initial) value of ψ_0 under geostatic conditions.

Initial work with determining ψ_0 from CPT data comprised triaxial testing of sands for which chamber test data was available to define the critical state locus (CSL) of each sand, and then processing the chamber test data to develop dimensionless relations (Been et al., 1987) of the form:

$$Q = k \exp(-m\psi_0)$$
[Eq. 6 - 1]

where Q is the normalised tip resistance defined as:

$$Q = \frac{q_t - p_0}{p'_0}$$
[Eq. 6 - 2]

where p_0 is the initial mean total stress, and p'_0 is the initial mean effective stress. The two coefficients k and m in Equation 6-1 differ from one sand to another.

As all analytical methods of interpreting ψ_0 from CPT must be verified against available calibration chamber data, the scatter in experimental results limits the interpretation method's accuracy. Experimentalists have tried to measure reproducibility of calibration chamber results by repeating tests on samples with the same density and stress conditions. These efforts have resulted in $\pm$ 25% error in measured Q in recent works (Hsu, 1999). However, the majority of available data suggest that $\pm50\%$ accuracy in measured Q is 'good' quality data. Of course, translating accuracy in Q to accuracy in ψ_0 includes some sort of interpretation, but a rough estimation based on average k and m values suggests that $\pm$ 0.05 is about the best accuracy that can be expected in prediction of any particular test in the available calibration chamber data.

Ghafghazi and Shuttle (2008) analysed a total of 301 calibration chamber tests and achieved an error of less than 0.04 with 78% confidence level and less than ±0.07 with 92% confidence level. Their results were improved to 84% and 97% respectively for cases where elasticity was measured using bender elements. This is deemed to be an excellent accuracy achievable in an analytical method. This method is used here for evaluating the state parameter at the Massey site.

The method involves two parallel tasks: the normalisation and processing of CPT tip resistance data, together with identification of soil behaviour and calculation of material specific correlations. The correlations are then used to calculate the state parameter. Figure 6-3 presents a summary of the method and the required steps.

Normalising and processing the CPT tip resistance data is done by estimating the stress state along the depth of interest. The total vertical and effective stresses can be calculated by estimating dry and saturated soil densities. The coefficient of earth pressure at rest (K_0) should be estimated or measured from in-situ tests such as SBP or dilatometer tests. The mean stress can then be calculated and the normalised tip resistance Q can be calculated from Equation 6-2. Central to the method is the application of a shape function which converts the calibration chamber test normalised tip resistance Q_{cc} to its spherical cavity expansion analysis equivalent Q_{sph}. Replacing the calibration chamber test normalised tip resistance Q_{cc} with its analogue in-situ normalised tip resistance Q and inverting Equation 4-3 (Ghafghazi and Shuttle, 2008) we can write:

$$Q_{sph} = \left(\frac{Q}{0.7}\right)^{0.59}$$
[Eq. 6 - 3]

210

6.5. Constitutive Modeling

The behaviour of the material is captured through constitutive model calibration to drained triaxial compression tests. The calibrated model is then used in a spherical cavity analysis to calculate Q_{sph}.

The reason to use a 'good' sand model for cavity expansion analysis is that, in general, part of the domain will be critical, parts dilating, and other parts contractive; with the exact behaviour being a function of position relative to the cone tip. The constitutive model adopted is NorSand (Jefferies, 1993; Jefferies and Shuttle, 2002), an isotropically hardening - isotropically softening generalised critical state model that captures a wide range of particulate soil behaviour. The reader is directed to Jefferies and Shuttle (2005) for a detailed discussion of the calibration procedures.

The CSL was identified based on the end points of 9 consolidated drained (CID) and 7 consolidated undrained (CIU) "UBC sample" triaxial compression tests as illustrated in Figure 6-4. The samples were prepared by moist tamping, and lubricated end platens were used to reduce the end friction. As not all of the tests reached the critical state, whether the sample was dilating or contracting was reported to help define the CSL. Corresponding data to determine the CSL of the "Massey" samples are also shown on Figure 6-4.

The remaining model calibration was based on 8 of the drained "UBC sample" triaxial compression tests (one test with unload-reload loops was not used). The elastic shear modulus was identified through bender element tests. Details of the testing are presented in detail in chapter 7 and appendix A. The calibration parameters for the UBC sample are presented in Table 6-1.

To accommodate the difference between the material tested at UBC and the material found at the site, model parameters that could be estimated using the Massey sample data replaced the "UBC" parameters in the analysis. The Massey sample data included 22 undrained triaxial tests and one drained triaxial compression test on undisturbed (frozen core) samples. The undrained tests were used to identify the critical state line (Γ, λ_e) (see Figure 6-4), and the critical state friction ratio (M_{tc}). This allowed the calibration parameters to be modified to match altering material behaviour caused by changing gradation. An adjustment to the hardening parameter H, which is affected by soil fabric, was made based on the drained test on the Massey sample (see Figure 6-5). The calibration parameters for the Massey sample are also presented in Table 6-1.

It is worth noting that the CSL in $e - \log p'$ is bilinear at lower stresses for both UBC and Massey samples. As discussed earlier in the thesis, the shape of the CSL is an arbitrary choice and does not affect the fundamentals of the model or the results. In this case a linear or a power law (Jefferies and Shuttle, 2011) relation could replace the familiar semi log representation. One should also notice that the measurements of the mean effective stress at low stresses become very sensitive to the accuracy of the testing equipment. At higher stresses (800-900 kPa for FRS), particle breakage controls the status of the CSL as discussed later in chapter 7. In this chapter the semi-log representation of the CSL is considered sufficient.

6.6.   Spherical Cavity Expansion Analysis

The spherical cavity expansion analogy idealises the CPT as a cavity in an infinite uniform medium under an isotropic stress state, with the internal pressure of the cavity initially equal to the mean effective stress p'_0. The cavity is monotonically expanded by increasing its radius until

a limiting (constant) pressure is obtained. This idealisation greatly simplifies the analysis because the spherical symmetry allows only radial displacements, in turn permitting a one-dimensional description of the problem. The corresponding stresses are a radial and two equal hoop stresses. The spherical cavity finite element code developed by Shuttle and Jefferies (1998) is used in this study. The code and finite element mesh remained the same, hence retaining the verified large displacement performance of it.

6.7. Inverse Form for Interpretation of CPT

Shuttle and Jefferies (1998) showed that Equation 6-1 may be used to recover ψ_0 from CPT data provided that k and m are functions of soil characteristics and the stress level. Using a spherical cavity expansion analysis, we can summarise the effect of different soil characteristics in the form of NorSand parameters in the following equation:

$$k_{sph} = f_1(G/p'_0, M_{tc}, N^*, H, \chi_{tc}, \lambda_e, \nu)$$ [Eq. 6 - 4a]

$$m_{sph} = f_2(G/p'_0, M_{tc}, N^*, H, \chi_{tc}, \lambda_e, \nu)$$ [Eq. 6 - 4b]

All the NorSand parameters in Equation 6-4 are constants, or known functions of ψ_0. Hence at a particular ψ_0, all the variables in Equation 6-4 take a single value except for G/p'_0 (the stress level effect) which is usually a function of both void ratio and stress level. This makes Q_{sph} a function of the stress level at a particular ψ_0 (Figure 6-6a). k_{sph} and m_{sph} can then be determined as functions of G/p'_0 (Figure 6-6b) in Equation 6-5.

$$k_{sph} = 9.82 + 0.336\ln\left(G_{max}/p_0'\right) \qquad \text{[Eq. 6 - 5a]}$$

$$m_{sph} = 1.77 + 0.49\ln\left(G_{max}/p_0'\right) \qquad \text{[Eq. 6 - 5b]}$$

Having the normalised tip resistance Q, Q_{sph} can be determined from Equation 6-3, and k_{sph} and m_{sph} from Equation 6-5, provided that the shear modulus G is independently available. The in-situ state parameter can then be calculated from Equation 6-6 which is directly deduced from writing Equation 6-1 for spherical cavity expansion:

$$\psi_0 = \frac{-\ln\left(\dfrac{Q_{sph}}{k_{sph}}\right)}{m_{sph}} \qquad \text{[Eq. 6 - 6]}$$

Combining Equations 6-1, and 6-3 and following the procedure in Figure 6-6, one can directly calculate the state parameter for the in-situ Massey site Fraser river sand from Equation 6-7 as

$$\psi_0 = \frac{-\ln\left(\dfrac{Q}{33.05 + 2.28\ln(G_{max}/p_0')}\right)}{3.01 + 0.83\ln(G_{max}/p_0')} \qquad \text{[Eq. 6 - 7]}$$

6.8.   Analysis and Results

Testing at the Massey site included a Frozen sampling core surrounded by six CPTs at a radius of approximately 5 m (Figure 6-1b). The Laval Large Diameter Sampler coring (shown as LDS on Figure 6-1b) was also located on the perimeter of the layout. Although the target zone was

identified as a fairly uniform layer, and the tests were relatively close, the CPT tip resistance measurements fell within a range between approximately 4 to 8 *MPa*. The tests plotted in Figure 6-7 suggested lower tip resistance values from 8 to 9 *m* depth and relative uniformity between 9 and 13 *m*. Parts of the logs obtained from tests M9401 and M9402 were ignored between 12 and 13 *m* due to their discrepancy with the trend established by the rest of the tests. The range of tip resistance measured within the target zones of the CPT selected for analysis, is plotted in Figure 6-8a. The normalised tip resistance Q is also plotted in Figure 6-8b as a range.

The shear wave velocity was determined through downhole seismic measurements for all CPTs. The results were shown in the form of elastic shear modulus G in Figure 6-9 with the range of interest and the average values plotted. The analyses were done using the average values at any given depth.

Considering $K_0 = 0.5$ a range of ψ_0 was calculated using Equation 6-7 (Figure 6-8c). Ghafghazi and Shuttle (2008) margins of error of ±0.04 and ±0.07 are also plotted.

The results obtained from the methods (see section 1.4.2) proposed by Konrad (1997), Been et al. (1987) and Plewes et al. (1992) are plotted in Figure 6-8d. To be able to directly compare methods, the average and standard deviation (SD) of ψ_0 data obtained from each method are summarised in Table 6-2.

6.9. Discussion and Conclusions

The samples trimmed from the cores obtained from ground freezing and Laval large diameter sampler are assumed to represent the real in-situ void ratio. An average void ratio of 0.96 with SD of 0.05 is obtained, translating into a state parameter of -0.055 with the same SD based on

Γ = 1.17 and λ_e = 0.035 obtained for Massey sample. The wide scatter in the measured void ratios, reflected in the large SD, covers a range of $-0.155 < \psi_0 < 0.01$. The scatter more likely stemmed from the ground sampling techniques, rather than being a characteristic of the ground, as widely ranging void ratios were measured in samples from adjacent points of the core. While the variation in the measured void ratios represents a wide range of sand behaviour, ranging from loose to dense, the geology of the site and all in-situ testing (including CPTs) imply a relatively uniform deposit associated with a narrower range of ground density and sand behaviour. This paradoxical observation in methods of obtaining the in-situ density from undisturbed samples of sands calls for a more cautious treatment of the results, and emphasises the need for better interpretation techniques for tests such as CPT.

The CSLs of UBC and Massey samples are plotted in Figure 6-10 along with that of series of tests on a slightly different gradation of Fraser river sand at University of Alberta (Chillarige, 1995). The in-situ measurements of void ratio are also plotted in this figure. The gradation of the "U of A sample" is also plotted in Figure 6-2. Although the three samples are of the same origin and have similar gradations, the variability in their CSLs is significant. This variability translates into a difference of 0.05 to 0.10 in the state parameter at the stress levels associated with Massey site.

Accepting the notion that the behaviour of the material is controlled by the state parameter (or other similar indexes) and not the void ratio (or relative density D_r) one can see that any direct measurement of void ratio, no matter how accurate (as in this case history), can lead to significant misrepresentations of the field behaviour. This misrepresentation will occur due to variations of the CSL, if the CSL is not rigorously determined for every variation of the material

gradation encountered. This can add significantly to the cost and difficulty of estimating the in-situ behaviour of the material by direct measurements of the void ratio.

On the contrary, the framework presented here has the advantage of directly providing the state parameter based on conveniently available CPT data. Once the CSL is established for a representative sample for capturing the essence of material behaviour, variations of the CSL due to local and limited material variability will have a second degree effect on the accuracy of the method, as discussed in detail by Shuttle and Jefferies (1998) in investigating the sensitivity of the interpretation to changes in Γ and λ_e.

As illustrated in Figure 6-8c, 98% of the undisturbed sampling measurement points fall within the $\pm\ 0.07$ error margins of the Ghafghazi and Shuttle (2008) method and 70.5% within the $\pm\ 0.04$ error margins. 20.5%, fall within the upper bound and lower bound lines, representing a zone of ideal accuracy for the information used in this work. The confidence levels are well comparable with those observed in validation of the method against calibration chamber testing results.

The accuracy offered by the $\pm\ 0.07$ error margins covers a wide range of possible state parameters (typically $-0.30 < \psi_0 < 0.05$) when combined with the variation in the original CPT data represented by upper and lower bound envelopes. However, the range is very similar to that covered by the frozen and LDS samples, suggesting that this method is as capable as the most expensive and cumbersome of ground sampling techniques for determining the soil's in-situ density. The average ψ_0 of -0.067 is also very close to that measured by ground sampling. The difference is close to ± 0.01; the ground sampling technique error margin given by Wride and Robertson (1997).

As shown in Table 6-2, amongst all interpretation methods, the Ghafghazi and Shuttle (2008) method provides the closest estimation for ψ_0 of Fraser river sand. Although the method appears more difficult than the others, the difficulty only lies in the analysis and modeling effort which is achievable in a matter of hours. With the exception of Plewes et al. (1992), all interpretation methods presented in Table 6-2 require knowledge of the Critical State Locus in $e - \log p'$ space. Performing a number of triaxial compression tests is the easiest and most common way of estimating the CSL. The only additional requirement of the Ghafghazi and Shuttle (2008) method is for these tests to be performed under drained conditions; a requirement that does not pose any additional laboratory testing effort.

Plewes et al. (1992) correlated the slope of the critical state line in $e - \log p'$ space to the CPT friction ratio based on experimental results, hence eliminating the need to experimentally obtain the CSL. However, the method does require laboratory testing to measure the critical state friction angle (or the analogous M_{tc}). Plewes et al. (1992) suggested using $M_{tc} = 1.2$ ($\phi_c = 30°$) for all soils, advising that doing so would cause less than 10% error in the estimated ψ_0. Likely due to the high M_{tc} of Fraser river sand, adopting the $M_{tc} = 1.2$ approximation changes the ψ_0 prediction by about 25% in these analyses, resulting in a less accurate prediction that puts the estimated ψ_0 in line with the other methods (see the last two columns of Table 6-2). Use of the measured M_{tc} results in a less negative (looser) state parameter that is closer to that implied by ground sampling techniques.

The success of these methods in obtaining the in-situ state parameter appears to be directly related to the level of material behaviour taken into consideration. Konrad (1997) does not account for any mechanical aspects of soil behaviour and returns the most discrepancy in estimated state parameter. The Been et al. (1987) method accounts for material compressibility

218

through the slope of the CSL. The Plewes et al. (1992) method adds the effect of the critical state friction angle to their framework resulting in an even better estimation. The Ghafghazi and Shuttle (2008) analytical procedure also accounts for both compressibility and friction angle, and importantly adds elasticity, as well as stress level, dilatancy, and fabric.

An overall comparison of the model parameters for Fraser river sand to those of other sands presented in Ghafghazi and Shuttle (2008) suggests that the most important factor that makes the other methods systematically biased towards a more negative state parameter in Fraser River sand is its high critical state friction angle. This is further confirmed by the fact that a correct M_{tc} value in the Plewes et al. (1992) method results in a better interpretation.

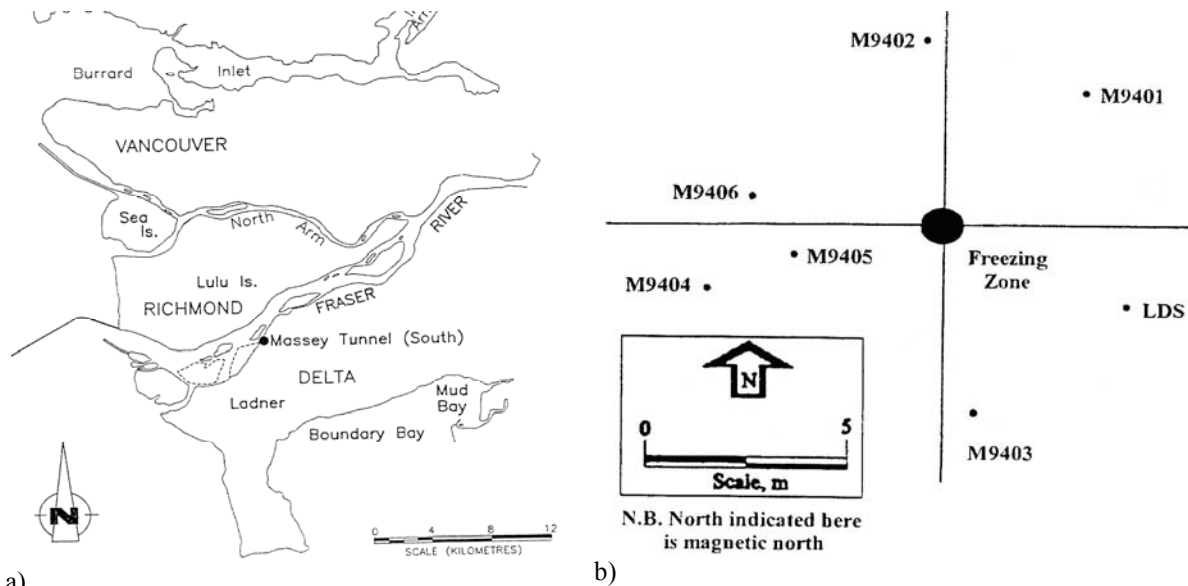Table 6 - 1 NorSand calibration parameters for Fraser river sand

Parameter	Critical State			Plasticity			Elasticity	
	Γ	λ_e	M_{tc}	H	χ_{tc}	N^*	$I_r = G/p'_0$	ν
UBC (moist tamped)	1.22	0.060	1.45	80-310 ψ_0	3.2	0.45	$\dagger 14.89 \dfrac{(2-e)^2}{1+e} \times \left(\dfrac{p'_0}{p_r}\right)^{0.42}$	0.2
Massey (undisturbed)	1.17	0.035	1.49	110-310 ψ_0	3.2	0.45	Seismic CPT $(650 < I_r < 800)$	0.2

$\dagger$ p_r is a reference pressure of 100 kPa. The correlation is obtained from bender element testing on some of the samples.

Table 6 - 2 ψ_0 interpretation summary

Interpretation method	Undisturbed sampling	Current work	Konrad (1997)	Been et al. (1987)	Plewes et al. (1992) $\dagger$	Plewes et al. (1992)
average ψ_0	-0.055	-0.067	-0.114	-0.092	-0.089	-0.071
SD	0.050	0.028	0.032	0.021	0.038	0.038

$\dagger$ $M_{tc} = 1.20$ is used in the formula

Figure 6 - 1 a) Massey site in the Fraser river delta; b) Layout of the Large Diameter Laval Sampler (LDS), the frozen core, and the CPTs (M9401 to M9406) relevant to the work at Massey site (after Wride and Robertson, 1997)
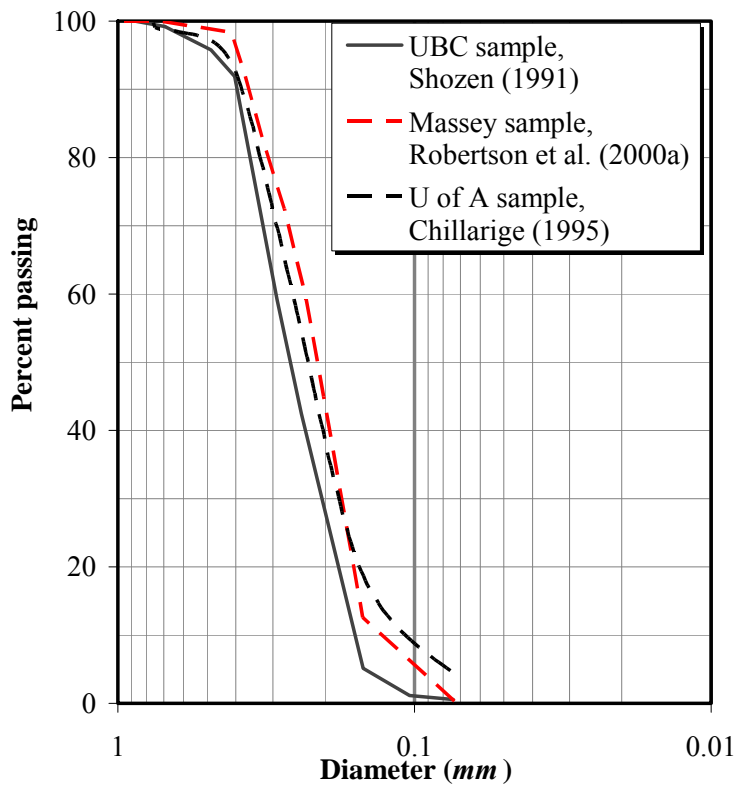

Figure 6 - 2 Gradation curves of Fraser river sand: UBC and Massey samples
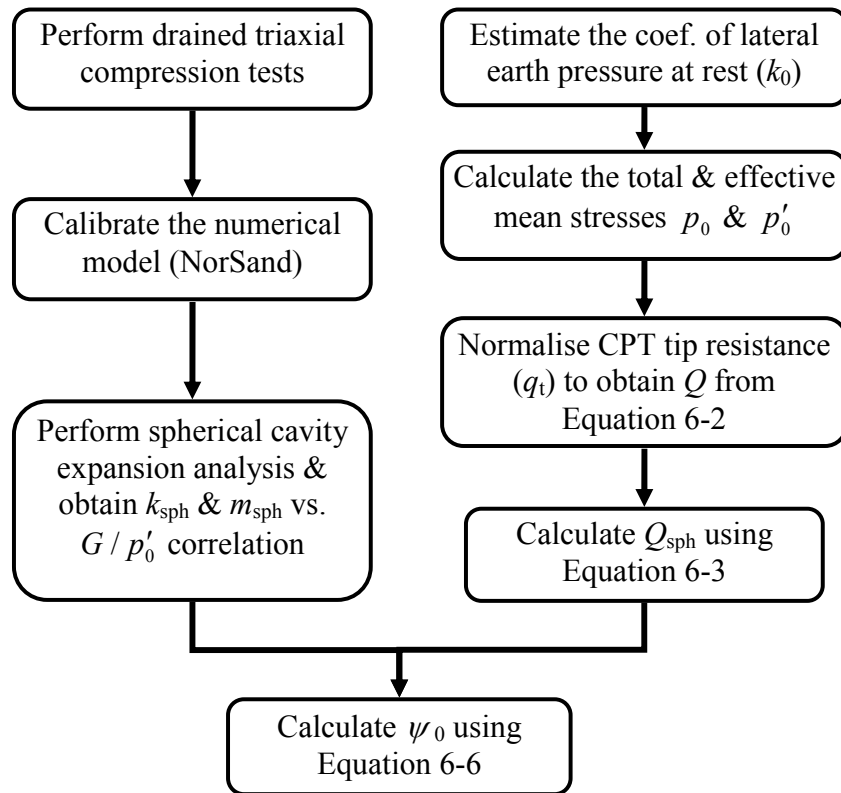
Figure 6 - 3 Flowchart for Ghafghazi and Shuttle (2008) method
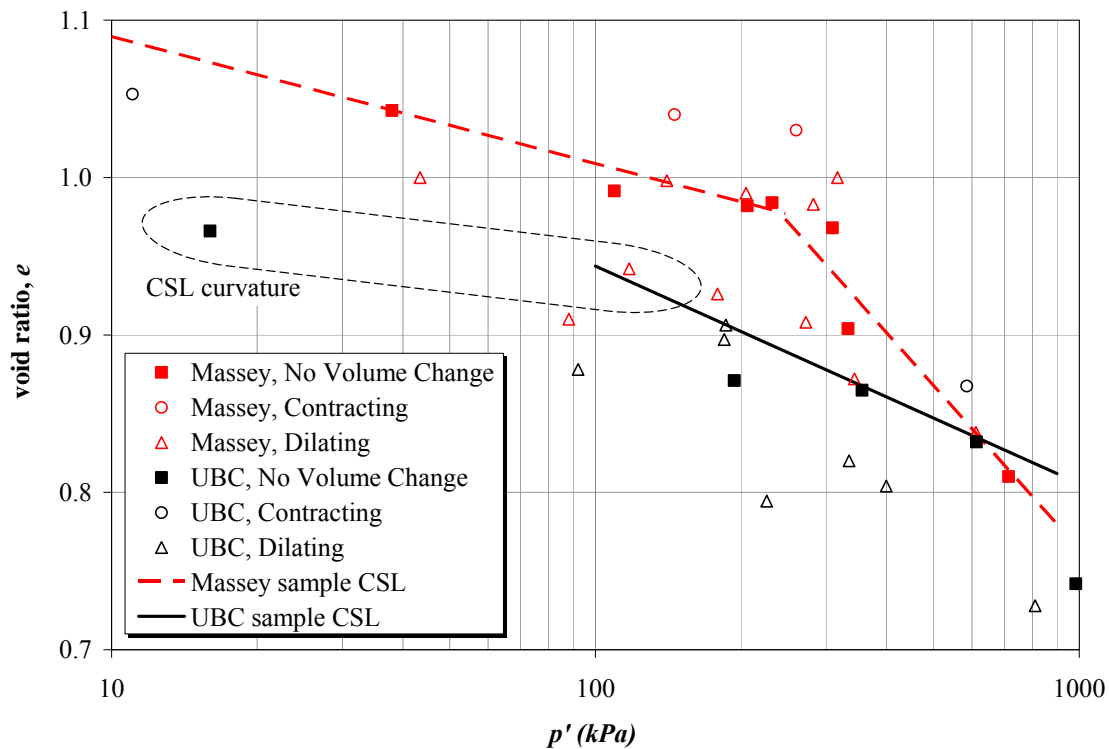
Figure 6 - 4 Critical State Loci for UBC and Massey samples; end points of drained and undrained tests are plotted with different signs assigned to tests that were contracting, dilating or had not volume change at the end of the test

222
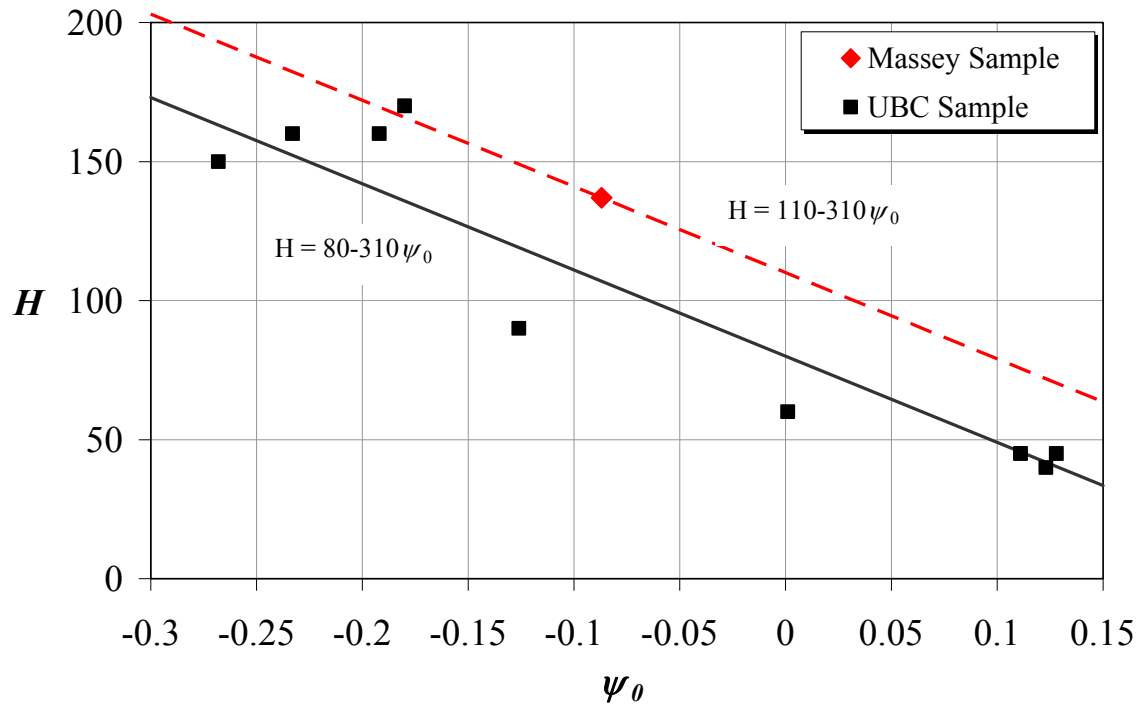
Figure 6 - 5 Variation of the hardening parameter H with the initial state parameter for UBC and Massey samples

a)

b)
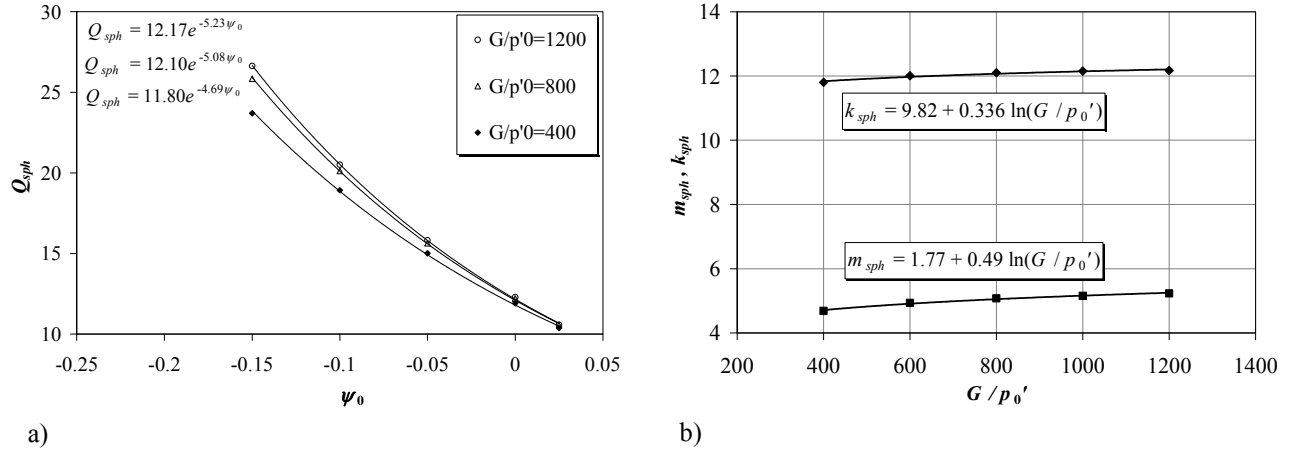
Figure 6 - 6 a) Q_{sph} vs. ψ_0 for range of $I_r = G/p_0'$; b) m_{sph} and k_{sph} vs. normalised shear modulus I_r
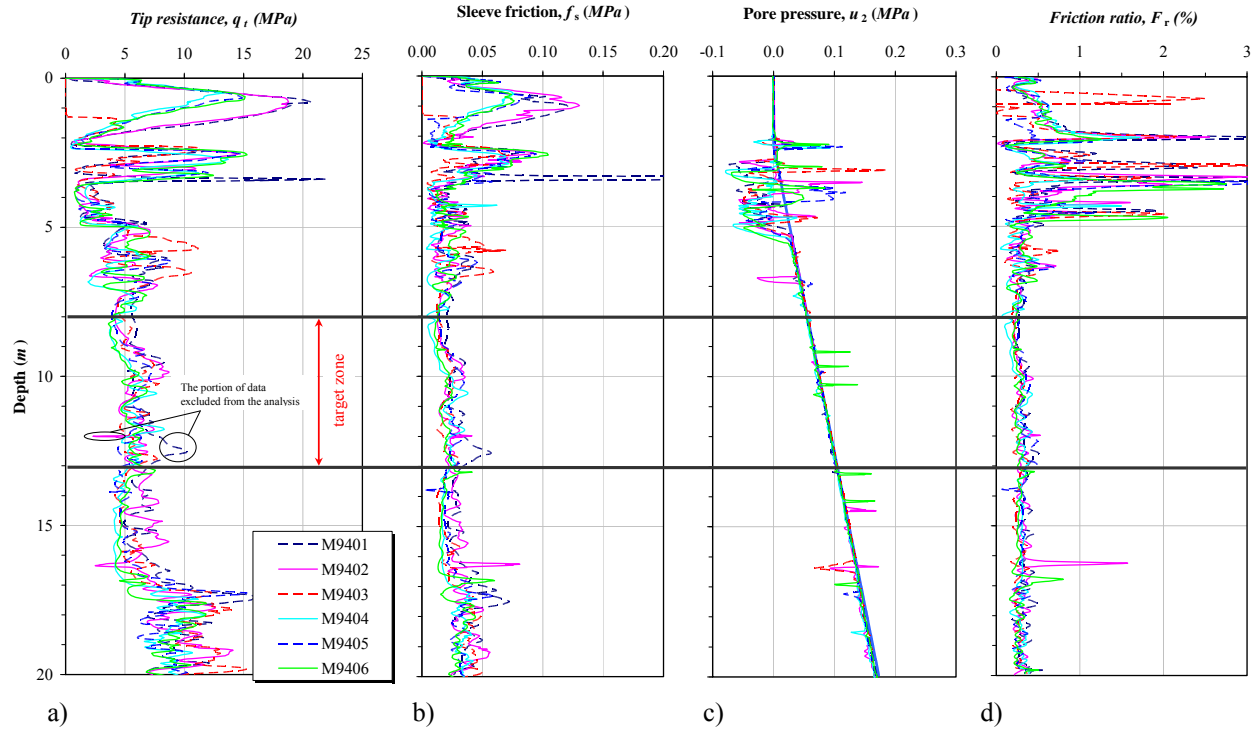
Figure 6 - 7 CPT data M9401 to M9406 a) Tip resistance b) Sleeve friction c) Pore pressure d) Friction ratio
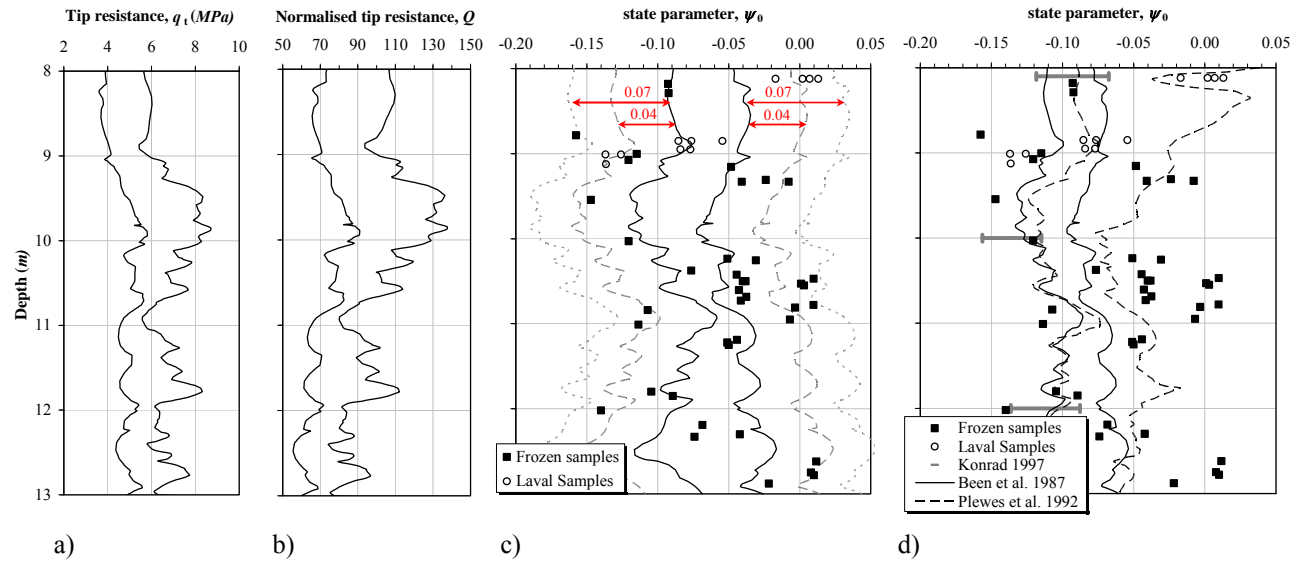
Figure 6 - 8 Upper and lower bound CPT response and state parameter interpretation for the target zone: a) Tip resistance b) Normalised tip resistance c) State parameter Interpretation (Ghafghazi and Shuttle, 2008) with ±0.04 and ±0.07 error margins d) Alternative methods of interpretation: Konrad (1997), Been et al. (1987), and Plewes et al. (1992)
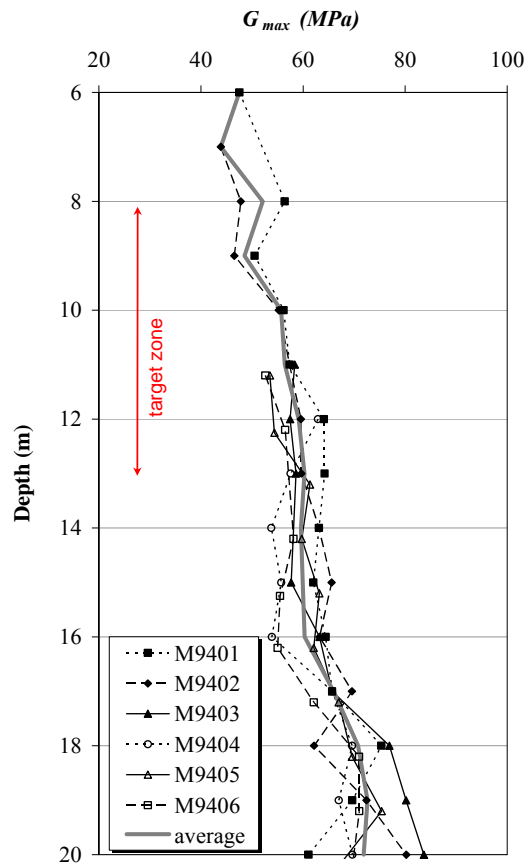
Figure 6 - 9 Shear modulus profile derived from shear wave velocity measurements from seismic CPTs, the average values and the target depth range
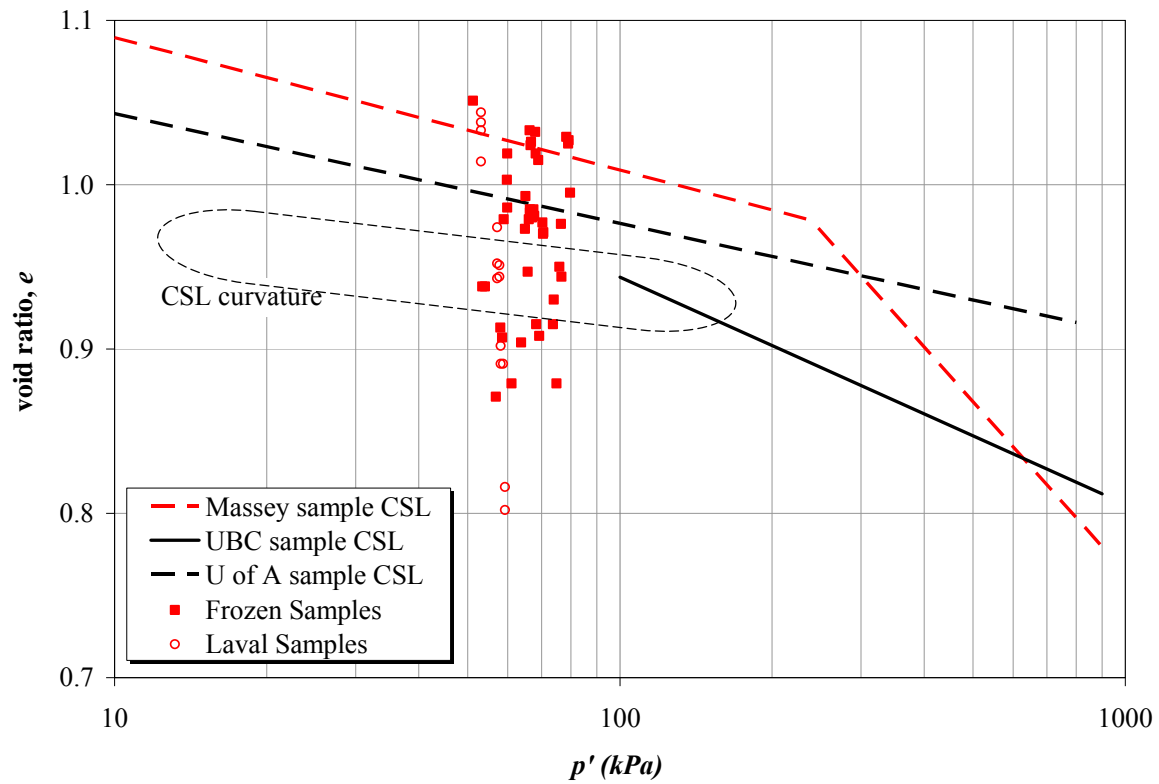
Figure 6 - 10 Comparison of Critical State Loci for UBC, Massey and U of A samples and the direct void ratio measurements

6.10. References

ASTM D2049-69 Test Method for Relative Density of Cohesionless Soils (Withdrawn 1983).

ASTM D4253 - 00(2006) Standard Test Methods for Maximum Index Density and Unit Weight of Soils Using a Vibratory Table.

ASTM D4254 - 00(2006)e1 Standard Test Methods for Minimum Index Density and Unit Weight of Soils and Calculation of Relative Density.

Been K., and Jefferies M.G. 1985. A State Parameter for Sands. Géotechnique, 35(2): 99-112.

Been K., Jefferies M.G., Crooks J.H.A. and Rothenburg L. 1987. The Cone Penetration Test in Sands. Part II: General Inference of State. Géotechnique, 37(3): 285-299.

Byrne, P.M. et al. 2000. CANLEX Full-Scale Experiment and Modelling. Canadian Geotechnical Journal, 37: 543–562.

Chillarige A.V. 1995. Liquefaction and Seabed Instability in Fraser River Delta. PhD Thesis, Department of Civil Engineering, University of Alberta, Canada.

Ghafghazi M. and Shuttle D.A. 2008. Interpretation of Sand State from Cone Penetration Resistance. Géotechnique, 58(8): 623–634.

Hsu H.H. 1999. Cone Penetration Tests in Sand under Simulated Field Conditions. PhD thesis, Department of Civil Engineering, National Chiao Tung University, Hsin Chu, Taiwan.

Jefferies M.G. 1993. Nor-sand: A Simple Critical State Model for Sand. Géotechnique, 43(1): 91-103.

Jefferies M.G. and Shuttle D.A. 2002. Dilatancy in General Cambridge-Type Models. Géotechnique, 52(9): 625-638.

Jefferies M.G. and Shuttle D.A. 2005. NorSand: Features, Calibration and Use. Proceedings of the specialty conference on Soil Constitutive Models: Evaluation, Selection, and Calibration. ASCE Geotechnical Special Publication, 128: 204-236.

Jefferies M.G. and Shuttle D.A. 2011. Understanding Liquefaction through Applied Mechanics. Proceedings of the 5th International Conference on Earthquake Geotechnical Engineering, Santiago, Chile, January 10 – 13, 2011.

Konrad J.M. 1997. In Situ Sand State from CPT: Evaluation of a Unified Approach at Two CANLEX Sites. Canadian Geotechnical Journal, 34: 120–130.

Plewes H.D., Davies M.P., and Jefferies M.G. 1992. CPT Based Screening Procedure for Evaluating Liquefaction Susceptibility. Proceedings of the 45th Canadian Geotechnical Conference, Toronto.

Robertson P.K., Wride (Fear) C.E., List B.R., Atukorala U., Biggar K.W., Byrne P.M., Campanella R.G., Cathro D.C., Chan D.H., Czajewski K., Finn W.D.L., Gu W.H., Hammamji Y., Hofmann B.A., Howie J.A., Hughes J., Imrie A.S., Konrad J.-M., Küpper A., Law T., Lord E.R.F., Monahan P.A., Morgenstern N.R., Phillips R., Piché R., Plewes H.D., Scott D., Sego D.C., Sobkowicz J., Stewart R.A., Watts B.D., Woeller D.J., Youd T.L., and Zavodni Z. 2000[a]. The Canadian Liquefaction experiment: an Overview. Canadian Geotechnical Journal, 37: 499–504.

Robertson P.K., Wride (Fear) C.E., List B.R., Atukorala U., Biggar K.W., Byrne P.M., Campanella R.G., Cathro D.C., Chan D.H., Czajewski K., Finn W.D.L., Gu W.H., Hammamji Y., Hofmann B.A., Howie J.A., Hughes J., Imrie A.S., Konrad J.-M., Küpper A., Law T., Lord E.R.F., Monahan P.A., Morgenstern N.R., Phillips R., Piché R., Plewes H.D., Scott D., Sego D.C., Sobkowicz J., Stewart R.A., Watts B.D., Woeller D.J., Youd

T.L., and Zavodni Z. 2000[b]. The CANLEX Project: Summary and Conclusions. Canadian Geotechnical Journal, 37: 563–591.

Shozen T. 1991. Deformation under the Constant Stress State and its Effect on Stress-Strain Behaviour of Fraser River Sand. MASc. thesis, Department of Civil Engineering, University of British Columbia, Vancouver, Canada.

Shuttle D.A., and Jefferies M.G. 1998. Dimensionless and Unbiased CPT Interpretation in Sand. International Journal for Numerical and Analytical Methods in Geomechanics, 22: 351-391.

Tavenas F.A. 1973. Difficulties in the Use of Relative Density as a Soil Parameter. Evaluation of Relative Density and its Role in Geotechnical Projects Involving Cohesionless Soils, American Society for Testing and Materials, Selig E.T., and Ladd R.S. (eds.), Philadelphia, ASTM Special Technical Publication 523: 478-483.

Wride (Fear) C.E., Hofmann B.A., Sego D.C., Plewes H.D., Konrad J.-M., Biggar K.W., Robertson P.K., and Monahan P.A. 2000[a]. Ground Sampling Program at the CANLEX Test Sites. Canadian Geotechnical Journal, 37: 530–542.

Wride (Fear) C.E., Robertson P.K., Biggar K.W., Campanella R.G., Hofmann B.A., Hughes J.M.O., Küpper A., and Woeller D.J. 2000[b]. Interpretation of In Situ Test Results from the CANLEX Sites. Canadian Geotechnical Journal, 37: 505–529.

Wride C.E., and Robertson P.K. 1997. The Canadian Liquefaction Experiment, Phase II Data Review Report, Massey and Kidd Sites, Fraser river delta, June 1997. ISBN 0-921095-49-X. Wride C.E. and Robertson P.K. (eds.), BiTech Publishers Ltd., Richmond, BC, Canada.

Chapter 7.

Particle Breakage and the Critical State of Sand[9]

7.1.   Introduction

In critical state soil mechanics shearing drives samples of particulate soils towards a state of

constant volume at a constant mean effective stress, termed the *critical state*. At high pressures

however, the particles tend to undergo breakage resulting in a continuous change to the soil's

gradation. The breakage also imposes additional compressibility on the soil giving rise to

ambiguities around the definition of the critical state condition as it relates to zero volume

change. In practice, high pressures often occur in deep penetration problems such as pile driving

and cone penetration testing, and at the base of large earth-fill dams. Hence the effect of particle

breakage becomes important for rigorous modelling of such problems within the critical state

framework.

---

[9] A version of this chapter has been submitted for publication. Ghafghazi M., Shuttle D.A., and Olivera R.R. 2010.
Particle Breakage and the Critical State of Sand.

A two or three part linear Critical State Locus (CSL) in $e - log\ p'$ space (where e is the void ratio and p' is the mean effective stress), similar to the one shown in Figure 7-1, has generally been accepted for the full range of p'. This agrees with the three zones of behaviour identified by Vesic and Clough (1968): very low pressures where dilatancy controls behaviour and breakage is negligible, higher pressures where breakage becomes more pronounced and suppresses dilatancy effects, and very high pressures where all effects of initial density vanish and sand behaves like an elastic material.

This second stress range (typically 1 $MPa < p' <$ 30 MPa), which more or less covers the higher end of stresses (all stresses are assumed to be effective in this chapter) of interest in geotechnical problems, has been less studied in comparison to the lower stress range. To date there is no consensus on whether a unique CSL exists for this stress range, and how it is affected by the continuous gradation change due to particle breakage. This work focuses on the critical state at the lower end of the second stress range (1 MPa to 3 MPa) where breakage becomes gradually dominant over dilatancy.

It is well accepted that shearing at high pressure changes the soil's gradation, which in turn contributes to volumetric compression (e.g. Lee and Farhoomand, 1967). The critical state is associated with a state of constant volume despite continued shearing. It is hence expected that for the sample to reach the critical state, a stable gradation should be reached for a specific stress level (Luzzani and Coop, 2002). This implies that such gradation would be more stable than the original one, and can sustain a higher level of stress without further breakage despite being formed by particles of exactly the same mineralogical combination. Hypothetically this is a viable proposition knowing that particle breakage drives the sample towards a more well-graded distribution which will establish more inter-particle contacts (Bishop, 1966) and thus reduce the

stress concentrations at particle level; however experimental evidence demonstrating the formation of such stable gradation related to a particular stress level is rather scarce in the literature.

Been et al. (1991), Konrad (1998), and Russell and Khalili (2004) all adopted the three part CSL framework as illustrated in Figure 7-1 and assumed that a continual constant volume state will be achieved once the tests approach the second part of the CSL. The data presented by Russell and Khalili (2004) (Figure 9 of their paper) suggest that for higher stress levels (above 1 *MPa*) the loose tests do not reach a constant volume and continue to contract. Lade and Yamamuro (1996) made the same observation on tests presented in Yamamuro and Lade (1996) and concluded that the critical state conditions can only be achieved at low pressures (the first part of CSL) or at extremely high pressures where particle breakage has ceased (the third part of CSL).

An experimental study on a granitic soil by Lee and Coop (1995) suggested that the amount of particle breakage at the critical state is path independent and solely a function of the value of p' on the CSL. In a later attempt to investigate whether the critical state can be achieved at higher stress levels, Coop et al. (2004) used ring shear tests to take samples of a carbonate sand to up to 100,000% shear strain. They concluded that particle breakage continues to very large strains beyond those reached in triaxial tests, but a constant gradation is reached at very large strains. This constant gradation is dependent not only on the stress level but also on the uniformity and particle size of the original gradation.

Theoretically, the change in gradation cannot continue indefinitely; it is always possible to imagine a gradation where all voids are filled with progressively smaller and smaller particles as proposed by McDowell et al. (1996). Such "fractal" gradation would be linear on a log-log plot

of particle size and proportion finer than that size. This condition of zero void space in the soil structure has been experimentally obtained by the early work of Bridgman (1918) for very high stresses falling on the third part of the CSL. But, for the range of stresses, strains and breakage of interest to this work, and much of geotechnical engineering, it appears safe to assume that breakage does not completely stop at higher stresses. Thus the idea of a CSL defined as a state of zero "total" volume change becomes irrelevant for the higher stress ranges.

Daouadji et al. (2001) first suggested that the changing gradation caused by the breakage imposes a downward shift on the CSL. Muir Wood (2007) developed this idea, suggesting that during shearing at higher stresses the CSL moves down towards a final location associated with the fractal gradation. He proposed a third dimension to the $e - log\ p'$ space called the "grading state index"; a parameter between 0 and 1 which identifies soil's state on a scale between uniform and fractal gradations. Muir Wood and Maeda (2008) showed, using a discrete element analysis, that the effect of particle breakage on the CSL location in $e - log\ p'$ space is essentially a parallel downward shift as a function of the grading state index. The current work builds upon this idea by proposing a simple conceptual framework to explain the movement of the CSL due to breakage. Triaxial testing on samples of a uniformly-graded natural sand before and after breakage is then presented to illustrate the utility of the framework.

7.2. Hypothesis

Basic difficulties with the proposition of a three part CSL, can be most easily illustrated using the state parameter concept (Been and Jefferies, 1985); the state parameter becomes ill-conditioned for the second part of the CSL (Jefferies and Been, 2000). But more importantly, its

evolution towards the three part CSL becomes logically questionable for stress paths that undergo a reduction in p'. For the test shown in Figure 7-1, the sample starts at an initial state parameter, ψ_0, which is defined as the difference between the initial void ratio and the CSL void ratio at the same initial p'. If that sample is now taken to the critical state, for example under undrained conditions, then the implication is that the sample has gone from a condition associated with a certain amount of breakage, to one with less, or no breakage. This is in contradiction to the fact that breakage is a "damage effect" which logically cannot be "reversed" by further shearing.

An alternative hypothesis is proposed here which explains how the breakage affects the CSL in $e - log\ p'$ space, when the breakage starts and how it contributes to the soil's compressibility. The new hypothesis is expanded from two assumptions:

1. For small amounts of particle breakage, the finer particles generated by the breakage process do not contribute to the soil's load carrying skeleton; and the breakage does not affect the overall characteristics of the particles forming the soil's load carrying skeleton.

2. Significant particle breakage in a particulate material does not occur unless two conditions are concurrently satisfied:
    i. The capability of the material for contraction merely by sliding and rolling of the particles is exhausted.
    ii. A stress threshold is surpassed.

The first statement is fairly intuitive provided only a relatively small number of soil particles break during shearing. It is known that breakage starts with the smallest load carrying particles

in the soil (Lee and Farhoomand, 1967; McDowell and Daniell, 2001). As long as the ratio of the particles that have undergone breakage remains small, the finer particles generated by the breakage do not contribute to the soil's load carrying skeleton; instead, they fall into the void space.

The idea that particle breakage does not commence until all sliding and rolling compressibility is suppressed is easy to hypothesise. Rolling is likely the first prevailing mechanism as it requires the least amount of energy to mobilise; once rolling is suppressed by an increase in confinement resulting from increased stress and reduced void space, sliding starts to dominate (Skinner, 1969). Breakage does not start while the particles have the opportunity to avoid loading by falling into the voids by merely rolling or sliding (compression). In loose samples the end of compression coincides with the critical state, while for dense samples it is followed by a tendency for dilation. At this stage, if the stresses are large enough to break the particles, breakage starts. The finer particles produced in the process are now capable of sliding and rolling into the voids and thus further reducing the sample's volume.

Inferences can be drawn from the above hypothesised behaviour. These inferences are developed here and then used to explain the observed experimental results to lend support to the credibility of the assumptions. The most fundamental implication of the first assumption is its effect on the CSL in $e - log\ p'$ space. A sample is expected to reach the critical state at a certain void ratio e_c. Now if the sample undergoes a finite amount of breakage, the particles chipped off bigger ones during shearing will cause a reduction in its void ratio (we limit the discussion to drained conditions considering the undrained condition a boundary constraint). This reduction in void ratio due to breakage is denoted as Δe_b. For small amounts of breakage the load bearing

235

skeleton will still reach the critical state at the expected "skeleton void ratio"; but the sample's overall void ratio will be lower by Δe_b.

The locus of the critical state void ratios (CSL) of the soil skeleton is a function of the current stress level as identified by the intercept Γ and the slope λ_{10} (the CSL shape is an arbitrary choice and does not affect the argument). Conversely the Δe_b generated is not related to the current stress level, instead being a function of the amount of breakage. Hence if the amount of breakage remains constant, the effect of breakage for the whole sample would be a parallel shift in the CSL ($\Delta\Gamma$). Equation 7-1 immediately follows from this argument:

$$\Delta\Gamma = \Delta e_b \qquad\qquad\qquad [\text{Eq. 7 - 1}]$$

For the second assumption, let us consider the expected behaviour for different initial states. For a loose sample starting at high stresses the CSL remains fairly unchanged as the soil particles preferentially roll and slide as the applied pressure increases, until the sample approaches the critical state. As the critical state is approached, the capacity for contraction decreases and particle breakage starts to shift the CSL downwards, and the sample follows it by further reduction in volume.

For a dense sample starting at higher stresses, the CSL remains unchanged until the initial contraction phase (related to sliding and rolling) ends. As contraction changes towards dilation, breakage starts, moving the CSL down and increasing the total contraction. Hence the contraction may be prolonged more than that expected in the absence of breakage, and some breakage may be observed before the overall contraction is replaced by dilation.

Breakage continues throughout the dilation phase and eventually the volume reduction caused by breakage, and the volume increase due to dilation, balance (Chandler, 1985; Baharom and Stallebrass, 1998). This transient constant volume stage may be called the "apparent critical state". Usually researchers have stopped shearing at this stage considering the sample to be at critical state (e.g. Russell and Khalili, 2004; Yamamuro and Lade, 1996). However, this may not necessarily be the case; breakage may continue beyond this point further reducing the sample's volume.

More insight into the breakage phenomenon can be gained by focusing on the state parameter and how it changes with regard to a moving CSL. The state parameter is defined as

$$\psi = e - e_c \qquad\qquad \text{[Eq. 7 - 2]}$$

where e_c is the critical void ratio for the current (with breakage) CSL and at the current mean effective stress.

Considering purely shear effects by holding mean stress constant, differentiating both sides of Equation 7-2 results in

$$\Delta\psi = \Delta e - \Delta e_c \qquad\qquad \text{[Eq. 7 - 3]}$$

If λ_{10} is constant, differentiating the CSL ($e_c = \Gamma - \lambda_{10}\log(p')$) gives

$$\Delta e_c = \Delta\Gamma \qquad\qquad \text{[Eq. 7 - 4]}$$

Combining Equation 7-1 with Equations 7-3 and 7-4 we can write

$$\Delta\psi = \Delta e - \Delta e_b \qquad \text{[Eq. 7 - 5]}$$

Separating the change in void ratio into two parts

$$\Delta e = \Delta e_{sr} + \Delta e_b \qquad \text{[Eq. 7 - 6]}$$

where Δe_{sr} is the change in void ratio caused by sliding and rolling.

From Equations 7-5 and 7-6 we obtain

$$\Delta\psi = \Delta e_{sr} \qquad \text{[Eq. 7 - 7]}$$

Equation 7-7 suggests that the breakage, and the change in the void ratio it induces, do not affect how the state parameter evolves. This implies that (while the initiation, and probably rate of breakage depend on the dilatancy caused by sliding and rolling of the particles) the sample moves towards the critical state irrespective of the breakage. The change in void ratio caused by the breakage is merely superimposed on that controlled by sliding and rolling.

Shearing of a sample at high stress constantly changes the gradation due to breakage, thus changing the CSL as defined in the absence of breakage. As breakage is associated with additional reduction in void volume (compressibility), reaching a stable critical state requires breakage to cease. So to understand how the CSL evolves with breakage it is necessary to eliminate the breakage from a sample undergoing shearing at high stresses. For such a sample,

this would only be possible if the particles became instantaneously unbreakable at the moment of interest during shearing. Since this is physically impossible, a compromise was to reduce the stresses to a level where no significant breakage happens and determine the CSL for a sample which has already undergone particle breakage. This is the rationale behind the testing program presented here.

7.3. Fraser River Sand

The tested material, Fraser River Sand (FRS), is an alluvial deposit widely spread in the Fraser river delta in the Lower Mainland of British Columbia, Canada. The gradation used in this research contains around 0.8% fines content and has D_{50} and D_{10} of 0.271 *mm* and 0.161 *mm* respectively. FRS is a uniform, angular to sub-angular with low to medium sphericity, medium grained clean sand. Figure 7-2 shows a microscopic picture of FRS grains. e_{min} and e_{max} are reported as 0.627 and 0.989 and G_s = 2.719 by Shozen (1991). The value of e_{min} was measured according to ASTM D2049 while e_{max} was reported as the initial deposition void ratio in the loosest state. The average mineral composition based on a petrographic examination is 25% quartz, 19% feldspar, 35% metamorphic rocks, 16% granites and 5% miscellaneous detritus.

7.4. Testing Program

The test program included 28 drained and 11 undrained triaxial tests using lubricated end platens to reduce stress non-uniformity within the samples. All samples were 142 *mm* in height and 71 *mm* in diameter and were prepared using the moist tamping technique. The samples were

239

flushed with CO_2 and de-aired water and back pressurised until a *B* value of 0.95 or greater was obtained. They were then consolidated and sheared until a steady state was reached, apparent shear localisation was observed, or the equipment limitations were met. The strain controlled shearing was applied at a constant rate of 5% per hour.

Special attention was paid to accurate measurement of the void ratios considering its significance to the arguments made. At the end of the shearing phase the drainage valves were closed. The sample was removed from the cell and the cell base, membrane and cap were dried before putting the setting in a freezer for 24 hours. The frozen sample was then extracted with extreme care making sure that no water or grains were lost during the process. This technique (Sladen and Handford, 1987) effectively eliminated loss of water during sample extraction, enabling accurate determination of water contents. A repeatability of 0.01 or better was obtained for three pairs of tests that were targeted to start from identical conditions. Corrections were applied for membrane penetration (Vaid and Negussey, 1984) and membrane force (Kuerbis and Vaid, 1990).

The initial stage of the testing program was aimed at measuring the critical state locus of FRS at low stress levels expected to be uninfluenced by particle breakage. Table 7-1 summarises these 16 lower stress tests.

To investigate the effect of particle breakage on CSL, an additional 8 samples (7 drained, 1 undrained) were sheared at higher levels of stress and dry sieved at the end of each test. Two samples (corresponding to sieve tests #1 and #2) were sieved before shearing and found to have fines contents of 0.7% and 0.9%. Table 7-2 provides details of these 8 tests referred to as the "parent tests", identified in the table by bold font. Information provided includes initial and final

stress level and void ratio, status of the sample with regards to the critical state at the end of the test, and the percentage fines following shearing.

Six samples showed an increase in their fines content following shearing. They were used to prepare samples for testing at lower stress levels to investigate the change in CSL due to breakage. Table 7-2 also provides details of the subsequent 15 tests performed on pre-sheared samples at lower stress levels.

7.5.   Results

Figure A-10a shows the deviator stress and volumetric strain plotted against axial strain for the drained tests presented in Table 7-1. Figure A-10b shows the deviator stress and the pore pressure plotted against the axial strain for the undrained tests presented in Table 7-1. A sample is considered at the critical state if the stress ratio and the volumetric strain (drained) or pore pressure (undrained) have reached a steady constant value.

To obtain the critical state parameters of FRS all the tests presented in Table 7-1 are plotted in Figure 7-3 as $e - \log p'$ state paths. Between 100 kPa and 900 kPa the CSL is approximated with $\Gamma = 1.22$ and $\lambda_{10} = 0.138$ ($\lambda_e = 0.06$) in the typical semi-log space idealisation. Below $p' = 100$ kPa the semi-log CSL idealisation does not match the data well and the CSL is plotted with a dashed line to illustrate uncertainty. As discussed in the previous chapter a bilinear semi-logarithmic representation of the CSL is also observed for other gradations of FRS and is not considered to be associated with a real change of behaviour. The dataset provides five tests that ended on the proposed CSL within a measured void ratio difference of 0.01 or less: CIU-M 200 kPa, CIU-L 390 kPa, CID-L 100 kPa, CID-M 400 kPa and CID-L 190 kPa UR. Another

241

three tests (CID-L 300 *kPa*, CIU-D 200 *kPa* and CID-D 200 *kPa* UR) delineate the same CSL with an error margin of ±0.05 or better. The location of the CSL is further assured by the fact that every single test below the proposed CSL was dilating and every single test above it was contracting at the end of their shearing phase. Any lowering of the CSL would undermine this basic principle of the critical state theory.

The CSL below 100 *kPa* is not important to the current work which focuses on a higher stress range. Above a particle 'breakage threshold' stress level particle breakage may occur. The approximate location of this threshold is shown on Figure 7-3, and is related to soil mineralogy, angularity, etc. Yamamuro et al. (1996) also showed an increase in particle breakage with reducing void ratio, suggesting the approximate threshold indicated on Figure 7-3 is in reality non-vertical. The exact location and nature of this breakage threshold is not important to the arguments presented, so the approximate threshold shown on Figure 7-3 is considered sufficient.

The deviator stress, pore pressure and volumetric strain have been plotted against axial strain for samples subjected to higher levels of stress in Figures A-11a to A-11c. Two of the parent samples (#1 and #2) were sieved before testing. At the end of each parent test the sample was sieved and then retested in the triaxial apparatus at lower levels of stress as summarised in Table 7-2 and shown in Figures A-11d to A-11f. Figure 7-4 illustrates the gradation curves for the sieve samples #1 and #2 before shearing and samples #1, #2 and #3 after. The remaining sieve tests were not plotted on this figure for clarity; their fines contents (FC) are reported in Table 7-2. Additional sieve tests were performed after shearing the pre-sheared samples whenever breakage was suspected to have occurred (tests starting at $p' = 600$ *kPa* or higher).

Post shearing fines content in the 8 samples ranged between 0.8% and 7.8%. Although more detailed indexes for quantifying particle breakage are available (e.g. Hardin, 1985; Miura and O-Hara, 1979), for simplicity the fines content has been used here to quantify particle breakage.

The tests performed on pre-sheared samples have been plotted in $e - log\ p'$ space along with their "parent" test (shown in bold) in Figures 7-5 to 7-12 in order to identify the effect of particle breakage on the CSL.

In Figure 7-5 the samples with an initial fines content of 4.1%, obtained by previously shearing sample CIU-D 1300 kPa to $p' = 2600\ kPa$ and $q = 3900\ kPa$, have been tested under drained and undrained conditions. The two undrained tests starting at $p' = 200\ kPa$ reached the critical state in the curved, low stress, zone of the CSL (see Figure 7-3) so these tests were discarded in determining the CSL. Hence the inferred location of CSL is biased towards Test "CIU-M #1 400 kPa".

The parent test CID-L 1600 kPa (Figure 7-6) on a virgin sample, was planned to be sheared drained near the equipment's pressure limit. Shortly after starting the test, the cell pump controlling the cell pressure failed and the cell pressure started decreasing. The test was continued until the sample failed. The sieve test performed post-shearing suggested no particle breakage had occurred and so no further tests were done on this sample.

The parent test shown on Figure 7-7 was performed on a loose drained sample consolidated to 1400 kPa and sheared to 43% axial strain. As expected for such large axial strains, towards the end of the test excessive bulging and shear localisation was observed, along with a drop in the measured deviator stress. At the end of the test the sample had 7.0% fines. This sample was then mixed with about 5% of its weight virgin sand (giving 6.3 % fines content) to produce enough material for the following tests. The mix was then tested loose at 200 kPa and 600 kPa mean

effective stresses respectively. The CSL was inferred based on the test at 200 *kPa*. Test CID-M #3 600 *kPa* was sieved and an increase in the fines content to 7.8% observed. To determine the change in CSL due to this further breakage, another test was conducted at 150 *kPa* suggesting a further drop in CSL.

The parent test in Figure 7-8 is similar to that in Figure 7-7; the difference being that the #5 sample shown in Figure 7-8 was sheared to a smaller strain (10%) and post test sieving showed a lower fines content of 1.9%. Two tests at 100 *kPa* and 300 *kPa* were performed on the sheared sample, which clearly showed a parallel shift in the CSL. The sample was then used in a test starting at 600 *kPa*. In this test, crossing the CSL, particle breakage was detected as indicated by the increase in fines content to 4.3%.

Test CID-D 600 *kPa* (Figure 7-9) was performed on a dense sample starting at p'=600 *kPa*. The fines content after shearing was 3.2%.

A dense sample at p'=600 *kPa* was sheared drained up to its peak strength as shown in Figure 7-10. Sieving detected no particle breakage. To confirm the absence of any effects on the CSL, one test at 100 *kPa* was performed on the sample which confirmed the original CSL.

Figures 7-11 and 7-12 plot tests from two nearly identical dense samples consolidated to just above 1000 *kPa*. The test in Figure 7-11 was stopped before the dilation phase. In Figure 7-12 the test was taken to larger strains until dilation ended and the sample started to contract again (see Figure A-11b). The test in Figure 7-11, which was stopped early, showed very little increase in its fines content. Two subsequent tests conducted on this sample indicated only a small CSL shift. Conversely, the more highly sheared sample (Figure 7-12) showed a significant fines increase, and a larger shift in the CSL.

The results presented in Figures 7-8, 7-11 and 7-12 suggest that for both loose and dense samples the effect of particle breakage on the location of CSL in $e - \log p'$ plot is a downward shift without a change in the slope of the line, consistent with the proposed varying Γ and constant λ_{10}. Postulating a parallel shift in CSL, it is possible to approximately locate the CSL with only one test at lower stresses using pre-sheared samples; the condition being that this test should have reached the critical state at the end of shearing. This approach was used to identify the CSL for the data presented in Figures 7-5 and 7-7.

7.6. Discussion

The critical state has been largely defined and tested in the absence of significant breakage of particles, when behaviour is controlled by sliding and rolling of the particles. The observation made at higher levels of stress has been that samples reach the critical state at lower void ratios than those expected by extrapolating the - usually but not necessarily - linear CSL in $e - \log p'$ space. This additional compressibility is understood to be caused by the breakage of soil particles resulting in generation of finer particles that fill the voids. The approach taken in this work is to distinguish between this additional compressibility caused by the breakage of soil particles and that caused by sliding and rolling (strictly speaking of plastic compressibility).

7.6.1. Influence of Breakage on CSL

These data suggest that particle breakage moves the CSL down (reducing Γ) without changing its slope (constant λ_{10}). This is in agreement with Muir Wood and Maeda (2008) who found that

the change in λ_{10} is negligible in comparison to the change in Γ. Looking at the tests on drained loose samples in Figures 7-7 and 7-8 it can be observed that a CSL extrapolation to higher stresses passes through the end point of the "parent" test. The end point of "CID-L 1400 *kPa*" is lower than that obtained from the extrapolation of the CSL drawn through the end point of "CID-M #3 200 *kPa*"; this test had 5% virgin soil added to the sample that has caused the CSL to move up relative to the CSL of CID-L 1400 *kPa*. The two consecutive tests again suggest that the test end point undergoing particle breakage ("CID-M #3 600 *kPa*") lies on an extrapolation of the CSL obtained from the test at the lower stress ("CID-L #3 150 *kPa*").

The end points of loose samples undergoing particle breakage are coincident with the CSL obtained from subsequent tests at lower stresses. Hence it can be inferred that samples undergoing particle breakage at higher stresses are at their CSL from a sliding and rolling point of view. In other words, the reduction in volume is entirely caused by the breakage phenomenon. So a sample being sheared at higher stresses is actually on its CSL defined as if the breakage stopped right away, but the line is continuously moving down parallel to the original CSL because of continuous breakage. This is the idea expressed by Equation 7-1 and shown in Figure 7-8. The data presented suggests that Equation 7-1 holds true some time after the sample has passed the original CSL.

7.6.2.   The Onset of Breakage

Let us now investigate when the breakage starts by considering test CID-L 1600 *kPa* (Figure 7-6) which was isotropically consolidated to a high confining pressure. The sample was sheared to 0.1% strain before failure of the cell pump occurred; shearing then continued until the sample

is is a rather strong

hint supporting the second assumption on which the conceptual model is based.

The drained tests on dense samples shown in Figures 7-9 to 7-12 start from 600 kPa and

1000 kPa and were taken to different levels of strain in order to investigate the initiation of

breakage. Test "CID-D 600 kPa-peak" was stopped around its peak strength when only some

slight dilation had occurred after the sample had undergone the initial contraction (see Figure

A-11b) expected from a dense sample. The consequent gradation test showed no increase in the

fines content and the test performed at 100 kPa confirmed no change in the CSL. In contrast,

test "CID-D 600 kPa", which was sheared until the dilation was completely suppressed, showed

a considerable amount of particle breakage (fines content increased to 3.2%). The tests starting

at 1000 kPa showed the same trend, suggesting that virtually all particle breakage occurs after

sliding and rolling compressibility is exhausted. This is consistent with Hyodo et al. (1999)

findings for undrained tests on sands, that particle breakage accelerates after the phase

transformation point. This observation can also be explained by assumption 2; that breakage

does not occur during the initial contraction phase in shearing of dense samples.

The proposed mechanism can be used to explain the behaviour seen in test "CID-L 1600 *kPa*" (and similarly the undrained test shown in Figure 7-1). Although starting at the highest mean effective stress of all tests, the sample showed no breakage in the sieve test performed afterwards because the sample contracted by sliding and rolling during the test and reached the CSL at a stress level lower than the 'particle breakage threshold'.

7.6.3.   The Influence of Breakage on Behaviour

Although test "CID-D 1000 *kPa*-peak" was stopped before the sample started dilating, some minor breakage was recorded; fines content increased from 0.8% to 1.0% and a small drop in the CSL was registered (Figure 7-11). It is possible to explain this using Equation 7-6: towards the end of the contraction phase and at the beginning of the dilation phase, Δe_{sr} becomes very small while breakage starts to kick in ($\Delta e_b \leq 0$). The resulting measured total Δe remains negative. Depending on the stress level, density, and the material, this effect can completely suppress the dilation phase and cause the sample to behave like a loose sample (Vesic and Clough, 1968) despite starting under the CSL.

A similar mechanism may occur during dilation when the sample is approaching the standard 'sliding/rolling' critical state. At this stage of the test the breakage may balance dilation, creating a state of zero volume change or "apparent critical state". The proposed hypothesis suggests that provided that breakage can continue with further shearing, compression will resume. This was observed in "CID-D 1000 *kPa*" on Figure A-11b as a resumption of contraction beyond 20% strain. For dense tests like "CID-D 1000 *kPa*", sheared to the "apparent

248

critical state" and beyond, the CSL is expected to follow the sample as it moves towards lower void ratios.

Although the tests presented in Figure 7-12 show that the CSL of the pre-sheared samples is significantly lower than the original CSL, the CSL of the pre-sheared samples is still well above the end point of the parent test. This could be due to localisation occurring post peak in dense samples, affecting both the volume changes and amount of breakage measured in the parent test. With localisation the whole sample has a smaller measured void ratio at the end of the test than it would have if the entire sample had dilated to the critical state. The same mechanism applies to particle breakage (Luzzani and Coop, 2002) resulting in a sample which is not only non-uniform in straining but also in gradation and amount of breakage. The pre-sheared sample is thus a mixture of materials with different degrees of breakage resulting in a higher CSL. This makes correlating the CSL with the sample's state at high stresses more difficult for dense samples.

Not considering localisation, it is expected for Equation 7-1 to similarly apply to dense samples once shearing has been continued far enough to initiate breakage. However, since in dense samples dilation occurs before the critical state is reached ($\Delta e_{sr} \geq 0$) it is not possible to directly measure Δe_b to verify the applicability of the equation.

The testing program presented here was not aimed at determining the exact nature of the stress level required to cause particle breakage (assumption 2.*ii*). But it appears that a breakage threshold around $p' = 900\ kPa$ marks the onset of measurable breakage for Fraser river sand.

It is well accepted that more particle breakage occurs during shearing than in isotropic compression (e.g. Bishop, 1966; Ueng and Chen, 2000), as also is observed here (test "CID-L 1600 *kPa*" with no breakage). The results of the current work do not suggest that no breakage

occurs in compression; likely just higher stress levels are required. Nevertheless, it is probable that the basics of the conceptual model are applicable to isotopic compression.

Although determining the CSL for samples undergoing breakage requires additional tests to be performed on sheared samples, the correlation between the shift in the CSL and the fines content produced by breakage is rather promising. Γ is plotted against the fines content in Figure 7-13 showing a direct relation between the two. And once this relation is established the CSL can be estimated for other samples by performing a sieve test.

The variation in Γ, ($\Delta\Gamma$), is plotted against the change in fines content for Fraser river sand as well as Kurnell sand (Russell and Khalili, 2002) in Figure 7-14. The kurnell sand data is plotted by applying the conceptual framework presented here to the triaxial compression and gradation test data presented by Russell and Khalili (2002). Despite the differences between the materials and the testing performed, the data presented in Figure 7-14 follow strikingly similar trends lending more support to the ideas presented.

7.6.4. The Influence of Breakage on CPT

In the context of the CPT analyses presented in earlier chapters, it is interesting that although particle breakage has been known (e.g. De Beer, 1963; Yang et al., 2010) to occur at the high stresses often induced by CPT, only a few of the preceding analyses have explicitly modelled the effects of particle breakage on CPT interpretation results. The hypothesis and data presented here allows additional insight into the effects of breakage on CPT interpretation.

Russell and Khalili (2002) considered breakage by incorporating a steepening CSL with increasing mean stress into a cavity expansion analysis using a critical state based model. The

fundamental issues with this approach were discussed earlier, but this approach was nevertheless able to partially address the effect of the additional compressibility caused by breakage on CPT analysis results. As expected, the result was a reduction in the limiting cavity expansion pressure, inferring an increase in the shape function required to match the chamber penetration resistance.

Although the framework adopted in this work for interpreting CPT does not account for the effects of breakage, it provides a basis for investigating its consequences on specific aspects of behaviour through the critical state parameters Γ, λ_{10}, and M_{tc}. The hypothesis and the data suggest a constant λ_{10} and a declining Γ due to breakage in zones around the cone where the stresses exceed the breakage threshold. The confined conditions around the cone and the large strain nature of deep penetration likely guarantee that the other requirement for the triggering of breakage (i.e. exhaustion of the capacity for sliding and rolling) be satisfied around the cone.

Similar to the findings of Russell and Khalili (2002), a declining Γ will likely result in a reduction in the limiting cavity expansion pressure. However, breakage as an energy dissipation mechanism can also add a component to the strength of the materials undergoing breakage. The effect will likely be analogous to an increase in M_{tc}. The increase is likely small as the energy dissipated in breakage is suggested to be around 10% of the energy dissipated in friction (McDowell et al., 2002). The added compressibility (declining Γ) will have a far more pronounced effect on cone penetration as a deformation controlled process. However, as mentioned in chapter 6, an increase in M_{tc} can still have significant implications for the interpretation of the state parameter from CPT.

One difficulty in incorporating the breakage phenomenon in the analysis of CPT is the inherent mismatch between the stress levels achieved in analysis and in reality, as reflected by the shape

function. Since breakage is governed by the stress level and in particular a stress threshold, if the numerical model is working at a lower stress range, it may not detect, or underestimate the amount of breakage and its consequences.

In the CPT interpretation framework adopted and developed in this work, the effects of particle breakage are implied in the shape function. By explicitly incorporating particle breakage into the framework one can expect further improvement in the accuracy in estimating the state parameter from the tip resistance. However, the current accuracy of the framework appears to be more constrained by the repeatability of the experimental data against which it is validated than by its simplifying assumptions, including its treatment of particle breakage.

7.7. Summary and Conclusions

The current work proposed a simple hypothesis to understand Critical State Locus movement due to shearing a particulate soil at stresses high enough to produce particle breakage. The conceptual model was tested using a series of triaxial compression tests on Fraser river sand, reaching p' levels of up to 3 MPa. The associated increase in the fines content of sheared samples ranged from zero to nearly 7%.

The main observations from the hypothesis and the associated testing performed are:

Measurable breakage only starts after the soil's contraction capacity is exhausted.

As postulated by Daouadji et al. (2001) and Muir Wood and Maeda (2008), breakage causes a downward parallel shift in the location of the CSL in $e - \log p'$ space.

The magnitude of this CSL shift is equal to the void ratio reduction due to breakage ($\Delta e_b = \Delta\Gamma$) and is directly correlated with the increase in fines content.

These observations contradict the widely adopted three part line used to model the effect of particle breakage on the CSL and it is recommended that future work idealises the CSL as a series of parallel loci each associated with a certain level of particle breakage.

The experimental observations also imply that since $\Delta e_b = \Delta \Gamma$, the state parameter is independent of breakage. The volume reduction caused by the breakage may simply be superimposed on the volume change controlled by stress-dilatancy. Hence it may be possible to uncouple the critical state framework and the breakage phenomenon.

The experimental data provided in this chapter are encouraging in the support they provide for the proposed hypothesis. More testing is needed to further investigate the generality of the ideas presented here and other aspects of breakage.

Table 7 - 1 Summary of testing program at lower stress level

Test name[*]	Initial conditions			End of Test					Remarks
	p' (kPa)	e	ψ_0[**]	Status[***]	ε_1 (%)	p' (kPa)	q (kPa)	e	
CIU-L 100 kPa	97.7	1.053	0.108	Con.	1.6	11.0	16.7	1.053	
CIU-L 200 kPa	201.9	0.963	0.061	CS	14.0	9.4	15.5	0.963	
CIU-M 200 kPa	200.2	0.897	-0.005	Dil.	10.2	184.6	273.5	0.897	
CIU-D 200 kPa	196.4	0.820	-0.083	Dil.	5.1	334.6	504.7	0.820	
CIU-L 300 kPa	301.0	0.966	0.088	CS	19.0	16.0	24.4	0.966	
CIU-D 390 kPa	388.4	0.906	0.044	Dil.	24.3	186.0	266.4	0.906	
CIU-M 400 kPa	393.3	0.832	-0.030	Dil.	19.6	613.6	896.5	0.832	
CID-D 50 kPa	50.3	0.753	-0.232	Dil.	25.1	92.1	126.7	0.878	
CID-L 100 kPa	102.1	0.948	0.005	CS	34.8	193.7	274.2	0.911	void ratio calculated from reconstitution density due to loss of water during retrieval
CID-D 115 kPa	113.9	0.668	-0.268	Dil.	21.7	226.0	336.9	0.794	
CID-L 300 kPa	302.9	1.005	0.128	Con.	29.1	585.9	847.1	0.868	
CID-D 410 kPa	409.6	0.634	-0.225	Dil.	24.3	811.1	1196.6	0.728	Some particle breakage expected
CID-D 515 kPa	514.5	0.689	-0.156	CS	28.4	984.3	1405.1	0.742	
CID-L 600 kPa	603.3	0.857	0.021	Con.	31.7	1134.9	1594.0	0.772	
CID-L 190 kPa UR	190.0	0.902	-0.004	CS	23.6	356.0	496.1	0.865	Un/Re-load cycles applied
CID-D 200 kPa UR	198.0	0.730	-0.173	Dil.	26.2	399.2	601.3	0.804	

[*] CIU, consolidated undrained test; CID, consolidated drained test; L, loose; M, medium dense; and D dense sample.

[**]The state parameter is obtained with respect to the original CSL defined in Figure 7-3.

[***]Con., contracting; CS, no change in volume or pore pressure i.e. critical state; and Dil., dilating.

Table 7 - 2 Summary of testing program at higher stress level and tests performed on pre-sheared samples

Test name	Initial conditions			End of Test					FC (%)	Sieve Test	Remarks
	P' (kPa)	e	ψ	Status	ε_1 (%)	p' (kPa)	q (kPa)	e			
CIU-D 1300 kPa*	1288.1	0.620	-**	CS	16.8	2584.4	3894.3	0.620	4.1	#1	Pre-testing fines content is 0.7 %
CID-D #1 100 kPa	102.2	0.698	-0.120	Dil.	1.9	209.8	317.1	0.774			
CIU-L #1 200 kPa	200.9	0.915	0.138	CS	18.7	5.7	8.1	0.915			
CIU-M #1 200 kPa	203.9	0.868	0.092	Con.	9.6	35.5	51.1	0.868			
CIU-M #1 400 kPa	394.0	0.820	0.084	CS	24.9	149.4	203.9	0.820			
CID-L 1600 kPa	1601.4	0.867	-	Con.	8.3	545.5	744.3	0.843	0.8	#2	Cell pump failed, but test continued down an arbitrary stress path. Pre-testing fines content is 0.9%
CID-D 1400 kPa	1396.2	0.839	-	Con.	10.7	2718.7	3950.5	0.600	7.0	#3	About 5% of the sample weight virgin FRS was added to the sample, reducing FC to 6.3%
CID-M #3 200 kPa	204.6	0.824	0.044	CS	43.0	392.2	560.9	0.746			
CID-M #3 600 kPa	614.9	0.780	0.065	CS	25.9	1193.0	1760.6	0.657	7.8	#3a	
CID-L #3 150 kPa	155.9	0.831	0.059	CS	28.4	274.4	363.5	0.739			
CID-D 1400 kPa-2	1403.5	0.849	-	Con.	39.4	2325.5	2744.7	0.736	1.9	#5	Test stopped early
CID-L #5 100 kPa	103.6	0.999	0.087	CS	9.8	186.5	249.3	0.883			
CID-L #5 300 kPa	303.617	0.9381	0.091	CS	35.0	563.5	780.4	0.809			
CID-L #5 600 kPa	604.103	0.8904	0.085	CS	32.3	1188.4	1762.4	0.729	4.3	#5a	Problems with cell pressure early in the test
CID-D 600 kPa	603.8	0.752	-	CS	31.8	1134.3	1594.8	0.748	3.2	#4	
CID-D 600 kPa-peak	578.3	0.701	-	Dil.	33.7	1321.0	2150.2	0.694	0.8	#6	Test stopped early
CID-L #6 100 kPa	104.4	1.004	0.063	CS	5.8	189.7	255.3	0.902			
CID-D 1000 kPa-peak	1003.4	0.666	-	Con.	31.3	2019.6	3027.3	0.643	1.0	#7	Test stopped early
CID-L #7 100 kPa	105.2	1.005	0.074	CS	23.1	187.2	246.0	0.898			
CID-L #7 300 kPa	302.7	0.954	0.086	CS	38.8	570.6	802.4	0.823			
CID-D 1000 kPa	1014.6	0.663	-	Con.	36.3	1880.8	2633.7	0.657	3.1	#8	
CID-L #8 100 kPa	104.1	0.982	0.095	CS	6.0	187.6	250.2	0.854			
CID-L #8 300 kPa	304.1	0.924	0.102	CS	34.4	559.5	765.6	0.788			

* Tests shown in bold provide the "parent" samples for the following tests after being sieved for gradation.
** The state parameter not stated for "parent" samples as CSL changes during test due to particle breakage.
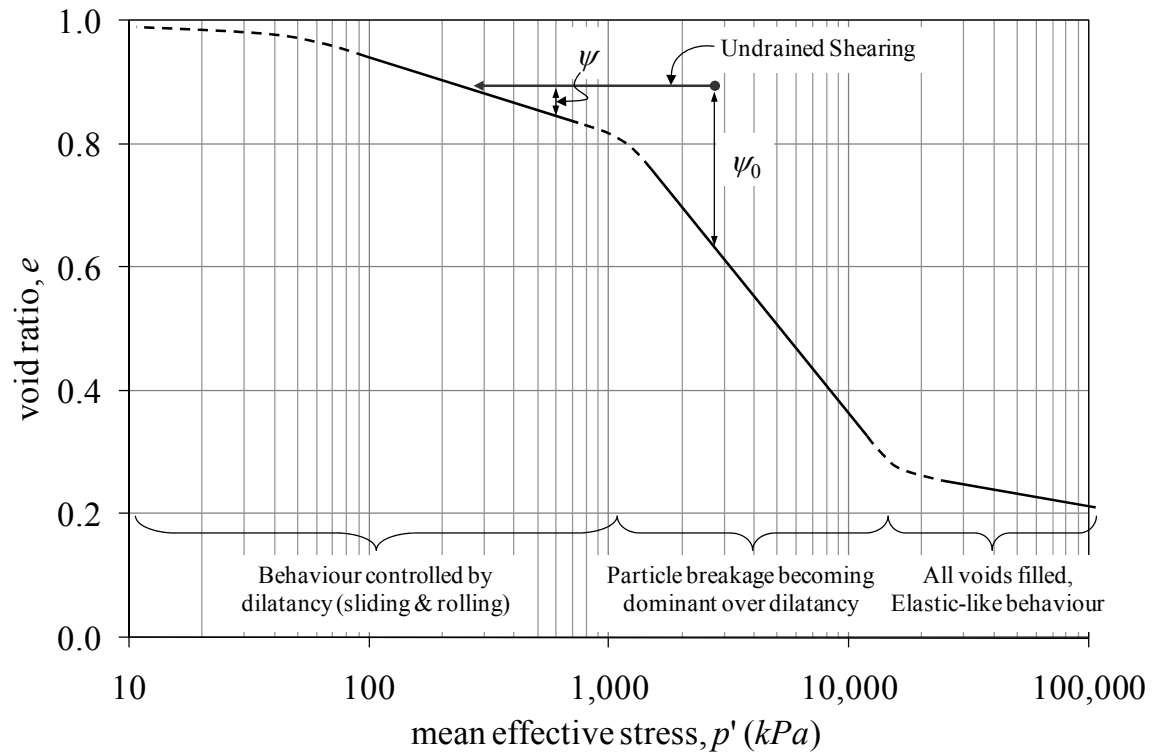
Figure 7 - 1 Full stress range CSL in $e - log\ p'$ space (after Russell and Khalili, 2004) and schematic undrained triaxial test
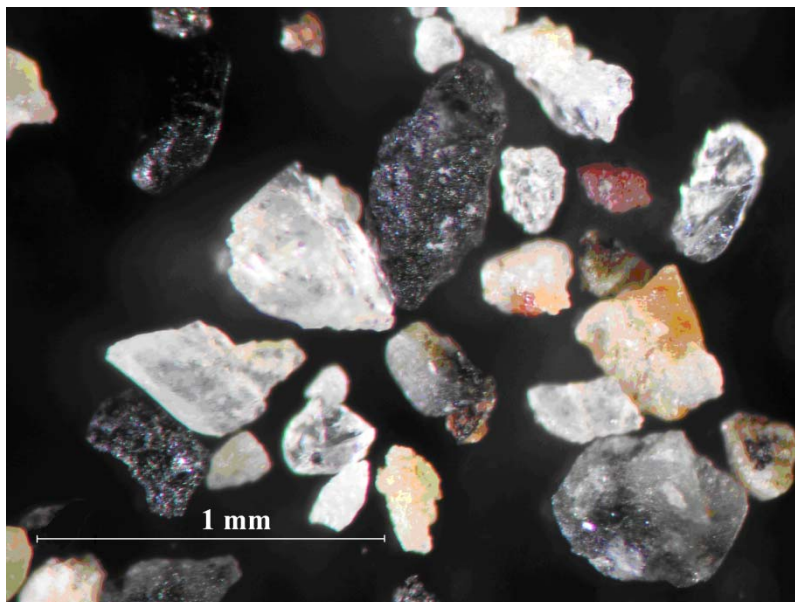

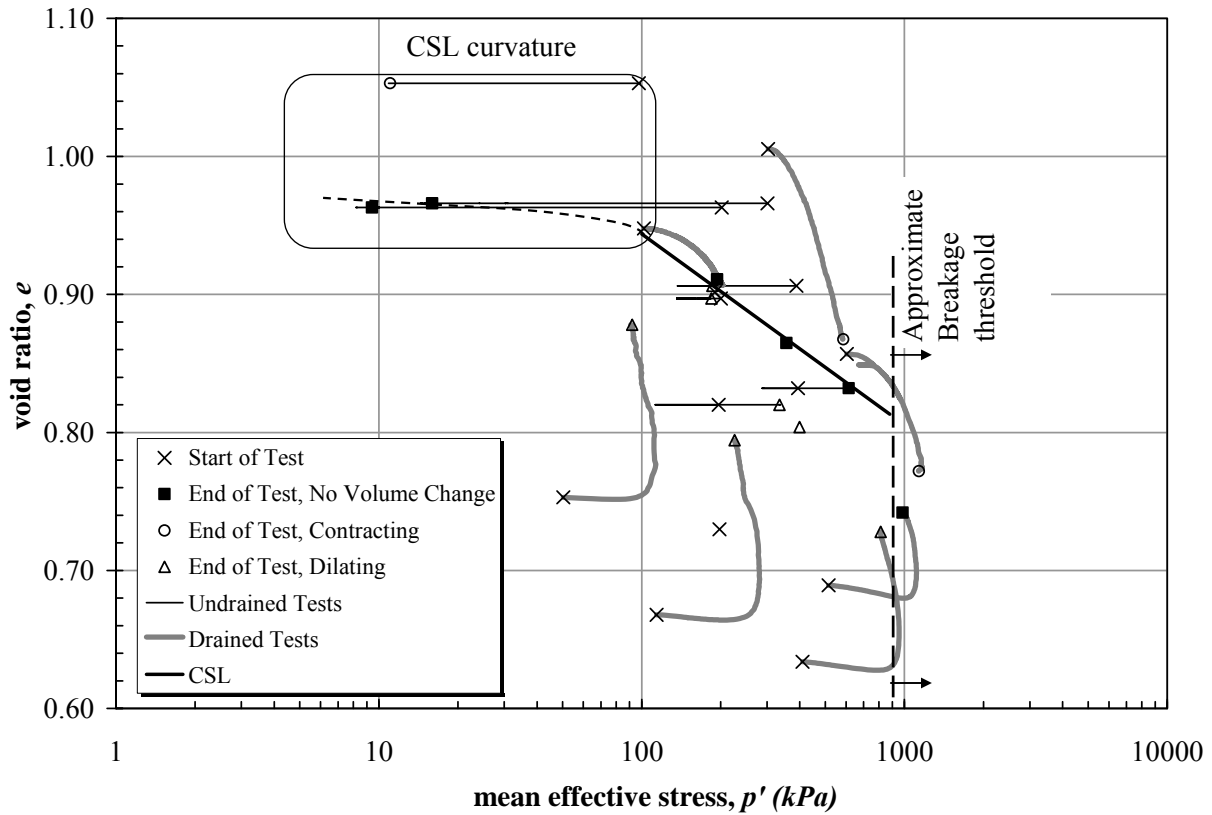Figure 7 - 2 Microscopic picture of FRS grains

Figure 7 - 3 Void ratio versus *p'* for virgin FRS tests summarised in Table 7-1 (for figure clarity only start and end points are plotted for cyclic tests)
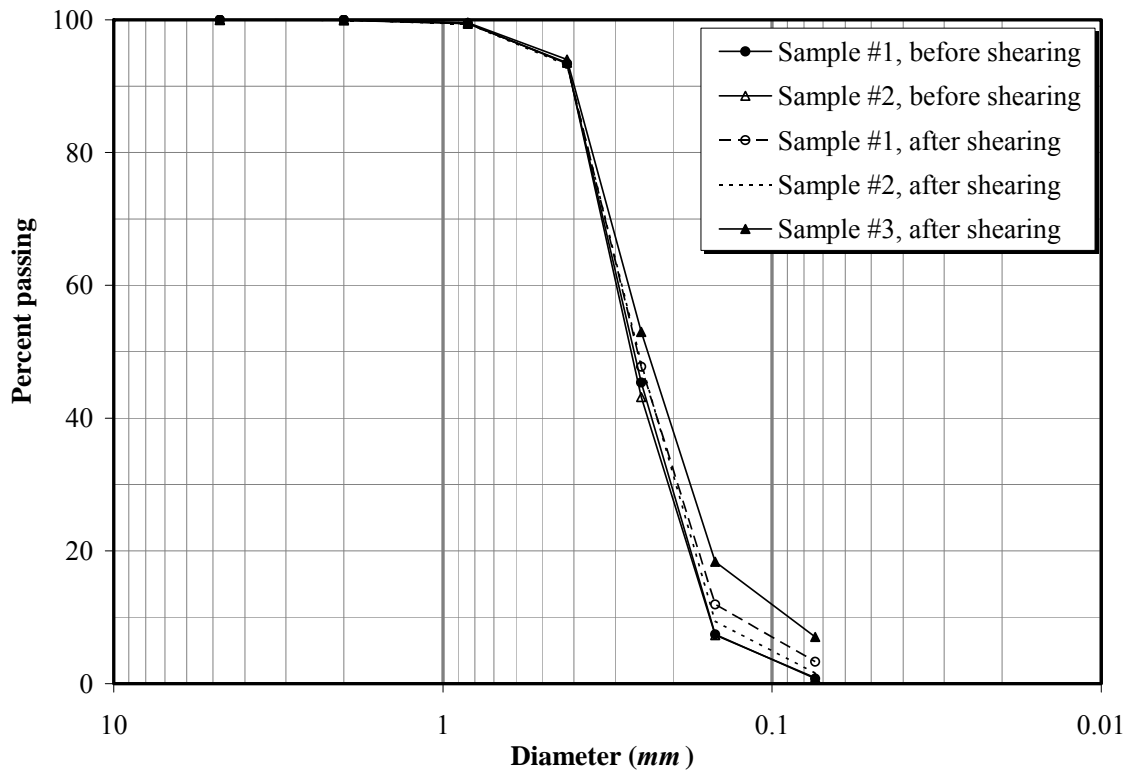
Figure 7 - 4 Gradation curve for samples of FRS before and after shearing
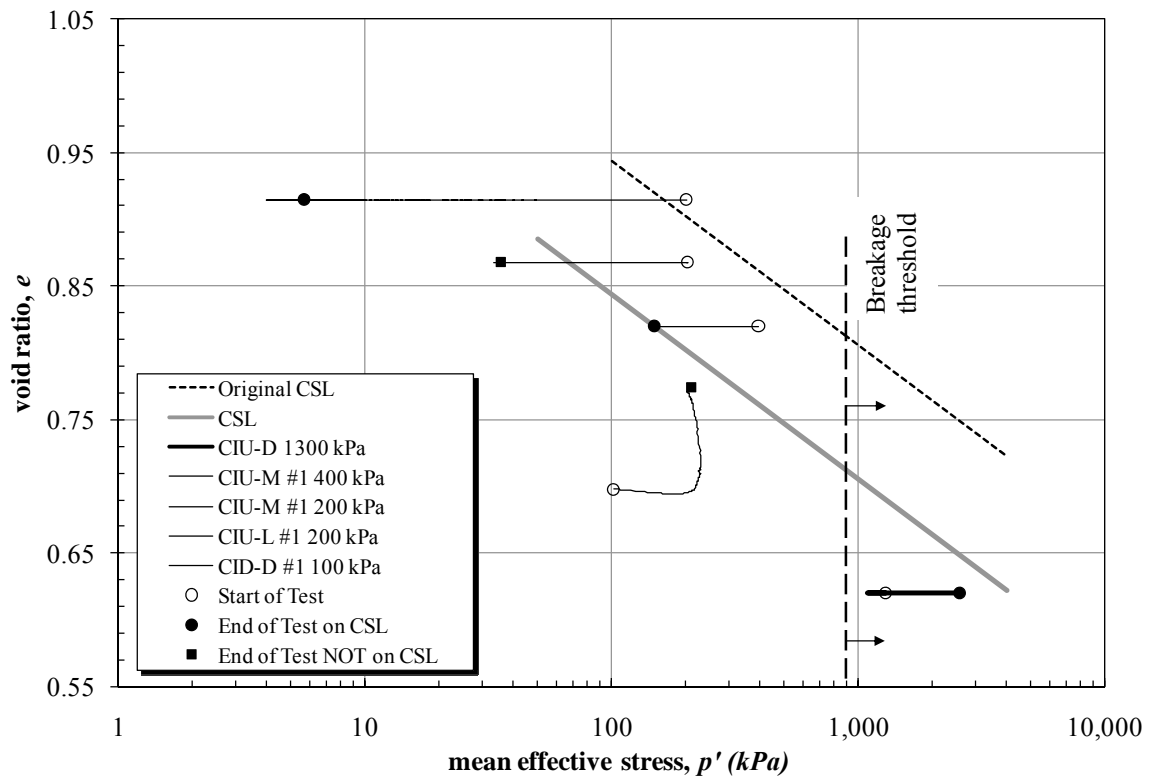

Figure 7 - 5 $e - log\ p'$ plot for all tests on sieve sample #1 in Table 7-2 (obtained from parent sample CIU-D 1300 *kPa*)
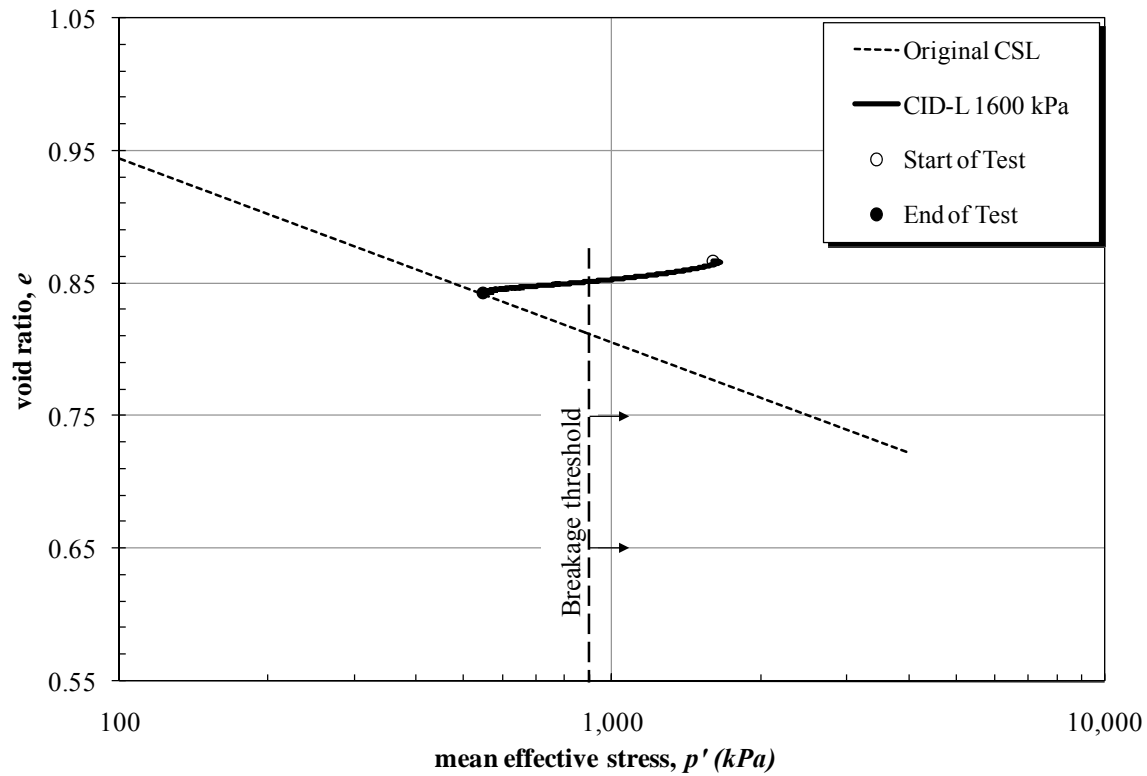
Figure 7 - 6 *e − log p'* plot for test CID-L 1600 *kPa* (sieve sample #2)
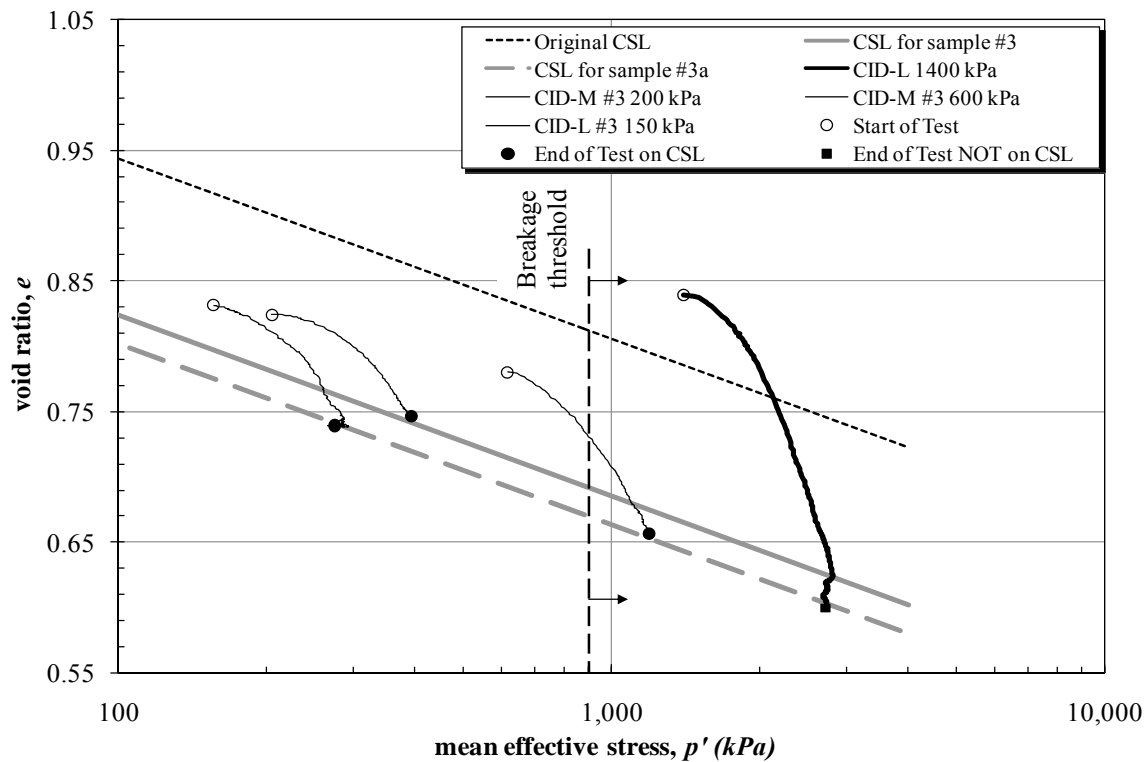
Figure 7 - 7 *e − log p'* plot for all tests on sieve sample #3 in Table 7-2 (obtained from CID-L 1400 *kPa*)
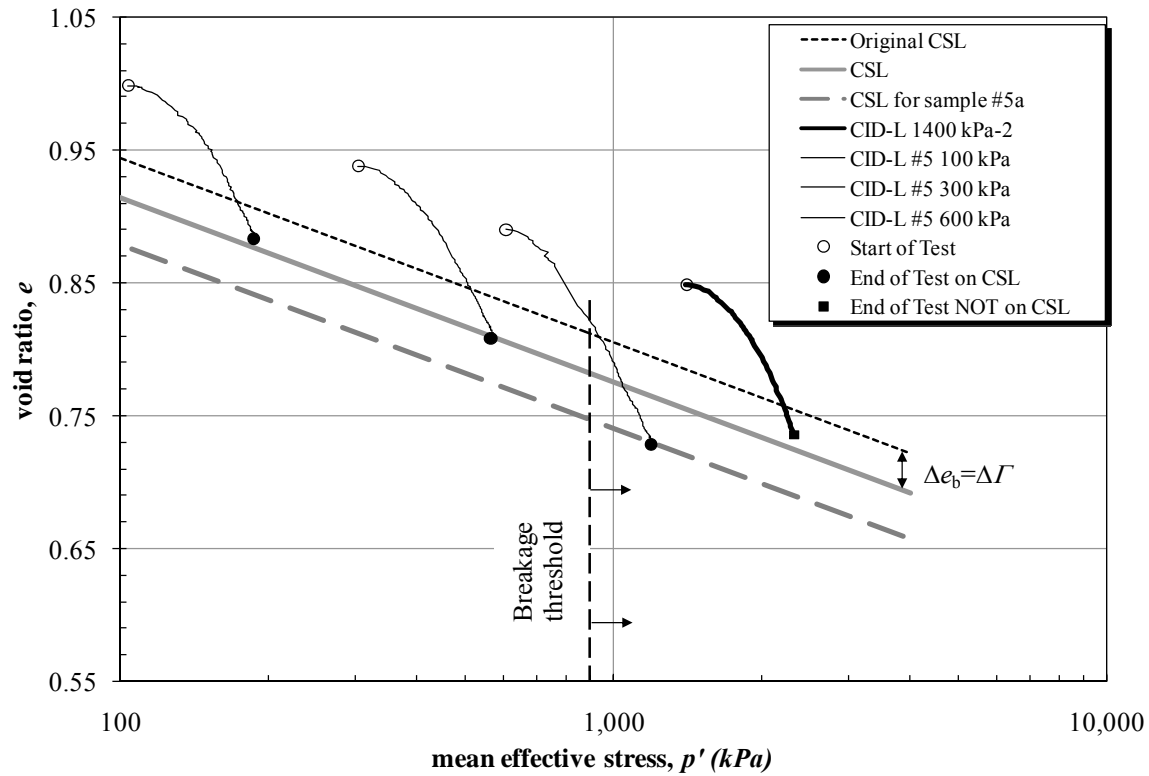
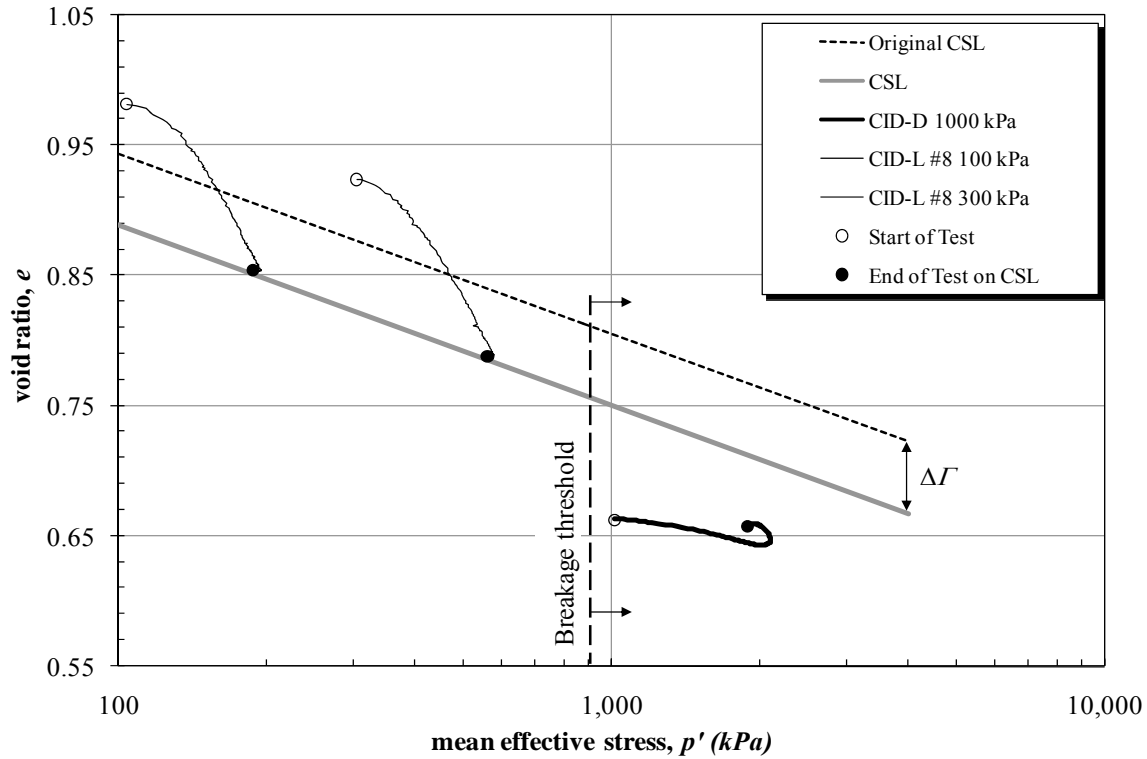Figure 7 - 8 $e - \log p'$ plot for all tests on sieve sample #5 in Table 7-2 (obtained from CID-L 1400 kPa-2)
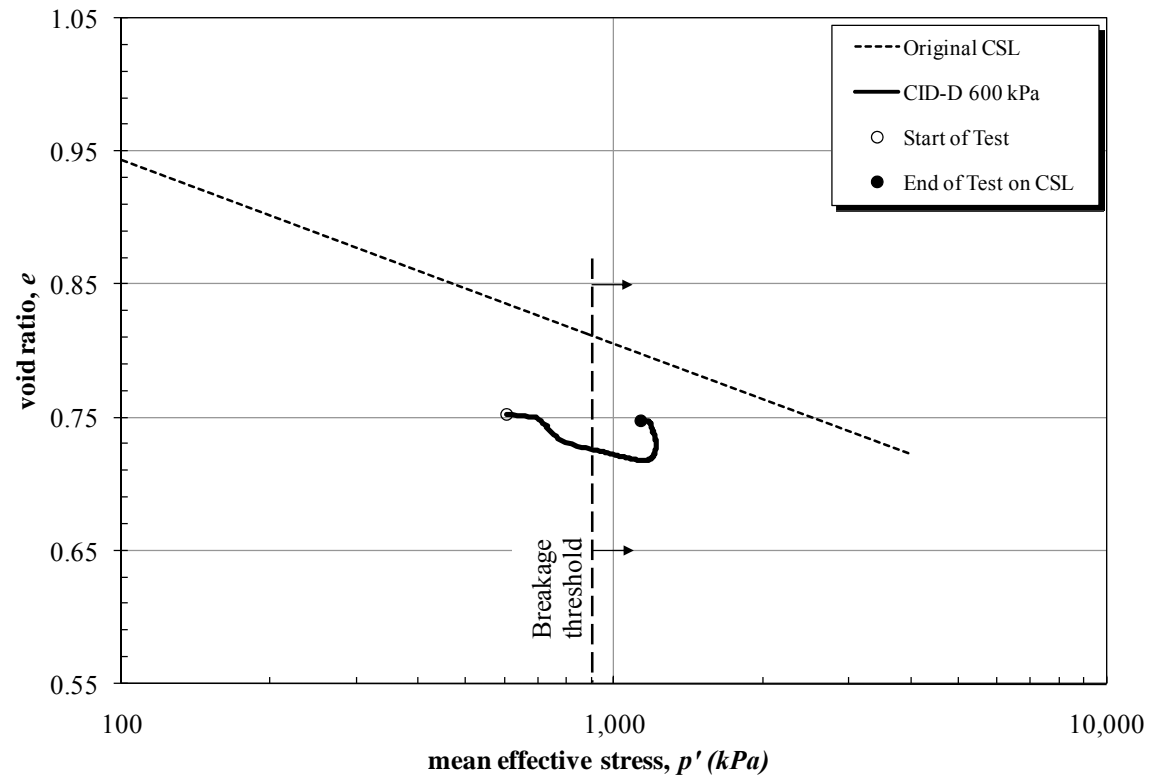
Figure 7 - 9 $e - \log p'$ plot for test CID-D 600 kPa (sieve sample #4)
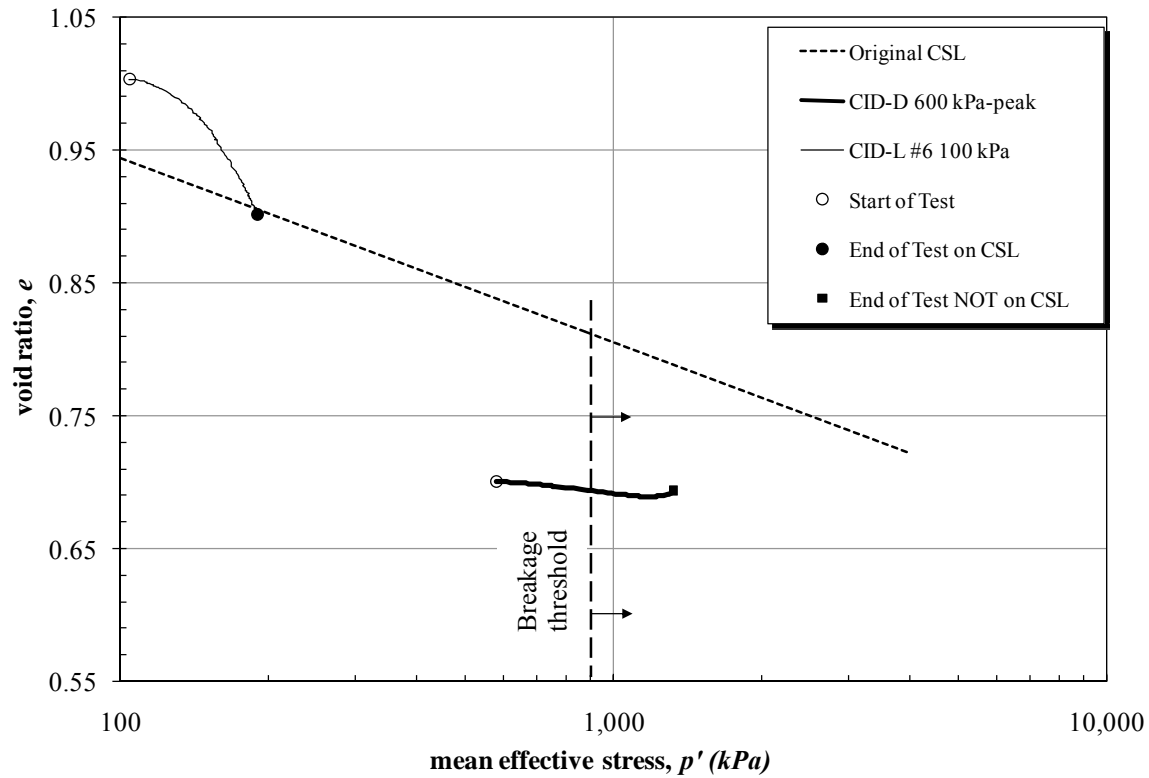
Figure 7 - 10 $e - log\ p'$ plot for all tests on sieve sample #6 in Table 7-2 (obtained from CID-D 600 kPa-peak)
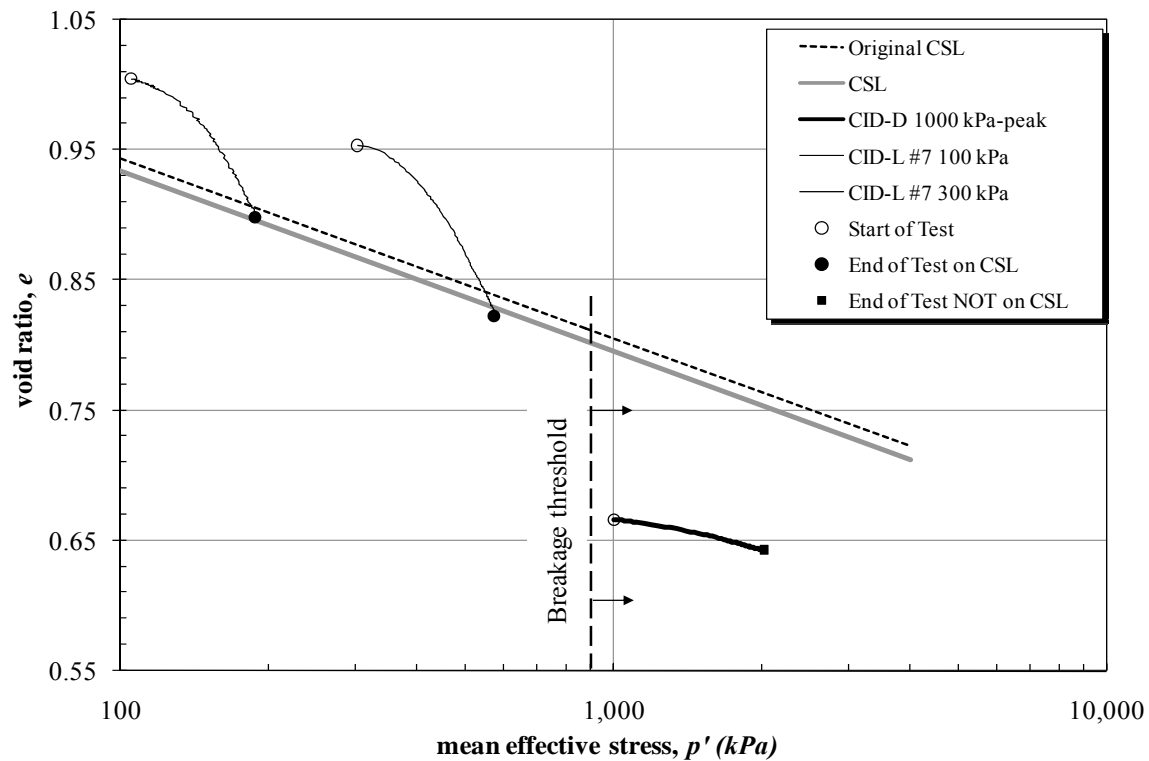
Figure 7 - 11 $e - log\ p'$ plot for all tests on sieve sample #7 in Table 7-2 (obtained from CID-D 1000 kPa-peak)

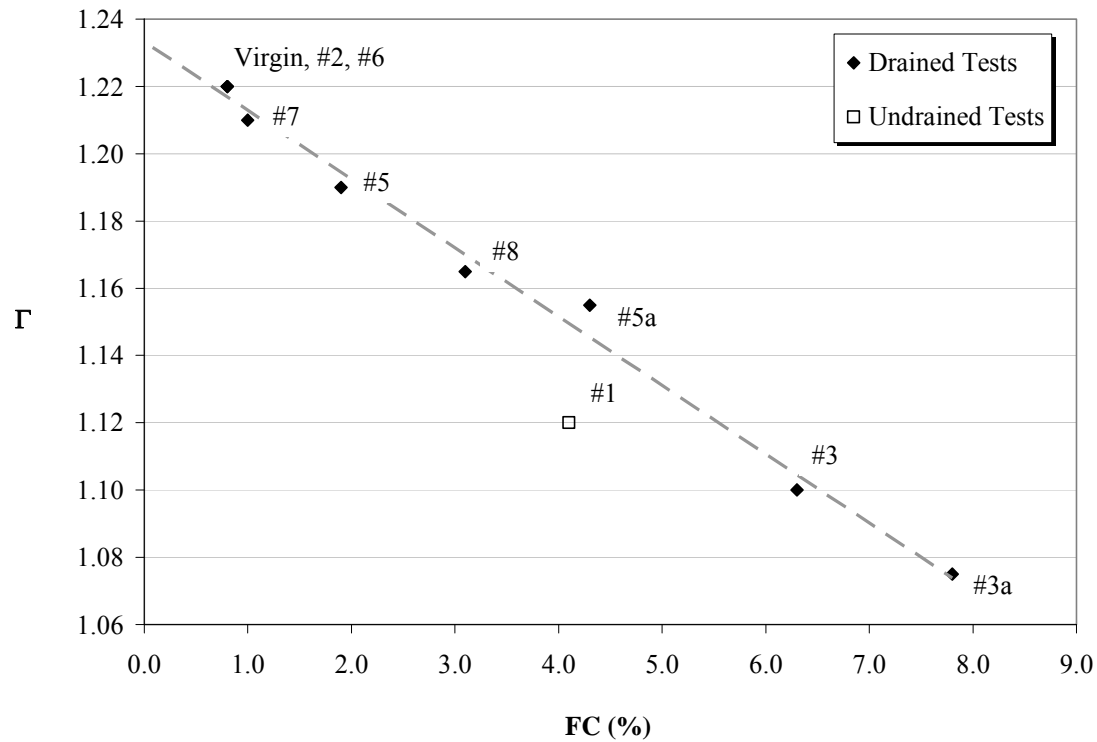Figure 7 - 12 *e – log p′* plot for all tests on sieve sample #8 in Table 7-2 (obtained from CID-D 1000 *kPa*)

Figure 7 - 13 Variation in Γ vs. fines content after shearing of FRS under drained and undrained conditions (Sieve test numbers are shown beside data points)
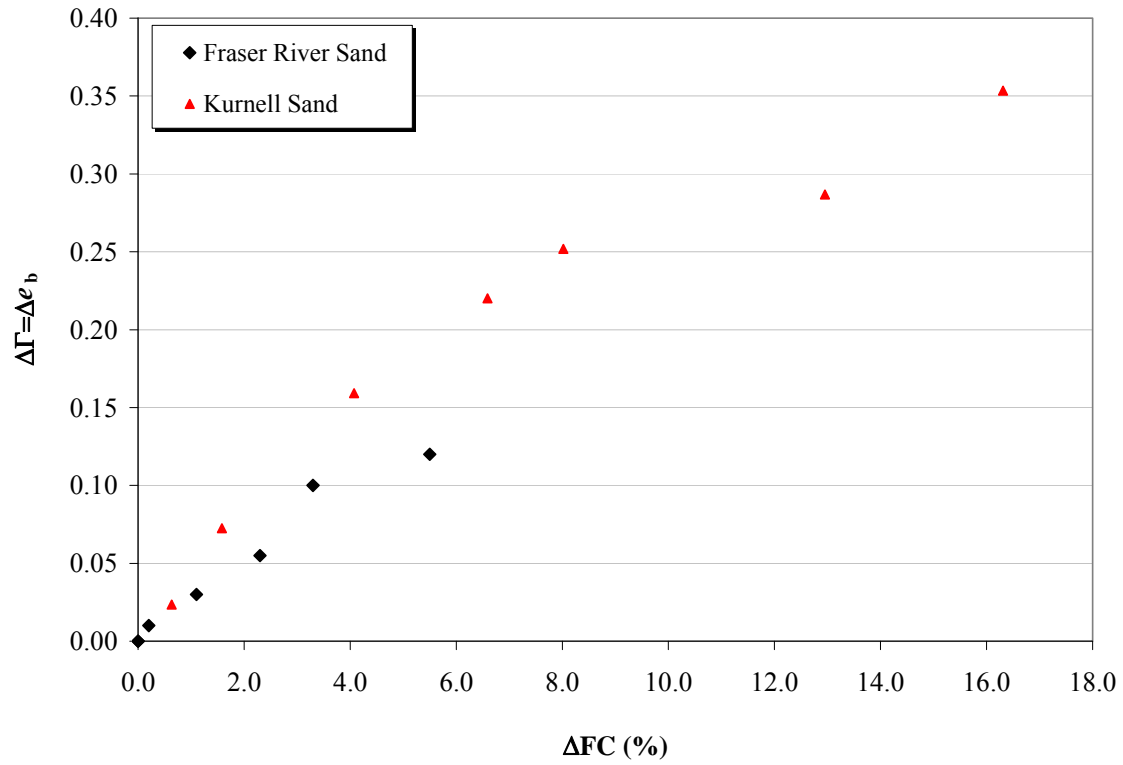
Figure 7 - 14 ΔΓ vs. the change in fines content after shearing at high pressures: comparison between FRS and Kurnell sand (Russell and Khalili, 2004)

7.8. References

Baharom B. and, Stallebrass S.E. 1998. A Constitutive Model Combining the Microscopic and Macroscopic Behaviour of Sands in Shear and Volumetric Deformation. Proceedings of the 4th European Conference on Numerical Methods in Geotechnical Engineering, Udine, 1998. Springer-Verlag Wien, New York, 263–273.

Been K., Jefferies M.G., and Hachey J. 1991. The Critical State of Sands. Géotechnique, 41(3): 365–381.

Been K., and Jefferies M.G. 1985. A State Parameter for Sands. Géotechnique, 35(2): 99-112.

de Beer E.E. 1963. The Scale Effect in the Transposition of the Results of Deep-Sounding Tests on the Ultimate Bearing Capacity of Piles and Caisson Foundations. Géotechnique, 13(1): 39-75.

Bishop A.W. 1966. Strength of Soils as Engineering Materials. 6th Rankine Lecture. Géotechnique, 16: 89-130.

Bridgman P.W. 1918. The Failure of Cavities in Crystals and Rocks under Pressure. American Journal of Science, 45: 243-268.

Chandler H.W. 1985. A Plasticity Theory without Drucker's Postulate, Suitable for Granular Materials. Journal of the Mechanics and Physics of Solids, 33: 215–226.

Coop M.R., Sorensen K.K., Bodas Freitas T., and Georgoutsos G. 2004. Particle Breakage During Shearing of a Carbonate Sand. Géotechnique, 54(3): 157-163.

Daouadji A., Hicher P. Y., and Rahma A. 2001. An Elastoplastic Model for Granular Materials Taking into Account Grain Breakage. European Journal of Mechanics - A/Solids, 20: 113–137.

Hardin B.O. 1985. Crushing of Soil Particles. ASCE, Journal of Geotechnical Engineering, 111(10): 1177-1192.

Hyodo M., Aramaki N., Nakata Y., and Inoue S. 1999. Particle Crushing and Undrained Shear Behaviour of Sand. Proceedings of the 9th International Offshore and Polar Engineering Conference, Brest, France, May 30-June 4, 1999. ISBN 1-880653-39-7.

Jefferies M.G., and Been K. 2000. Implications for Critical State Theory from Isotropic Compression of Sand. Géotechnique, 50(4): 419-429.

Konrad J.M. 1998. Sand State from Cone Penetrometer Tests: A Framework Considering Grain Crushing Stress. Géotechnique, 48(2):201–215.

Kuerbis R.H., and Vaid Y.P. 1990. Corrections for Membrane Strength in the Triaxial Test. Geotechnical Testing Journal, 13(4): 361-369.

Lade P.V., and Yamamuro J.A. 1996. Undrained Sand Behaviour in Axisymmetric Tests at High Pressures. Journal of Geotechnical Engineering, 122(2): 120-129.

Lee I.K., and Coop M.R. 1995. Intrinsic Behaviour of a Decomposed Granite Soil. Géotechnique, 45(1): 117-130.

Lee K.L., and Farhoomand I. 1967. Compressibility and Crushing of Granular Soil in Anisotropic Triaxial Compression. Canadian Geotechnical Journal, 4(1): 68-86.

Luzzani L., and Coop M.R. 2002. On the Relationship between Particle Breakage and the Critical State of Sands. Soils and Foundations, 42(2): 71-82.

McDowell G.R., Bolton M.D., and Robertson D. 1996. The Fractal Crushing of Granular Materials. Journal of the Mechanics and Physics of Solids, 44(12): 2079-2101.

McDowell G.R., and Daniell C.M. 2001. Fractal Compression of Soil. Géotechnique, 51(2): 173-176.

McDowell G.R., Nakata Y., and Hyodo M. 2002. On the plastic hardening of sand. Géotechnique, 52(5): 349-358.

Miura N., and O-Hara S. 1979. Particle-Crushing of a Decomposed Granite Soil under Shear Stresses. Soils and Foundations, 19(3): 1-14.

Muir Wood, D. 2007. The Magic of Sands – The 20th Bjerrum lecture presented in Oslo, 25 November 2005. Canadian Geotechnical Journal, 44: 1329-1350.

Muir Wood D., Maeda K. 2008. Changing Grading of Soil: Effect on Critical States. Acta Geotechnica, 3: 3-14.

Russell A.R., and Khalili N. 2002. Drained Cavity Expansion in Sands Exhibiting Particle Crushing. International Journal of Numerical and Analytical Methods in Geomechanics, 26(4): 323–340.

Russell A.R., and Khalili N. 2004. A Bounding Surface Plasticity Model for Sands Exhibiting Particle Crushing. Canadian Geotechnical Journal, 41(6): 1179-1192.

Shozen T. 1991. Deformation under the Constant Stress State and its Effect on Stress-Strain Behaviour of Fraser River Sand. MASc. thesis, Department of Civil Engineering, University of British Columbia.

Skinner A.E. 1969. A Note on the Influence of Interparticle Friction on the Shearing Strength of a Random Assembly of Spherical Particles. Géotechnique, 19: 150-157.

Sladen J.A., and Handford G. 1987. A potential systematic error in laboratory testing of very loose sands. Canadian Geotechnical Journal, 24: 462-466.

Ueng T.-S., and Chen T.-J. 2000. Energy Aspects of Particle Breakage in Drained Shear of Sands. Géotechnique, 50(1):65-72.

Vaid Y.P., and Negussey D. 1984. A Critical Assessment of Membrane Penetration in the Triaxial Test. Geotechnical Testing Journal, 7(2): 70-76.

Vesic A.S., and Clough G.W. 1968. Behavior of Granular Materials under High Stresses. Journal of the Soil Mechanics and Foundations Division, ASCE, 94 (SM3): 661-688.

Yamamuro J.A., and Lade P.V. 1996. Undrained Sand Behaviour in Axisymmetric Tests at High Pressures. Journal of Geotechnical Engineering, ASCE, 122(2): 109-119.

Yamamuro, J.A., Bopp, P.A. and Lade, P.V. 1996. One dimensional compression of sands at high pressures. Journal of Geotechnical Engineering, ASCE, 122(2): 147-154.

Yang Z.X., Jardine R.J., Zhu B.T., Foray P., and Tsuha C.H.C. 2010. Sand Grain Crushing and Interface Shearing During Displacement Pile Installation in Sand. Géotechnique, 60(6): 469-482.

Chapter 8.

Summary and Conclusion

8.1. Summary

The Cone Penetration Test (CPT) has been widely used for evaluating the in-situ conditions of soils because of its continuous data measurement and repeatability at relatively low cost. The test is even more attractive in cohesionless soils such as sands, silts and tailings due to difficulties associated with retrieving undisturbed samples in them.

The behaviour of cohesionless soils strongly depends on their density as well as stress level. An index that captures both the effects of void ratio and mean stress on soil behaviour is the state parameter, ψ (Been and Jefferies, 1985).

Determining the state parameter from CPT data is done through a process referred to as interpretation. Both experimental and analytical approaches have been used to develop interpretation techniques. Analytical solutions have certain advantages but they have to be verified and validated against experimental data. Most analytical solutions to date are either too

complicated to be applicable to real engineering projects, or fail to capture the essential characteristics of the problem. Even those that appear competent in dealing with the cone penetration problem have not been verified and validated against a sufficiently wide range experimental data. Such verification and validation is necessary to provide confidence in both the accuracy and the range of ground conditions to which any analytical framework can be applied in practice.

An analytical framework for the interpretation of the state parameter from CPT tip resistance, q_c was laid out, verified, validated, and discussed. The cone penetration was analysed as the expansion of a spherical cavity with a large strain finite element code using a critical state soil model (NorSand) capable of accounting for both elasticity and plastic compressibility.

The framework is simple enough to be used in real engineering projects, and still sufficiently detailed to capture the essential characteristics of the problem. The framework relies on material-specific and independent calibration of the numerical model through triaxial tests. Special attention was paid to the critical state friction angle, ϕ_c as one of the parameters having a pronounced effect on the interpretation results.

Different methods of determining the state parameter were discussed, and the confidence and accuracy in its determination was quantified.

The efficiency of the method was further investigated by analysing two well documented case histories confirming that consistent results could be obtained from different in-situ testing methods using the proposed analysis technique. Consequently, cumbersome large scale testing methods such as Calibration Chamber (CC) testing can be substituted by a combination of triaxial testing and finite element analysis producing soil specific correlations.

One of the difficulties in understanding the cone penetration problem is the less researched effect of high stresses developing around the cone on the behaviour of the soil. A series of triaxial tests on Fraser river sand were performed focusing on the effects of particle breakage on the location of the CSL. Particle breakage was shown to cause additional compression in the soil and a parallel shift in the Critical State Locus (CSL).

8.2. Major Topics of Research

1. Four different methods of obtaining the critical state friction angle, ϕ_c from drained triaxial tests were examined through two independent and extensive databases of triaxial testing on clean sand. The purpose was to identify the most suitable method of determining the critical friction angle for use in calibrating the NorSand constitutive model to laboratory test data.

2. A statistical evaluation of a drained triaxial compression test database on Erksak sand was performed to determine accuracy and confidence level in determining the critical state friction angle. Recommendations were made on the number and distribution of the tests necessary to achieve different levels of accuracy in determining the critical state friction angle.

3. A framework for evaluating in-situ soil state parameter, ψ_0 from CPT tip resistance, q_c was developed based on a spherical cavity expansion analogy. A database of nine normally consolidated soils, including laboratory standard and natural sands as well as tailings materials, was used to verify the framework. A unique and consistent shape function between the normalised measured CPT tip resistance and spherical cavity

270

expansion limit pressures was identified. The spherical analysis results were then used to back calculate ψ_0 for 301 calibration chamber tests and the resulting states were compared to those measured in the lab.

4. In order to validate the proposed framework for obtaining ψ_0 from q_c data, cylindrical and spherical cavity expansion analyses were used to interpret the state parameter from in-situ Self-Bored Pressuremeter (SBP) and CPT in an hydraulically placed clean quartz sand in the Beaufort Sea.

5. The developed framework for determining ψ_0 was applied to a site in the Fraser river delta in British Columbia, Canada, that has been extensively investigated as part of the CANadian Liquefaction EXperiment (CANLEX) project. The void ratios obtained from the cores obtained from ground freezing and Laval large diameter sampler were used to validate the approach.

6. Particle Breakage is known to occur at stress levels similar to those often generated during CPT penetration, although this phenomenon is rarely considered as part of CPT interpretation. The final aspect of this research was to develop a simple hypothesis explaining the material behaviour during the shearing a particulate soil at stresses high enough to produce particle breakage. The hypothesis was tested using a series of triaxial compression tests on Fraser river sand.

The following sections (i.e. sections 8.2.1 to 8.2.6) summarise the conclusions derived from the work in this research with respect to the items above.

8.2.1. Determination of the Critical State Friction Angle from Triaxial Tests - Summary of Findings

Four methods reported in the literature for obtaining the critical state friction angle, ϕ_c (or the equivalent critical state friction angle M_{tc}) were summarised and the advantages and disadvantages of each method were investigated using previously published data from drained triaxial tests on two sands.

The "maximum contraction", although widely reported in the literature, is inconsistent with the definition of the critical state and was found to give unrealistic estimates of M_{tc}. The "end of test" method was also found to be problematic. The large strain levels required to reach the critical state were generally not achieved in these triaxial tests and, combined with the potential for localisation, the "end of test" method provided poor estimates of M_{tc}.

Two methods are recommended for obtaining reliable values of ϕ_c: The 40 year old Bishop (1972) method which uses an extrapolation of the peak friction angle (or stress ratio) versus minimum dilatancy to the zero dilatancy axis; and an application of the stress-dilatancy method which involves extrapolation of the complete stress-dilatancy path to zero dilatancy.

While both methods did provide reliable values of ϕ_c, they had differing advantages and limitations. Most triaxial testing programs include only a limited number of tests. The Bishop method, although very simple, is sensitive to any outlying data points (associated with poor quality tests). Conversely, an advantage of the Stress-Dilatancy method is that it yields an estimate of M_{tc} for every single test, so it is much simpler to discard outlying values making it especially helpful when dealing with a small number of tests. The Stress-Dilatancy method usually has better resolution if high-scan-rate data is available for processing; an issue of less

importance when using the Bishop method. However, the use of post peak data in the Stress-Dilatancy method requires cautious application of it due to the possibility of shear banding and stress localisation post peak. It is therefore recommended that the whole stress-dilatancy path of tests be plotted and used in conjunction with the Bishop approach; obtaining the benefits of both methods.

8.2.2. Confidence and Accuracy in Determination of Critical State Friction Angle - Summary of Findings

A statistical evaluation of a drained triaxial compression test database was performed to determine accuracy and confidence level in determining ϕ_c. The critical state friction angle was obtained from a dataset comprising 34 triaxial tests using the methodology proposed by Bishop (1972); ϕ_c being obtained using linear regression. It was assumed that the correct ϕ_c was obtained if all 34 tests were included in the analysis. In determining the accuracy of smaller realisations of the dataset it was assumed that any test program will include at least one loose ($D_r = 26$ %), one medium dense ($D_r = 56$ %) and one dense ($D_r = 70$ %) sample tested under drained triaxial compression conditions.

Results were presented as error in ϕ_c versus number of tests for confidence levels of 75%, 85%, 90% and 95%. As the number of tests increased from 3 to 8 a large increase in accuracy was observed at all confidence levels. Hence it is recommended that any commercial testing program for evaluation of ϕ_c includes at least 6 tests (6 tests yielding an accuracy of $\pm1.0°$ from university quality data with 90% confidence). For academic purposes, where accuracy of $\pm0.5°$ with 90% confidence may be needed, more than 20 tests may be required.

Although the presented results were developed using one comprehensive academic testing program, their application to commercial data was encouraging. Although (unsurprisingly) the errors from the commercial dataset were slightly larger, the academic database provided a reasonable upper bound on likely achievable accuracy.

In conclusion, although soil type and gradation might be expected to affect sample uniformity during reconstitution and hence influence the repeatability (and hence accuracy) of the triaxial testing program, distributing the triaxial tests over a wide range of initial D_r, or ideally initial ψ, should provide greater accuracy in ϕ_c for fewer tests.

8.2.3. Interpretation of Sand State from CPT Tip Resistance - Summary of Findings

A framework for evaluation of in-situ soil state parameter ψ_0 from CPT tip resistance q_c data was developed based on a spherical cavity expansion analogy. Central to the approach is a shape function that relates the calculated normalised spherical cavity expansion pressure and the measured calibration chamber tip resistance.

A database of nine normally consolidated soils, including laboratory standard and natural sands as well as tailings materials, was selected for which both calibration chamber tests and triaxial tests were available. The NorSand critical state soil model was calibrated for each of the nine soils using the triaxial data. Spherical cavity expansion analysis was then performed on 301 normally consolidated calibration chamber tests and the results compared to those obtained experimentally. All nine soils followed the same trend with a scatter equivalent to that observed for the most intensely tested calibration chamber sand, Ticino. A unique and consistent shape function between the normalised experimental CPT and spherical cavity limit pressures was

identified.

Estimation of accuracy of the proposed framework is constrained by the repeatability seen in the calibration chamber data. For known soil properties (from triaxial compression tests) the soil specific k and m relations recover the q_c trend line to near perfect accuracy, and without bias. Individual calibration chamber results cannot be recovered to this accuracy, but this appears to be a consequence of the intrinsic variability in the calibration chamber data. For the nine soils, it was shown that the normalised cone resistance can be analytically reproduced with an accuracy of ±70% with 89% confidence. This accuracy is close to that observed in recovering the state parameter in calibration chamber data itself.

The spherical analysis results were then used to back calculate ψ_0 for all 301 chamber tests and the resulting states compared to those measured in the laboratory. The method predicted ψ_0 to within ±0.04 with 78% confidence and to within ±0.07 with 92% confidence.

Two sources of error were explicitly identified; inherent variability in the calibration chamber testing and the soil's elastic modulus. Clearly no analytical method can predict ψ_0 with accuracy higher than the repeatability of the dataset itself. In some of the most extensively investigated sets of data (calibration chamber tests on Ticino sand) the tip resistance can vary by a factor of two, despite ostensibly identical initial conditions. This inherent variability between calibration chamber tests likely accounts for about half the observed error. Part of the lack of repeatability seen in the chamber test data could credibly be caused by changes in the elastic modulus G. For Ticino sand the estimated error in interpreted ψ_0 due to a ± 50% variation in G was estimated to be up to ±0.03. Hence, it is recommended that G be measured in-situ to eliminate an unnecessary source of error. Where G is adequately measured, the accuracy of the state parameter estimation is virtually the same as that of costly calibration chamber tests.

8.2.4. Evaluation of Sand State from SBP and CPT: A Case History - Summary of Findings

The interpretation framework was used to interpret the in-situ state parameter from CPT in a hydraulically placed clean quartz sand in Beaufort Sea. An analogous technique was used for obtaining ψ_0 from in-situ SBP tests in an adjacent borehole. Calibration chamber test data available for the site were modified by the means of the analytical method for fabric effects to replicate in-situ soil conditions and used as reference.

Data from the CPT and SBP tests were evaluated independently, and plotted for comparison. Six of the seven evaluations indicate good correspondence between estimates for ψ_0 estimating the state parameter with a difference of 0 to 0.05. This is considered a very good level of consistency when compared to the common scatter observed in calibration chamber tests performed under controlled conditions in laboratory.

In comparison to CPT, SBP tends to estimate more negative (denser) values of ψ_0 by approximately 0.02, indicating a denser deposit. Although small, this bias in the estimate is non-conservative relative to the CPT interpretation; so the results should be cautiously applied to engineering problems.

There was one problematic SBP test, for which the SBP curve fitting estimated a ψ_0 value of -0.26 compared to $\psi_0 = -0.16$ from CPT data at the same depth. Although the CPT data confirms that the test was done on the densest material in the borehole, the SBP estimate seems unrealistic, especially as no densification effort had been undertaken at the site. However, this test was continued to the lowest strain (2.8%) amongst all the SBP tests done at the site. Other tests were taken to 5.5% to 10.5% strain. Thus, it could be speculated that any SBP test taken to

strains of less than about 5% should be treated with extreme caution when it comes to determining the state parameter.

CPT results appeared more consistent, and the state parameter values were more reasonable with respect to site conditions. However, since CPT calibration chamber testing was used as the reference, and no independent measurement of the in-situ state is available, it is not possible to say whether the CPT or SBP gave the "correct" answer; but the CPT and SBP results were close enough to be considered "in general agreement" with each other and the expected site conditions.

The mismatch between the state parameters obtained from SBP and CPT may be due to the geometry correction applied to the SBP. The correction is applied to account for the difference in cylindrical cavity expansion analysis that assumes infinite pressuremeter length and the real pressuremeter geometry. The current correlations, based on limited experimental data, do not account for the possible effects the material (its density amongst other characteristics) in which the test is being done may have on the correction.

One should keep in mind that although the CPT appears to produce a more reasonable and consistent state parameter interpretation for the site investigated, an estimate of horizontal stress is required for the adopted CPT interpretation. An adjacent pressuremeter test was used to obtain the horizontal stress at this site, hence the accuracy of CPT inferred state parameter relies in part on SBP measurement.

8.2.5.   Interpretation of the Sand State from CPT in Fraser River Sand: A Case History - Summary of Findings

The interpretation framework presented in Chapter 4 was applied to the Massey Tunnel site, an extensively investigated site in Fraser river delta in British Columbia, Canada. The effect of soil fabric on the interpretation results was considered by adjusting the calibration parameters with respect to tests on undisturbed samples. The accuracy of the method was evaluated by comparison to in-situ density measurements and compared to other methods of interpreting the state parameter from CPT.

The samples trimmed from the cores obtained from ground freezing and Laval large diameter sampler were considered to represent the real in-situ void ratio. The state parameter was obtained using the framework developed in Chapter 4 for the range of CPT tip resistances measured in the site. $\pm\ 0.07$ and $\pm\ 0.04$ error margins were identified to be able to compare the confidence level of the interpretation to the data used in developing the framework. The results were then compared to the state parameters calculated from the in-situ void ratio measurements. 98% of the undisturbed sampling measurement fell within the $\pm\ 0.07$ error margins and 70.5% within the $\pm\ 0.04$ error margins. These confidence levels compare very well with the 92% and 78% observed in the calibration chamber data used in developing the framework. 20.5% of the data were coincident with ψ_0 calculated for the range of CPT resistances, representing ideal accuracy for the information used in this work.

Direct measurements of the void ratio yielded an average void ratio of 0.96 with standard deviation (SD) of 0.05, translating into an average state parameter of -0.055 with the same SD. The wide scatter in the measured void ratios, reflected in the large SD, covers a range of

278

$-0.155 < \psi_0 < 0.01$. Part of the scatter likely stems from the ground sampling techniques, rather than being a characteristic of the ground, as widely ranging void ratios were measured in samples from adjacent points of the coring. While the variation in the measured void ratios represents a wide range of sand behaviour, ranging from loose to dense, the geology of the site and all in-situ testing (including CPTs) imply a relatively uniform deposit associated with a narrower range of ground density and sand behaviour. This paradoxical observation in methods of obtaining the in-situ density from undisturbed samples of sands calls for a more cautious treatment of the experimental results and emphasises the need for better interpretation techniques for tests such as CPT.

The accuracy offered by the ± 0.07 error margins covers a wide range of possible state parameters (typically $-0.30 < \psi_0 < 0.05$) when combined with the range of the original CPT data. However, the range is very similar to that covered by the frozen and Laval large diameter samples, suggesting that this method is as capable as the most expensive and cumbersome of ground sampling techniques for determining the soil's in-situ density. The average ψ_0 of -0.067 differs from the -0.055 average measured by ground sampling by -0.012. This difference is close to ±0.01; the ground sampling technique error margin given by Wride and Robertson (1997).

The results were compared to those obtained from Been et al. (1987), Plewes et al. (1992) and Konrad (1997) methods. Amongst all interpretation methods the one presented in Chapter 4 provided the closest estimation of ψ_0 for Fraser river sand. Although the method appears to be more difficult than the others, the difficulty lies only in the analysis and modeling effort which is achievable in a matter of hours. With the exception of Plewes et al. (1992), all interpretation methods require knowledge of the CSL in $e - \log p'$ space. Performing a number of triaxial compression tests is the easiest and most common way of estimating CSL. The only additional

requirement of the present method is for these tests to be performed under drained conditions; a requirement that does not pose any additional laboratory testing effort.

Plewes et al. (1992) correlated the slope of the critical state line in $e - \log p'$ space to the CPT friction ratio based on experimental results, hence eliminating the need to experimentally obtain the CSL. However, the method does require laboratory testing to measure ϕ_c (or the analogous M_{tc}). Plewes et al. (1992) suggested using $M_{tc} = 1.2$ ($\phi_c = 30°$) for all soils, advising that doing so would cause less than 10% error in the estimated ψ_0. However, using $M_{tc} = 1.2$ for Fraser river sand puts the estimated ψ_0 in line with the other methods (with an average ψ_0 of -0.089), resulting in a more negative (denser) state parameter than that implied by ground sampling techniques.

The success of these methods in obtaining ψ_0 appears to be directly related to the level of material behaviour taken into consideration. Konrad (1997) does not account for any mechanical aspects of soil behaviour and returns the most discrepancy in estimated state parameter (with an average ψ_0 of -0.114). The Been et al. (1987) method accounts for material compressibility through the slope of the CSL (with an average ψ_0 of -0.092). The Plewes et al. (1992) method adds the effect of the critical state friction angle to their framework resulting in an even better estimation (with an average ψ_0 of -0.071). The framework presented in this thesis also accounts for both compressibility and friction angle, and importantly adds elasticity, as well as stress level, dilatancy, and fabric.

An overall comparison of the model parameters for Fraser river sand to those of other sands presented in Chapter 4 suggests that the most important factor that makes the other methods systematically biased towards a more negative state parameter in Fraser river sand is its high

critical state friction angle. This is further confirmed by the fact that a correct M_{tc} value in the Plewes et al. (1992) method results in a markedly better interpretation.

8.2.6.   Particle Breakage and the Critical State of Sand - Summary of Findings

The current work involved using laboratory testing to assess a hypothesis for particle breakage; of importance to CPT due to the high pressures encountered at the cone tip. The hypothesis explained the CSL movement due to shearing a particulate soil at stresses high enough to produce particle breakage. This conceptual model was tested using a series of 39 triaxial compression tests on Fraser river sand, reaching p' levels of up to 3 *MPa*. The associated increase in the fines content of sheared samples ranged from zero to nearly 7%.

The main aspects of the hypothesis that are confirmed by laboratory testing were:

- Measurable breakage only starts after the soil's contraction capacity is exhausted.

- Breakage causes a downward parallel shift in the location of the CSL in $e - \log p'$ space.

- The magnitude of this CSL shift is equal to the void ratio reduction due to breakage ($\Delta e_b = \Delta \Gamma$) and is directly correlated to the increase in fines content.

These observations on the parallel shift in the CSL contradict the widely adopted three part line used to model the effect of particle breakage on the CSL (e.g. Russell and Khalili, 2004). It is recommended that future work idealises the CSL as a series of parallel loci each associated with a certain level of particle breakage.

The hypothesis also implies that since $\Delta e_b = \Delta\Gamma$, the state parameter is independent of breakage. The volume reduction caused by the breakage may simply be superimposed on the volume change controlled by stress-dilatancy. Hence for small amounts of breakage the critical state framework found in many, and arguably most, advanced constitutive models for soil remains valid even in the presence of particle breakage; particle breakage can be treated as an uncoupled phenomenon that changes Γ.

The work presented here lays out a conceptual framework for the idea of parallel CSLs (Daouadji et al., 2001) and provides experimental evidence for it. The simplicity of the hypothesis and its implications on the evolution of the state parameter towards the critical state under particle breakage provides a basis for modelling of the phenomenon within a critical state soil mechanics context.

8.3.   Contributions

The main contributions of this dissertation to the current state of knowledge in the fields researched are:

1. A correlation was provided between the number of triaxial tests required to achieve certain accuracy and confidence levels in determining the critical state (constant volume) friction angle in laboratory.

2. An analytical framework for estimating the in-situ state parameter of sands was verified against an unprecedentedly extensive database of calibration chamber tests, and validated against two well documented case histories. It was shown that the confidence

and accuracy achieved through the framework is comparable to the best and most expensive laboratory and field methods.

3. A simple hypothesis was put forward to explain the effects of particle breakage on the critical state and behaviour of sand. A significant number of triaxial tests were performed for the first time to investigate the matter. The hypothesis was demonstrated to successfully explain the behaviour observed in the tests.

8.4. Limitations

The results presented in this thesis were obtained based on a series of assumptions and verified against a limited set of data. Application of this work to other situations should take account of such limitations. The following specific limitations can be pointed out with regards to different portions of the work:

1. The confidence and accuracy levels in determining the critical state friction angle were obtained for a clean quartz sand. Soil type and gradation are expected to affect sample uniformity during reconstitution and hence influence the repeatability (and hence accuracy) of the triaxial testing program.

2. The framework for interpretation of the state parameter was developed for drained penetration. The methodology is not applicable to finer grained materials and/or higher rates of penetration where development of excess pore water pressure around the cone is expected.

3. The constitutive model used to represent soil, Norsand, is applicable to granular soils. Hence the methodology presented does not apply to cohesive or cemented materials.

4. An important assumption of the cavity expansion analysis is a uniform homogeneous medium around the expanding cavity. The current framework is therefore not capable of capturing the effects of phenomena such as closely layered soils and soils with significantly anisotropic stress-strain behaviour.

5. The framework is verified and validated for an extensive database of calibration chamber tests and in-situ measurements of the state parameter. However, all the materials comprising the database are more or less sand size materials with fines contents not exceeding 6%. The extension of its use to other cohesionless materials such as silts and fines rich sands and materials with significantly different minerologies (e.g. Calcareous sands) should be sufficiently examined as such data become available.

6. The experimental work done to investigate the effects of particle breakage on the critical state of the sands was limited to one suite of testing on Fraser river sand. Further testing is needed to confirm the generality of the results. Testing with a range of material types is also needed to extend the theoretical framework to link the reduction in Γ during particle breakage to the encountered stress-strain path.

7. The stress and strain levels achieved in investigating the effects of particle breakage were limited by the constraints of the triaxial testing apparatus. Hence the amount of particle breakage was limited and it did not become clear how far the observed trends would continue as more breakage occurs under higher stress and strain levels.

8.5.   Future Studies

The work presented in this thesis focused on interpreting the state parameter from CPT tip resistance. The critical state friction angle and the particle breakage phenomenon were further investigated as factors with great influence on the interpretation. The following work is recommended to be undertaken as part of future research on this subject:

1. Studying the effect of over-consolidation ratio on the proposed CPT interpretation methodology. The current work only considered normally consolidated soils, but over-consolidated soils are common in practice and calibration chamber data are available with over-consolidated samples.

2. Further laboratory testing to tie the amount of particle breakage to the shear strain and stress level. And investigating how the stress path taken can affect particle breakage. Such research can provide the experimental evidence for a new framework for modeling the particle breakage phenomenon. It will be then possible to investigate the effects of including particle breakage in CPT interpretation.

3. Modelling the CPT using an axisymmetric geometric approximation. A more realistic geometric approximation enables investigation of the effect of sleeve friction on interpretation of the state parameter. Accurate geometry also allows investigation of the effect of soil layering on CPT resistance. The understanding gained from these simulations could be used directly, or incorporated into the current framework.

4. Investigating the effect of lateral stress on CPT tip resistance and its implications. This issue has been previously investigated, but the addition of new chamber testing using

more advanced chambers and application of more sophisticated constitutive models can illuminate the previous discussions on this subject.

In the absence of material-specific data, careful consideration should be given when extrapolating the methods and data presented in this thesis to other cases involving different materials. The analysis presented here reduces the need for prohibitively expensive and cumbersome calibration chamber tests to a few triaxial tests on reconstituted samples, followed by a limited amount of numerical analysis. The geotechnical community is moving away from the use of rule of thumb correlations for interpreting CPT data except for problems with insignificant consequences (Robertson, 2009). As requirements are expanding to require analysis of the consequences of geotechnical problems such as liquefaction, more projects will find the resources to justify the additional efforts required for adopting methods such as those presented here.

8.6.   References

Been K., and Jefferies M.G. 1985. A State Parameter for Sands. Géotechnique, 35(2): 99-112.

Been K., Jefferies M.G., Crooks J.H.A., and Rothenburg L. 1987. The Cone Penetration Test in Sands. Part II: General Inference of State. Géotechnique 37(3): 285-299.

Bishop A.W. 1972. Shear strength parameters for undisturbed and remolded soil specimens. In Proceedings, Roscoe Memorial Symposium, Cambridge University. Edited by R.H.G. Parry. G.T. Foulis & Co. Ltd., Yeovil, U.K., 3–139.

Daouadji A., Hicher P. Y., and Rahma A. 2001. An Elastoplastic Model for Granular Materials Taking into Account Grain Breakage. European Journal of Mechanics - A/Solids, 20: 113–137.

Konrad J.-M. 1997. In Situ Sand State from CPT: Evaluation of a Unified Approach at Two CANLEX Sites. Canadian Geotechnical Journal. 34: 120–130.

Muir Wood D. 2007. The Magic of Sands. The 20th Bjerrum lecture presented in Oslo, 25 November 2005, Canadian Geotechnical Journal, 44: 1329-1350.

Plewes H.D., Davies M.P., and Jefferies M.G. 1992. CPT Based Screening Procedure for Evaluating Liquefaction Susceptibility. Proceedings of the 45th Canadian Geotechnical Conference, Toronto.

Robertson P.K. 2009. Interpretation of Cone Penetration Tests – A Unified Approach. Canadian Geotechnical Journal, 46: 1337-1355.

Russell A.R., and Khalili N. 2004. A Bounding Surface Plasticity Model for Sands Exhibiting Particle Crushing. Canadian Geotechnical Journal, 41(6): 1179-1192.

Wride C.E. and Robertson P.K. 1997. The Canadian Liquefaction Experiment, Phase II Data Review Report, Massey and Kidd Sites, Fraser River Delta, June 1997. ISBN 0-921095-49-X. Wride C.E. and Robertson P.K. (eds.), BiTech Publishers Ltd., Richmond, BC, Canada.

Appendix A

Triaxial Tests on Fraser River Sand

Procedures and Results

A.1.   Testing Equipment

Triaxial tests were carried out using a computer-controlled triaxial system capable of consolidating and shearing soil specimens along user specified stress paths. Figure A-1 presents a picture of the equipment and the triaxial set set-up. The system consisted of a load frame, two pressure/volume actuators (flow pumps) and a high resolution analog data acquisition system all connected and controlled by a computer via interface modules.

The pressure/volume actuators generated and controlled pressures up to 2100 *kPa* (300 *psi*) and flow rates ranging from 25 *ml/min* to 0.000025 *ml/min*. The system also included one load cell, one deformation sensor, three pressure sensors and one temperature sensor. Load cells with 500, 2000 and 10,000 *lbs* (227, 907 and 4536 *kg* respectively) capacities were available for obtaining the optimum accuracy from the tests. Two of the pressure sensors had a range of -68 *kPa* to 2100 *kPa* (-10 *psi* to 300 *psi*) and were used in the pressure/volume control pumps; the third sensor had a range of -68 *kPa* to 1380 *kPa* (-10 *psi* to 200 *psi*) and was used for pore pressure measurements. Linear displacement transducers had a range of 76.2 *mm* (3.0 *in*). All electronic measurement devices were connected to the loading frame and then into the laboratory PC; data was logged electronically recording 200 measurement every hour giving a typical data set of 600 measurements in a test taken to 15% axial strain.

The triaxial cell was equipped with 'frictionless' end platens. These platens had a diameter of 74 *mm.* and the samples were prepared with a split mould (Figure A-2) with a diameter of 71.5 *mm.* The split mould height was 142.8 *mm* for a sample height to diameter ratio of 2.

A.2. Test Procedures

The vacuum split mould was attached to the triaxial cell base with a membrane connected to the bottom platen (Figure A-3). The top of the membrane was folded over the split mould and the membrane was held open with a vacuum pressure. Samples were prepared by mixing distilled water with the soil (Figure A-4) to a moisture content of 5% with a weight precision of 0.01 *g*. Six layer mass portions were determined using the undercompaction method proposed by Ladd (1978). The six mass portions of the moist soil were then placed in the mould (Figure A-5) and compacted with the tamping rod (Figure A-6) in six equal thickness lifts (each 1/6 the total sample height in the mould). The method was employed to ensure that each layer, and thus the entire sample, is prepared to the target density and void ratio. Prior to the next lift being placed, the surface of the previous lift was scarified to a depth of 1 *mm* to 2 *mm*. After tamping of the sixth lift, the top cap platen was placed on the sample, the membrane turned up and the o-rings applied to seal the membrane to the top cap (Figure A-7). Then the vacuum was switched from the split mould to the sample through the drainage port. At this point a vacuum pressure of about 20 *kPa* was applied. While under the vacuum pressure, sample height and diameter were measured to a precision of ±0.01 *mm*. Each dimension was measured at four different locations and the average values were recorded as sample dimensions.

Triaxial tests were carried out using lubricated enlarged end platens aimed at reducing stress non-uniformities and minimizing the end restrain. The procedure developed by Tatsuoka et al. (1984) was used by using two rubber membranes (0.21 *mm* thickness) separated by a smear of high-vacuum silicon-based grease.

The triaxial cell was assembled following the measurement of the sample dimensions. The cell was filled with water and a 20 kPa seating cell pressure was incrementally applied to the sample while reducing the vacuum on the sample. Then, CO_2 gas was slowly percolated through the sample for a period of two to four hours. Following flushing with CO_2, de-aired water was allowed to flow through the sample under less than 2 m driving head for 8 to 12 hours.

Sample dimensions during saturation were monitored by the displacement of the top cap and chamber volume changes.

The sample pore pressure lines were then connected to the pressure/volume actuators and back pressure was applied. The back pressure saturation was carried out by increasing the cell pressure and measuring the response in pore pressure. The cell pressure was increased in increments until a $B \geq 0.95$ for drained tests or $B \geq 0.98$ for undrained tests was achieved.

After completing the saturation phase, the sample was consolidated to the required pressure in incremental steps. The volume change during the consolidation process was continuously monitored.

The sample was then sheared at a constant rate of 5% per hour. The tests aimed at locating the CSL were prepared to a loose state and sheared until a steady state of constant volume was achieved. Dense samples were sheared until clear shear banding was detected in the sample. Some of the tests were stopped at lower strain levels to investigate the particle breakage occurred at intermediate states of shearing as explained in Chapter 7.

At the end of the shearing phase the drainage valves were closed keeping and all pore water in the sample. The cell's confining fluid was drained and after removing the chamber sleeve, the cell pedestal together with the sample and the loading cap were gently wiped and put into a freezer for a minimum 24 hours. After the specimen was frozen, the membrane, top and bottom

platens were carefully removed and any soil grains remaining on them carefully brushed into the sample pan. The sample was then dried in a laboratory oven for determining the final water content. This water content was used to calculate the void ratio at the end of shearing. This technique (Sladen and Handford, 1987) effectively eliminated loss of water during sample extraction, enabling accurate determination of void ratio at the end of the test. It also allowed for determining the void ratio to the end of the back-pressurisation phase by back tracking the void ratio changes during shearing and isotropic consolidation with the accuracy provided by the flow pumps.

Corrections were applied for membrane penetration (Vaid and Negussey, 1984) and membrane force (Kuerbis and Vaid, 1990).

A.3. Repeatability of Test Results

The confidence in experimental observations is greatly enhanced by the repeatability of the results. Repeatability is achieved by consistent reproduction of the void ratio, fabric (through reconstitution method), repeatability of the procedures, duplication of the stress paths, and the measurement accuracy. A repeatability of 0.01 or better in void ratio measurement was achieved for three pairs of tests that were targeted to start from identical conditions; and, there was corresponding near-perfect repeatability in measurement of stresses and strains as illustrated in Figures A.8 and A.9.

A.4.   Test Results

Figure A.10a shows the deviator stress and volumetric strain plotted against axial strain for the drained tests presented in Table 7-1. Figure A.10b shows the deviator stress and the pore pressure plotted against the axial strain for the undrained tests presented in Table 7-1.
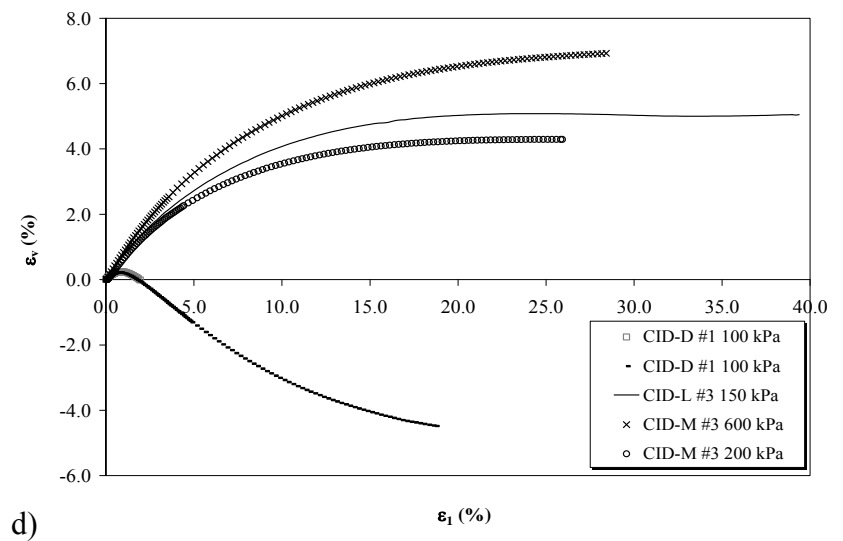
The deviator stress, pore pressure and volumetric strain are plotted against axial strain for samples subjected to higher levels of stress in Figures A-11a to A-11c . At the end of each parent test the sample was sieved and then retested in the triaxial apparatus at lower levels of stress as summarised in Table 7-2 and shown in Figures A-11d to A-11f .
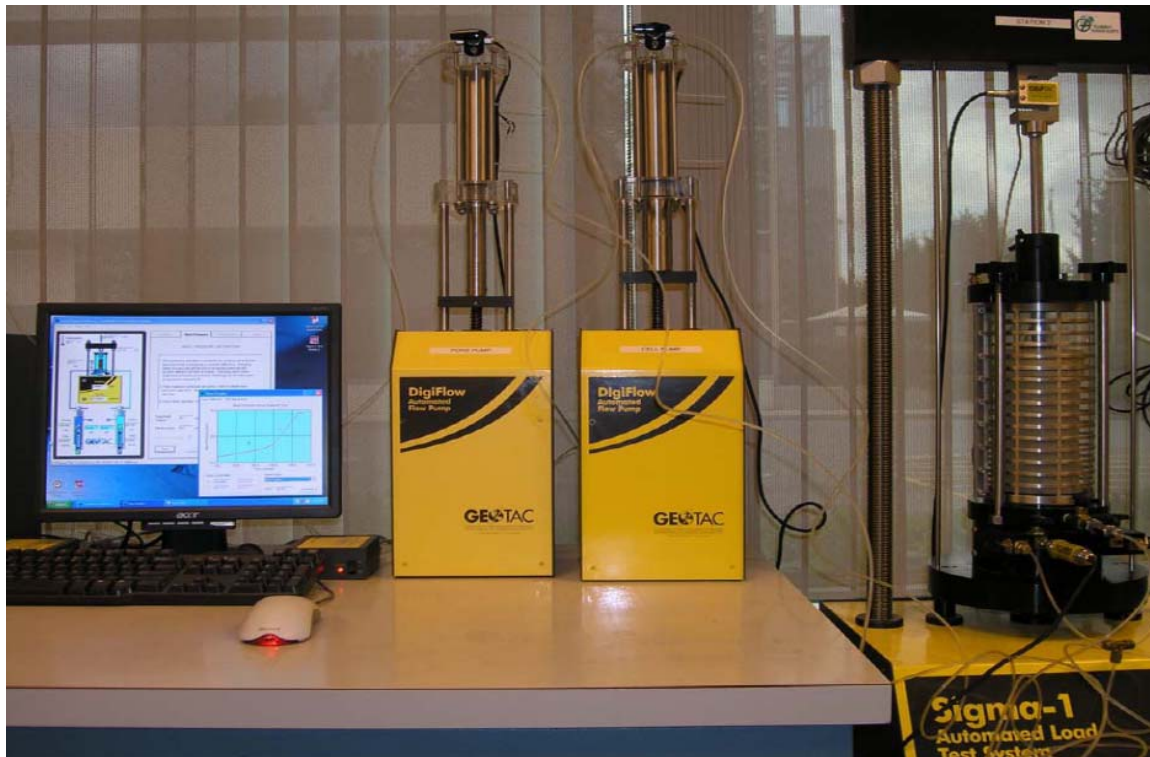
Figure A - 1 Triaxial test loading frame, pressure pumps and cell set-up

Figure A - 2 Split mould device

Figure A - 3 Triaxial base with split mould and membrane

Figure A - 4 Adding water for sample preparation

Figure A - 5 Sample preparation in layers

Figure A - 6 Sample compaction

Figure A - 7 Prepared sample before cell assembly
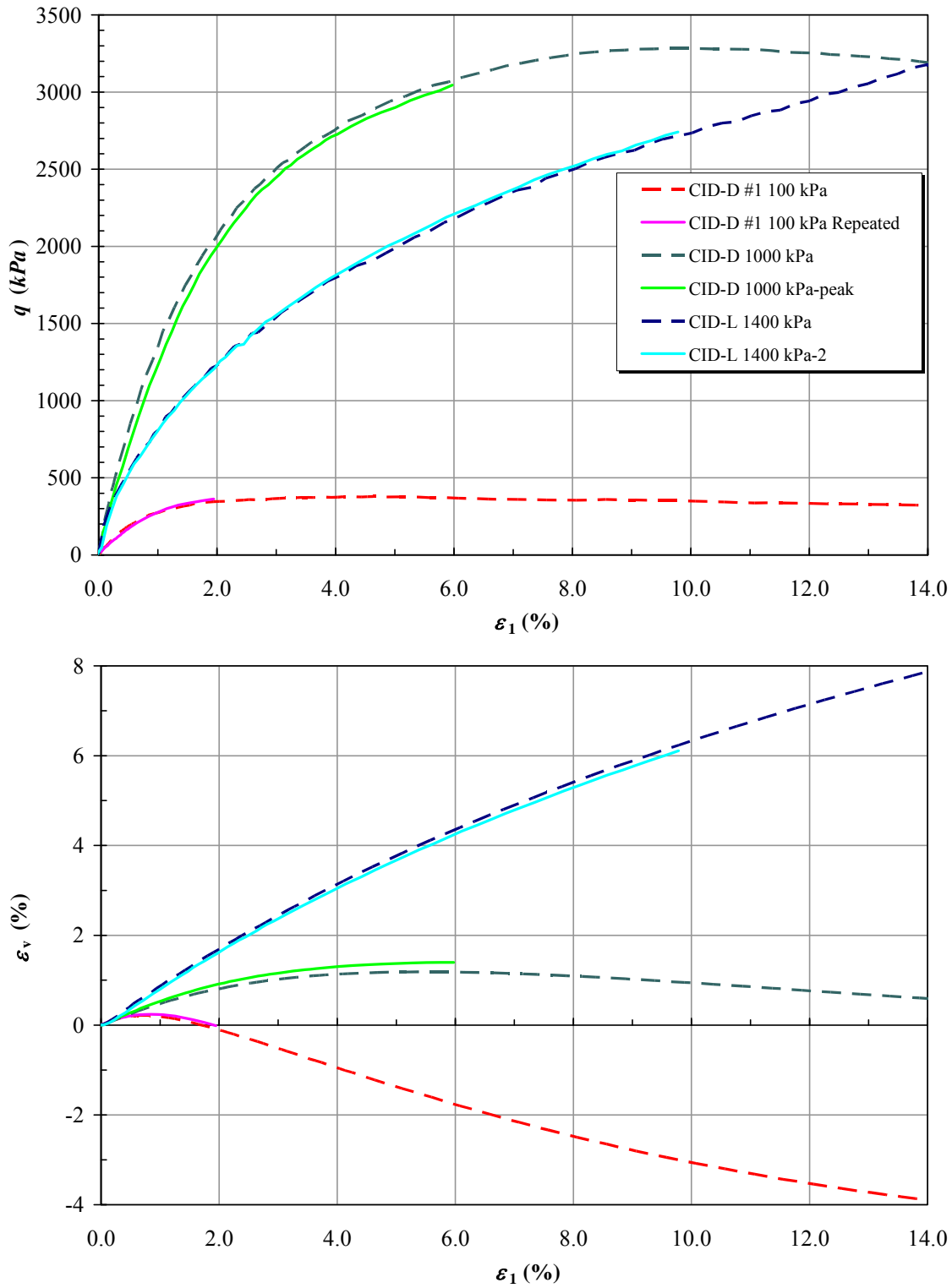
Figure A - 8 Deviator stress and volumetric strain versus axial strain for three pairs of tests starting from identical density and stress states
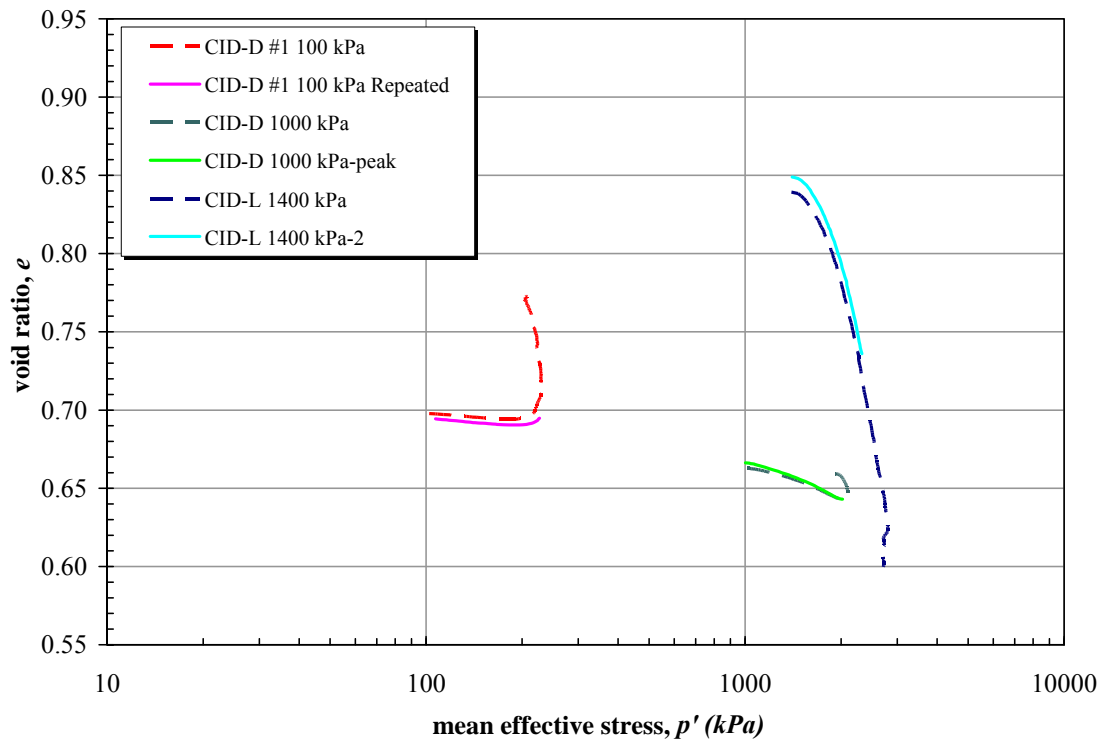
Figure A - 9 Void ratio versus mean effective stress for three pairs of tests starting from identical density and stress states
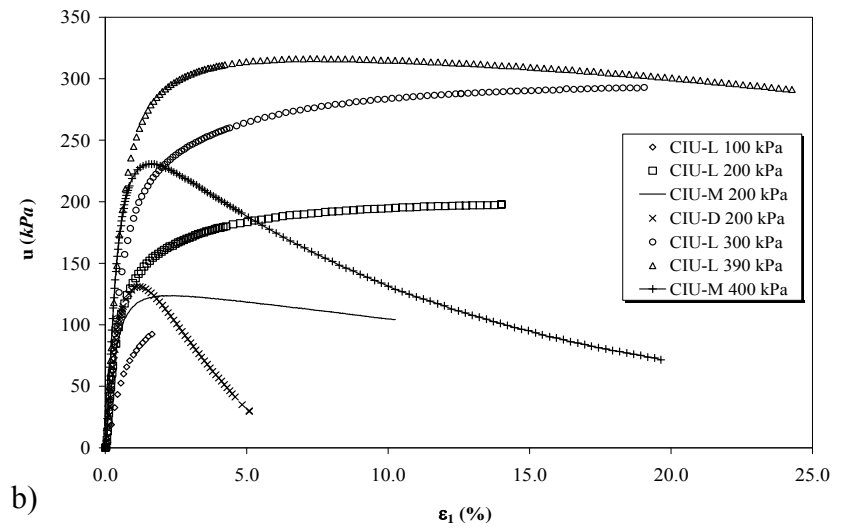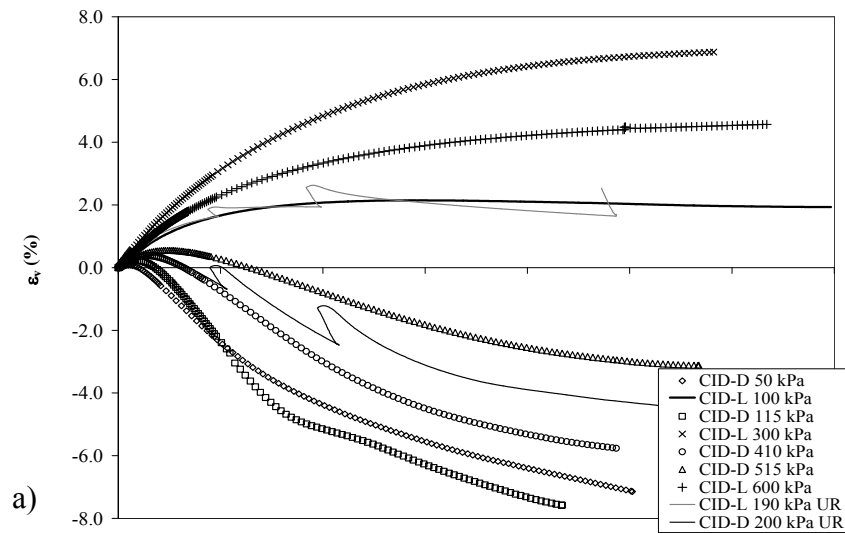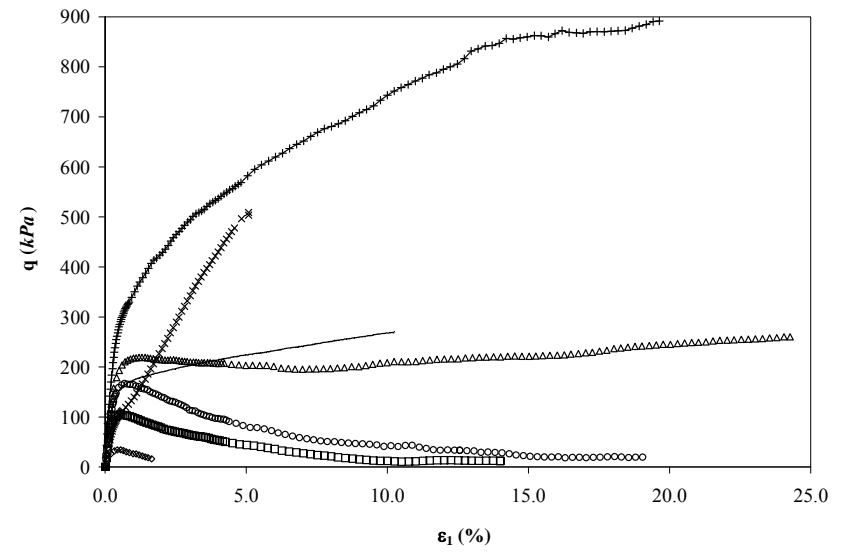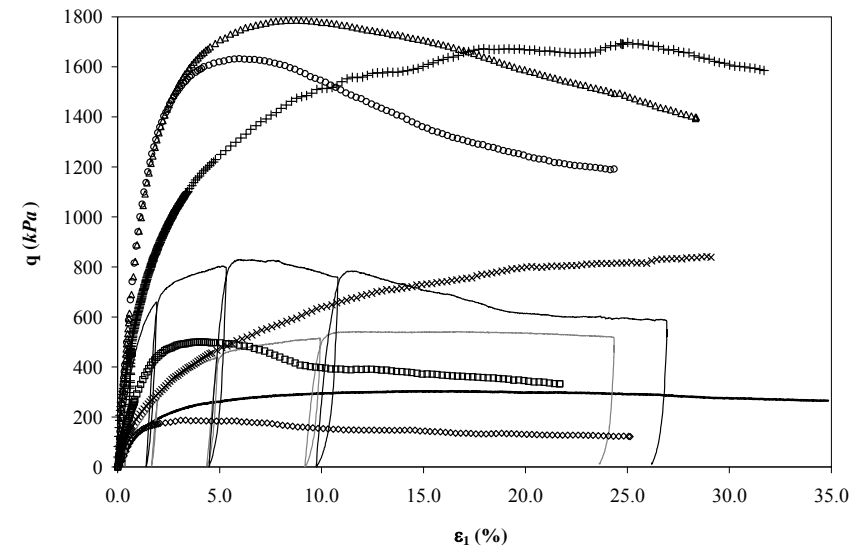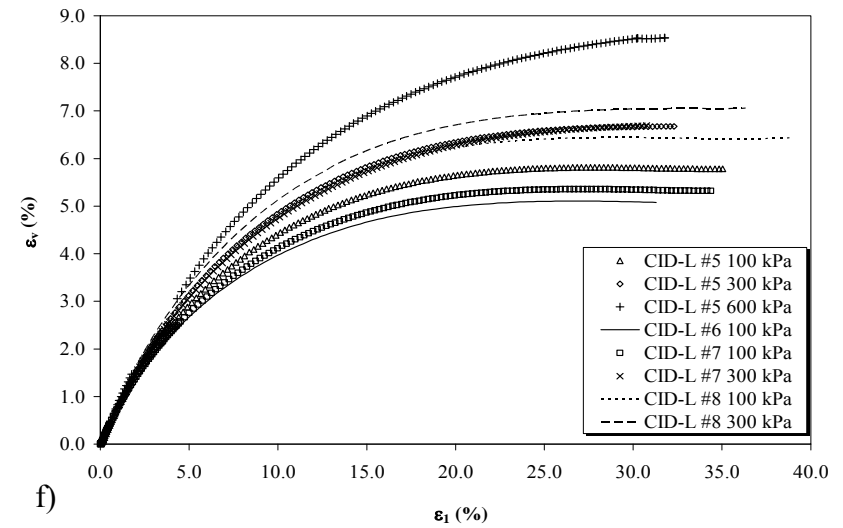
Figure A - 10 Deviator stress, pore pressure and volumetric strain plotted against the axial strain for tests aimed at determining the CSL for virgin FRS, summarised in Table 7-1
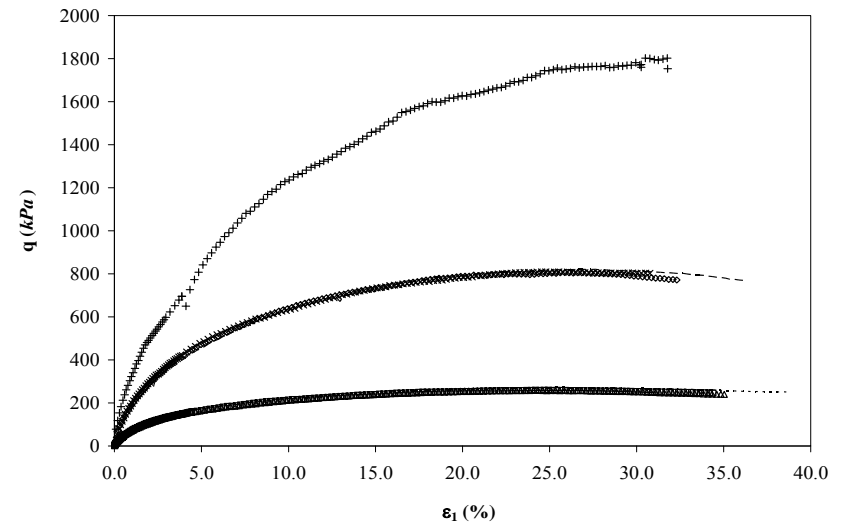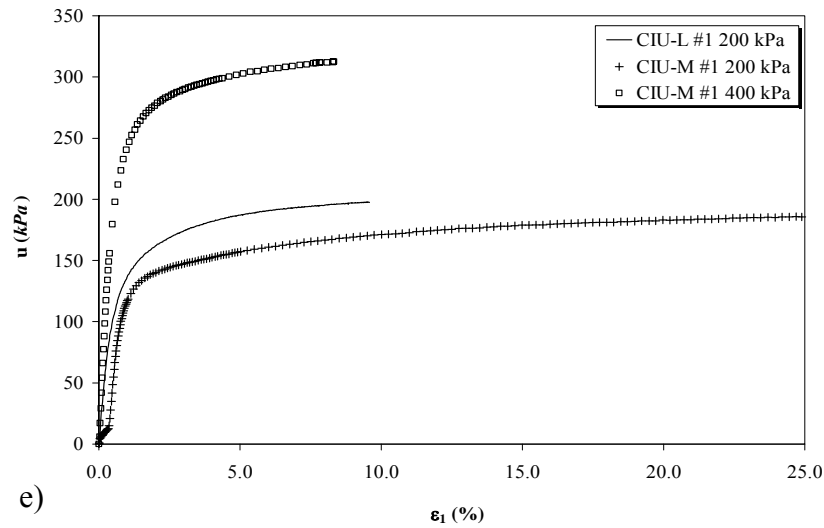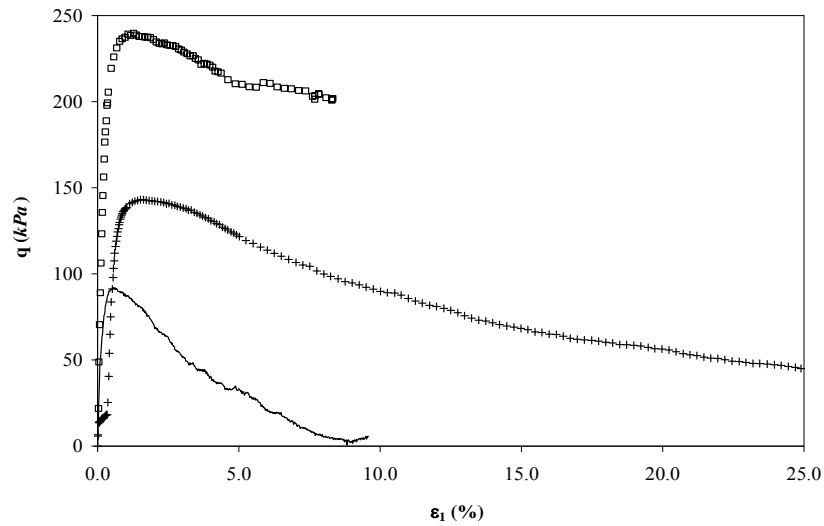
c)

d)

306
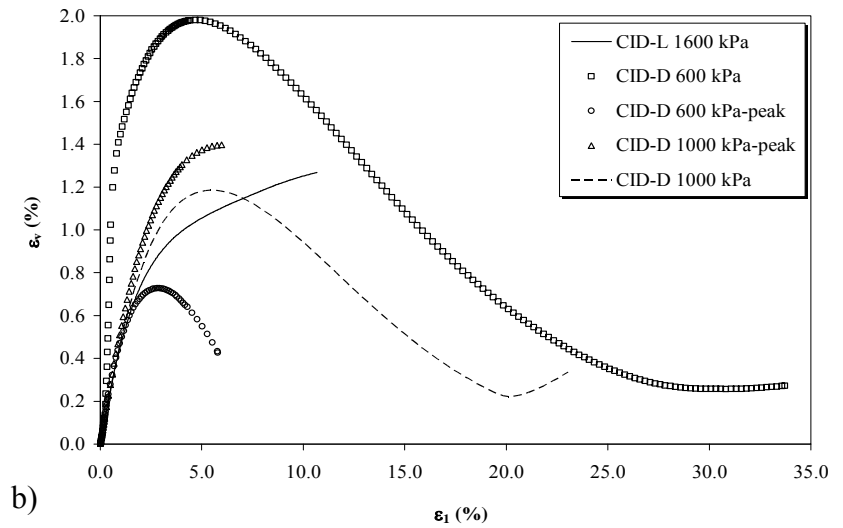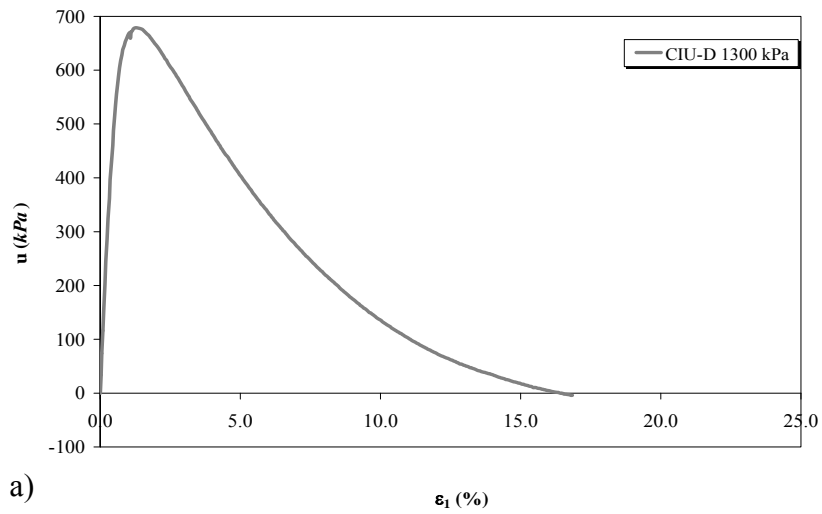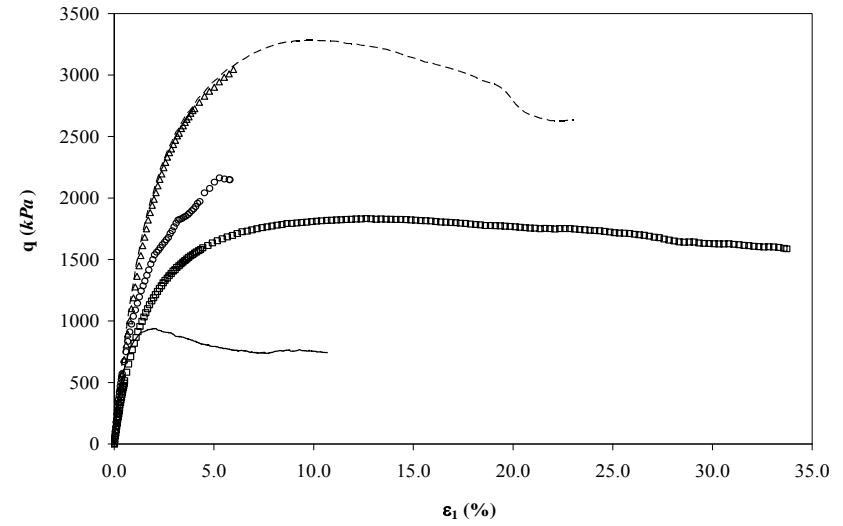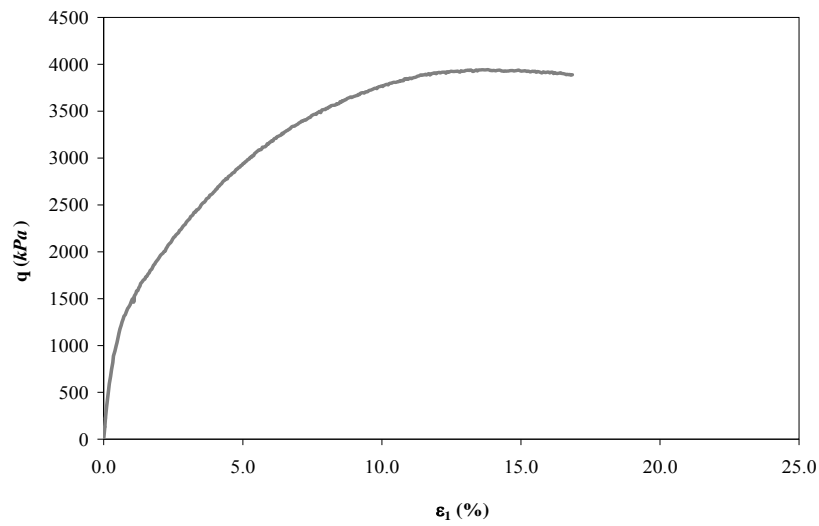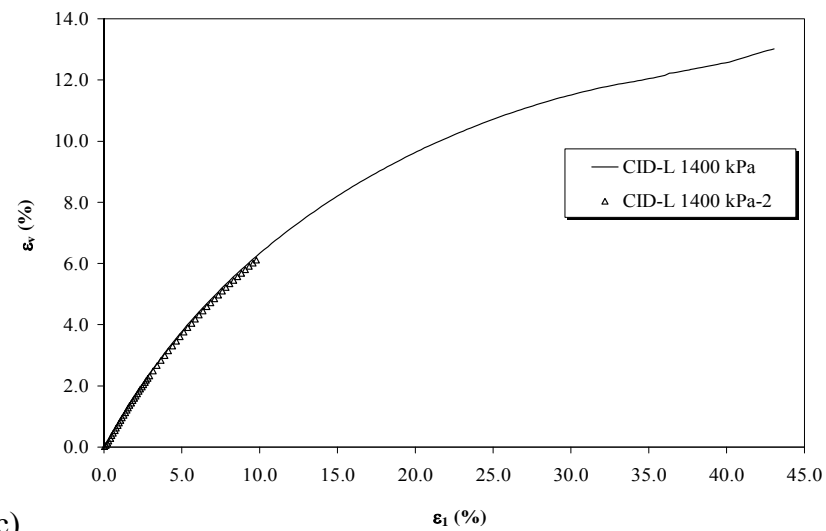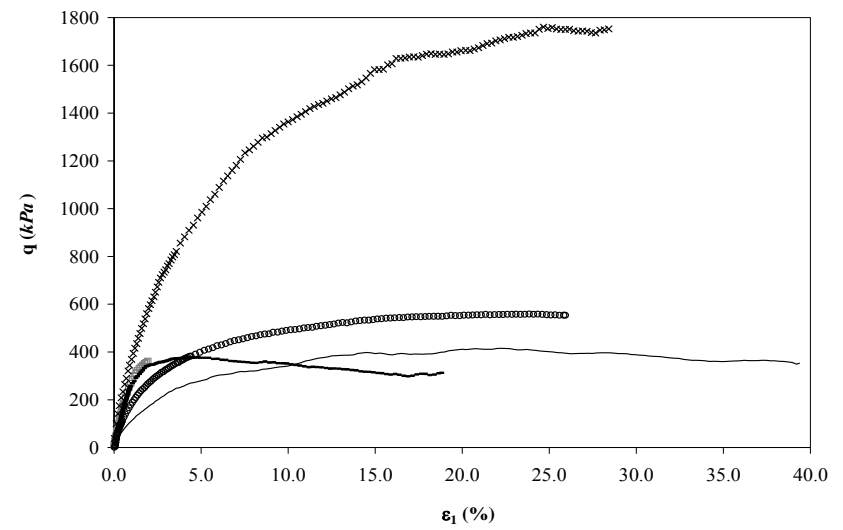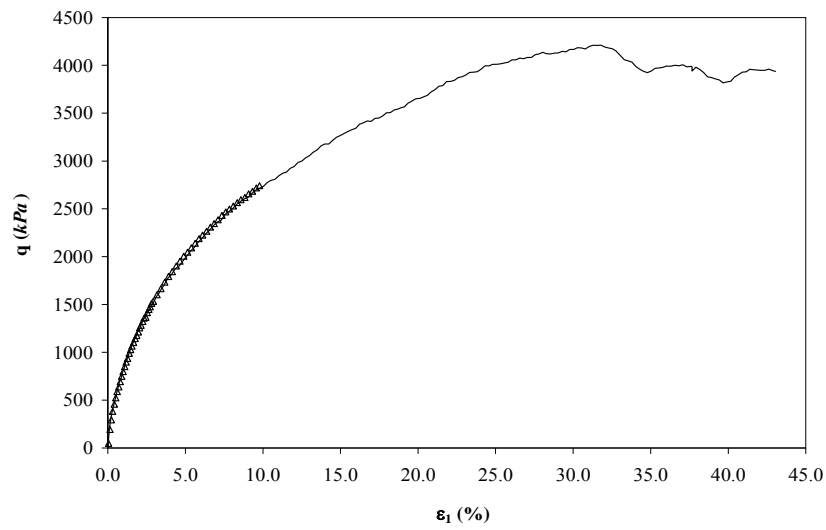
Figure A - 11 Deviator stress, pore pressure and volumetric strain plotted against the axial strain for tests aimed at determining the effects of particle breakage on FRS, summarised in Table 7-2

A.5. References

Kuerbis R.H., and Vaid Y.P. 1990. Corrections for Membrane Strength in the Triaxial Test. Geotechnical Testing Journal, 13(4): 361-369.

Ladd R.S. 1978. Preparing test specimens using undercompaction. Geotechnical Testing Journal, 1(1): 16-23.

Negussey D., Wijewickreme W.K.D., and Vaid, Y.P. 1988. Constant Volume Friction Angle of Granular Materials. Canadian Geotechnical Journal, 25: 50-55.

Sladen J.A., and Handford G. 1987. A potential systematic error in laboratory testing of very loose sands. Canadian Geotechnical Journal, 24: 462-466.

Tatsuoka F., Molenkamp F., Torii T., and Hino T. 1984. Behavior of lubrication layers of platens in element tests. Soils and Foundations, 24(1): 113-128.